

# CONTROLLABLE SUSPENSION DESIGN USING MAGNETORHEOLOGICAL FLUID

ANRIA STRYDOM

October 2013

Pretoria

South Africa

UNIVERSITY OF PRETORIA



UNIVERSITEIT VAN PRETORIA  
UNIVERSITY OF PRETORIA  
YUNIBESITHI YA PRETORIA

Submitted in partial fulfilment of the requirements for the degree **Masters in Mechanical Engineering** in the FACULTY OF ENGINEERING, THE BUILT ENVIRONMENT AND INFORMATION TECHNOLOGY (EBIT).



---

---

## Dissertation Summary

---

---

**Title:** Controllable Suspension Design Using Magnetorheological Fluid  
**Author:** ANRIA STRYDOM  
**Supervisor:** Prof. P.S. Els  
**Co-Supervisor:** Dr. S. Kaul  
**Department:** Mechanical and Aeronautical Engineering, University of Pretoria  
**Degree:** Masters in Mechanical Engineering

The purpose of this study is to mitigate the compromise between ride comfort and handling of a small single seat off-road vehicle known as a Baja. This has been achieved by semi-active control of the suspension system containing controllable magnetorheological (MR) dampers and passive hydro-pneumatic spring-damper units.

MR fluid is a viscous fluid whose rheological properties depend on the strength of the magnetic field surrounding the fluid, and typically consists of iron particles suspended in silicone oil. When a magnetic field is applied to the fluid, the iron particles become aligned and change the effective viscosity of the fluid. The use of MR fluid in dampers provides variable damping that can be changed quickly by controlling the intensity of the magnetic field around the fluid. Various benefits associated with the use of MR dampers have led to their widespread implementation in automotive engineering.

Many studies on conventional vehicles in the existing literature have demonstrated the conflicting suspension requirements for favourable ride comfort and handling. Generally, soft springs with low damping are ideal for improved ride comfort, while stiff springs with high damping are required for enhanced handling. This has resulted in the development of passive suspension systems that provide either an enhanced ride quality or good drivability, often targeting one at the expense of the other.

The test vehicle used for this study is distinct in many ways with multiple characteristics that are not commonly observed in the existing literature. For instance, the absence of a differential in the test vehicle driveline causes drivability issues that are aggravated by increased damping.

The majority of existing MR damper models in the literature are developed for uniform excitation and re-characterisation of model parameters is required for changes in input conditions. Although recursive models are more accurate and applicable to a wider range of input conditions, these models require measured force feedback which may not always be available due to limitations such as

packaging constraints. These constraints required the development of alternative MR damper models that can be used to prescribe the current input to the damper.

In this study parametric, nonparametric and recursive MR damper models have been developed and evaluated in terms of accuracy, invertibility and applicability to random excitation. The MR damper is used in parallel with passive damping as a certain amount of passive damping is always present in suspension systems due to friction and elastomeric parts.

Most of the existing studies on suspension systems have been performed using linear two degree of freedom vehicle models that are constrained to specific conditions. Usually these models are implemented without an indication of the ability of these models to accurately represent the vehicles that these studies are intended for.

For this study, a nonlinear, three-dimensional, 12 degrees of freedom vehicle model has been developed to represent the test vehicle. This model is validated against experimental results for ride comfort and handling. The MR damper models are combined with the model of the test vehicle, and used in ride comfort and handling simulations at various levels of passive damping and control gains in order to assess the potential impact of suspension control on the ride quality and drivability of the test vehicle.

Simulation results show that lower passive damping levels can significantly improve the ride comfort as well as the handling characteristics of the test vehicle. Furthermore, it is observed that additional improvements that may be obtained by the implementation of continuous damping control may not be justifiable due to the associated cost and complexity.

---

---

## Samevatting van Verhandeling

---

---

<b>Titel:</b>	Beheerbare Suspensie Ontwerp met Magnetoreologiese Vloeistof
<b>Outeur:</b>	ANRIA STRYDOM
<b>Studieleier:</b>	Prof. P.S. Els
<b>Mede-Studieleier:</b>	Dr. S. Kaul
<b>Departement:</b>	Meganiese en Lugvaartkundige Ingenieurswese, Universiteit van Pretoria
<b>Graad:</b>	Meesters in Meganiese Ingenieurswese

Die doel van hierdie studie is om die kompromie tussen die ritgemak en hantering van 'n klein enkelsitplek veldvoertuig, bekend as 'n Baja, te verminder. Dit word bereik deur die semi-aktiewe beheer van die voertuig se suspensie, wat uit beheerbare magnetoreologiese-(MR) dempers en passiewe hidro-pneumatiese veer-demper eenhede bestaan.

MR-vloeistof is 'n viskeuse stof waarvan die reologiese eienskappe afhanklik is van die sterkte van die magneetveld om die vloeistof, en bestaan tipies uit ysterparikels gesuspendeer in silikonolie. Wanneer die vloeistof aan 'n magneetveld blootgestel word, word die partikels opgelyn en sodoende word die effektiewe viskositeit van die vloeistof verander. Die gebruik van MR-vloeistof in dempers verskaf varieërbare demping wat vinnig verander kan word deur die intensiteit van die magneetveld om die vloeistof te beheer. Verskeie voordele geassosieer met die gebruik van MR-dempers het gelei tot die wye implementering van die dempers in voertuigingenieurswese.

Verskeie studies in die huidige literatuur demonstreer dat suspensie-karakteristieke vir optimale ritgemak en hantering van konvensionele voertuie in konflik met mekaar is. In die algemeen is sagte vere met lae demping ideal vir verbeterde ritgemak, waar harde vere met hoë demping nodig word om die hantering van die voertuig te verbeter. Hierdie konflik het gelei tot die ontwikkeling van passiewe suspensiestelsels wat óf verbeterde ritkwaliteit, óf gewenste hantering lewer, waar die een aspek gewoonlik bevoordeel word ten koste van die ander.

Die toetsvoertuig wat in hierdie studie gebruik word is uniek met verskeie eienskappe wat nie tradisioneel in die bestaande literatuur beskryf word nie. Byvoorbeeld, die afwesigheid van 'n ewenaar in die voertuig se dryflyn veroorsaak swak stuurvermoë wat deur die verhoging van demping vererger word.

Die meerderheid van die MR dempermodelle wat in die huidige literatuur beskryf word is ontwikkel vir uniforme opwekking en her-karakterisering van modelparameters moet uitgevoer word

indien die insette verander. Alhoewel rekursiewe modelle meer akkuraat is en van toepassing is op 'n groter verskeidenheid van insette, benodig hierdie modelle die terugvoer van gemete dempingskrag, wat nie noodwendig beskikbaar is nie as gevolg van beperkings soos beskikbare ruimte in die suspensie opstelling. As gevolg van hierdie beperkings moet 'n alternatiewe MR-dempermodel ontwikkel word wat in staat is om die stroom inset na die demper voor te skryf.

In hierdie studie is parametriese, nie-parametriese en rekursiewe MR-dempermodelle ontwikkel en ge-evalueer in terme van akkuraatheid, omkeerbaarheid en toepasbaarheid op willekeurige opwekking. Die MR-demper word in parallel met passiewe dempers gebruik aangesien 'n sekere mate van passiewe demping altyd in suspensiestelsels teenwoordig is as gevolg van wrywing en die teenwoordigheid van elastomeriese komponente.

Die meerderheid van die studies op suspensiestelsels wat tans beskikbaar is, is uitgevoer op lineêre twee-vryheidsgraad voertuigmodelle wat beperk is tot sekere omstandighede. Gewoonlik word hierdie modelle geïmplementeer sonder om 'n aanduiding te gee van die vermoë van die modelle om die werklike voertuie waarvoor die studies uitgevoer is te verteenwoordig.

Vir hierdie studie is 'n nie-lineêre, drie-dimensionele, 12-vryheidsgraad voertuigmodel ontwikkel om die toetsvoertuig voor te stel. Die model is gevalideer teenoor eksperimentele resultate vir ritgemak en hantering. Die MR-dempermodelle is gekombineer met die voertuigmodel en geïmplementeer in ritgemak en hantering simulasies teen verskeie vlakke van passiewe demping en beheer faktore om die potensiële impak van suspensiebeheer op die ritkwaliteit en stuurbaarheid van die toetsvoertuig te ondersoek.

Simulasieresultate toon aan dat laer passiewe dempingsvlakke beide die ritgemak en die hantering van die toetsvoertuig verbeter. Verder is gevind dat addisionele verbeteringe wat behaal kan word deur die implementering van kontinue dempingbeheer nie noodwendig motiveerbaar is nie as gevolg van die ekstra koste en kompleksiteit wat daarmee gepaard gaan.

---

---

## *ACKNOWLEDGEMENTS*

---

---

The Author would like to thank the following persons:

- The Sasol Laboratory staff for their help with the experimental work performed in the laboratory facilities.
- The Baja team of 2011, including Joachim Stallman, for their assistance with the experimental work concerning the validation of the Baja simulation model.
- A special thanks to the Baja vehicle driver, Michael Kapp, who had to sacrifice a lot of his time for the performance of vehicle baseline testing, as well as the experimental determination of the Baja centre of mass and moments of inertia.
- Theunis Botha for his help with the debugging of the Baja simulation models and the implementation of a steering controller which fell beyond the scope of this project.
- The Vehicle Dynamics Group of the University of Pretoria for their support and advice regarding various aspects of the project.
- The Author's immediate family and friends for their support and advice.
- Lastly a special thanks to the project supervisors, namely Prof. P.S. Els (supervisor) from the University of Pretoria and Dr. S. Kaul (co-supervisor) from the University of Mount Union. Without their guidance successful completion of the project would not have been possible.





---

---

# *TABLE OF CONTENTS*

---

---

Dissertation Summary.....	i
Samevatting van Verhandelng .....	iii
Acknowledgements .....	v
Table of Contents.....	vii
List of Symbols.....	xi
List of Abbreviations .....	xv
List of Figures.....	xvii
List of Tables .....	xxiii
1 Introduction.....	1.1
2 Literature Survey .....	2.1
2.1 Ride Comfort and Handling.....	2.1
2.1.1 Ride Comfort .....	2.2
2.1.2 Handling.....	2.3
2.1.3 The Ride Comfort and Handling Compromise .....	2.5
2.1.4 Conclusion .....	2.6
2.2 Vehicle Suspension Systems Classification.....	2.6
2.2.1 Passive Suspension Systems .....	2.7
2.2.2 Semi-Active Suspension Systems .....	2.7
2.2.3 Active Suspension Systems .....	2.9
2.2.4 Conclusion .....	2.9
2.3 Vehicle Modelling .....	2.10
2.3.1 The Quarter Car Vehicle Model.....	2.10
2.3.2 Higher Order Mathematical Models .....	2.11
2.3.3 Computer Simulation Models .....	2.12
2.3.4 Validation of Vehicle Models .....	2.12
2.3.5 Conclusion .....	2.13
2.4 Suspension Control.....	2.13
2.4.1 Skyhook-, Groundhook-, and Hybrid Control .....	2.13

2.4.2	Other Control Algorithms Used in Suspension Control.....	2.18
2.4.3	Conclusion .....	2.18
2.5	Controllable Dampers .....	2.19
2.6	Magnetorheological Dampers.....	2.20
2.6.1	Magnetorheological Damper Technology.....	2.20
2.6.2	Magnetorheological Damper Modelling .....	2.21
2.6.3	Commonly Used Magnetorheological Damper Models.....	2.23
2.6.4	Conclusion .....	2.32
2.7	Literature Summary and Problem Statement .....	2.32
3	Magnetorheological Damper Characterization .....	3.1
3.1	Experimental Work.....	3.1
3.2	Magnetorheological Damper Models.....	3.7
3.2.1	Bingham Model.....	3.8
3.2.2	Bouc-Wen Model.....	3.13
3.2.3	Kwok Model .....	3.17
3.2.4	Polynomial Model.....	3.20
3.2.5	Generalised Batch Least Square (BLS) Model .....	3.25
3.2.6	Recursive Models.....	3.30
3.3	Conclusion .....	3.35
4	Baja Vehicle Modelling .....	4.1
4.1	The Baja Vehicle.....	4.1
4.2	Experimental Work.....	4.2
4.2.1	Determination of Centre of Mass.....	4.3
4.2.2	Determination of Moments of Inertia .....	4.5
4.2.3	Hydro-Pneumatic Spring-Damper Unit Characterization .....	4.9
4.2.4	The Tyre Model .....	4.15
4.3	The Vehicle Simulation Model .....	4.16
4.4	Baseline Vehicle Testing .....	4.20
4.4.1	Instrumentation .....	4.20
4.4.2	Bump Test Experimental Setup .....	4.22
4.4.3	Slalom Test Experimental Setup.....	4.23
4.5	Model Validation .....	4.24

4.5.1	Bump Test Results .....	4.25
4.5.2	Slalom Test Results.....	4.29
4.6	Conclusion .....	4.34
5	Simulation Results: Control Implementation on Vehicle Model .....	5.1
5.1	Simulated Suspension Control.....	5.1
5.2	Ride Comfort Results.....	5.3
5.2.1	Ride Comfort Baseline Results .....	5.3
5.2.2	Ride Comfort Simulation Results .....	5.4
5.2.3	The Optimal Ride Comfort Suspension .....	5.9
5.2.4	Ride Comfort Results Summary .....	5.13
5.3	Handling Results.....	5.13
5.3.1	Handling Baseline Results .....	5.13
5.3.2	Handling Simulation Results .....	5.15
5.3.3	The Optimal Handling Suspension .....	5.25
5.3.4	Handling Results Summary .....	5.30
5.4	Addressing the Combined Ride Comfort and Handling Problem.....	5.32
5.5	Conclusion .....	5.33
6	Conclusions and Future Work.....	6.1
6.1	Conclusions.....	6.1
6.2	Recommendations.....	6.4
6.2.1	MR Damper Models.....	6.4
6.2.2	Vehicle Modelling.....	6.4
6.2.3	Suspension Control Simulations .....	6.5
6.3	Future Work.....	6.5
	References.....	R.1
	Appendix A: Experimental Moment of Inertia Results .....	A.1
	Appendix B: Baja Pacejka '89 Tyre Model Properties.....	B.1



---



---

## *LIST OF SYMBOLS*

---



---

### ENGLISH SYMBOLS:

Symbol	Description	Unit
<i>A</i>	Amplitude	m
	Area	m <sup>2</sup>
	Bouc-Wen model parameter	-
<i>a</i>	LuGre friction model parameter	various
	Polynomial model parameter	various
	Skyhook-groundhook bias factor	-
<i>b</i>	Distance to centre of gravity	m
	Polynomial- and modified Bingham model parameter	various
<i>c</i>	Damping coefficient	Ns/m
	Polynomial model parameter	various
<i>d</i>	Distance	m
<i>F</i>	Force	N
$\hat{F}$	Predicted or estimated MR damper force	N
<i>f</i>	Frequency	Hz
<i>G</i>	Hybrid damper force gain	Ns/m
<i>g</i>	Gravitational acceleration ( $1g = 9.81m/s^2$ )	m/s <sup>2</sup>
<i>H</i>	Height, distance, dimension	m
<i>H</i>	Magnetic flux	Vs
<i>h</i>	Height of centre of gravity	m
<i>I</i>	Current	A
	Identity matrix	-
	Inertia	kgm <sup>2</sup>
<i>K</i>	RLS variable	-
<i>k</i>	Spring stiffness	N/m
<i>L</i>	Length	m
<i>M, m</i>	Mass	kg
<i>m</i>	Number of independent variables	-
<i>n</i>	Bouc-Wen model parameter	-
	Model order	-
	Number of points	-
<i>P</i>	Pressure	Pa
	RLS variable	-
<i>t</i>	Time	s
<i>T</i>	Temperature	°C
	Torque or moment	Nm

Symbol	Description	Unit
$v$	Voltage	V
$x$	Displacement	m
	Longitudinal direction	-
	Spring deflection	m
	System inputs	various
$X''$	Longitudinal acceleration	$m/s^2$
$\dot{x}$ or $x'$	Velocity	m/s
$y$	Lateral direction	-
	System output	various
$Y''$	Lateral acceleration	$m/s^2$
$Z$	Vertical displacement	m
$z$	Evolutionary or hysteretic variable (MR damper models)	m
	Vertical direction	-
$Z'$	Vertical velocity	m/s
$\dot{z}$	Evolutionary variable derivative (MR damper models)	m/s
$Z''$	Vertical acceleration	$m/s^2$

**GREEK SYMBOLS:**

<b>Symbol</b>	<b>Description</b>	<b>Unit</b>
$\alpha$	Bouc-Wen model parameter	N/m
	Kwok model parameter	N/m
	Pitch angle	rad
	Tyre slip angle	°
$\alpha'$	Pitch rate	°/s
$\beta$	Bouc-Wen model parameter	/m <sup>2</sup>
	Kwok model parameter	s/m
	Roll angle	rad
$\beta'$	Roll Rate	°/s
$\gamma$	Bouc-Wen model parameter	/m <sup>2</sup>
	Forgetting factor	-
	Yaw angle	rad
$\gamma'$	Yaw rate	°/s
$\delta$	Hyperbolic tangent model parameter	various
	Kwok model parameter	-
	Logarithmic decrement	-
$\Delta$	Change	-
$\zeta$	Damping ratio	-
$\theta$	BLS model coefficients	various
	Tilted angle	° or rad
$\theta'$	Angular rate	°/s or rad/s
$\ddot{\theta}$	Angular acceleration	°/s <sup>2</sup> or rad/s <sup>2</sup>
$\hat{\theta}$	Model coefficients vector	-
$\kappa$	Percentage tyre longitudinal slip	-
$\lambda$	Forgetting factor	-
$\rho$	Projection algorithm constant	-
$\sigma$	Damper force skyhook-groundhook contribution	-
	LuGre friction model parameter	various
$\tau$	Oscillation period	s
$\varphi$	Regressor vector (BLS model)	-
$\Phi$	Regressor matrix (BLS model)	-
$\omega$	Frequency	rad/s
	Rotational speed	rad/s

**SUBSCRIPTS:**

<b>Subscript</b>	<b>Symbol</b>	<b>Description</b>
$0$	$F$	Force offset
$0, 1, 2, 3, \dots$	$A, a, \sigma, \delta$	Number of
$axis$	$d$	Distance to axis
	$I$	About axis through centre of gravity (pitch, roll or yaw)
$Baja$	$M$	Mass of Mini-Baja vehicle
$c$	$F$	Friction force
$cm$	$X, Y, Z$	At centre of mass
$components$	$I$	Inertia of object
$controllable$	$c$	Variable damping coefficient
$d$	$F$	Desired damping force; Passive damper force
	$\omega, \tau$	Damped
$f$	$F$	Front of vehicle
$fac$	$c$	Damping factor
$force$	$L$	Distance to force
$g$	$Z$	Ground or road profile
$gnd$	$c, \sigma$	With regard to groundhook control
$i$	$a, b, c, y, \varphi$	Number of
$j$	$x$	Number of
$meas$	$F$	Measured force
$MR$	$F, x, \dot{x}, x'$	With regard to MR damper
$n$	$\omega$	Natural frequency
$O$	$I, T$	About axis
$pitch$	$I$	With regard to pitch axis
$R$	$T$	About rotation point
$r$	$F$	Rear of vehicle
$roll$	$I$	With regard to roll axis
$s$	$F$	Spring force
	$k, c$	Suspension
	$X'', Y'', Z, Z', Z'', M$	Sprung mass
$SA, sa$	$F$	Semi-active
$sd$	$F, x, x'$	With regard to hydro-pneumatic spring-damper unit
$sky$	$c, \sigma$	With regard to skyhook control
$steer$	$x$	Steering rack displacement
$su$	$Z, Z'$	Relative to sprung and unsprung masses
$t$	$F, K, P, x, x', \varphi$	Time step number
	$c, F, k, T$	Tyre
$u$	$Z, Z', Z'', m$	Unsprung mass
$x$	$F$	Longitudinal force
$y$	$F$	Lateral force
$yaw$	$I$	With regard to yaw axis
$z$	$F, T$	Vertical, about vertical axis



---

---

## *LIST OF ABBREVIATIONS*

---

---

4S <sub>4</sub>	4 State Semi-active Suspension System
AAP	Average Absorbed Power
ADAMS	Automatic Dynamic Analysis of Mechanical Systems
BLS	Batch Least Squares
BS	British Standard
CAD	Computer Aided Design
CF	Crest Factor
CVT	Continuously Variable Transmission
DADS	Dynamic Analysis and Design System
DOF	Degrees of Freedom
eDAQ	Electronic Data Acquisition
ER	Electrorheological
HiL	Hardware-in-the-Loop
IMU	Inertial Measurement Unit
ISO	International Organisation for Standardisation
LMS	Least Mean Square
LQG	Linear Quadratic Gaussian
LVDT	Linear Variable Differential Transformer
MR	Magnetorheological
MSDV	Motion Sickness Dose Value
MTVV	Mean Transient Vibration Value
NRMS	Normalised Root Mean Square
RLS	Recursive Least Square
RMS	Root Mean Square
SUV	Sport Utility Vehicle
TLD	Tuned Liquid Damper
TSD	Tuned Sloshing Damper
VDI	“Verein Deutscher Ingenieure” (Society of German Engineers)
VDV	Vibration Dose Value



---



---

## ***LIST OF FIGURES***

---



---

Figure 2-1: Ride comfort and handling trade-off schematic (Simon 2001).....	2.5
Figure 2-2: Quarter car vehicle model. ....	2.10
Figure 2-3: Ideal skyhook configuration (left), and semi-active skyhook configuration (right). ....	2.14
Figure 2-4: Ideal groundhook configuration (left), and semi-active groundhook configuration (right).....	2.15
Figure 2-5: Ideal hybrid configuration (left), and semi-active hybrid configuration (right).....	2.17
Figure 2-6: Pressure-driven flow mode: pre-yield flow (left), and post-yield flow (right).....	2.21
Figure 2-7: Principle of a MR damper. ....	2.21
Figure 2-8: Bingham model (left), and extended Bingham model (right). ....	2.24
Figure 2-9: Bouc-Wen model (left), and Phenomenological model (right).....	2.25
Figure 3-1: MR damper characterization experimental setup.....	3.2
Figure 3-2: An example of measured MR damper data.....	3.4
Figure 3-3: Measured force-displacement response to 30mm amplitude and 2Hz sinusoidal excitation. ....	3.5
Figure 3-4: Measured force-velocity response to 30mm amplitude and 2Hz sinusoidal excitation. ....	3.5
Figure 3-5: Measured force-displacement and force-velocity response to a 30mm sinusoidal excitation at 1.0A. ....	3.6
Figure 3-6: MR damper damping curves. ....	3.7
Figure 3-7: Random displacement excitation signals used for MR damper model development.....	3.8
Figure 3-8: Bingham model force-displacement (left) and force-velocity (right) relationship in response to 30mm amplitude at 2Hz sinusoidal excitation. ....	3.9
Figure 3-9: Modified and delayed Bingham model force-displacement (left) and force-velocity (right) relationship in response to 30mm amplitude at 2Hz sinusoidal excitation. ....	3.10
Figure 3-10: Modified and delayed Bingham model predicted force-displacement (left) and force-velocity (right) relationship in response to a random displacement input signal at 1.50A.....	3.11
Figure 3-11: Comparison of measured MR damper forces and forces predicted by modified and delayed Bingham model developed using Random #1 input at 1.50A.....	3.12
Figure 3-12: Bouc-Wen model force-displacement (left) and force-velocity (right) relationship in response to 30mm amplitude at 2Hz sinusoidal excitation. ....	3.14
Figure 3-13: Bouc-Wen model predicted force-displacement (left) and force-velocity (right) relationship in response to a random displacement input signal at 1.50A.....	3.15

Figure 3-14: Comparison of measured MR damper forces and forces predicted by Bouc-Wen model developed using Random #1 input at 1.50A..... 3.16

Figure 3-15: Kwok model force-displacement (left) and force-velocity (right) relationship in response to 30mm amplitude at 2Hz sinusoidal excitation. .... 3.17

Figure 3-16: Kwok model predicted force-displacement (left) and force-velocity (right) relationship in response to a random displacement input signal at 1.50A..... 3.19

Figure 3-17: Comparison of measured MR damper forces and forces predicted by Kwok model developed using Random #1 input at 1.50A. .... 3.20

Figure 3-18: Polynomial model force-displacement (left) and force-velocity (right) relationship in response to 30mm amplitude at 2Hz sinusoidal excitation. .... 3.21

Figure 3-19: Displacement determined polynomial model force-displacement (left) and force-velocity (right) relationship in response to 30mm amplitude at 2Hz sinusoidal excitation. .... 3.23

Figure 3-20: Acceleration determined polynomial model predicted force-displacement (left) and force-velocity (right) relationship in response to a random displacement input signal. .... 3.24

Figure 3-21: Comparison of measured MR damper forces and forces predicted by polynomial model developed using Random #1 input at several current levels ( $n = 7$ ). .... 3.25

Figure 3-22: BLS model force-displacement (left) and force-velocity (right) relationship in response to 30mm amplitude at 2Hz sinusoidal excitation. .... 3.26

Figure 3-23: BLS model predicted force-displacement (left) and force-velocity (right) relationship in response to a random displacement input signal. .... 3.28

Figure 3-24: Comparison of measured MR damper forces and forces predicted by BLS model developed using Random #1 input at several current levels. .... 3.29

Figure 3-25: LMS model with measured force feedback force-displacement (left) and force-velocity (right) relationship in response to 30mm amplitude at 2Hz sinusoidal excitation. .... 3.31

Figure 3-26: LMS model with measured force feedback predicted force-displacement (left) and force-velocity (right) relationship in response to a random displacement input signal. .... 3.32

Figure 3-27: Comparison of measured MR damper forces and forces predicted by LMS model with measured force feedback developed using Random #1 input at several current levels. .... 3.33

Figure 3-28: Parameter history of LMS algorithm with measured force feedback. .... 3.34

Figure 3-29: LMS model with calculated force feedback force-displacement (left) and force-velocity (right) relationship in response to 30mm amplitude at 2Hz sinusoidal excitation. ....	3.35
Figure 4-1: Baja vehicle on an incline during the 2009 competition. ....	4.1
Figure 4-2: Experimental determination of the centre of gravity. ....	4.3
Figure 4-3: Obtaining the position of the centre of gravity. ....	4.4
Figure 4-4: Height of Baja sprung mass centre of mass as a function of lifted angle. ....	4.4
Figure 4-5: Baja vehicle axis system. ....	4.5
Figure 4-6: Schematic presentation of rigid body pivot motion (pitch). ....	4.6
Figure 4-7: Experimental determination of pitch moment of inertia. ....	4.7
Figure 4-8: Spring deflection decay. ....	4.8
Figure 4-9: Measured angular rates during pitch excitation of vehicle sprung mass. ....	4.8
Figure 4-10: Measured angular rates during roll excitation of vehicle sprung mass. ....	4.9
Figure 4-11: Measured angular rates during yaw excitation of vehicle sprung mass. ....	4.9
Figure 4-12: Hydro-pneumatic spring-damper unit section (Wehrmeyer 2011). ....	4.10
Figure 4-13: Hydro-pneumatic spring-damper unit characterization experimental setup (Wehrmeyer 2011). ....	4.11
Figure 4-14: Average front spring characteristic. ....	4.12
Figure 4-15: Average rear spring characteristic. ....	4.12
Figure 4-16: Front and rear pneumatic spring characteristics. ....	4.13
Figure 4-17: Force-displacement relationship of rear spring-damper unit. ....	4.14
Figure 4-18: Force-velocity relationship of rear spring-damper unit. ....	4.14
Figure 4-19: Front and rear hydraulic damper characteristics. ....	4.15
Figure 4-20: Tyre characterization experimental setup. ....	4.16
Figure 4-21: Pacejka '89 tyre model side force characteristic. ....	4.17
Figure 4-22: Pacejka '89 tyre model brake force characteristic. ....	4.17
Figure 4-23: Pacejka '89 tyre model self-aligning torque characteristic. ....	4.17
Figure 4-24: Baja simulation model schematic. ....	4.18
Figure 4-25: Graphic illustration of Baja simulation model. ....	4.19
Figure 4-26: Instrumented Baja vehicle for baseline testing. ....	4.22
Figure 4-27: Schematic representation of instrumentation installed on Baja vehicle. ....	4.22
Figure 4-28: Bumps implemented in bump test. ....	4.23
Figure 4-29: Schematic of bump test setup. ....	4.23
Figure 4-30: Schematic of slalom test setup. ....	4.24
Figure 4-31: Bump test measured and simulation speed input. ....	4.25
Figure 4-32: Bump test vehicle body angular rates results. ....	4.26

Figure 4-33: Bump test suspension deflection results.....	4.27
Figure 4-34: Bump test vehicle body acceleration results. ....	4.27
Figure 4-35: Bump test unsprung mass vertical acceleration results. ....	4.28
Figure 4-36: Slalom test measured and simulation steer input. ....	4.29
Figure 4-37: Slalom test measured and simulation speed input.....	4.29
Figure 4-38: Slalom test vehicle body angular rates results. ....	4.30
Figure 4-39: Slalom test suspension deflection results. ....	4.31
Figure 4-40: Slalom test vehicle body acceleration results.....	4.32
Figure 4-41: Slalom test unsprung mass vertical acceleration results. ....	4.33
Figure 5-1: Front and rear passive damper characteristics for various passive damping factors.....	5.2
Figure 5-2: ADAMS/Simulink co-simulation environment. ....	5.3
Figure 5-3: Belgian paving measured results: Vertical acceleration of the sprung mass.....	5.4
Figure 5-4: Belgian paving measured results: Vertical acceleration of the four wheels.....	5.5
Figure 5-5: Speed input for ride comfort (Belgian paving) tests. ....	5.5
Figure 5-6: Belgian paving simulation results: Weighted RMS acceleration of sprung mass for various skyhook gain and passive damping contributions. ....	5.6
Figure 5-7: Belgian paving simulation results: RMS acceleration of rear right wheel for various skyhook gain and passive damping contributions. ....	5.7
Figure 5-8: Belgian paving simulation results: Weighted RMS acceleration of sprung mass for various groundhook gain and passive damping contributions.....	5.8
Figure 5-9: Belgian paving simulation results: RMS acceleration of rear right wheel for various groundhook gain and passive damping contributions. ....	5.9
Figure 5-10: Optimal ride comfort: Time traces for skyhook control implementation (rear right corner). ....	5.10
Figure 5-11: Prescribed input current to MR dampers.....	5.11
Figure 5-12: Comparison of the prescribed semi-active forces and the forces delivered by the MR dampers. ....	5.11
Figure 5-13: Force-velocity relationship of polynomial model compared to prescribed semi-active forces.....	5.12
Figure 5-14: Slalom test measured results: Suspension deflection. ....	5.14
Figure 5-15: Slalom test measured results: Lateral- and longitudinal acceleration, and yaw rate. ....	5.14
Figure 5-16: Steer input for handling (single lane change) tests. ....	5.15
Figure 5-17: Inaccurate prescribed forces due to relative damper velocity error. ....	5.16
Figure 5-18: Sprung mass pitch, roll and yaw angles during single lane change test for various passive damping factors and skyhook gains.....	5.17

Figure 5-19: Sprung mass pitch, roll and yaw rates during single lane change test for various passive damping factors and skyhook gains.....	5.18
Figure 5-20: Vertical tyre forces during single lane change test for various passive damping factors and skyhook gains. ....	5.19
Figure 5-21: Path followed during single lane change test for various passive damping factors and skyhook gains. ....	5.19
Figure 5-22: Lateral- and longitudinal acceleration response during single lane change test for various passive damping factors and skyhook gains. ....	5.20
Figure 5-23: Sprung mass angles during single lane change test for various passive damping factors and groundhook gains.....	5.21
Figure 5-24: Sprung mass pitch, roll and yaw rates during single lane change test for various passive damping factors and groundhook gains. ....	5.22
Figure 5-25: Vertical tyre forces during single lane change test for various passive damping factors and groundhook gains.....	5.23
Figure 5-26: Path followed during single lane change test for various passive damping factors and groundhook gains. ....	5.23
Figure 5-27: Lateral- and longitudinal acceleration response during single lane change test for various passive damping factors and groundhook gains. ....	5.24
Figure 5-28: Optimal handling: Time traces for skyhook control implementation (front left corner). ....	5.26
Figure 5-29: Optimal handling: Time traces for suspension forces (front left corner). ....	5.27
Figure 5-30: Prescribed input current to MR dampers.....	5.27
Figure 5-31: Force-velocity relationship of polynomial model compared to prescribed semi-active forces.....	5.28
Figure 5-32: Force-velocity relationship of polynomial model compared to prescribed semi-active forces.....	5.29
Figure 5-33: Sprung mass angles during single lane change test with implementation of MR damper model.....	5.30
Figure 5-34: Vertical tyre forces during single lane change test with implementation of MR damper model.....	5.31
Figure 5-35: Belgian paving simulation results: Weighted RMS acceleration of sprung mass for various skyhook gain and passive damping contributions. ....	5.33





---



---

## ***LIST OF TABLES***

---



---

Table 2–1: Classification of suspension systems.....	2.8
Table 3–1: Displacement excitation imposed on MR damper for damper characterization. ....	3.3
Table 3–2: Computed Bingham model parameters for a sinusoidal input. ....	3.9
Table 3–3: Computed modified and delayed Bingham model parameters for a sinusoidal input. ....	3.10
Table 3–4: Computed modified and delayed Bingham model parameters for a random input signal. ....	3.11
Table 3–5: Modified and delayed Bingham model predicted force RMS and NRMS errors for random input signals. ....	3.12
Table 3–6: Computed Bouc-Wen model parameters for a sinusoidal input. ....	3.13
Table 3–7: Computed Bouc-Wen model parameters for a random input signal.....	3.14
Table 3–8: Bouc-Wen model predicted force RMS and NRMS errors for random input signals. ....	3.16
Table 3–9: Computed Kwok model parameters for a sinusoidal input.....	3.18
Table 3–10: Computed Kwok model parameters for a random input signal. ....	3.18
Table 3–11: Kwok model predicted force RMS and NRMS errors for random input signals.....	3.19
Table 3–12: Computed polynomial model parameters. ....	3.21
Table 3–13: Computed displacement determined polynomial model parameters. ....	3.22
Table 3–14: Computed acceleration determined polynomial model parameters. ....	3.23
Table 3–15: Computed BLS model parameters for a sinusoidal input. ....	3.26
Table 3–16: Computed BLS model parameters for a random input signal.....	3.27
Table 3–17: Comparison of BLS and LMS models.....	3.31
Table 3–18: Summary of developed MR damper current independent models.....	3.36
Table 3–19: Summary of developed MR damper current dependent models.....	3.37
Table 3–20: Summary of developed MR damper recursive models. ....	3.37
Table 4–1: Centre of mass properties of Baja sprung mass. ....	4.5
Table 4–2: Equipment installed on Baja vehicle for baseline testing. ....	4.21
Table 5–1: Ride comfort and handling simulation results summary. ....	5.36
Table A–1: Roll moment of inertia results.....	A.1
Table A–2: Pitch moment of inertia results. ....	A.1
Table A–3: Yaw moment of inertia results.....	A.1



---

# *1 INTRODUCTION*

---

Improvement of ride comfort characteristics and enhancement of handling capabilities are widely recognised as two important aspects of design in vehicle dynamics. Both of these features are vital for overall drivability of a vehicle, and have been thoroughly discussed in the existing literature in vehicle dynamics, suspension design and rigid body dynamics. Improvements in ride comfort have been directly correlated with reduction of occupant fatigue allowing the driver to focus on the road conditions and the flow of traffic for longer periods of time. Enhanced handling capabilities are important to enable a driver to easily keep the vehicle on the required path or to manoeuvre a vehicle better in situations where sudden swerving or lane changing becomes necessary. Increasing demands for vehicle safety, better ride quality and improved handling have resulted in an extensive amount of research in the design and analysis vehicle suspension systems over the last few decades. This research has been further supplemented by rapid advances in controller design, the discovery of smart materials and the increasing use of microcontrollers.

It has been clearly demonstrated through numerous studies and experimental data that, in general, low damping and soft spring characteristics of a suspension system improve ride quality by isolating the vehicle body from road disturbance inputs. On the contrary, high damping and a stiff spring setting of the suspension system improve handling by reducing body roll and increasing road-tyre contact. This leads to an inevitable compromise in passive suspension systems to strike a balance between ride comfort and handling. The design decision is also influenced by the primary use of the vehicle with key distinctions drawn between on-road and off-road application in order to determine suspension settings for a specific level of ride comfort and handling capability.

Recent studies in suspension design have attempted to address the trade-off between ride comfort and handling through the design of controlled suspension systems, such as semi-active suspensions. The suspension settings of these systems can be altered through a control law in order to mitigate the design trade-off and enable the suspension system to better accomplish both design objectives with a reduced compromise between ride comfort and handling.

A semi-active suspension system consists of variable dampers and, in rare cases, variable springs with an ability to change the settings with time. In many cases a semi-active suspension consisting of variable dampers with fixed springs is implemented, which requires a lower energy input to change the damping characteristics of the suspension system. An example of a controllable damper is the so called “magnetorheological (MR) damper”. The damping characteristics of an MR damper can be

changed reversibly and continuously in milliseconds between upper and lower physical limits. The various positive aspects of MR dampers have led to extensive research in the use of MR technology in vehicle suspensions. Numerous studies have shown that semi-active suspension control using variable damping has the ability to considerably improve the ride comfort and handling behaviour of a vehicle.

In semi-active control of variable dampers, the ideal damping forces are prescribed by an appropriate control law using specific measurements (usually related to the dynamic response of the vehicle). The damper state is then altered and regulated by a damper controller so as to produce the desired damping forces. One commonly used control law for semi-active control of suspension systems is hybrid control, comprised of skyhook- and groundhook control. This strategy aims to improve ride comfort by “hooking” the vehicle body to a stationary reference in the sky (thereby reducing vehicle body movement), and enhancing handling by “hooking” the wheels to a stationary reference at the road surface (thereby increasing road-tyre contact). The damper is controlled so as to yield damping forces that will realise, or at least approximate, the “hooking” action.

Many of the semi-active suspension control studies in the existing literature have been performed by using linear two degree of freedom models, under simple excitation conditions, with the primary focus on ride comfort. Some of the studies have made unsubstantiated claims regarding improvements in handling capabilities. These studies have focussed on in-plane dynamics, while handling behaviour is known to be largely related to the lateral, roll and yaw degrees of freedom. Also, the focus of the research on MR damper modelling has been limited to accurate model development, with very limited attention paid to realistic excitation conditions that the damper might be subjected to. This is especially important for the suspension system in an off-road application. Furthermore, a robust model of the MR damper becomes even more important when the model is incorporated into real-time control so as to be capable of providing a controllable suspension system that can withstand excitation inputs that are typically seen by an off-road application.

The purpose of this study is to implement semi-active suspension control on a test vehicle, which is mostly limited to off-road usage, by using MR dampers. The suspension characteristics are studied and tested so as to yield a balance between ride comfort and handling characteristics. This study further aims to gain insight into the feasibility of using skyhook- and groundhook control for ride quality and handling improvement by using a higher order nonlinear model of the test vehicle.

The test vehicle used in this study is a small single seat off-road vehicle known as a Baja that competes in an annual international competition hosted by the SAE International (**Baja SAE, 2013**). The specific vehicle has been designed and manufactured by a team of students from the University of Pretoria. The main motivation for using a small vehicle as a test platform is the relatively small size, requiring fairly small MR dampers that are affordable and easily available commercially. Also, the

design of the vehicle permits ease of usage and easy access to the frame and suspension components for modifications and repairs in order to accommodate the MR dampers. Since the Baja is small, the typical equipment in a small engineering laboratory is sufficient to determine the vehicle centre of mass and moments of inertia required for vehicle modelling. The choice of the test vehicle also presents unique challenges and constraints that may not represent the usage of a conventional automobile. The absence of a differential in the driveline of the vehicle is one such constraint. However, the test vehicle represents many features commonly seen in off-road vehicles.

A thorough literature survey of all relevant topics related to this study is presented in Chapter 2. These topics include ride comfort and handling, classification of vehicle suspension systems, vehicle modelling, suspension control, controllable dampers and magnetorheological (MR) dampers. The research question is also formulated in this chapter. In Chapter 3, multiple models are developed to represent the dynamic characteristics of the MR damper. These models are used for analysis and suspension control simulation. The experimental setup used for data collection and validation of the models is also discussed. The development of the vehicle model used for simulating suspension control is presented in Chapter 4. Experimental work and characterization involved in the development of the simulation model are discussed and the model is validated for ride comfort and handling simulations. The semi-active suspension control simulation process is discussed in Chapter 5. The MR damper model chosen from Chapter 3 is implemented in the simulations, and ride comfort and handling results are evaluated and discussed. The ideal suspension characteristics in favour of optimal ride comfort and handling behaviour are presented. Overall conclusions are drawn in Chapter 6, along with recommendations based on the findings from this study and a discussion on future work.



---

## 2 LITERATURE SURVEY

---

This chapter provides the necessary background of this study, and discusses the broader context of the problem addressed by this research. Possible shortcomings in existing research are also identified in this chapter and the literature survey is used to define the problem statement.

The two main functions of the suspension system on a vehicle, namely to provide ride comfort and driving stability (handling), are discussed in Section 2.1, p2.1. Possible measures to quantify ride and handling are identified. Suspension classification is given in Section 2.2, p2.6, with the focus on semi-active suspensions as a solution to the ride comfort and handling compromise. Vehicle models implemented in the literature for suspension studies are discussed in Section 2.3, p2.10. Section 2.4, p2.13, deals with several suspension control strategies identified in the literature. Different controllable damping devices are discussed in Section 2.5, p2.19, and MR damper technology, including the modelling of MR dampers, is discussed in Section 2.6, p2.20.

### 2.1 Ride Comfort and Handling

The suspension system of a vehicle serves two primary purposes: to isolate the vehicle body from the forces transmitted by external excitation, and to improve road-holding and handling (**Guglielmino et al. 2008**). **Savaresi et al. (2010)** explains that the suspension can be seen as a low-pass filter which attenuates the effects of a disturbance, such as an irregular road profile excitation, on an output variable. When ride comfort is the main objective the output variable is typically the body acceleration. When road-holding is the design goal tyre deflection is the output variable. It is commonly accepted that a passive suspension system is a compromise between favourable ride comfort and handling. Vehicles with a soft suspension and low damping provide good ride comfort at the expense of handling, while a firm suspension and high damping offers excellent handling with a rough ride (**Els et al. 2007, Nell and Steyn 2003**). The passive suspension compromise and other factors such as demands on operating efficiency, have initiated the implementation of controlled suspension systems in passenger vehicles. Possible solutions to the ride comfort and handling compromise consist of advanced suspension technologies that allow independent tuning of the sprung mass natural frequency, ride height and damping (**Cao et al. 2011, Guglielmino et al. 2008**).

Ride comfort and handling is discussed in Section 2.1.1, p2.2, and Section 2.1.2, p2.3 respectively. The ride comfort and handling compromise is discussed in Section 2.1.3, p2.5.

### 2.1.1 Ride Comfort

There are various definitions of ride comfort found in the literature. According to **Gillespie (1992)** the ride of a vehicle is connected to the quality of a car judged in terms of the vibration environment. More specifically, the ride can be seen as the low frequency (up to 5Hz) vibration of the sprung mass of the vehicle. **Els (2006)** states that the ride comfort of a vehicle is in general associated with the vertical dynamics of the vehicle body in response to road input excitation. **Blundell and Harty (2004)** adds that ride studies are mainly focused on the acceleration environment.

A passenger's perception of a vehicle is influenced by the magnitude and direction of vibrations imposed on the vehicle body. Since passenger vehicles travel at high speed, they experience a broad spectrum of vibrations. The lower end of the spectrum, 0-25Hz, is classified as ride which refers to tactile and visual vibrations. The higher end of the spectrum, 25Hz-20kHz, are aural vibrations categorised as noise. (**Gillespie 1992, Blundell and Harty 2004**).

**Els (2005)** compared the objective methods of ride comfort quantization to subjective comments of passengers transported over off-road terrain in a military vehicle. The objective methods included the ISO 2631 standard (**International Organisation for Standardisation, 1997**), BS 6841 (**British Standards Institution, 1987**), Average Absorbed Power or AAP (**Pradko and Lee 1966**), and VDI 2057 (**Hohl, 1984**). Seven tests were performed over different terrains, at two different tyre pressures, and at two speeds. The subjective ride comfort ratings were determined by seven groups of eight to nine passengers each. Passengers of various postures, age groups and qualifications were used, and the tests were performed in a different order for each group. The passengers had to complete a questionnaire to indicate the level of comfort/discomfort experienced. The objective ride comfort ratings were determined from measured acceleration data according to the methods of ISO 2631, BS 6841, AAP and VDI 2057. Seatpad accelerometers were used to measure the lateral, longitudinal and vertical acceleration on different seats, while seven accelerometers were used to measure the roll, pitch, and yaw acceleration of the vehicle body. Good correlations between the subjective and objective ratings were achieved. When the objective values increased, the subjective values also increased. It was concluded that for unweighted, ISO 2631, and BS 6841, the vertical acceleration gave the best correlation between subjective and objective ride comfort values. The same conclusion was made for AAP and VDI 2057 where only vertical values were used. Correlation for roll, pitch and yaw acceleration was poor. The motion sickness dose value (MSDV), crest factor (CF), and mean transient vibration value (MTVV) had little or no correlation to subjective ride comfort. The overall conclusion from the investigation was that any of the four objective methods can be used to determine the ride comfort of off-road vehicles over rough terrain. The vertical values should be used for all four



methods and the root mean square (RMS) value is sufficient for ISO 2631, BS 6841 and unweighted values.

**Dong et al. (2010)**, **Els et al. (2007)**, and **Ahmadian and Pare (2000)** used RMS vertical acceleration of the vehicle body to quantify ride comfort. **Nell and Steyn (2003)**, considered the vibration dose values (VDVs) of BS 6841, and **Fischer and Isermann (2004)** considered normalised vertical acceleration.

### 2.1.2 Handling

According to **Gillespie (1992)** the term “handling” refers to the objective properties of the vehicle of interest when changing direction (such as directional response), including qualities that affect the driver’s ability to maintain control. Handling, therefore, does not only refer to the capabilities of the vehicle, but to the performance of the driver-vehicle combination.

Another property associated with handling is the road-holding capability of the vehicle. Adequate road-holding maximises wheel tracking to road roughness, and guarantees road contact regardless of road profile and load transfer conditions. The road-holding capability is important since the wheel load determines the lateral and longitudinal forces that can be generated at the wheels (**Savaresi et al. 2010**). **Fischer and Isermann (2004)** refer to driving safety instead of handling as the optimal dynamic behaviour of a vehicle, which is obtained by avoidance of wheel oscillations since a non-bouncing wheel is required for transferring of road-contact forces. Thus the tyre load variation is used as an indicator to quantify safety. To improve ride stability the tyre must be kept in contact with the road surface, which is achieved by decreasing the resonance peak at the natural frequency of the wheels (typically near 10Hz).

**Sharp and Pan (1991)** mention that improved steering behaviour is observed in vehicles with less body roll, and to improve the handling performance of vehicles they are often made stiffer in roll by adding or stiffening anti-roll bars. Active electro-hydraulic actuators located in the anti-roll bars were used to eliminate body roll response to steering inputs.

Roll over is related to handling, but a vehicle’s handling capability and resistance to roll over is not necessarily the same. Handling concerns the response of a vehicle experienced by the driver, while roll over refers to the tendency of the roll motion of a vehicle to increase due to a manoeuvre induced disturbance (**Uys et al. 2006a**). The static roll over threshold is often used for a first order estimate of a vehicle’s resistance to roll over, defined as half of a vehicle’s track width divided by its centre of gravity height (**Gillespie 1992**).

**Uys et al. (2006a)** note that a single unambiguous objective handling criterion has eluded the vehicle science community despite several studies regarding the topic, and performed a study in order

to establish relationships that can be used to quantify vehicle handling performance. Many research works were consulted to summarise suggestions and conclusions on handling criteria. An experimental investigation was executed in which three vehicles equipped with measurement apparatus were driven by four drivers over two different handling tracks. It was concluded that roll angle, lateral acceleration and yaw rate are interrelated. It was suggested that the vehicle body roll angle could be a suitable metric to measure handling, but acceptable levels need to be determined.

In addition to the roll angle response, **Choi et al. (2001)** also considered the pitch angle at various acceleration magnitudes to compare the performance of an electrorheological (ER) suspension to a conventional passive suspension during the performance of a squat test (sudden acceleration at idle stage). It is stated that the improvement in pitch motion directly relates to improvement of the steering stability of the test vehicle. **Ha et al. (2009)** used roll and pitch angle results from a bump and random road test to compare the ride comfort and handling of an uncontrolled and skyhook controlled suspension. In an experimental study to compare the performance of semi-active suspensions to a conventional passive suspension of a quarter car test rig, **Ivers and Miller (1989)** used the normalised RMS tyre contact force as an indication of road-holding.

According to **Els et al. (2007)** handling tests fall in two groups: steady state- and dynamic handling tests. The most widely used steady state handling test is the constant radius test, discussed in detail by **Gillespie (1992)**. Dynamic handling tests can either be closed loop where a human driver tries to steer the vehicle through a prescribed path, or open loop where the steering angle vs. time is prescribed. A popular example of a closed loop test is the severe double lane change test (**International Organisation for Standardisation, 1999**). Open loop tests include the Fishhook roll over test (**Garrott et al. 2001**) and step steer and pulse steer tests (**International Organisation for Standardisation, 1988**).

There is a peculiarity associated with the test vehicle used in this study since there is no differential to distribute the power between the left and right driving wheels, and therefore the vehicle handles quite differently from conventional vehicles. It has been determined that this unique characteristic results in distinct suspension requirements for desirable handling behaviour because the yaw response of the vehicle is restricted. During handling manoeuvres it is required that the inner rear wheel of the test vehicle lifts up in a turn, in order to improve the yaw response of the vehicle by generating oversteer. Quad bikes and Karts often don't have differentials and are, therefore, included in this category of vehicles. While there are numerous studies in the existing literature on the use of differentials to control the handling behaviour of vehicles, studies on vehicles without differentials aren't very common.

### 2.1.3 The Ride Comfort and Handling Compromise

Many sources agree that favourable ride comfort and handling have conflicting criteria (**Dong et al. 2010**, **Els et al. 2007**, **Fischer and Isermann 2004**, **Uys et al. 2006a**). Three case studies performed by **Els et al. (2007)** indicated that the spring and damper characteristics required for ride comfort and handling lie on opposite extremes of the design space. A soft spring and low damping is required for improved ride comfort, while a stiff spring with high damping is required for improved handling (**Els et al. 2007**, **Fischer and Isermann 2004**, **Nell and Steyn 2003**), resulting in a trade-off situation. The ride comfort and handling trade-off is expressed graphically by **Simon (2001)**, as shown in Figure 2-1, p2.5.

Due to the nature of passive suspensions, they provide a compromise between ride comfort and handling. The ride comfort of some luxury vehicles may be excellent while the handling capability is undesirable, while sports vehicles provide great handling but the ride is rough. The trade-off problem is especially prominent in off-road vehicles where high ground clearance, large suspension travel and soft springs are required for good off-road capability, but have made these vehicles prone to roll over when operating at high speeds on smooth roads (**Els et al. 2007**). In order to address the ride comfort and handling compromise, semi-active (on/off or continuous) and active suspension systems have been introduced in some vehicles. These systems are capable of offering varying stiffness and damping, and active systems can also aid wheel motion and reduce body roll.

There are numerous examples of solutions to the ride comfort and handling trade-off problem in the literature. **Els (2006)** developed a 4-State Semi-active Suspension System (4S<sub>4</sub>) that can switch between low and high stiffness, and low and high damping. Switching occurs within a few milliseconds and is regulated by a decision making control strategy. **Simon (2001)** implemented

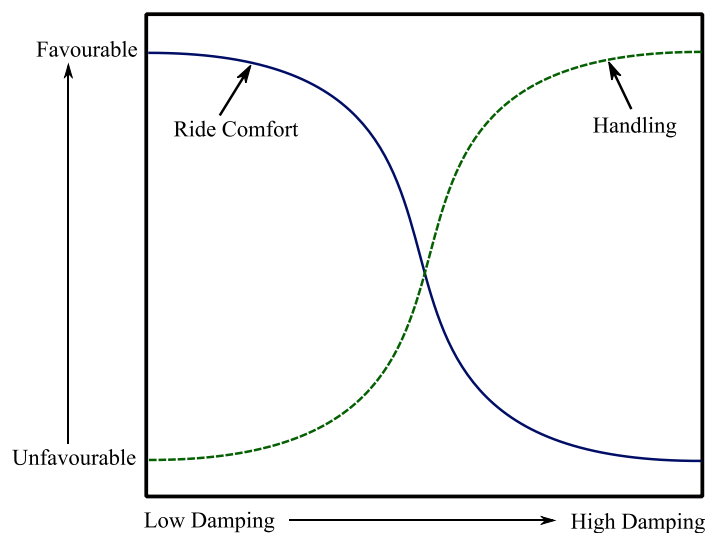


**Figure 2-1: Ride comfort and handling trade-off schematic (Simon 2001).**

magnetorheological (MR) dampers and skyhook control to adjust damping in order to reduce roll over propensity of a sport utility vehicle (SUV). **Nell and Steyn (2003)** implemented two-state semi-active dampers on a  $6 \times 6$  high mobility off-road vehicle in order to improve its handling capabilities. **Sharp and Pan (1991)** developed an active anti-roll bar used to improve handling by reducing vehicle body roll.

#### 2.1.4 Conclusion

The results of the study by **Els (2005)** (discussed in Section 2.1.1, p2.2) motivated the use of BS 6841 (**British Standards Institution, 1987**) weighted RMS vertical acceleration values for ride comfort evaluation in this study. Vertical acceleration measurements are easily obtainable using readily available accelerometers. To simplify the process of vehicle modelling and simulation, the single lane change test (an open loop test) was chosen to evaluate the handling of the test vehicle. This eliminates the need for a complex driver model (steering controller) used to track a prescribed path. In the single lane change test the steering angle is prescribed as a function of time, as compared to closed loop tests where the driver aims to steer the vehicle through a prescribed path. Lateral drift occurring during the simulation process is addressed by implementation of a road profile modelled as two tracks independent of lateral position, rather than a three-dimensional surface. Where road-holding and the body roll angle are often used as metrics to evaluate handling, these metrics are not applicable to the test vehicle. While there are numerous studies in the existing literature on the use of differentials to control the handling behaviour of vehicles, studies on vehicles without differentials is uncommon.

## 2.2 Vehicle Suspension Systems Classification

Vehicle suspension systems are either passive (uncontrolled), or controlled. Controllable suspension systems include active and semi-active suspensions. While the fixed spring and damper settings of a passive suspension are chosen in favour of ride comfort or handling, this compromise may be improved through the implementation of controlled suspension systems consisting of variable dampers or springs. Semi-active and active suspensions aim to reduce the compromise between comfort and handling since these suspensions can adapt to various driving conditions (**Els et al. 2007**, **Fischer and Isermann 2004**). Numerous positive aspects of semi-active suspension systems have led to these systems becoming increasingly popular, and today semi-active suspension systems are available on a large number of passenger vehicles, mostly high-end luxury vehicles (**Cao et al. 2011**).

A summary of the classification of suspension systems is given in Table 2–1, p2.8 using the studies in the existing literature, **Fischer and Isermann (2004)**, p1356, **Els (2006)**, p1.4, and **Savaresi et al. (2010)**, p24.

### 2.2.1 Passive Suspension Systems

The traditional suspension system that has been used in vehicles is the passive suspension system featuring springs and hydraulic dampers. The properties of the passive suspension remain fixed during its design life, resulting in a compromise between ride comfort and handling (Els 2006, Cao et al. 2011). The main distinguishing feature of passive suspension systems is that they merely impart forces in response to motion, storing and dissipating the vibratory energy of a vehicle. While passive suspensions offer design simplicity and may perform well when subjected to the conditions they were designed for, they cannot adapt to varying loading and driving conditions and are therefore limited in performance and capability (Dyke et al. 1998, Lai and Liao 2002, Ha et al. 2009). The limitations of passive suspensions are discussed in detail by Cao et al. (2011).

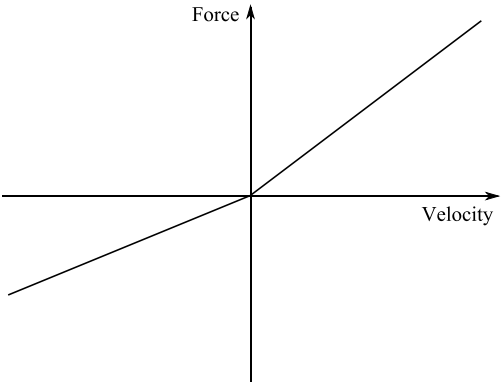
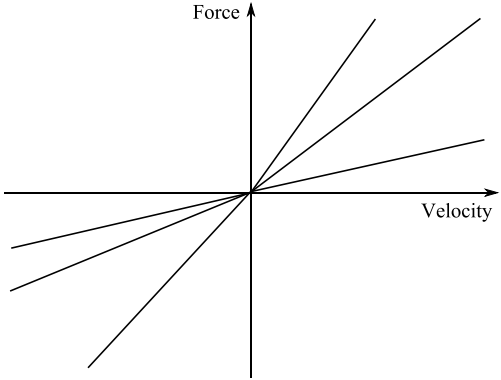
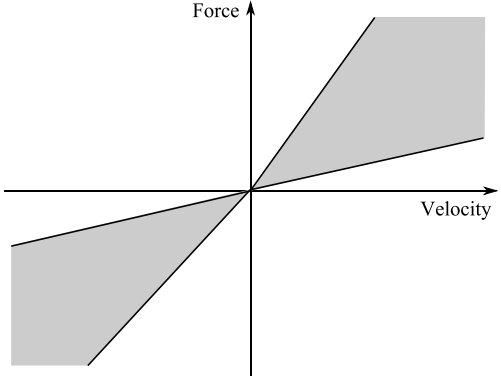
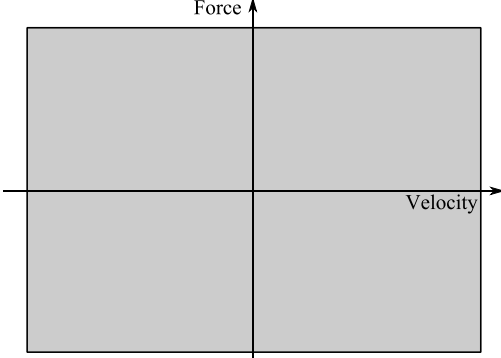
### 2.2.2 Semi-Active Suspension Systems

According to Housner et al. (1997) a semi-active device can be seen as a controllable passive device. The characteristics of such a device can be adjusted with time, but it cannot supply energy to the controlled system, it can only store or dissipate energy. In vehicle applications a semi-active suspension refers to a suspension of which the damping and/or the stiffness can be adjusted as required. The characteristics of semi-active dampers can be changed in fixed steps, or continuously, depending on the damper technology (Spencer et al. 1997, Dyke et al. 1998, Fischer and Isermann 2004).

Many factors have resulted in wide acceptance and implementation of semi-active suspension systems, including low power requirements, adaptability, system simplicity, ease of implementation and low cost. Furthermore, semi-active suspensions are inherently stable and considered to be fail-safe as they merely absorb or store vibratory energy by reacting to relative motion, and revert to a passive suspension system in the event of control failure (Ivers and Miller 1991, Spencer et al. 1997, Dyke et al. 1998, Ahmadian and Pare 2000, Jansen and Dyke 2000, Lai and Liao 2002, Dong et al. 2010, Cao et al. 2011). Another note-worthy benefit of semi-active suspensions is that several semi-active control laws (skyhook control and its variations such as groundhook- and hybrid control) are model-free control algorithms, and therefore do not require prior knowledge of the system parameters and excitations (Cao et al. 2011).

The most common semi-active dampers utilised in vehicles are either hydraulic dampers or MR dampers implemented discretely (with predefined damping states) or continuously (bound by minimum and maximum damping levels). A summary of recent production and prototype applications of controllable suspension systems is provided by Els (2006).

**Table 2-1: Classification of suspension systems.**

Class	Damper Characteristic	Energy Requirements
<p><b>Passive:</b></p> <p>Properties remain fixed at design values.</p> <p>Resists motion.</p>		None
<p><b>Semi-Active Discret:</b></p> <p>Properties can change reversibly between predefined states.</p> <p>Resists motion.</p>		Low (50W)
<p><b>Semi-Active Continuous:</b></p> <p>Properties can change reversibly between predefined upper and lower limits.</p> <p>Resists motion.</p>		Low (50W)
<p><b>Active:</b></p> <p>Properties can change reversibly between predefined upper and lower limits.</p> <p>Resists and aids motion.</p>		High (1-7kW, can be much higher depending on vehicle and application.)

### 2.2.3 Active Suspension Systems

In contrast to passive suspension systems (which only apply forces in response to motion), active suspension systems provide additional force inputs by active devices, such as hydraulic actuators, and are therefore used to aid and resist motion. Full roll and pitch control, and ideal skyhook control, can be performed by active systems. Since active control forces are not dependent on the relative motion between the vehicle body and the wheel, active suspensions are more flexible and applicable to an extensive range of input conditions (**Ivers and Miller 1991, Dyke et al. 1998, Fischer and Isermann 2004**).

Although active suspensions can be far more effective than semi-active and passive suspensions, there are many obstacles associated with active systems that obstruct commercialisation, including high cost, system complexity, substantial power requirements, sensor and maintenance requirements, increased weight, sophisticated control algorithms and dangerous failure modes (**Ivers and Miller 1991, Lai and Liao 2002, Ha et al. 2009, Dong et al. 2010, Cao et al. 2011**). **Dyke et al. (1998)** and **Ivers and Miller (1991)** explain that unmodelled system dynamics and nonlinearities could result in instabilities generated by the active system, and since active suspensions are capable of briefly pulling the tyres off the road, loss of traction could occur.

### 2.2.4 Conclusion

As compared to fully active suspension systems, semi-active suspension systems are cost-effective and safe, with much lower energy requirements, requiring a minimal amount of modification to the vehicle. These benefits associated with semi-active suspensions have resulted in the wide acceptance and implementation of semi-active devices, especially semi-active dampers, in vehicle suspension systems during the past three decades (**Ivers and Miller 1991, Cao et al. 2011**).

According to **Fischer and Isermann (2004)**, semi-active suspension systems have the potential to improve ride comfort by 30%, and handling by approximately 25%. Although even greater improvements are achievable by active suspension systems, the energy demand of semi-active suspensions is orders of magnitude lower than active suspensions. These advantages have led to the widespread implementation of semi-active dampers as the preferred choice for suspension control. These factors are further complemented by affordability, fast switching between continuous damping levels, and ease of implementation. All these advantages have led to the use of semi-active MR dampers in this study.

## 2.3 Vehicle Modelling

Vehicle models used in the existing literature range from simple linear quarter car models up to nonlinear full vehicle models. Some of the frequently used conventional vehicle mathematical models, as well as simulation models, are discussed in this section. The validation of some of these models is also briefly discussed.

### 2.3.1 The Quarter Car Vehicle Model

A quarter car model is a simplified two degrees of freedom vehicle model often used in suspension design. It is a basic model as it only includes vertical motion of the vehicle body and wheel without taking into account the pitch and roll motion of the vehicle (**Guglielmino et al. 2008**). A schematic of the quarter car model is shown in Figure 2-2, p2.10. According to **Savaresi et al. (2010)** the quarter car model describes the interactions between the suspension system, the tyre and the vehicle body in a corner of a vehicle, and consists of four elements:

- The sprung mass (also referred to as the sprung mass,  $M_s$ ) representing the vehicle body (usually contains a quarter of the vehicle body mass).
- The unsprung mass,  $m_u$ , that includes the wheel, brake and calliper.
- A spring element (and often a damper element) representing the tyre.
- A spring and damper element representing the suspension system.

The stiffness and damping of the suspension is denoted by  $k_s$  and  $c_s$  respectively, and the tyre stiffness and damping is denoted by  $k_t$  and  $c_t$  respectively. The input to the quarter car model is the vertical displacement of the road profile as a function of time.

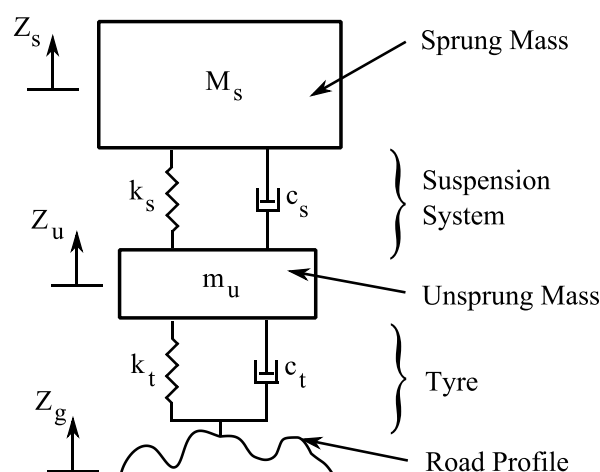


Figure 2-2: Quarter car vehicle model.



Quarter car models are often used to demonstrate vehicle suspension related principles. **Fischer and Isermann. (2004)** implemented a quarter car model and test rig to develop methods for identification, control, and fault detection in a mechatronic concept of an active- and semi-active suspension. **Dong et al. (2010)** implemented five semi-active control algorithms using a quarter car model containing a MR damper as a benchmark model for numerical comparison analysis. The performance of the five controllers is validated and compared using the numerical simulation and actual road test results. In a study by **Du et al. (2005)** semi-active  $H_\infty$  control of a MR damper is implemented on a quarter car model to improve the sprung mass acceleration, suspension deflection and tyre deflection of a passive suspension system. **Ahmadian and Pare (2000)** used a quarter car model and test rig to demonstrate the effect of suspension control on the sprung mass and unsprung mass transmissibility.

### 2.3.2 Higher Order Mathematical Models

The quarter car model is often extended to a four degrees of freedom half vehicle model, involving either the pitch ( $\alpha$ ) or roll ( $\beta$ ) motion of the sprung mass. The implementation of this model requires more information about the modelled vehicle: the location of centre of mass of the vehicle body has to be determined, as well as the pitch or roll moments of inertia. While the mass distribution can be easily obtained, accurate determination of moments of inertia is much more challenging. A numerical analysis of a passive pitch oriented half vehicle model is performed by **Savaresi et al. (2010)**.

A vertical full vehicle model is also often used in vehicle modelling. Two half vehicle models are joined to form a seven degrees of freedom model: vertical motion of the four wheels, and vertical, pitch and roll motion of the sprung mass. **Savaresi et al. (2010)** point out the following modelling assumptions:

- Suspension kinematics are neglected, resulting in only vertical forces being imposed on the vehicle body.
- Anti-roll bars aren't considered.
- The vehicle chassis plane is assumed to be parallel to the road surface where in reality vehicles are inclined in order to, among other things, reduce aerodynamic resistance.

**Guglielmino et al. (2008)** introduces a full vehicle model of which the front suspensions are independent, and the rear suspensions are connected through a rigid axle. Full vehicle models are often expanded to include more degrees of freedom, as in a study by **Ha et al. (2009)** where a six wheel drive military vehicle is considered. **Carrera Akutain et al. (2007)** developed a seven degrees of freedom simulation model of a small race vehicle similar in appearance to the test vehicle used in this work.

### 2.3.3 Computer Simulation Models

Increased processing power provided by computers has allowed the use of more complex models of higher degrees of freedom. As explained by **Blundell and Harty (2004)**, specialised software codes automatically assemble the equations of motion of the modelled vehicle and perform numerical integration in order to find the time-domain solution of these equations. In order to successfully use software codes, it is necessary that the user comprehend the complexities involved with the computational methods implemented. Popular numerical multi-body simulation codes include Dynamic Analysis and Design System (DADS) and Automatic Dynamic Analysis of Mechanical Systems (ADAMS).

**Els et al. (2007)** developed a 14 degrees of freedom first order simulation model using DADS software in order to perform a ride comfort and handling trade-off study on a Land Rover Defender vehicle. The encouraging results obtained from the simulation model motivated the development of a more detailed computer model in order to quantify favourable suspension characteristics. The model was developed using ADAMS software. **Thoresson et al. (2009)** performed a mathematical comparative study in which simplified models of the work of **Els et al. (2007)** were developed in order to decrease computational effort. It was concluded that the simplified models exhibit similar trends as the full simulation model developed using ADAMS software, but that the absolute values differ. The simplified models were scaled in order to be more representative of the full model.

### 2.3.4 Validation of Vehicle Models

Since increased computing power allows for more complex models that require more data to define them, simulation models should be developed in relation to the problems they intent to solve, and should be of minimum complexity while being capable of providing a solution of acceptable accuracy. As a consequence of the popularity of computer model implementation, the reliability of computer predictions has been an issue of growing concern for several decades. In order to obtain meaningful results from computer models, the models need to be adequately validated (**Blundell and Harty 2004, Bernard and Clover 1994 and Babuska and Oden 2004**). According to **Bernard and Clover (1994)** validation is the process of gaining confidence that the calculations yield useful insights into the behaviour of the simulated vehicle. **Heydinger et al. (1990)** argues that validation should be addressed by comparing the output of computer simulation models with vehicle test results. The importance of validating simulation models for the correct parameters is demonstrated in a study by **Kat and Els (2011)**.

Often in the literature basic quarter car models are implemented without commenting on the ability of these models to accurately represent the actual vehicles that the studies are intended for. The model

developed by **Els et al. (2007)** was successfully validated for ride comfort and handling simulation, using data obtained from discrete bump tests and double lane change manoeuvres. The model developed by **Carrera Akutain et al. (2007)** was validated using measured data from driving over two bumps a distance apart.

### 2.3.5 Conclusion

Implementation of semi-active suspension control requires an accurate simulation model of the test vehicle used in this study. Both ride comfort and handling of the vehicle are investigated in this study, thus the needs to accurately represent the vertical, as well as the lateral, roll, pitch, and yaw degrees of freedom. Such a model is complex and computationally intensive, therefore a computer simulation model will be developed using ADAMS View software. The model will be adequately validated in order to comprehend the shortcomings of the model, and to establish the accuracy of the simulation results.

## 2.4 Suspension Control

Upon comparison of the suspension control strategies in the existing literature, hybrid control has been identified as the strategy that is implemented in this study. This decision is based on the relative ease of implementation, and the fact that hybrid control is often implemented to address the ride comfort and handling compromise as the control strategy can be easily biased for either ride comfort or handling. In this section suspension control strategies found in the existing literature are discussed, with the emphasis on skyhook-, groundhook- and hybrid control.

### 2.4.1 Skyhook-, Groundhook-, and Hybrid Control

Skyhook control (discussed in Section 2.4.1.1, p2.13) is a comfort oriented semi-active control approach, and groundhook control (discussed in Section 2.4.1.2, p2.15) is a road-holding oriented semi-active control approach. Hybrid control (discussed in Section 2.4.1.3, p2.16) consists of the combination of skyhook- and groundhook control and aims to reduce the vertical acceleration of the vehicle body as well as mitigate the dynamic tyre force.

#### 2.4.1.1 Skyhook Control

The principle of the ideal skyhook control approach (initially developed by **Crosby and Karnopp, 1973**) is to connect the sprung mass to a hypothetical reference in the sky with the suspension damper in order to limit the vertical motion of the vehicle body (**Savaresi et al. 2010**). Skyhook control is used to improve the trade-off between resonance control and high frequency isolation of the sprung

mass that is inherent in passive dampers (Song, 1999). Implementation of the skyhook principle on the quarter car model is shown in Figure 2-3 (left), p2.14, where  $c_{sky}$  is the damping coefficient of the ideal skyhook damper. The ideal skyhook principle requires a fictional reference in the sky that remains fixed in the vertical direction, but is able to move in the horizontal direction. The ideal skyhook system is realised in practice by replacing the passive damper of the quarter car model with a controllable semi-active damper that allows imitation of the skyhook behaviour. The realization of the ideal skyhook principle using controllable dampers is shown in Figure 2-3 (right). The damping coefficient,  $c_{controllable}$ , varies with time in order to produce the required damping force that is determined by the skyhook control law. Comparing the required damping force of the ideal skyhook configuration to the semi-active skyhook configuration in Figure 2-3, it is apparent that if the sprung mass is moving upwards ( $\dot{Z}_s > 0$ ) and the sprung mass and unsprung mass are moving away from each other ( $\dot{Z}_{su} > 0$ ), the force delivered by the skyhook damper and the controllable damper will be in the same direction (relative to the sprung mass), downwards. The force delivered by the controllable semi-active damper is set to equal the force that will be produced by the skyhook damper:

$$\dot{Z}_s \dot{Z}_{su} > 0: F_{SA} = c_{sky} \dot{Z}_s \quad [ 1 ]$$

In Equation 1  $F_{SA}$  is the ideal damping force delivered by the semi-active damper, and the skyhook damping coefficient,  $c_{sky}$ , is:

$$c_{sky} = 2\zeta\sqrt{k_s M_s} \quad [ 2 ]$$

When the unsprung and sprung masses are separating ( $\dot{Z}_{su} > 0$ ) and the sprung mass is moving downwards ( $\dot{Z}_s < 0$ ), the skyhook damper force in Figure 2-3 (left), will be applied upwards. However, since the controllable damper in the semi-active configuration in Figure 2-3 (right), is located below the sprung mass it will exert a downward force in order to oppose the motion. Thus, in

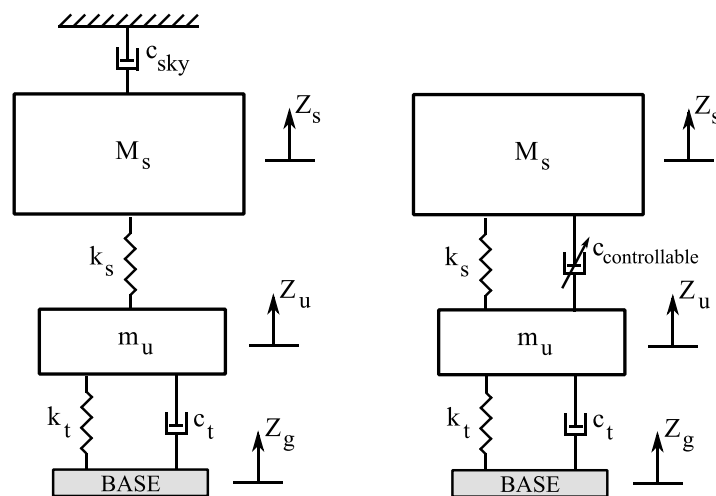


Figure 2-3: Ideal skyhook configuration (left), and semi-active skyhook configuration (right).

an attempt to approximate the skyhook behaviour as best as possible, the damping force is minimized (by setting it to zero):

$$\dot{Z}_s \dot{Z}_{su} \leq 0: F_{SA} = 0 \quad [ 3 ]$$

#### 2.4.1.2 Groundhook Control

The principle of the ideal groundhook control approach is to connect the unsprung mass to a hypothetical reference on the ground with the suspension damper, in order to limit the vertical motion of the tyre and thereby improve handling performance (Guglielmino et al. 2008). The ideal groundhook configuration is shown in Figure 2-4 (left), p2.15, where  $c_{gnd}$  is the damping coefficient of the ideal groundhook damper. Similar to the ideal skyhook configuration shown in Figure 2-3 (left), p2.14, the ideal groundhook configuration requires a fictional ground reference that remains fixed in the vertical direction while being able to move in the horizontal direction. The groundhook principle is approximated by using a semi-active controllable damper between the sprung and unsprung mass that allow for variable damping characteristics. The two degree of freedom quarter car model is modified to the semi-active suspension shown in Figure 2-4 (right), where the damping coefficient,  $c_{controllable}$ , varies in order to produce the required damping force determined by the groundhook control law. Comparing the required damping force of the ideal groundhook configuration to the semi-active groundhook configuration in Figure 2-4, it is apparent that if the unsprung mass is moving upwards ( $\dot{Z}_u > 0$ ) and the sprung mass and unsprung mass are moving towards each other ( $\dot{Z}_{su} < 0$ ), the force delivered by the groundhook damper and the controllable damper will be in the same direction (relative to the unsprung mass), downwards. The force delivered by the controllable semi-active damper is set equal to the force that will be produced by the groundhook damper, shown in Equation 4, p2.15:

$$\dot{Z}_u \dot{Z}_{su} < 0: F_{SA} = -c_{gnd} \dot{Z}_u \quad [ 4 ]$$

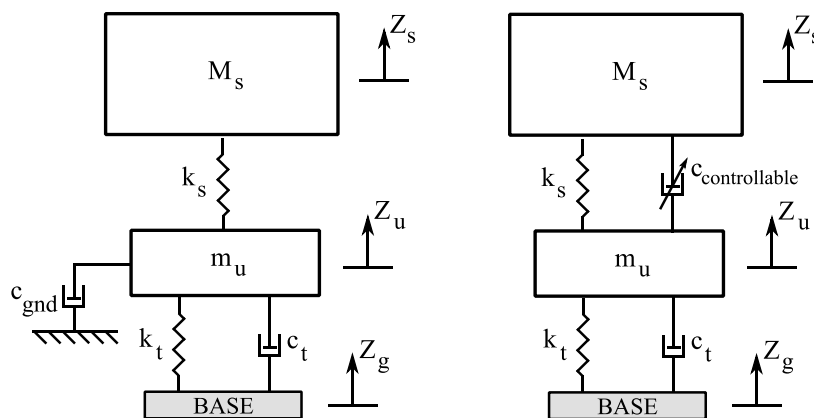


Figure 2-4: Ideal groundhook configuration (left), and semi-active groundhook configuration (right).

In Equation 4  $F_{SA}$  is the damping force delivered by the semi-active damper, and the groundhook damping coefficient,  $c_{gnd}$ , is:

$$c_{gnd} = 2\zeta\sqrt{k_t m_u} \quad [ 5 ]$$

However, when the sprung and unsprung masses are separating ( $\dot{Z}_{su} > 0$ ) and the unsprung mass is moving upwards ( $\dot{Z}_u > 0$ ), the required semi-active force and the groundhook damper force will be in different directions. Therefore, to approximate the groundhook configuration as best as possible, the damping force is minimized (by setting it to zero). The same holds when the sprung and unsprung masses are moving towards each other ( $\dot{Z}_{su} < 0$ ) while the unsprung mass moves downwards ( $\dot{Z}_u < 0$ ):

$$\dot{Z}_u \dot{Z}_{su} \geq 0: F_{SA} = 0 \quad [ 6 ]$$

### 2.4.1.3 Hybrid Control

While the skyhook control strategy minimizes vehicle body motion (improving ride comfort) at the cost of unsprung mass motion, the groundhook control strategy minimizes the unsprung mass motion (improving handling) at the cost of vehicle body motion. The hybrid control strategy is a combination of skyhook- and groundhook control and aims to reduce vehicle body acceleration as well as unsprung motion (**Guglielmino et al. 2008**). The hybrid control configuration is shown in Figure 2-5 (left), p2.17, and is realised using a semi-active controllable damper, shown in Figure 2-5 (right). The hybrid control strategy is a combination of the skyhook- and groundhook control laws:

$$\begin{aligned} \dot{Z}_s \dot{Z}_{su} > 0: \quad \sigma_{sky} &= \dot{Z}_s \\ \dot{Z}_s \dot{Z}_{su} \leq 0: \quad \sigma_{sky} &= 0 \\ \dot{Z}_u \dot{Z}_{su} < 0: \quad \sigma_{gnd} &= -\dot{Z}_u \\ \dot{Z}_u \dot{Z}_{su} \geq 0: \quad \sigma_{gnd} &= 0 \end{aligned} \quad [ 7 ]$$

In Equation 7,  $\sigma_{sky}$  and  $\sigma_{gnd}$  are the skyhook control and groundhook control contributions to the semi-active damper force,  $F_{SA}$ :

$$F_{SA} = G[a\sigma_{sky} + (1 - a)\sigma_{gnd}] \quad [ 8 ]$$

In Equation 8,  $G$  is a constant gain and  $a$  is the relative ratio between skyhook- and groundhook control strategies implemented in hybrid control. If  $a$  is set to 1, hybrid control is switched to skyhook control, on the other hand, if  $a$  is set to 0, hybrid control is switched to groundhook control. The skyhook- and groundhook contributions are equal when  $a$  is set to 0.5.

Hybrid control can be implemented in various forms (**Savaresi et al. 2010**):

- 2-State skyhook- and groundhook control: This is an on/off strategy that switches between high and low damping. The control strategy is driven by either the vehicle body velocity ( $\dot{Z}_s$ ) or the unsprung mass velocity ( $\dot{Z}_u$ ), and the suspension deflection velocity ( $\dot{Z}_{su}$ ).

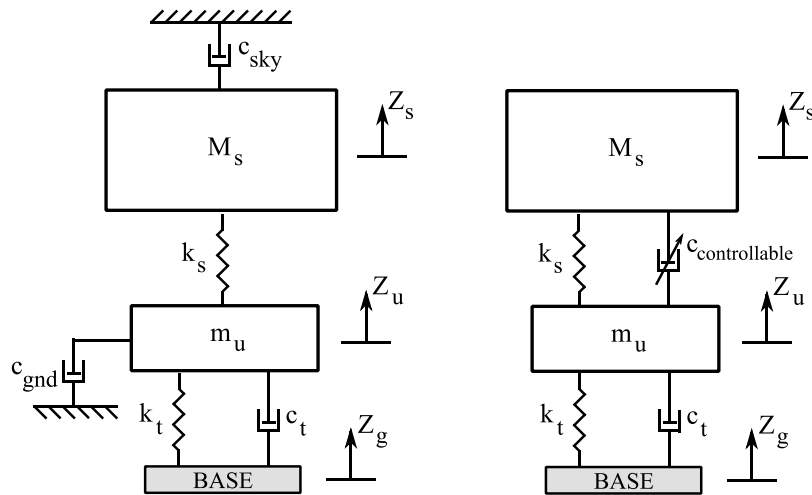


Figure 2-5: Ideal hybrid configuration (left), and semi-active hybrid configuration (right).

- Linear approximation damper control: This is suitable for use with a continuously variable damper since the control strategy provides an infinite number of damping coefficients. This control strategy has been discussed in Section 2.4.1.1, p2.13, and Section 2.4.1.2, p2.15. The vehicle body velocity ( $\dot{Z}_s$ ) or the unsprung mass velocity ( $\dot{Z}_u$ ), and the suspension deflection velocity ( $\dot{Z}_{su}$ ) are used to determine the damping factor.
- Acceleration driven skyhook damper control: This control strategy is similar to the 2-state skyhook control strategy as the damper switches between minimum and maximum damping. However, vehicle body acceleration ( $\ddot{Z}_s$ ), instead of velocity, is used to determine the outcome. This strategy minimizes the vertical body acceleration when the road profile is not available, and is not applicable to a groundhook control strategy in order to improve road-holding.
- Power driven skyhook damper control: A control strategy which has four possible damping factor outcomes. The suspension deflection ( $Z_{su}$ ), suspension deflection velocity ( $\dot{Z}_{su}$ ), and the suspension stiffness ( $k_s$ ) is required to determine the outcome. This control strategy, like the acceleration driven damper control strategy, is only applicable to a skyhook control strategy in order to improve ride comfort.

**Ahmadian and Pare (2000)** implemented skyhook-, groundhook- and hybrid control on a quarter car test rig to demonstrate the effect of changes in the control gain and bias factor on the sprung mass and unsprung mass transmissibility. Semi-active control results are compared to passive results. **Dong et al. (2010)** implemented skyhook- and hybrid control (with a bias factor of 0.8) on a small passenger vehicle in a comparative study. The effectiveness of various semi-active control strategies were compared by using vertical acceleration of the sprung- and unsprung mass. **Ha et al. (2009)** demonstrated that the roll and pitch response of a six wheeled military vehicle can be reduced by

implementation of skyhook control. **Carrera Akutain et al. (2007)** implemented a unique hybrid control strategy including a pitch hook, and a hybrid- plus extended groundhook control strategy, on four different suspension compositions. It was concluded that body pitch motion can be significantly reduced, while wheel hop control improvements are inconsequential.

#### 2.4.2 Other Control Algorithms Used in Suspension Control

Numerous control strategies have been adopted for semi-active suspension systems. A few of the popular control algorithms include skyhook control (and its variations including groundhook and hybrid control, discussed in Section 2.4.1, p2.13), linear quadratic Gaussian (LQG), sliding mode, and  $H_\infty$  control. According to **Fischer and Isermann (2004)** sliding mode control is usually implemented due to nonlinearities of actuators (in the case of active suspensions), and robust controllers such as  $H_\infty$  controllers are developed to deal with varying parameters and input conditions of suspension systems.

**Dong et al. (2010)** implemented skyhook-, hybrid-, LQG-, sliding mode-, and fuzzy logic controllers on a quarter car model excited by various inputs such as step, bump, sinusoidal, and random inputs. It was concluded that the performance of the controlled system is highly dependent on the control algorithm utilised. Each semi-active controlled system performed better than the passive system in some aspect. The sliding mode controller was found to be the most appropriate for use with MR dampers in suspension control. **Lai and Liao (2002)** developed a sliding mode controller for a single degree of freedom system aimed at producing ride comfort results achieved by an ideal skyhook suspension. **Du et al. (2005)** implemented  $H_\infty$  control on a quarter car suspension model. The controller utilises the suspension deflection and vehicle body velocity as feedback signals in order to determine the desired damping forces.

Several fuzzy logic and neural network control schemes have also been developed and evaluated in the literature. Examples include studies by **Yildirim (2004)**, **Yu et al. (2006)**, **Yu et al. (2009)**, **Dong et al. (2010)** and **Chen et al. (2012)**.

Clipped optimal-, decentralised bang-bang-, modulated homogeneous friction-, maximum energy dissipation-, and Lyapunov control is often implemented in studies concerning seismic protection by use of controllable MR dampers (**Jansen and Dyke 2000**, **Dyke and Spencer 1997**, and **Dyke et al. 1998**).

#### 2.4.3 Conclusion

Favourable results from other studies regarding skyhook, groundhook, and hybrid control implementation, as well as controller simplicity, have motivated the use of these control schemes for



this study. Also, hybrid control can easily be biased in favour of ride comfort or handling, and is therefore suitable for addressing the ride comfort and handling trade-off situation which forms part of this investigation.

## 2.5 Controllable Dampers

**Housner et al. (1997)** provide a list of semi-active controllable dampers that have been implemented in structural control. These include variable-orifice-, variable-friction-, controllable tuned liquid (TLD)-, and controllable fluid dampers.

A variable-orifice damper consists of a conventional hydraulic fluid damper and a controllable electromechanical valve to alter flow resistance. **Nell and Steyn (2003)** have implemented a hydraulic damper with a controlled bypass valve on a high mobility off-road vehicle to enable switching between two damping modes.

A variable-friction damper consisting of two braking pads on opposite ends of a sliding rod has been implemented in structural control of a five storey building by **Hirai et al. (1996)**. By adjusting the pressure applied by the top braking pad, the friction force is altered according to a control input.

Controllable TLDs are based on passive tuned sloshing dampers (TSD) where the liquid in a sloshing tank is used to add damping to a structural system. The effectiveness of the passive TSD is improved by developing a semi-active device in which the length of the tank is altered in order to change the properties of the damping device (**Housner et al. 1997**).

Controllable fluid dampers contain fluids that have the ability to undergo a change in viscosity when a magnetic or electric field is applied to the fluid. Two popular fluids commonly used in controllable fluid dampers are electrorheological (ER) and magnetorheological (MR) fluids. According to **Guglielmino et al. (2008)** and **Ahmadian and Pare (2000)**, the use of MR dampers in automotive engineering has become increasingly popular, and **Savaresi et al. (2010)** state that the three main technologies available presently are electrohydraulic (variable-orifice) dampers, MR dampers and ER dampers, with controllable air-damping suspensions soon to be introduced.

According to **Housner et al. (1997)** controllable devices containing electrically controlled valves or mechanisms are known to exhibit reliability and maintenance issues. However, controllable fluid dampers are reliable since they contain no moving parts other than the piston. Over the last two decades MR fluids have exhibited some distinct advantages over ER fluids, such as yield strength, lower sensitivity to impurities and variations in temperature, and easy stabilization. **Lai and Liao (2002)** mention that MR dampers are favourable for implementation in vehicle suspension systems due to their high yield strength, good stability, broad operational temperature range, and fast response

times compared to variable-orifice dampers. These favourable characteristics of MR dampers have led to the decision to use MR dampers as controllable damping devices implemented in this study.

## 2.6 Magnetorheological Dampers

MR dampers are promising semi-active devices implemented presently in automotive engineering. The working principle of MR dampers lies in the ability of the MR fluids to undergo a change in its rheological properties in accordance to alterations in the magnetic field strength applied to the fluid. By controlling the field intensity (i.e. controlling the current in an electromagnet), variable damping is produced. Although MR fluids were discovered in the 1940s, these fluids have only been extensively studied in recent years owing to a number of properties favourable for real-life engineering applications (**Guglielmino et al. 2008**).

### 2.6.1 Magnetorheological Damper Technology

MR fluids fall within a family of fluids, including ferro fluids and ER fluids, whose rheological properties depend on the strength of an electrical or magnetic field.

MR fluids consist of a mixture of micron-sized (5-10 $\mu$ m) magnetically polarizable particles, such as iron particles, suspended in a carrier fluid such as silicone oil. Additional substances are added to the fluid to prevent gravitational settling of the particles, as well as to enhance stability, improve lubrication, and inhibit wear. When a magnetic field is applied to the fluid, the particles become arranged in chains aligned in the direction of the external field, causing the free-flowing liquid to behave like a semi-solid. This change in state occurs within a few milliseconds and is completely reversible. Very low power input is required (12-24V; 1-2A; less than 50W), the fluid is insensitive to impurities and remains stable over a wide range of temperatures (-40-150°C) (**Dyke et al. 1998, Spencer et al. 1997, Housner et al. 1997, and Savaresi et al. 2010**). A detailed analysis of MR fluids properties and applications are given in **Jolly et al. (1999)**.

According to **Guglielmino et al. (2008)** the rheological behaviour of MR fluids can be separated into two distinct regions, namely pre- and post-yield. In the pre-yield region particle chain stretching occurs with occasional ruptures, resulting in elastic solid like behaviour of the MR fluids. In the post-yield region there is equilibrium between chain ruptures and chain reformations, resulting in viscous Newtonian fluid like behaviour.

MR fluids are implemented in various operation modes, including pressure-driven flow-, direct shear-, and squeeze-film mode. MR dampers used in automotive suspensions typically operate in pressure-driven flow mode since large-magnitude damping forces and large displacements can be

provided. Chain formations and ruptures present in pressure-driven flow mode is shown in Figure 2-6, p2.21 (based on **Guglielmino et al. (2008), p169**).

A MR damper (conceptually represented in Figure 2-7, p2.21, based on **Guglielmino et al. (2008), p15**, and **Savaresi et al. (2010), p29**) is very similar to a conventional viscous damper, the main differences being the MR fluid and an electromagnet embedded inside the damper piston which delivers a magnetic field in the orifices, also referred to as a magnetic choke. By controlling the electromagnet current, continuously variable damping can be produced without employing moving parts such as valves or variable orifices.

## 2.6.2 Magnetorheological Damper Modelling

The semi-active control of a MR damper based suspension system is discussed by **Wang and Liao (2011)** and **Lai and Liao (2002)**. The semi-active control system consists of a system controller and a damper controller. The system controller uses the measured system outputs to determine the desirable MR damper force, and the damper controller determines the required voltage (or current) input in order for the damper to track the desired damping force. The damper controller uses the desired force as prescribed by the system controller and the monitored or predicted force of the MR damper to generate the MR damper command voltage. **Wang and Liao (2011)** point out that the semi-active

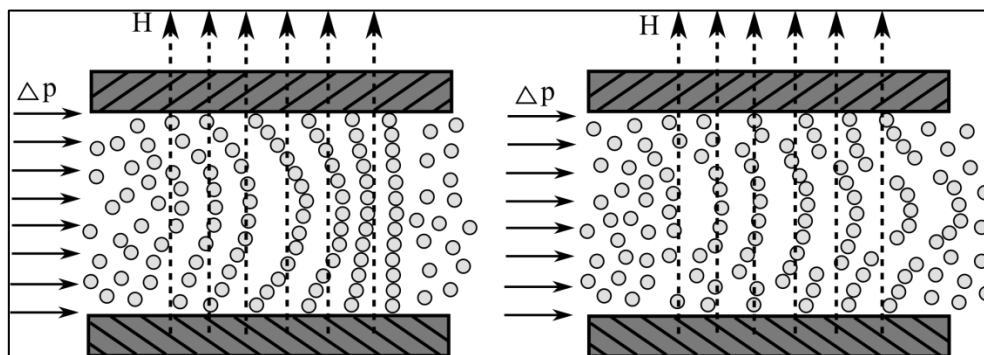


Figure 2-6: Pressure-driven flow mode: pre-yield flow (left), and post-yield flow (right).

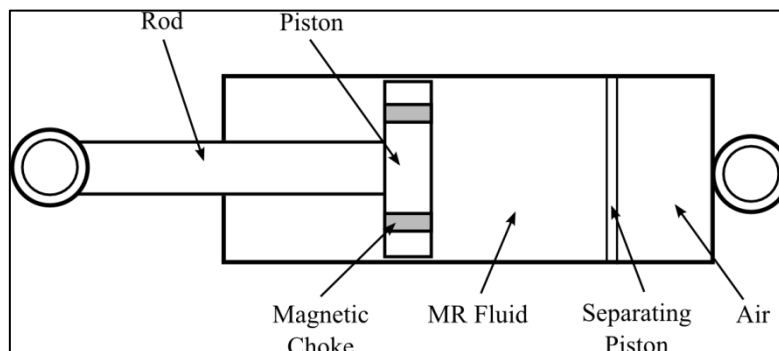


Figure 2-7: Principle of a MR damper.

control system requires an accurate damper model that relates the MR damper force to the damper excitation state, often used as feedback to the damper controller. A model that determines the required current or voltage to deliver the desirable MR damper force is also required. **Şahin et al. (2010)** state that the effective control of a MR damper depend on accurate control algorithms that are able to take maximum advantage of the unique features of a MR damper. Therefore damper models that accurately describe the nonlinear and saturation effects of the dampers are required. According to **Du et al. (2005)** the success of MR dampers in semi-active vehicle suspension applications is determined by the accurate modelling of the MR dampers and the selection of an appropriate control strategy, where the choice of control strategy is often related to the choice of MR damper model.

A list of MR damper model requirements is provided by **Wang and Liao (2011)**. According to the authors, besides high accuracy (small difference between predicted and measured data), MR damper models must be simple, robust, adaptable and reversible. Identification and implementation of simple models is easier, and a robust model is favourable for online implementation as it can withstand adverse conditions. Variations in operating conditions require an adaptive model, and model reversibility is required in order to determine both the damper force and the required damper voltage according to the desired force. **Spencer et al. (1997)** mention that a MR damper model must accurately capture the nonlinear and hysteretic behaviour of the damper, and be applicable to a wide range of input conditions without being numerically challenging.

To date several MR damper models have been developed and verified in the existing literature. A topical review of parametric MR damper models has been done by **Wang and Liao (2011)**, and the classification of MR damper models has also been discussed. MR damper models are characterised as quasi-static and dynamic. Typical properties used in quasi-static models include pressure gradients and yield stresses of the MR fluid. Since quasi-static models are insufficient to describe the nonlinear behaviour of MR dampers under dynamic loading, these models are mainly used in the design process of MR dampers. The shortcomings of quasi-static models are overcome by dynamic models.

Dynamic MR damper models can be classified into two main categories namely parametric and nonparametric models. According to **Wang and Liao (2011)**, **Şahin et al. (2010)** and **Song et al. (2005)**, parametric models represent the MR damper as a collection of linear and/or nonlinear springs, dampers, and other physical elements such as friction elements and hysteretic operators in various arrangements. **Wang and Liao (2011)** and **Song et al. (2005)** state that nonparametric models consist of analytic expressions developed from working principles that are based on experimental data. In a comparative study by **Şahin et al. (2010)** it is mentioned that the variables associated with parametric models have physical meaning, while those of nonparametric models do not necessarily have physical meaning. The majority of parametric models can further be categorised as evolutionary models (containing a nonlinear ordinary differential equation) and algebraic models. According to **Wang and**

**Liao (2011)**, parametric and nonparametric models can further be classified as dynamic or inverse dynamic. Dynamic models predict the output force as a function of various inputs such as the relative displacement of the damper and applied voltage or current. The inverse dynamic models return the voltage or current required in order to deliver a certain force magnitude under specific input conditions (such as relative piston velocity). Thus the dynamic models are used to predict the damping force while the inverse dynamic models are used to prescribe the command voltage to the damper.

There are several problems associated with many of the currently available MR damper models. **Song et al. (2005)** point out that accurate parametric models (such as the Bouc-Wen model) are difficult to solve numerically due to the presence of stiff differential equations used to model sharp transition nonlinearity, and that these models often do not include the magnetic field saturation effect. **Şahin et al. (2010)** concluded that more complicated parametric models containing differential equations result in high computational effort while offering no appreciable advantage over the simpler algebraic models which are capable of more accurate modelling of the nonlinear hysteretic behaviour of MR dampers. **Kaul (2011)** demonstrated that changes in the applied voltage or operating conditions require repeated characterization of model parameters and concluded that this aspect renders the majority of parametric models unsuitable for online identification processes. Although **Wang and Liao (2011)**, **Song et al. (2005)** and **Boada et al. (2011)** mention that nonparametric models are robust, flexible, suitable for a wider operating range, and capable of modelling the saturation effect more accurately with computational efficiency, **Şahin et al. (2010)** argue that these models can be complex and require large experimental datasets for validation.

In works by **Kaul (2011)** and **Alvarez and Jiménez (2002)** parametric and nonparametric models are implemented recursively to address the problem of repeated characterization for changes in input and operating conditions. **Kaul (2011)** concluded that since recursive model parameters are updated as new data becomes available, the models are computationally less expensive and can, therefore, be implemented in adaptive control algorithms.

### 2.6.3 Commonly Used Magnetorheological Damper Models

Some of the MR damper models often discussed and implemented in the literature are listed in this section. These include the less frequently discussed Batch Least Squares (BLS) model, and recursive algorithms applicable to specific nonparametric models.

#### 2.6.3.1 Parametric Dynamic Models

According to **Wang and Liao (2011)** parametric dynamic models include Bingham-based models, bi-viscous models, viscoelastic-plastic models, stiffness-viscosity-elasto-slide models, hysteretic

operator-based models such as the Bouc-Wen-, Dahl-, and LuGre models, hyperbolic tangent function-based models, sigmoid function-based models, equivalent models and phase transition models. The commonly used MR damper parametric models are discussed in this section.

### 2.6.3.1.1 Bingham Model

**Stanway et al. (1987)** developed an ER damper model known as the Bingham model. This model consists of a Coulomb friction element in parallel with a viscous damper, as shown in Figure 2-8 (left), p2.24. The damping force,  $F$ , as a function of piston velocity,  $\dot{x}$ , is given in simplified form as:

$$F = F_c \text{sgn}(\dot{x}) + c\dot{x} + F_0 \quad [9]$$

In Equation 9,  $F_c$  is the friction force,  $c$  is the damping coefficient,  $F_0$  is the force offset due to the accumulator in the damper, and  $\text{sgn}$  denotes the signum function. The Bingham model was implemented by **Spencer et al. (1997)** to model the dynamics of a MR damper. It was concluded that although the Bingham model reasonably predicts the force-displacement behaviour of the damper, the force-velocity relationship is not accurately modelled. The Bingham model delivers a one-to-one relationship between the force and velocity, while the experimental data is not one-to-one. The authors also implemented an extension of the Bingham model developed by **Gamota and Filisko (1991)**, which consists of the Bingham model in series with a standard model of a linear solid, shown in Figure 2-8 (right), p2.24. The extended model was successful in capturing the force-velocity relationship of the damper, but a significant shortcoming of the model is its computational burden associated with the stiff governing equations. A selection of Bingham model-based dynamic models have also been discussed by **Wang and Liao (2011)**.

### 2.6.3.1.2 Bouc-Wen Model

According to **Wang and Liao (2011)** a popular model used to represent hysteretic behaviour of MR dampers is the Bouc-Wen model, initially formulated by **Bouc (1971)** and generalised by **Wen (1976)**. The damping force,  $F$ , is computed as follows:

$$F = kx + c\dot{x} + az + F_0 \quad [10]$$

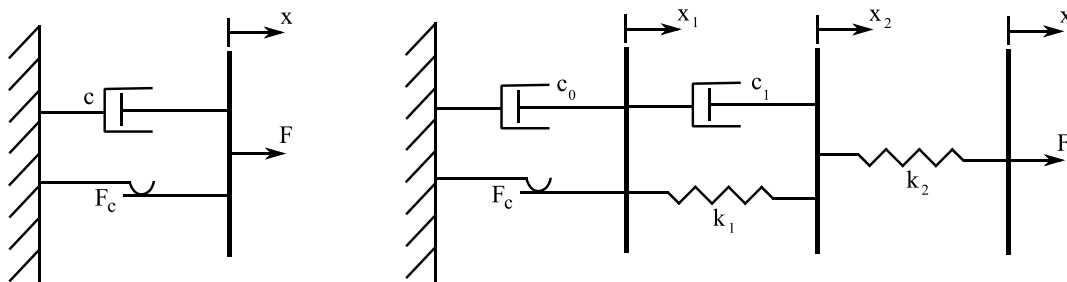


Figure 2-8: Bingham model (left), and extended Bingham model (right).

In Equation 10,  $x$  and  $\dot{x}$  represent the relative displacement and velocity of the damper piston,  $k$  is the spring stiffness,  $c$  is the damping coefficient,  $F_0$  is the force offset due to the accumulator in the damper,  $\alpha$  is a constant, and  $z$  is the evolutionary variable governed by:

$$\dot{z} = -\gamma z |\dot{x}| |z|^{n-1} - \beta \dot{x} |z|^n + A \dot{x} \quad [11]$$

In Equation 11, the shape of the force-velocity characteristic is adjusted by  $\gamma$ ,  $\beta$ ,  $n$  and  $A$ . The influences of these parameters are discussed in detail by **Guglielmino et al. (2008)**. The Bouc-Wen model is shown in Figure 2-9 (left), p2.25. Although the Bouc-Wen model is favourable as its equations are less stiff than those of the extended Bingham model, the Bouc-Wen model is incapable of accurately modelling the transition between pre-yield and post-yield regions of the force-velocity relationship. The Bouc-Wen model was implemented by **Spencer et al. (1997)** to model a MR damper. According to the authors the accuracy of the Bouc-Wen model was comparable to the extended Bingham model at resembling the force-velocity relationship, but did not show accurate representation of the roll-off between pre-yield and post-yield regions. A voltage dependent version of the Bouc-Wen model was implemented in a comparative study by **Jansen and Dyke (2000)** on a shear mode paddle-type MR damper. **Spencer et al. (1997)** proposed a modified Bouc-Wen model, often referred to as the Phenomenological model in the literature, and a voltage dependent version of this model was implemented by **Dyke et al. (1998)** in a study concerning seismic protection. The Phenomenological model (or modified Bouc-Wen model) is shown in Figure 2-9 (right), p2.25. **Lai and Liao (2002)** used a voltage dependent modified Bouc-Wen model to represent a MR damper used for vibration control in a suspension system. **Du et al. (2005)** pointed out that although the Phenomenological model can accurately describe the behaviour of MR dampers, corresponding inverse dynamic models are difficult to obtain due to the nonlinear characteristics of the dynamic model. **Şahin et al. (2010)** compared the Bouc-Wen-, modified Bouc-Wen-, and voltage dependent modified Bouc-Wen models to several other parametric MR damper models. The ordinary Bouc-Wen

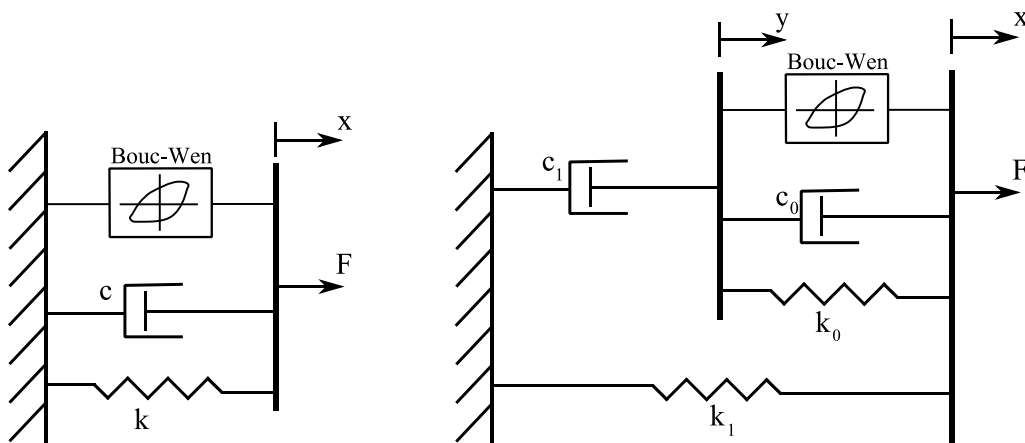


Figure 2-9: Bouc-Wen model (left), and Phenomenological model (right).

model yielded the worst results while the voltage dependent modified Bouc-Wen model was one of the most accurate models used in the study. A number of Bouc-Wen models, including voltage dependent models, current dependent models, and models for shear mode dampers and large-scale MR dampers, have been discussed by **Wang and Liao (2011)**.

#### 2.6.3.1.3 Modified LuGre Friction Model

A popular model used for friction dynamics is the LuGre friction model introduced by **De Wit et al. (1995)**. A modified version of the LuGre model was proposed by **Alvarez and Jiménez (2002)**. In this model the damping force,  $F$ , is a function of voltage,  $v$ , and velocity,  $\dot{x}$ :

$$F = \sigma_0 z v + \sigma_1 \dot{z} + \sigma_2 \dot{x} \quad [12]$$

In Equation 12,  $\sigma_0$ ,  $\sigma_1$ , and  $\sigma_2$  are model parameters, and the internal variable,  $z$ , is given by:

$$\dot{z} = \dot{x} - \sigma_0 a_0 |\dot{x}| z (1 + a_1 v) \quad [13]$$

In Equation 13  $a_0$  and  $a_1$  are constant parameters. The authors implemented the modified LuGre friction model in a recursive least squares (RLS) algorithm to ensure parameter convergence during MR damper characterization. **Şahin et al. (2010)** compared the modified LuGre friction model to several other parametric MR damper models. The modified LuGre friction model yielded moderately accurate results.

#### 2.6.3.1.4 Kwok Model

According to **Şahin et al. (2010)** the Kwok model is a hyperbolic tangent function-based algebraic model proposed by **Kwok et al. (2006)** and is expressed as follows:

$$F = c \dot{x} + kx + \alpha z + F_0 \quad [14]$$

In Equation 14,  $F$ ,  $x$ , and  $\dot{x}$  are the damper force, displacement and velocity respectively,  $c$  and  $k$  are the damping coefficient and spring stiffness,  $F_0$  is the force offset due to the accumulator in the damper,  $\alpha$  is a constant, and the hysteretic variable,  $z$ , is given by:

$$z = \tanh[\beta \dot{x} + \delta \operatorname{sgn}(x)] \quad [15]$$

$\beta$  and  $\delta$  in Equation 15 influence the shape of the force-velocity hysteresis curve. **Kwok et al. (2006)** pointed out that the proposed model is computationally efficient and is, therefore, favourable for controller design and implementation. The Kwok model is a very accurate model compared to other parametric models in the study by **Şahin et al. (2010)**.

#### 2.6.3.1.5 Hyperbolic Tangent Model

**Simon (2001)** developed a current dependent hyperbolic tangent model to describe the properties of a MR damper used in skyhook control of a SUV suspension. The force exerted by the damper,  $F$ , is



expressed as a function of damper current,  $I$ , and relative damper velocity,  $\dot{x}$ :

$$F = (\delta_1 I + \delta_2)(\tanh[\delta_3 \dot{x}] + \delta_4 \dot{x} + \delta_5) \quad [16]$$

The model parameters  $\delta_1$  to  $\delta_5$  in Equation 16 are constants determined by using a best fit technique. The required damper current to deliver the desired damping force,  $F_d$ , can be determined by the damper inverse model:

$$I = \frac{1}{\delta_1} \left[ \frac{F_d}{(\tanh[\delta_3 \dot{x}] + \delta_4 \dot{x} + \delta_5)} - \delta_2 \right] \quad [17]$$

**Kaul (2011)** demonstrated that the model is incapable of representing hysteretic behaviour, and as such **Simon (2001)** used the model to generate damping curves rather than time dependent force-velocity plots.

### 2.6.3.2 Nonparametric Dynamic Models

According to **Wang and Liao (2011)** nonparametric models include the polynomial model, the multi-function model, the black-box model, the query-based model, the neural network model, the fuzzy model, the wavelets model, and the Ridgenet model. Some of the commonly used nonparametric models are discussed in this section.

#### 2.6.3.2.1 Polynomial Model

According to **Du et al. (2005)** the polynomial model (initially developed by **Choi et al. 2001**) is convenient and effective because the inverse model can be obtained in an analytical form and can therefore easily be implemented in an open-loop control system. A shortcoming of the polynomial model is its inability to characterise the damper behaviour in the pre-yield region. In the polynomial model the hysteresis loop is divided into positive acceleration (lower loop) and negative acceleration (upper loop). The lower loop or the upper loop is fitted by the polynomial and a least square optimization method is used to determine the appropriate model parameters for both the positive and negative acceleration data sets. The damping force,  $F$ , is expressed as a function of damper current,  $I$ , and damper piston velocity,  $\dot{x}$ :

$$F = \sum_{i=0}^n a_i \dot{x}^i \quad [18]$$

The order of the polynomial in Equation 18,  $n$ , is chosen by trial and error. There exists a linear relationship between the model parameters,  $a_i$ , and the damper current,  $I$ :

$$a_i = b_i + c_i I, \quad i = 0, 1, 2, \dots, n \quad [19]$$

Thus the damper force is expressed by:

$$F = \sum_{i=0}^n (b_i + c_i I) \dot{x}^i \quad [ 20 ]$$

In Equation 20,  $b_i$  and  $c_i$  are determined by a linear fit. Once the model parameters are determined, the required damper current to deliver the desired damping force,  $F_d$ , can be determined by the inverse model as:

$$I = \frac{F_d - \sum_{i=0}^n b_i \dot{x}^i}{\sum_{i=0}^n c_i \dot{x}^i} \quad [ 21 ]$$

**Du et al. (2005)** mention that although the desired damper force prescribed by the system controller can be any value (and thus in any direction), the MR damper is a passive device and the current should be restricted to a range between zero and the maximum allowable current value. It is concluded that the polynomial model is accurate under various excitation conditions without modification of the model parameters.

#### 2.6.3.2.2 Batch Least Squares Model

**Kaul (2011)** developed a nonparametric model referred to as a batch least squares (BLS) model to describe the behaviour of a small paddle-type MR damper. The BLS model was compared to a Bouc-Wen model (discussed in Section 2.6.3.1.2, p2.24) and a Hyperbolic Tangent model (discussed in Section 2.6.3.1.5, p2.26).

According to **Tham (1999)** a general relationship between a dependent variable (the output,  $y$ ) and  $m$  independent variables (inputs,  $x$ ) can be written as:

$$y_i = \theta_1 x_{i1} + \theta_2 x_{i2} + \theta_3 x_{i3} + \dots + \theta_m x_{im} \quad [ 22 ]$$

where:

- $y_i$  = the  $i$ 'th observation of the dependent variable,
- $x_{ij}$  = the  $i$ 'th observation of the  $j$ 'th independent variable,
- $\theta_j$  = the coefficient associated with the  $j$ 'th independent variable.

Equation 22, p2.28, is expressed in vector notation as:

$$y_i = [x_{i1} \quad x_{i2} \quad x_{i3} \quad \dots \quad x_{im}] \begin{bmatrix} \theta_1 \\ \theta_2 \\ \theta_3 \\ \vdots \\ \theta_m \end{bmatrix} \quad [ 23 ]$$

Equation 23 is also written as:

$$y_i = \phi_i^T \hat{\theta} \quad [ 24 ]$$

where  $\phi_i^T$  is the regressor vector and its entries are the known time history inputs (such as displacement and velocity) to the system.  $\hat{\theta}$  is a vector containing the estimated model coefficients. Once a suitable regressor vector is identified the model coefficients are determined as follows:

$$\hat{\theta} = (\Phi^T \Phi)^{-1} \Phi^T y \quad [ 25 ]$$

In Equation 25,  $y$  is the  $n \times 1$  column vector consisting of  $n$  measured outputs, and  $\Phi$  is the  $n \times m$  matrix consisting of the regressor vectors ( $\phi_i^T$ ) as its rows.

The regressor vector of the model developed by **Kaul (2011)** contains three measurements of displacement, one measurement of velocity, one product of absolute measured velocity and measured MR damper force, and three measurements of MR damper force. The regressor was determined by changing the model order and regressor coefficients iteratively. The regressor vector that was identified is as follows:

$$\phi_t^T = [x_{t-1} \quad x_{t-2} \quad x_{t-3} \quad \dot{x}_{t-1} \quad |\dot{x}_{t-1}|F_{t-1} \quad F_{t-1} \quad F_{t-2} \quad F_{t-3}] \quad [ 26 ]$$

The subscript  $t-i$  in Equation 26 refers to the  $i^{\text{th}}$  previous measured data point. Since three time history data points are required to calculate the MR damper force, predicted MR damper force values are available from  $t = 4$  to  $t = n$ , where  $n$  is the total number of measured points. Once  $\Phi$  is compiled for all regressor vectors  $\phi_{t=4}^T$  to  $\phi_{t=n}^T$  the BLS model coefficients are determined according to Equation 25, where  $y$  is a column vector consisting of the measured MR damper forces. The MR damper force is then predicted as:

$$F_t = \phi_t^T \hat{\theta} \quad [ 27 ]$$

Note that Equation 27 is analogous to Equation 24, p2.28. **Kaul (2011)** found that the BLS model very accurately predicts the MR damper force when separate characterization is performed for each current level. It is mentioned that characterization for a data set of increasing current levels together is possible, but results in a higher RMS error. The increase in RMS errors for such data sets is attributable to the increase in hysteretic behaviour and the effect of saturation with increasing current levels. **Kaul (2011)** concluded that parametric models such as the Bouc-Wen model may not be viable in on-line applications since repeated characterization is computationally intensive. Recursive models based on the BLS model are advantageous over parametric models because these models are much more computationally efficient and applicable to continuously changing input conditions. It should however be noted that for the implementation of this model, the measured damper force is required as feedback.

### 2.6.3.3 Recursive Models

According to **Kaul (2011)** the shortcomings of parametric models, such as inadequate modelling of hysteresis and saturation, and the need for repeated characterization, can be overcome by

implementation of recursive models. While parametric models work well within limited bounds of input conditions used to characterise the damper, recursive algorithms continuously update the model parameters as data becomes available, and are therefore applicable to a wider range of input conditions. Recursive models also provide advantages over parametric models with regards to computation time.

To overcome the problem of repeated characterization associated with parametric and nonparametric models **Kaul (2011)** implemented three recursive algorithms to model a paddle type MR damper: least mean square (LMS), recursive least square (RLS), and a Projection algorithm. The recursive algorithms contain the regressor vector of the BLS model discussed in Section 2.6.3.2.2, p2.28. Initial model coefficients were obtained from a BLS model developed using the first few measured data points. **Alvarez and Jiménez (2002)** also implemented a RLS identification algorithm on a modified LuGre friction model using the MR damper model proposed by **Spencer et al. (1997)** to generate artificial forces in response to a defined displacement and voltage input. The identification scheme was then implemented on the same inputs, thus obtaining parameter convergence within 1.5s. The force response to a varying displacement input was not explored in this paper. According to **Boada et al. (2011)** the main advantages of the method described by **Alvarez and Jiménez (2002)** are that the model is less complex while still capturing the essential characteristics of MR dampers, and is suitable for real-time parameter identification. **Terasawa et al. (2004)** implemented a different voltage dependent modified LuGre friction model in an adaptive algorithm to address the issue of uncertainty in model parameters. The error between the measured MR damper force and the force predicted by the model is used in an adaptive law to update the model parameters. Contrary to the model proposed by **Alvarez and Jiménez (2002)** the model proposed by **Terasawa et al. (2004)** is invertible as the voltage is not included in the internal deformation state equation. In the experimental work the damper was excited by a random velocity input ranging between -0.15m/s and 0.15m/s with a constant voltage between 0.6V and 1.3V for a duration of approximately 2s. It was concluded that the proposed adaptive identification method thoroughly describes the hysteretic behaviour of the MR damper. **Boada et al. (2011)** implemented a recursive lazy learning algorithm based on RLS to model the behaviour of a MR damper similar to the damper used in this study. The neural network used in the lazy learning algorithm is adjusted by minimizing the error between the measured MR damper force and the force predicted by the model. The MR damper force in response to a sinusoidal displacement input of fixed amplitude and frequency is predicted using the proposed recursive method. The current level is kept constant for all runs, and is increased from 0A to 1.2A. The accuracy of the proposed method has been compared to that of several popular MR damper models, including the Bingham model and the Bouc-Wen model. It is concluded that the neural model satisfactorily captures the hysteretic and nonlinear behaviour of the MR damper.

Three recursive algorithms are discussed in this section: RLS, LMS, and Projection algorithm. Implementation of these algorithms requires that the model is linearised in the parameters and can therefore be decomposed into a regressor vector and a model coefficients vector as shown in Equation 23, p2.28, and Equation 27, p2.29.

### 2.6.3.3.1 Least Mean Square Algorithm

According to **Ljung and Soderstrom (1985)** the LMS algorithm is a good alternative to the RLS algorithm when there are uncertainties regarding the choice of the regressor, or when the regressor does not completely satisfy the conditions of RLS. The LMS algorithm updates the model parameters according to:

$$\hat{\theta}_t = \hat{\theta}_{t-1} + \gamma_1 \phi_t [F_{t,meas} - \hat{F}_t] \quad [28]$$

In Equation 28,  $\gamma_1$  is the forgetting factor, also known as the gain sequence, which determines the extent to which the new data influences the model parameters, and causes a trade-off between model tracking capability and insensitivity to noise. The forgetting factor is constrained by  $0 < \gamma_1 \leq 1$ .  $\hat{\theta}_t$  and  $\hat{\theta}_{t-1}$  are the time varying parameter estimates at the current ( $t$ ) and previous ( $t - 1$ ) time intervals. In the LMS algorithm the predicted force is calculated as:

$$\hat{F}_t = \phi_t^T \hat{\theta}_{t-1} \quad [29]$$

Note that Equation 29 is analogous to Equation 27, p2.29. A starting value of  $\hat{\theta}_0$  is required and may be arbitrarily selected (**Kaul 2011**).

### 2.6.3.3.2 Projection Algorithm

The Projection algorithm is expressed as:

$$\hat{\theta}_t = \hat{\theta}_{t-1} + \frac{\gamma_2 \phi_t}{\rho + \phi_t^T \phi_t} [F_{t,meas} - \hat{F}_t] \quad [30]$$

In Equation 30,  $\rho$  is an additional constant selected to be strictly greater than zero in order to avoid division by zero, while  $\gamma_2$  is analogous to the forgetting factor in Equation 28, p2.31 and is constrained such that  $0 < \gamma_2 < 2$  (**Kaul 2011**).

### 2.6.3.3.3 Recursive Least Square Algorithm

The RLS algorithm updates the model parameters as follows:

$$\hat{\theta}_t = \hat{\theta}_{t-1} + K_t [F_{t,meas} - \hat{F}_t] \quad [31]$$

In Equation 31  $K_t$  is computed as:

$$K_t = P_{t-1} \phi_t [\lambda + \phi_t^T P_{t-1} \phi_t]^{-1} \quad [32]$$

In Equation 32,  $\lambda$  is a forgetting factor analogous to  $\gamma_l$  in Equation 28 and can be approximated as  $\lambda \approx 1 - \gamma_1$ , with  $0 < \lambda \leq 1$ .  $P_t$  in Equation 32 is computed as:

$$P_t = [I - K_t \phi_t^T] \frac{P_{t-1}}{\lambda} \quad [ 33 ]$$

A starting value of the time-varying matrix  $P_0$  is required and a large positive definite matrix is generally used.  $I$  is an identity matrix of the same order as  $P$ .

#### 2.6.4 Conclusion

Several important conclusions can be drawn from the literature review. The applications of developed models are usually limited to specific input conditions since MR damper models are mostly developed for sinusoidal displacement inputs of fixed frequency and amplitude, which is not realistic from a vehicle implementation point of view. These models are rarely verified with random displacement excitation comparable to road disturbance inputs. Current independent models are developed for a discrete current level setting and re-characterization of model parameters is then required to accommodate changes in supplied current.

While there has been a lot of focus on developing models of improved accuracy in response to uniform (for example sinusoidal) inputs, not enough work has been done in order to develop models of acceptable accuracy applicable to non-uniform (random) excitation. Often models developed using uniform excitations are implemented in random excitation situations without prior verification of applicability to changes in excitation conditions.

The focus of MR damper modelling is also concerned with predicting the MR damper force for a specific input current. There are very few invertible models that can be used to determine the current input in order to deliver the desired damping force.

Little research has been done towards implementation of recursive (adaptive) models implementing least square based methods to determine model parameters. Also, the available recursive models are often used to obtain parameter convergence, or to update model parameters for changes in current levels. The effects of changes in excitation conditions have not been explored as yet. Recursive models also require the measuring of actual MR damper forces for error feedback, which is often difficult to execute due to constraints in vehicle design and allowable costs.

## 2.7 Literature Summary and Problem Statement

Based on the discussion of the existing literature, some topics that need further investigation have been identified from the literature review and are listed in this section:

1. *Passive suspension systems inevitably provide a compromise in ride comfort and handling due to conflicting suspension requirements. In order to improve the performance of the vehicle-driver combination, this compromise needs to be mitigated. A possible solution to reduce the suspension trade-off has been identified in the literature, namely semi-active suspension control by implementation of MR damper control.*
2. MR damper models are developed for specific input conditions and become unreliable when the input conditions change, requiring re-characterization of model parameters for new input conditions. Uniform excitation has been thoroughly investigated, while random excitation, to which dampers in a suspension application are typically subject to, is seldom explored. Also, the capability of developed models to prescribe the required current setting in order to yield favourable damping forces requires further investigation. *There exists a need for an invertible MR damper model applicable to a wider range of input conditions including random excitation.*
3. Vehicle models regularly implemented in suspension studies involve several assumptions and simplifications, such as linearity in suspension and tyre forces, reduced degrees of freedom, etc. The ability of vehicle models to represent physical vehicles is rarely investigated. *An adequately validated, higher-order, nonlinear vehicle simulation model is required.*

The main research question addressed by this study is: *Can MR suspension technology be implemented to improve the ride comfort and handling characteristics of a Baja vehicle by using hybrid control, without causing a trade-off situation?*

It has been established in the literature that vertical acceleration values provide good correlation between subjective and objective ride comfort ratings. The results of numerous ride comfort studies motivated the use of BS 6841 (**British Standards Institution, 1987**) weighted RMS vertical acceleration values for ride comfort evaluation in this study.

Closed loop handling tests require a driver model to track a prescribed path. An open loop single lane change test (where a steer input is defined as a function of time) has been chosen for this study in order to simplify the modelling process. Yaw rate has been identified as a measure to evaluate the handling (or directional response) of the test vehicle. The body roll angle and vertical tyre forces will also be analysed as these metrics have often been used in the existing literature to assess handling and road-holding. These metrics will be implemented with caution due to the lack of a differential in the test vehicle that requires a different interpretation of the results as compared to conventional vehicles.

The vertical, lateral, roll, pitch and yaw degrees of freedom should be included in the vehicle simulation model since both the ride comfort and handling is addressed in this study. The model

should also contain nonlinearities in order to model the suspension and the tyres as accurately as possible. A simulation model will be developed using ADAMS View software. The model will also be validated by comparing measured data to simulation results.

To address the ride comfort and handling compromise a control strategy that can be biased for either ride comfort or handling is required. Since hybrid control (comprising of skyhook- and groundhook control) have been widely implemented in semi-active control studies, this study will incorporate hybrid control as well. Furthermore, hybrid control is a model-free strategy and can therefore be implemented without prior knowledge of system parameters or excitations, and is thus attractive for use in this study.

Although studies have shown that active suspensions are very effective in addressing the ride comfort and handling compromise, these systems are very complex, expensive, and require a lot of power during operation. Semi-active suspensions are simple, can easily be implemented, and have low energy requirements. Semi-active control is thus very appealing since variable damping can be incorporated to reduce the compromise between ride-comfort and handling at little additional cost.

Controllable dampers used in suspension control include variable-orifice- and controllable fluid dampers, such as MR dampers. Compared to variable orifice dampers, MR dampers provide faster switching between a wide range of damping levels. MR dampers are also more reliable and less sensitive to impurities and variations in operating temperature. These favourable characteristics of MR dampers, and their widespread implementation in controllable suspensions, have led to the use of MR dampers in this study.

MR damper models frequently implemented in the existing literature have been discussed in the literature review, along with some less familiar models, such as the BLS model and the recursive models. Although many models are discussed in the literature, no superior model has been identified. In this study some commonly used parametric models (including the Bingham-, Bouc-Wen- and Kwok models) are developed, in addition to the polynomial and BLS nonparametric models. A recursive LMS model is also implemented using measured and calculated force feedback. In addition so sinusoidal displacement excitation (as is the norm in the literature), random excitations are also used to better evaluate the accuracy of the models when the input conditions change. In an attempt to develop models that are applicable to a wider range of input conditions, current dependent models are also developed in order to eliminate the need for re-characterization with changes in supplied current.

The main list of tasks performed as part of this study is as follows:



1. Development of an adequate MR damper model. This model is needed to predict the damping force exerted under specific input conditions such as relative piston velocity and input current.
2. Development of a vehicle model to simulate suspension control. This model has to be accurate and should therefore be validated against test results for ride comfort and handling. The development of the simulation model involves the following tasks:
  - i. A complete computer aided design (CAD) model is required to define the geometry of the test vehicle.
  - ii. Experimental determination of specific characteristics such as the centre of mass and moments of inertia of the vehicle body.
  - iii. Characterization of the hydro-pneumatic spring-damper units to obtain spring and passive damping characteristics of the existing spring-damper system of the test vehicle.
  - iv. Development of a suitable tyre model required by the vehicle simulation model.
  - v. Data collection is needed in order to compare simulation results and thereby validate the model. This includes experimental MR damper tests and vehicle tests for both ride and handling.
3. Determination of the ideal suspension and control settings for optimal ride comfort and handling. This requires simulations of semi-active suspension control.

It may be noted that optimal ride comfort and optimal handling suspension characteristics may not be the same for all ride comfort and handling tests. In this study the rough Belgian paving track has been identified as the excitation source used for the ride comfort evaluation, and the single lane change test is used for handling evaluation.

One of the constraints in this study is the damping capabilities of the relatively small MR dampers used for this study. To overcome this constraint, passive damping is not eliminated from the suspension, but instead retained in the existing test vehicle in conjunction with the MR dampers. This is often the case in all conventional suspension systems where passive damping is always present due to inherent friction and elastomeric components, although these contributions are almost always assumed to be small and therefore neglected. Similarly the MR damper itself has some passive damping when the control current is zero. In this study only variable damping is considered while the spring characteristics are kept fixed. Also, additional constraints such as test vehicle suspension layout, and system complexity have led to an inability to directly measure the MR damper forces. As a result MR damper forces are not included in the damper models, and the damper controller design falls beyond the scope of the project.



---

## 3 *MAGNETORHEOLOGICAL DAMPER CHARACTERIZATION*

---

In order to obtain suspension characteristics for desirable ride comfort and handling for the Baja vehicle used in this study, the damping of the suspension is used as an adjustable variable. In order to achieve this, damping provided by the MR damper is varied by adjusting the current supplied to the MR damper. It may be noted that this damping is in addition to the passive damping provided by the hydro-pneumatic spring-damper unit. The vehicle state (such as changes in vertical acceleration, body pitch and roll, and suspension displacement) is used as input to a control algorithm (such as hybrid control) that specifies the required damping force in order to obtain optimal damping for the desired ride comfort and handling of the vehicle. Once the required damping force is specified, the current in the MR damper must be adjusted accordingly. A damper control algorithm compares the actual force exerted by the MR damper to the required force. If the actual force is smaller than the required force the current supplied to the MR damper is increased until the difference in the forces is below a specified tolerance. Similarly, if the required force is smaller than the actual force delivered by the MR damper the current is reduced or switched off. For simulation purposes a MR damper model is required to define the relationship between the damper inputs (such as displacement and current) and the corresponding force output. For semi-active suspension control implementation, an inverse MR damper model is required in order to determine the necessary current setting that will deliver the prescribed MR damper force. Several MR damper models have been developed in this study from experimental data, as described in Section 3.1, p3.1. The MR damper models developed in this work are discussed in Section 3.2, p3.7.

### 3.1 Experimental Work

The MR damper used in this study is manufactured by LORD Corporation and is suitable for use in semi-active seat suspension systems (Part Number: RD-8041-1, **LORD Corporation 2013**). The choice of this damper is based on cost and availability considerations, since MR dampers suitable for vehicle applications generally aren't sold to academic institutions, perhaps due to reasons related to intellectual property protection.

The MR damper is a continuously variable mono-tube damper that contains high-pressure nitrogen gas. The outer diameter of the damper is 42mm, its extended length is 250mm with a 73mm stroke. A safety clearance of 6mm is recommended to prevent damage to the damper, resulting in a 67mm

usable stroke. The annular orifice and electromagnetic coil is contained in the piston, and current is delivered to the coil via leads routed through the hollow damper shaft. A current input of 1A can be delivered constantly to the damper and a maximum allowable current of up to 2A intermittently. The damper requires an input voltage of 12V DC. The resistance of the coil is  $5\Omega$  at ambient temperature and  $7\Omega$  at a maximum operating temperature of  $71^{\circ}\text{C}$ . The mass of the MR damper is approximately 0.92kg. The response time of the MR damper is specified as less than 15ms.

The experimental setup used for data collection is shown in Figure 3-1, p3.2. The MR damper is connected by means of clevises to a supporting frame at the top, and to a moment-insensitive 1ton load cell at the bottom. The load cell is connected to a 25kN hydraulic actuator. The MR damper circuit is connected to a variable voltage DC power supply. Due to a lack of heat dissipation through convection in laboratory conditions, a cooling fan is used to ensure that the damper does not exceed its maximum operating temperature. A controlled displacement input is imposed on the MR damper and is measured by the internal displacement transducer (LVDT) of the hydraulic actuator. Sinusoidal displacement inputs, with various fixed amplitudes and frequencies, as well as random displacement

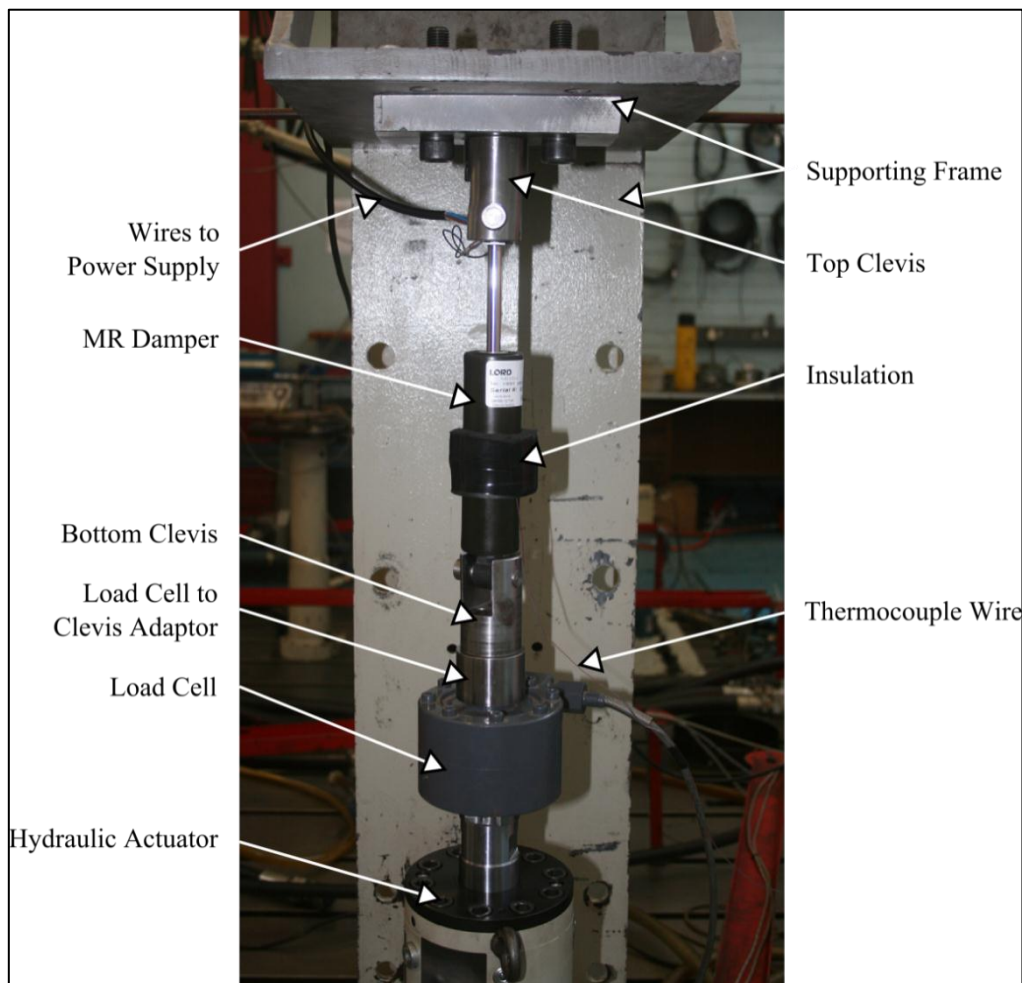


Figure 3-1: MR damper characterization experimental setup.

inputs are used. Table 3–1, p3.3 shows a list of displacement inputs imposed on the MR damper as well as the current supplied to the damper during experimental work. For a sinusoidal displacement input of constant amplitude and frequency the current through the damper is measured and increased by increments of 0.2A or 0.25A, ranging from 0A to 2A. The force exerted by the damper is measured by the load cell, and the temperature of the damper casing is measured using a thermocouple that is insulated from the atmosphere. The damper displacement, damping force, input current, and damper casing temperature are measured using an electronic data acquisition (eDAQ) system at a sampling frequency of 500Hz using a linear-phase low-pass filter with a roll-off start frequency of 167Hz. The relative velocity over the damper is calculated using backward difference numerical differentiation.

An example of two sets of measured data is shown in Figure 3-2, p3.4. The measured temperature, input current, damping force and input displacement are shown as a function of time. A 35mm stroke at 0.8Hz sinusoidal displacement input is imposed on the MR damper. The current input to the

**Table 3–1: Displacement excitation imposed on MR damper for damper characterization.**

	Stroke [mm]	Frequency [Hz]	Current [A] ; Increment [A]		Stroke [mm]	Frequency [Hz]	Current [A] ; Increment [A]
1	64	0.10	0.0-2.0 ; 0.2	24	30	7.00	1.0
2	60	0.10	1.0	25	28	1.40	0.0-2.0 ; 0.2
3		0.20	0.0-2.0 ; 0.2	26		2.00	
4		0.25	1.0	27	22	2.20	0.0-2.0 ; 0.2
5		0.50		28		2.80	
6		1.00		29		3.40	
7		2.00	0.0-2.0 ; 0.25	30		4.00	
8		2.50	1.0	31		4.60	
9		3.00		32	5.00	0.0-2.0 ; 0.2	
10		3.50		33	5.60		
11		55	0.40	0.0-2.0 ; 0.2	34		6.00
12	35	0.60	0.0-2.0 ; 0.2	35	20		7.00
13		0.80		36	8.00		
14		1.00		37	9.00		
15		1.20		38	10.00		
16	30	0.10	1.0	39	10	12.00	0.0-2.0 ; 0.2
17		0.50		40	6	13.00	0.0-2.0 ; 0.2
18		1.00		41	5	14.00	0.0-2.0 ; 0.2
19		2.00	42	15.00			
20		3.00	0.0-2.0 ; 0.25	43	2	18.00	0.0-2.0 ; 0.2
21		4.00	1.0	44		20.00	
22		5.00		45		Random #1	
23		6.00		46	Random #2	0.0-2.0 ; 0.25	

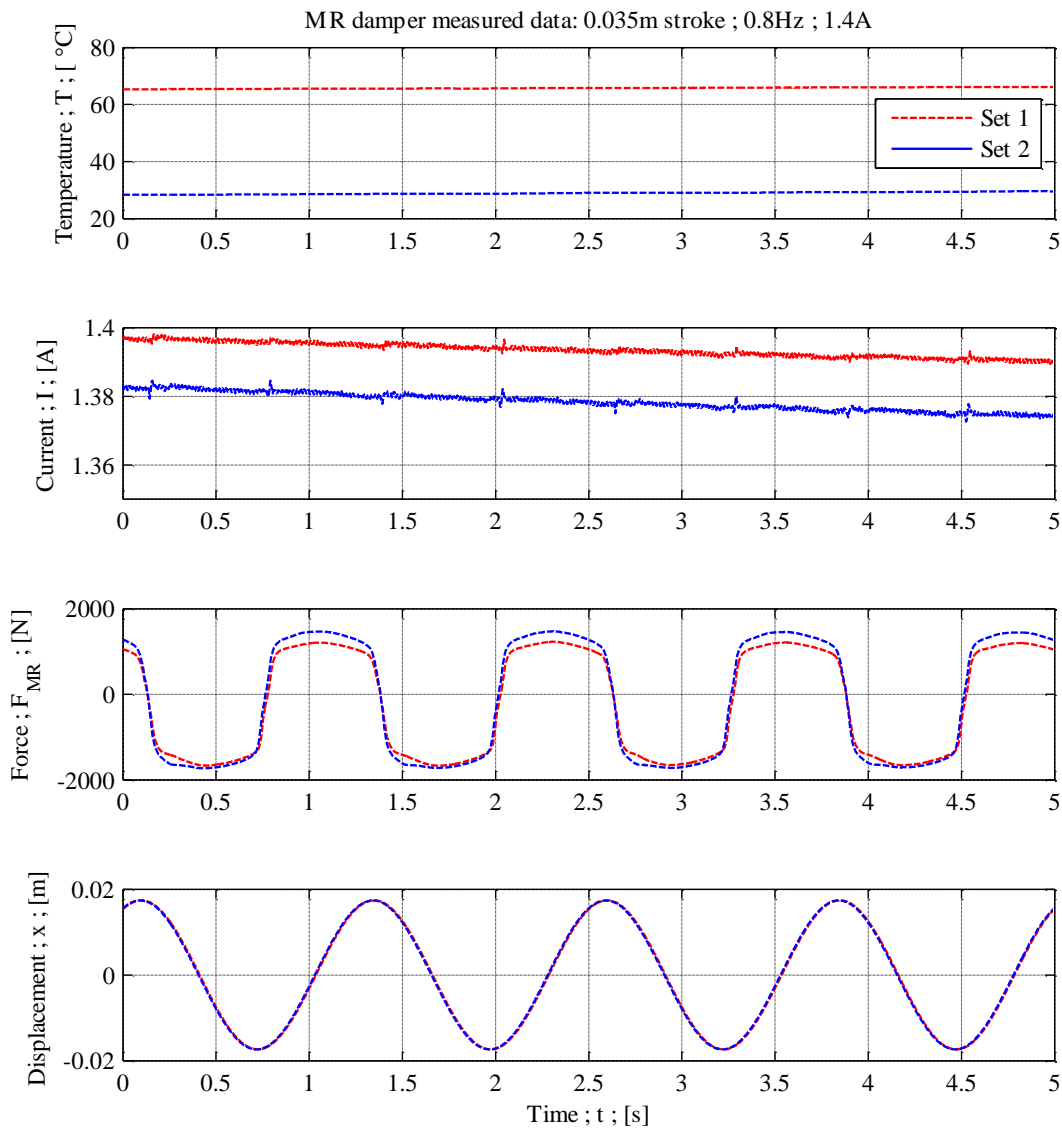


**Figure 3-2: An example of measured MR damper data.**

damper is approximately 1.4A. As the electromagnetic coil in the damper piston heats up, the resistance of the coil increases, resulting in a corresponding current drop. The peak force exerted by the MR damper in the two data sets is 1.2kN, and 1.5kN respectively. The measured peak force in the second set is higher even though a lower input current is supplied to the MR damper. This phenomenon is attributed to a higher viscosity of the MR fluid at lower temperatures. These results clearly demonstrate the significant influence of temperature on the damping characteristics of the MR damper used in this study.

The force-displacement and force-velocity response of the damper to a sinusoidal displacement input of 30mm amplitude at a frequency of 2Hz is shown in Figure 3-3, p3.5 and Figure 3-4, p3.5. There are several remarkable characteristics associated with the data collected from the MR dampers

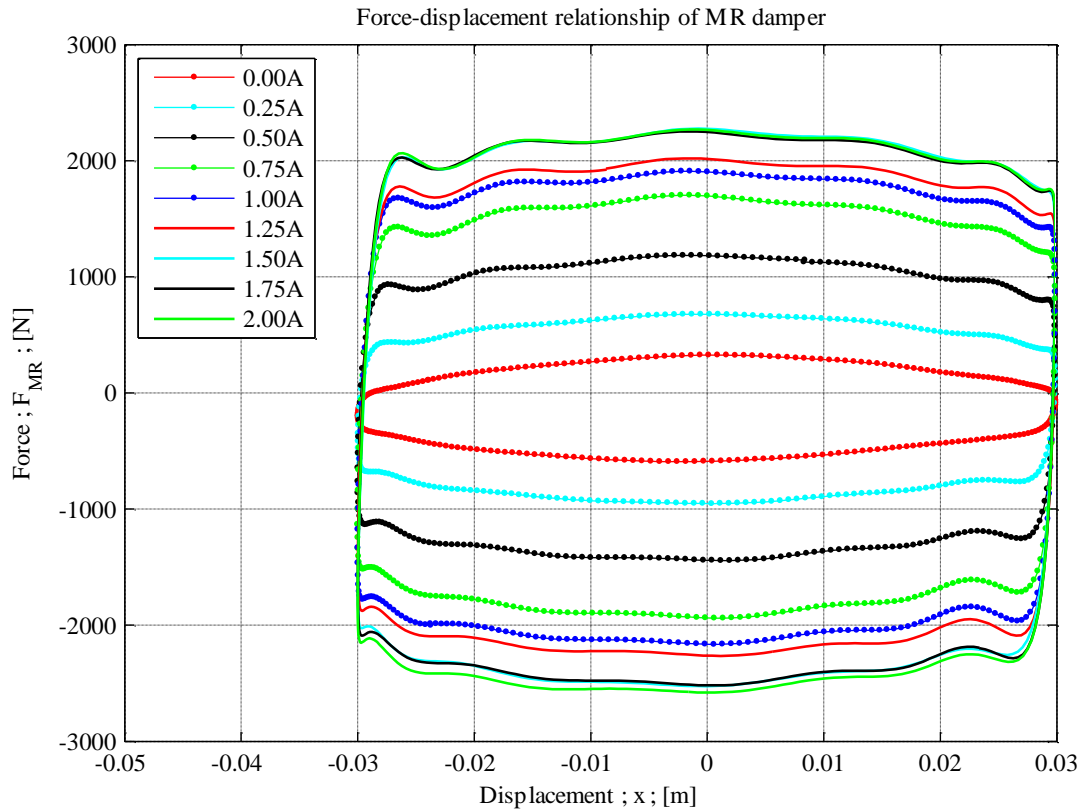


Figure 3-3: Measured force-displacement response to 30mm amplitude and 2Hz sinusoidal excitation.

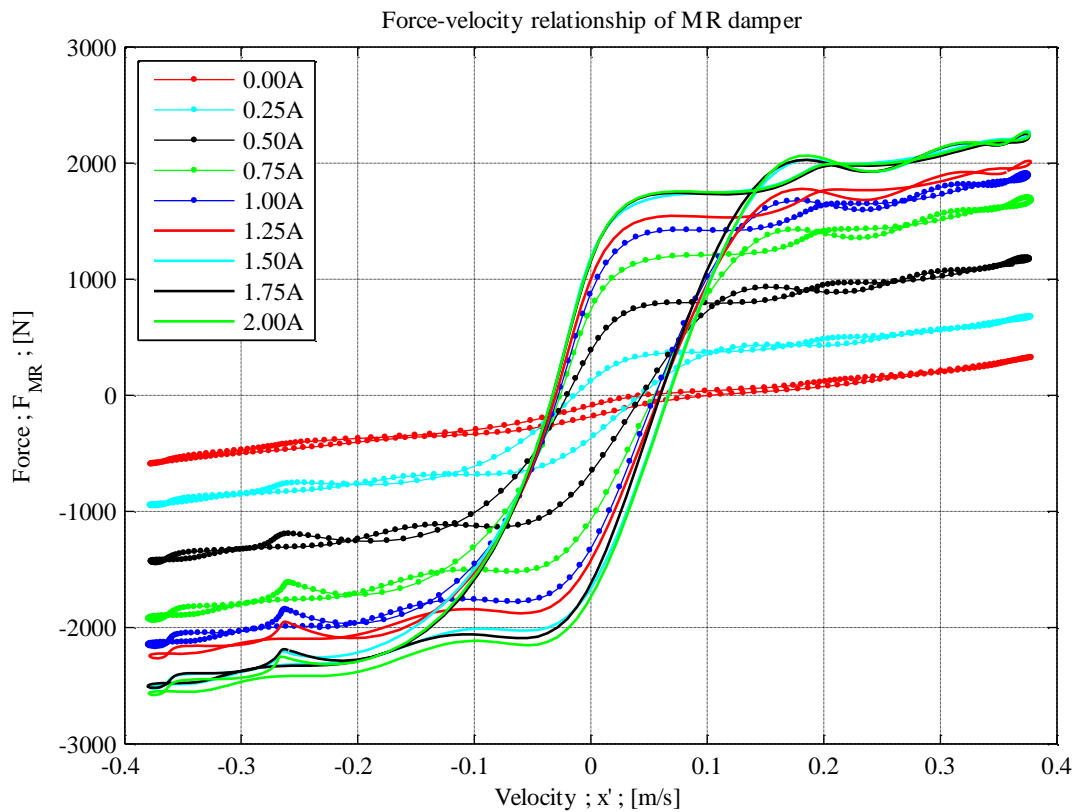


Figure 3-4: Measured force-velocity response to 30mm amplitude and 2Hz sinusoidal excitation.

for this study. The most desirable characteristic is an increase in damping force as the current level is increased. Due to this exceptional characteristic MR dampers are implemented in semi-active control applications where variable damping is desired. MR dampers exhibit hysteresis which proceeds counter clockwise with increasing time. The current supplied to the MR damper, as well as the excitation conditions (including frequency and amplitude), influence the mean slope of the hysteretic curve of the force-velocity relationship, referred to as the viscous damping coefficient. The hysteretic curve can be separated into two distinct regions: the pre-yield region at low velocities where strong hysteresis is present, and the post yield region at higher velocities where the relationship approximates linearity. The existence of a roll-off effect between the pre-yield and post-yield regions can also be detected, where the force decreases swiftly when the velocity approaches zero. According to **Wang and Liao (2011)** the roll-off effect is caused by blow-by of fluid between the damper piston and cylinder which is introduced to eliminate harshness of ride in vehicle applications. When no current is supplied to the damper, it behaves passively, as can be deduced from the near elliptical force-displacement relationship and almost linear force-velocity relationship at 0.0A. The peak force as well as the nonlinearity in the force-velocity relationship are dependent on excitation frequency, as shown in Figure 3-5, p3.6. It can also be observed from Figure 3-3 and Figure 3-4, p3.5, that current levels above 1.25A do not result in a significant increase in damping force. This characteristic is commonly referred to as saturation. The damping characteristics of the MR damper are shown in Figure 3-6, p3.7. These are generated by plotting the maximum force as a function of the corresponding velocity for various displacement inputs. The maximum damping force obtained experimentally is 2.65kN, and the force range is approximately 1.7kN.

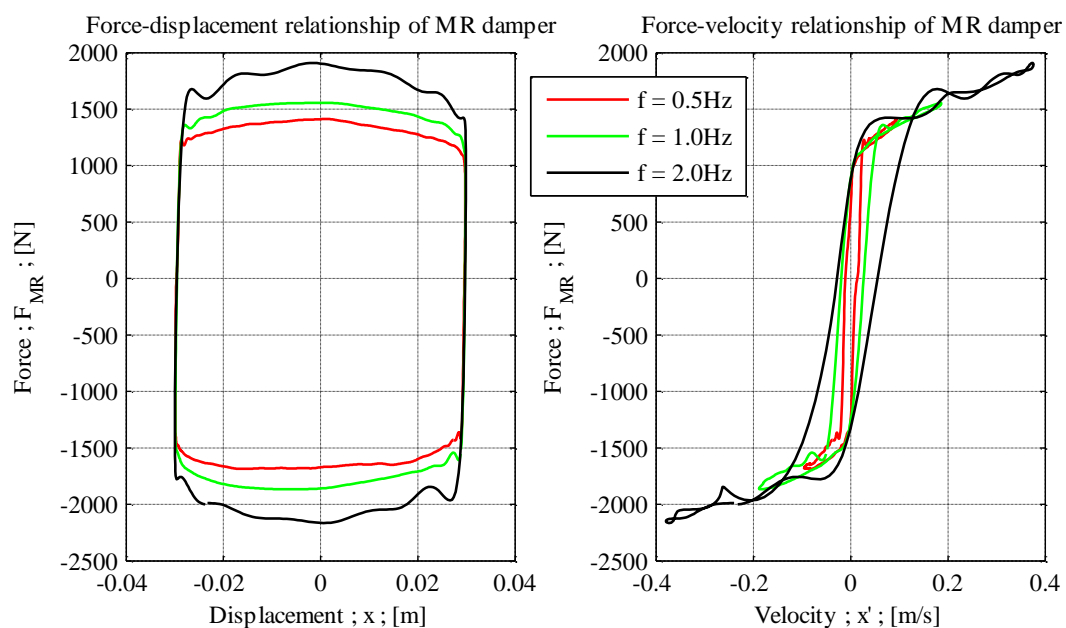


Figure 3-5: Measured force-displacement and force-velocity response to a 30mm sinusoidal excitation at 1.0A.



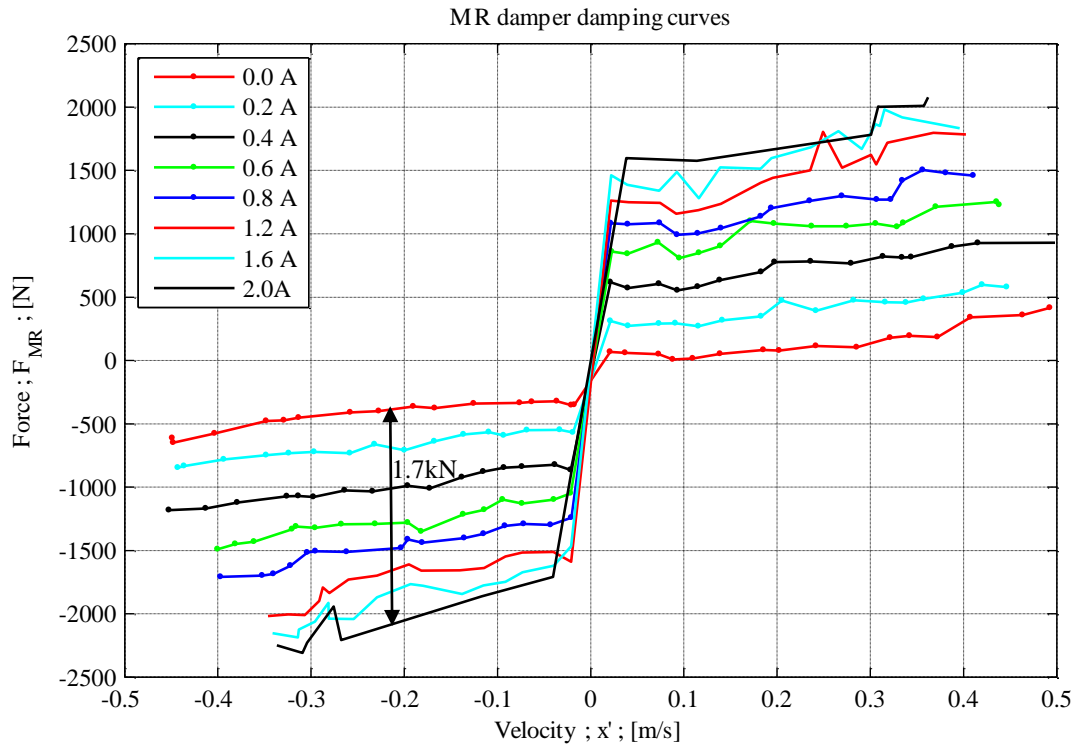


Figure 3-6: MR damper damping curves.

### 3.2 Magnetorheological Damper Models

In this subsection the MR damper models that have been developed in this study, by implementing the least squares based constrained nonlinear optimization, are discussed. The model parameters are computed so as to minimize the RMS error of the difference between the MR damper force predicted by the model ( $\hat{F}$ ) and the measured MR damper force ( $F$ ). The RMS error is computed as:

$$RMS\ Error = \sqrt{\frac{1}{n} \sum_{i=1}^n (\hat{F}_i - F_i)^2} \quad [34]$$

The accuracy of the models is compared by using the normalised RMS (NRMS) error, computed as follows:

$$NRMS\ Error = \frac{RMS\ Error}{|F_{max}|} \times 100\% \quad [35]$$

MR damper models are developed by using sinusoidal displacement inputs at fixed amplitude and frequency, and at multiple current inputs. In addition to sinusoidal displacement inputs, random displacement signals are also implemented. These random displacement signals, shown in Figure 3-7, p3.8, were generated to exhibit frequency content that is similar to the MR damper displacements that were measured when the test vehicle was driven over a rough Belgian paving track (designed to excite a vehicle at a wide range of frequencies) at Gerotek Test Facilities (Gerotek, 2008).

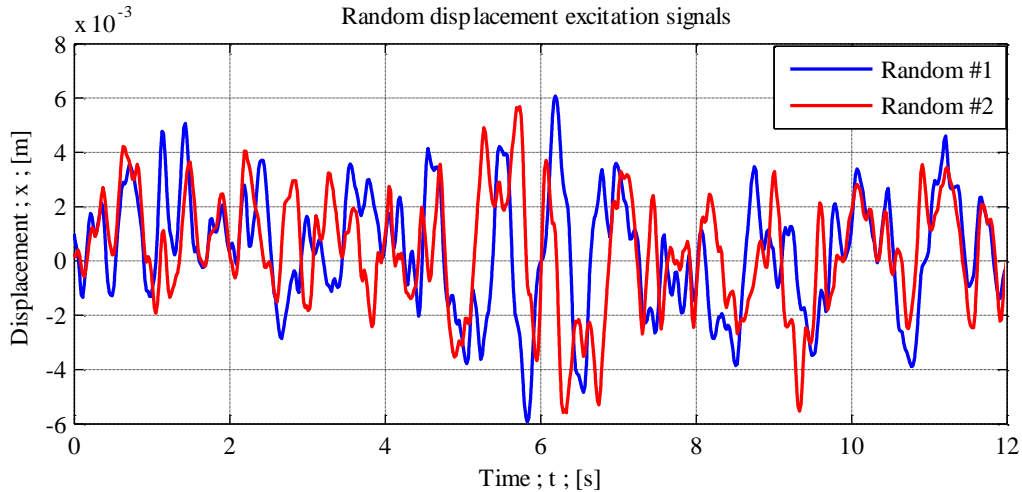


Figure 3-7: Random displacement excitation signals used for MR damper model development.

### 3.2.1 Bingham Model

The computed Bingham model parameters (previously discussed in Section 2.6.3.1.1, p2.24) for a sinusoidal displacement input of 30mm amplitude at 2Hz with input currents of 0.50A and 1.75A are shown in Table 3–2, p3.9. Two models have been developed, each applicable to a different current setting. From Figure 3-8, p3.9 it can be deduced that although the Bingham model represents the force-displacement relationship of the MR damper fairly accurately, it is not capable of accurately representing the force-velocity characteristic. This is especially the case at low velocities since the Bingham model can't model hysteretic behaviour.

An additional difficulty concerning the Bingham model is its computational burden due to the discontinuity caused by the signum function. This issue can be addressed by replacing the signum function with a continuous function that approximates its behaviour. This results in the modified Bingham model given by:

$$F = F_c \left[ \frac{2 \tan^{-1}(b\dot{x})}{\pi} \right] + c\dot{x} + F_0 \quad [36]$$

The parameters in Equation 36 have the same physical meaning as in Equation 9, p2.24, with the addition of  $b$ , which is a form factor (**Guglielmino et al. 2008**).

The accuracy of the Bingham model is improved by introducing hysteresis as a result of delaying the velocity signal (**Guglielmino et al. 2008**). The computed modified and delayed Bingham model parameters for a sinusoidal displacement input of 30mm amplitude at 2Hz with an input current of 0.50A and 1.75A are given in Table 3–3, p3.10. The force-displacement and force-velocity relationship predicted by the model is shown in Figure 3-9, p3.10. The model corresponding to 0.50A is delayed by 0.008s and the model corresponding to 1.75A is delayed by 0.012s. It can be discerned that the force-displacement relationship shows an improvement, and the model exhibits hysteretic

**Table 3–2: Computed Bingham model parameters for a sinusoidal input.**

Bingham Model Parameters						
30mm amplitude at 2Hz sinusoidal input						
Parameters		$F_c$	$c$	$F_0$	RMS Error [N] (NRMS Error)	
Input Current	0.50A	519.76	2241.1	-137.56	200.55	(13.81%)
	1.75A	955.85	4186.6	-147.02	503.55	(19.99%)

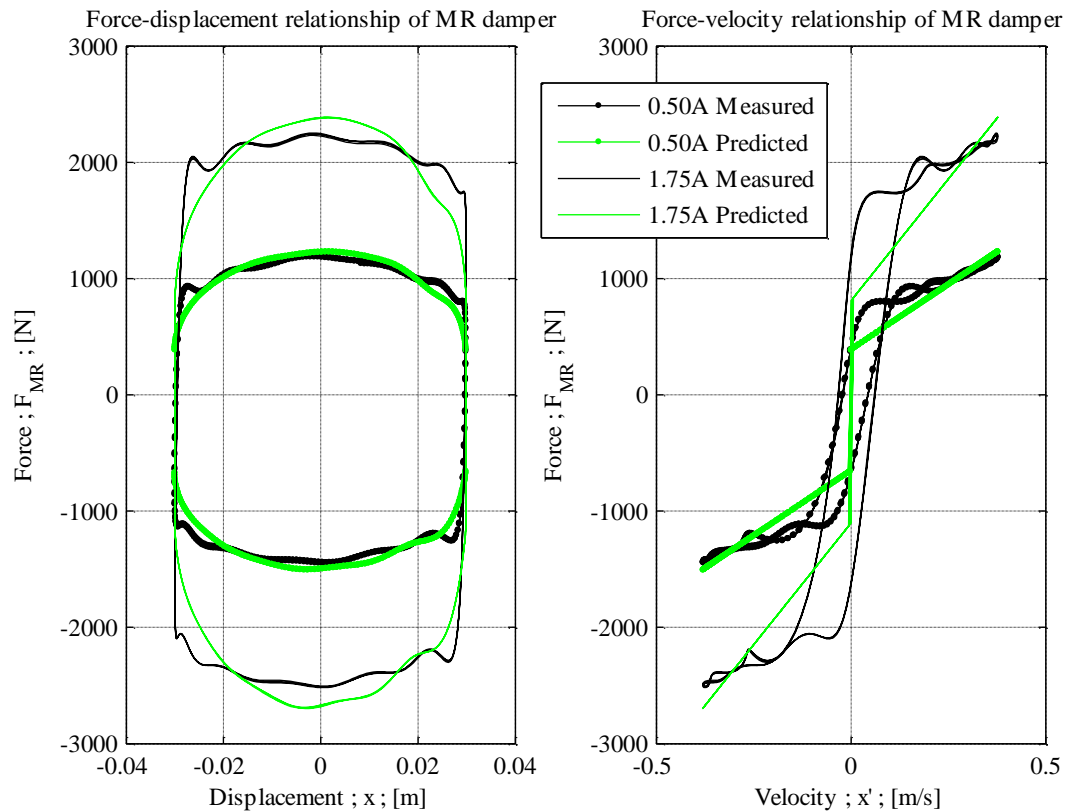


**Figure 3-8: Bingham model force-displacement (left) and force-velocity (right) relationship in response to 30mm amplitude at 2Hz sinusoidal excitation.**

behaviour, with a very smooth roll-over from the pre-yield to the post-yield region in the force-velocity relationship. As indicated by the RMS and NRMS errors in Table 3–2, p3.9, and Table 3–3, p3.10, the modified and delayed Bingham model yields a significant improvement in accuracy.

Various modified Bingham models for increasing current levels have been developed using a random displacement input signal. The computed modified Bingham model parameters are provided in Table 3–4, p3.11. The delay in the velocity is altered for each model so as to yield the most accurate results. For current levels of 1.00A and higher the optimal delay remains constant at 0.006s,

**Table 3–3: Computed modified and delayed Bingham model parameters for a sinusoidal input.**

Modified and Delayed Bingham Model Parameters								
30mm amplitude at 2Hz sinusoidal input								
Parameters		$F_c$	$b$	$c$	$F_0$	RMS Error [N] (NRMS Error)		Delay [s]
Input Current	0.50A	1000.4	38.134	852.65	-140.46	53.180	(3.66%)	0.008
	1.75A	2185.9	34.537	621.95	-157.34	100.10	(3.97%)	0.012

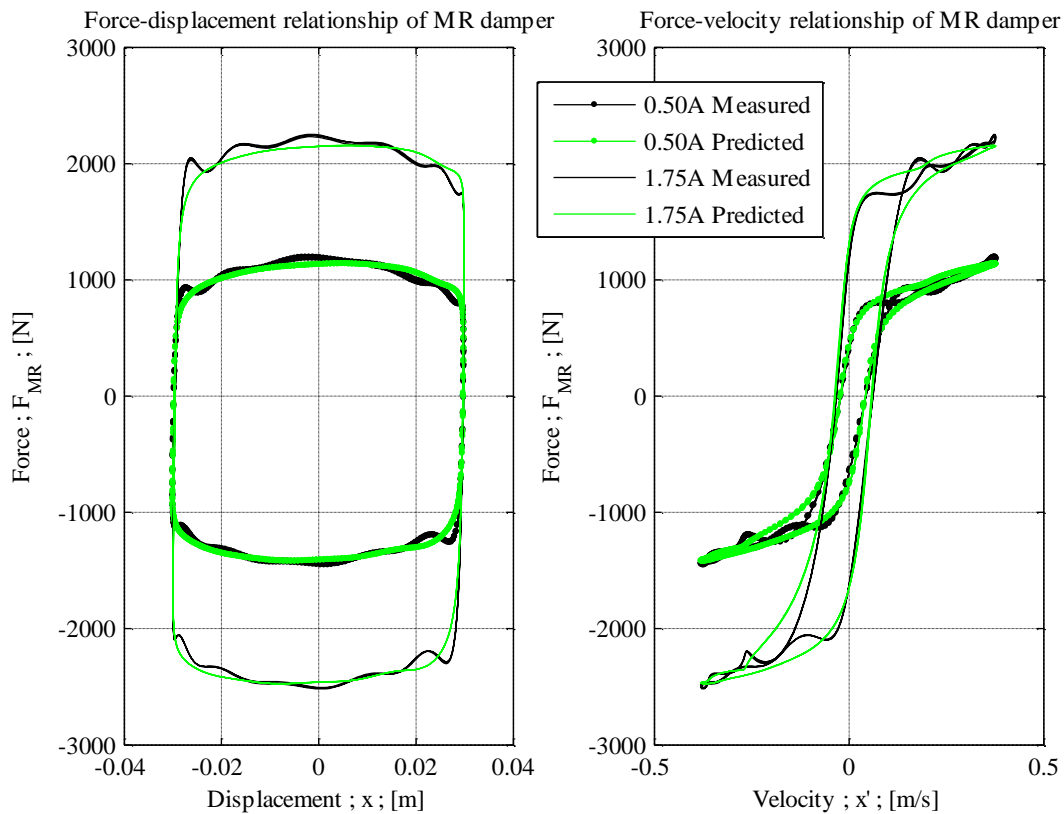


**Figure 3-9: Modified and delayed Bingham model force-displacement (left) and force-velocity (right) relationship in response to 30mm amplitude at 2Hz sinusoidal excitation.**

while the delay varies between 0.0s and 0.004s for lower current levels. As the current is increased, the accuracy of the model deteriorates as demonstrated by higher NRMS error values in Table 3–4. The force-displacement and force-velocity relationship predicted by the Bingham model at 1.50A is compared to measured data in Figure 3-10, p3.11, and the top graph of Figure 3-11, p3.12. The model exhibits a wide hysteretic loop which covers the majority of the measured force-velocity data.

The applicability of each Bingham model from Table 3–4, p3.11 to changes in the displacement input has been investigated by implementing the models developed using Random input #1 on Random input #2. The RMS and NRMS errors of the models implemented on Random input #2 are

compared to the original errors in Table 3–5, p3.12. Similar velocity delays are introduced in the models. The RMS errors of the models implemented on Random signal #1 and #2 are comparable, and it is thus concluded that the modified and delayed Bingham models of the respective current

**Table 3–4: Computed modified and delayed Bingham model parameters for a random input signal.**

Modified and Delayed Bingham Model Parameters							
Random (#1) signal input							
Parameters	$F_c$	$b$	$c$	$F_0$	RMS Error [N] (NRMS Error)		Delay [s]
0.00A	796.65	1.7133	413.41	-135.74	23.424	(3.44%)	0
0.25A	571.35	19.413	779.37	-133.71	94.238	(8.60%)	0.002
0.50A	1169.5	19.457	630.58	-142.89	190.32	(11.56%)	0.004
0.75A	1654.3	19.142	597.38	-153.15	267.01	(12.77%)	0.004
1.00A	1947.2	19.497	536.13	-176.75	333.82	(14.05%)	0.006
1.25A	2137.2	19.109	496.22	-189.53	366.36	(14.33%)	0.006
1.50A	2295.6	18.556	397.51	-199.99	396.35	(14.83%)	0.006
1.75A	2398.4	18.293	349.64	-210.50	419.04	(15.21%)	0.006
2.00A	2473.2	17.599	436.05	-229.44	449.97	(15.82%)	0.006

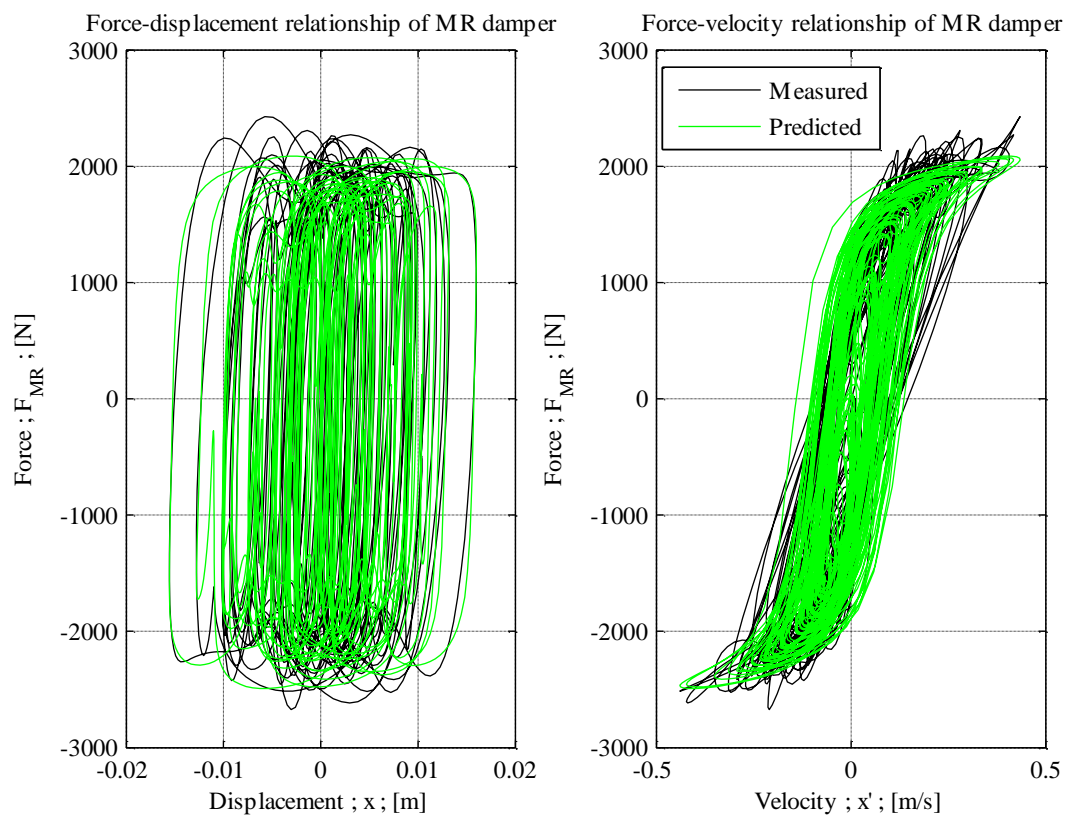


**Figure 3-10: Modified and delayed Bingham model predicted force-displacement (left) and force-velocity (right) relationship in response to a random displacement input signal at 1.50A.**

Table 3-5: Modified and delayed Bingham model predicted force RMS and NRMS errors for random input signals.

Modified and Delayed Bingham Model Errors						
Signals	Random #1			Random #2		
	RMS Error [N] (NRMS Error)	Delay [s]		RMS Error [N] (NRMS Error)	Delay [s]	
Input Current	0.00A	23.424 (3.44%)	0	25.937 (3.08%)	0	
	0.25A	94.238 (8.60%)	0.002	99.641 (8.08%)	0.002	
	0.50A	190.32 (11.56%)	0.004	201.69 (11.45%)	0.004	
	0.75A	267.01 (12.77%)	0.004	279.40 (12.65%)	0.004	
	1.00A	333.82 (14.05%)	0.006	349.94 (14.00%)	0.004	
	1.25A	366.36 (14.33%)	0.006	389.49 (14.58%)	0.006	
	1.50A	396.35 (14.83%)	0.006	435.73 (15.07%)	0.006	
	1.75A	419.04 (15.21%)	0.006	464.40 (15.65%)	0.006	
	2.00A	449.97 (15.82%)	0.006	461.55 (15.71%)	0.006	

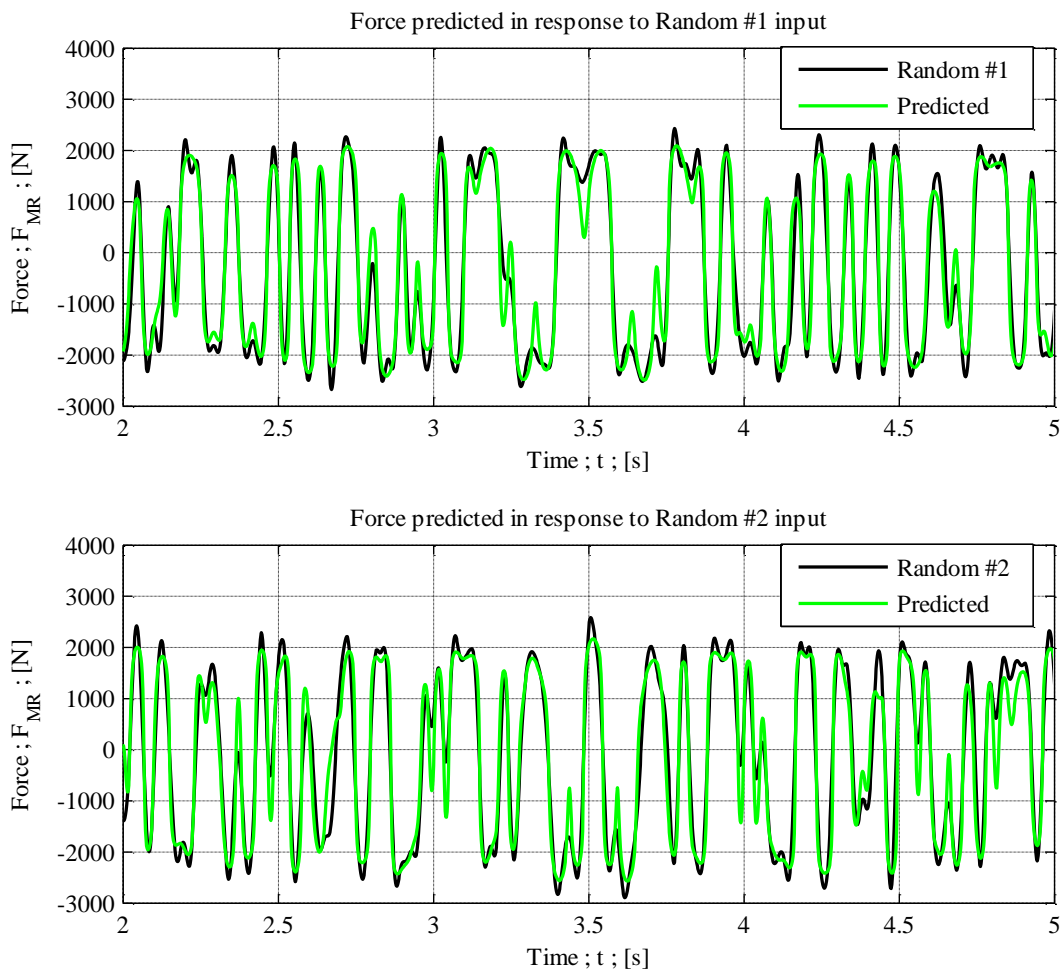


Figure 3-11: Comparison of measured MR damper forces and forces predicted by modified and delayed Bingham model developed using Random #1 input at 1.50A.

levels will deliver similar results when implemented on random displacement inputs of similar frequency content. The MR damper force predicted at 1.50A (see Table 3–4) is compared to the measured force in response to the two random input displacements in Figure 3-11, p3.12.

### 3.2.2 Bouc-Wen Model

The computed Bouc-Wen model parameters (previously discussed in Section 2.6.3.1.2, p2.24) for a sinusoidal displacement input of 30mm amplitude at 2Hz with current settings of 0.50A and 1.75A are shown in Table 3–6, p3.13. The Bouc-Wen model implemented in this study is not voltage dependent (although complex voltage dependent models can be found in the literature) therefore separate models have been developed for each current setting. It may be noted that for the development of the Bouc-Wen models, the displacement and velocity inputs have been converted to mm and mm/s, resulting in damping and stiffness coefficients in Ns/mm and N/mm (in Table 3–6, p3.13 and Table 3–7, p3.14). The force-displacement and force-velocity relationships predicted by the Bouc-Wen models are shown in Figure 3-12, p3.14. The force-velocity relationship of the MR damper is accurately represented by the Bouc-Wen models, including the transition between the pre-yield and post-yield regions. The transition is shaper than exhibited by the modified and delayed Bingham models (refer to Figure 3-9, p3.10), and the Kwok models (refer to Figure 3-15, p3.17). From the measured MR damper force-velocity response (Figure 3-4, p3.5) it is apparent that the MR damper exhibits strain-softening behaviour, therefore  $\beta > 0$  (Guglielmino et al. 2008).

Bouc-Wen models applicable to several discrete current levels have been developed using a random displacement excitation signal. The computed Bouc-Wen model parameters are given in Table 3–7, p3.14. The accuracy of the models remains between 10.57% and 11.25% for supplied current levels above 0.50A. This is a significant improvement over the capabilities of the modified Bingham- and Kwok models, which show a deterioration in accuracy with increasing current levels. The force-displacement and force-velocity relationship predicted by the Bouc-Wen model at 1.50A is shown in Figure 3-13, p3.15, and the top graph of Figure 3-14, p3.16. It is demonstrated that sufficient hysteresis is obtained in comparison to the Kwok model (Figure 3-16, p3.19).

**Table 3–6: Computed Bouc-Wen model parameters for a sinusoidal input.**

<b>Bouc-Wen Model Parameters</b>										
30mm amplitude at 2Hz sinusoidal input										
Parameters		$c$	$k$	$\alpha$	$\gamma$	$\beta$	$n$	$A$	$F_0$	RMS Error [N] (NRMS Error)
Input Current	0.50A	1.5883	1.0914	312.86	1.2951	1.1295	1.9083	11.818	-141.28	69.733 (4.80%)
	1.75A	2.3488	2.1274	608.80	1.8997	1.1930	1.0173	7.818	-142.18	144.68 (5.74%)

The applicability of the developed Bouc-Wen models (from Table 3–7, p3.14) to changes in excitation conditions are evaluated by implementing the models on a different random displacement input (instead of the input used to develop the models). The RMS and NRMS errors of models

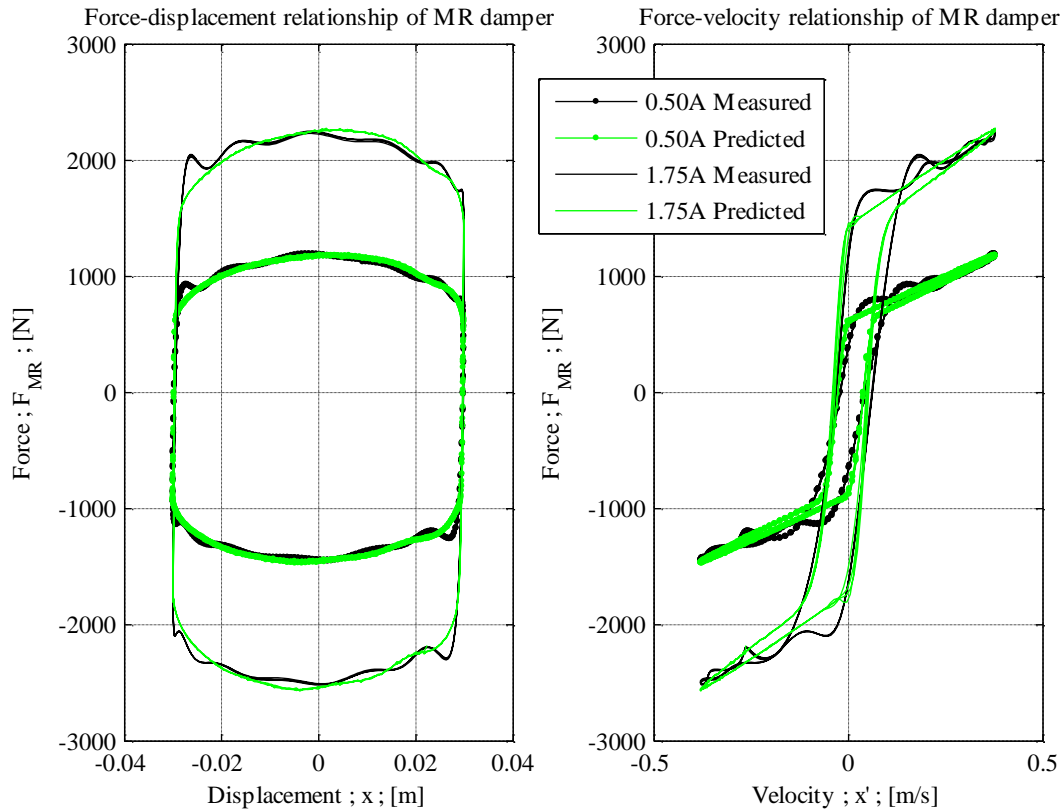


Figure 3-12: Bouc-Wen model force-displacement (left) and force-velocity (right) relationship in response to 30mm amplitude at 2Hz sinusoidal excitation.

Table 3–7: Computed Bouc-Wen model parameters for a random input signal.

Bouc-Wen Model Parameters										
Random (#1) signal input										
Parameters	$c$	$k$	$\alpha$	$\gamma$	$\beta$	$n$	$A$	$F_0$	RMS Error [N] (NRMS Error)	
0.00A	1.1834	0.0000	3.3549	1.1644	1.0275	2.1517	22.185	-135.48	23.500	(3.45%)
0.25A	1.8118	0.0713	139.94	1.3247	1.0606	2.3332	10.421	-136.00	94.400	(8.62%)
0.50A	2.4984	0.0718	327.86	0.9157	0.8237	2.3986	6.3104	-138.99	179.37	(10.89%)
0.75A	2.7915	1.1425	327.16	1.5311	0.7378	1.4002	9.3525	-137.34	235.31	(11.25%)
1.00A	3.3343	1.2334	310.97	0.8832	0.7244	1.2930	7.7126	-136.72	259.56	(10.93%)
1.25A	3.5942	1.2330	329.88	0.8717	0.6292	1.1579	6.4695	-136.88	277.70	(10.86%)
1.50A	3.6001	1.2689	343.61	1.1214	0.5025	1.0928	6.7952	-135.44	282.65	(10.57%)
1.75A	3.6895	1.5417	344.68	1.0934	0.6927	1.0996	7.6236	-137.51	299.44	(10.87%)
2.00A	3.6911	1.8978	371.66	0.8501	0.5031	1.2371	6.8306	-138.92	304.11	(10.69%)



developed using the first random input and implemented on a new random displacement input signal are given in Table 3–8, p3.16. The NRMS errors of the models implemented on displacement input Random #1 and Random #2 are comparable. Thus, a Bouc-Wen model developed using a random displacement signal of specified frequency content can be seen as applicable to other random signals with similar frequency content. The time trace of the MR damper force predicted at 1.50A is compared to the measured force in response to the two random displacement inputs in Figure 3-14, p3.16.

The shape of the Bouc-Wen hysteretic loop depends on the parameters  $\gamma$ ,  $\beta$ ,  $n$  and  $A$ . The identification of these parameters is not a straightforward task as the dependence between the hysteretic operator,  $z$ , and the shape parameters is highly nonlinear and is not easy to investigate analytically. Although parameter identification through least square based methods (implemented in this study) is possible, it may not be the best choice. Black-box optimization methods based on artificial intelligence techniques such as genetic algorithms could yield more accurate results (Guglielmino et al. 2008).

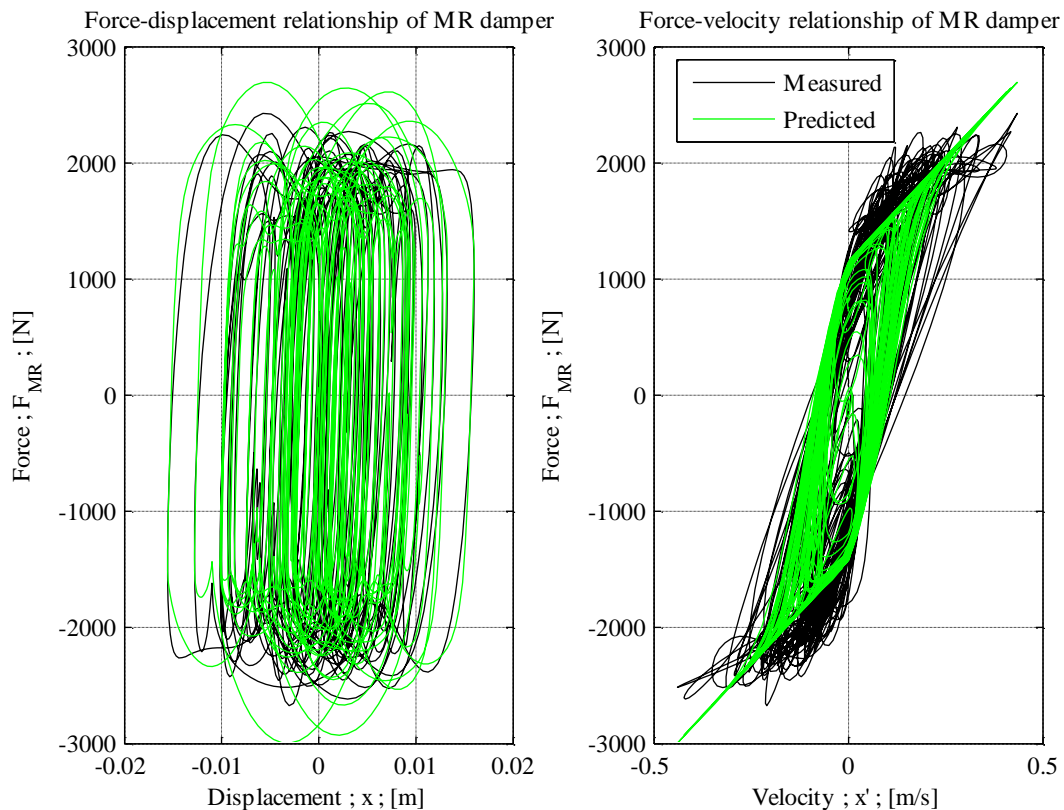


**Figure 3-13: Bouc-Wen model predicted force-displacement (left) and force-velocity (right) relationship in response to a random displacement input signal at 1.50A.**

**Table 3–8: Bouc-Wen model predicted force RMS and NRMS errors for random input signals.**

<b>Bouc-Wen Model Errors</b>					
Signals	Random #1		Random #2		
	RMS Error [N] (NRMS Error)		RMS Error [N] (NRMS Error)		
Input Current	0.00A	23.500	3.45%	25.340	3.01%
	0.25A	94.400	8.62%	94.007	7.62%
	0.50A	179.37	10.89%	177.54	10.07%
	0.75A	235.31	11.25%	235.62	10.67%
	1.00A	259.56	10.93%	262.23	10.49%
	1.25A	277.70	10.86%	280.07	10.48%
	1.50A	282.65	10.57%	284.14	9.83%
	1.75A	299.44	10.87%	311.11	10.48%
	2.00A	304.11	10.69%	301.70	10.27%

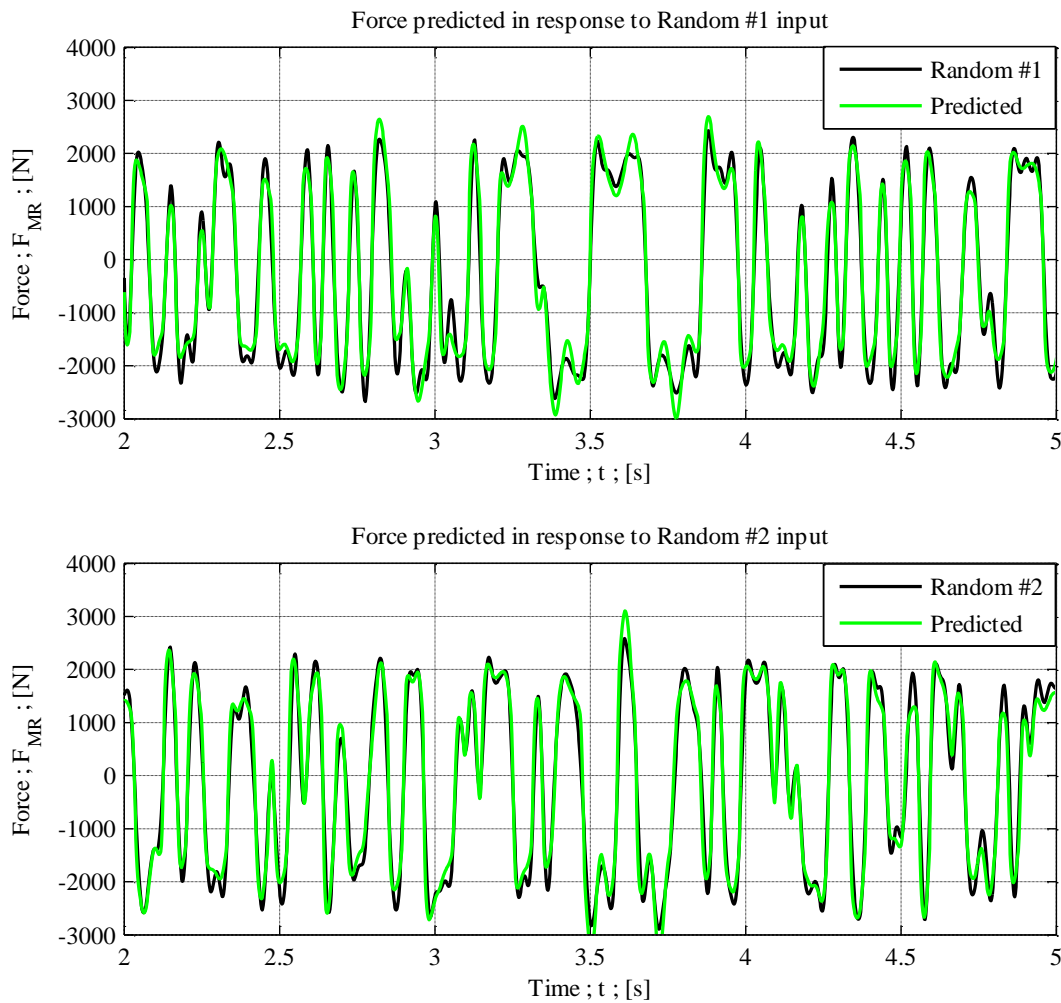


**Figure 3-14: Comparison of measured MR damper forces and forces predicted by Bouc-Wen model developed using Random #1 input at 1.50A.**

### 3.2.3 Kwok Model

The computed Kwok model parameters (previously discussed in Section 2.6.3.1.4, p2.26) for a sinusoidal displacement input of 30mm amplitude at 2Hz with an input current of 0.50A and 1.75A are given in Table 3–9, p3.18. Since the Kwok model is not voltage or current dependent, re-characterization for changes in current settings is required. Therefore two models have been developed for the different current settings. The predicted force-displacement and force-velocity relationships of the Kwok models for the MR damper used in this study are compared to measured data in Figure 3-15, p3.17. As compared to the Bingham model, the Kwok model accurately represents the force-velocity relationship largely due to a thorough exhibition of hysteretic behaviour. The transition between the pre-yield and post-yield regions is more accurate than predicted by the modified and delayed Bingham models and the Bouc-Wen models.

Several Kwok models have been developed using a random displacement input signal, with a new model for each current setting. The computed Kwok model parameters are provided in Table 3–10, p3.18. As the current level increases the accuracy of the Kwok model deteriorates. The force-displacement and force-velocity relationship predicted by the Kwok model at 1.50A is

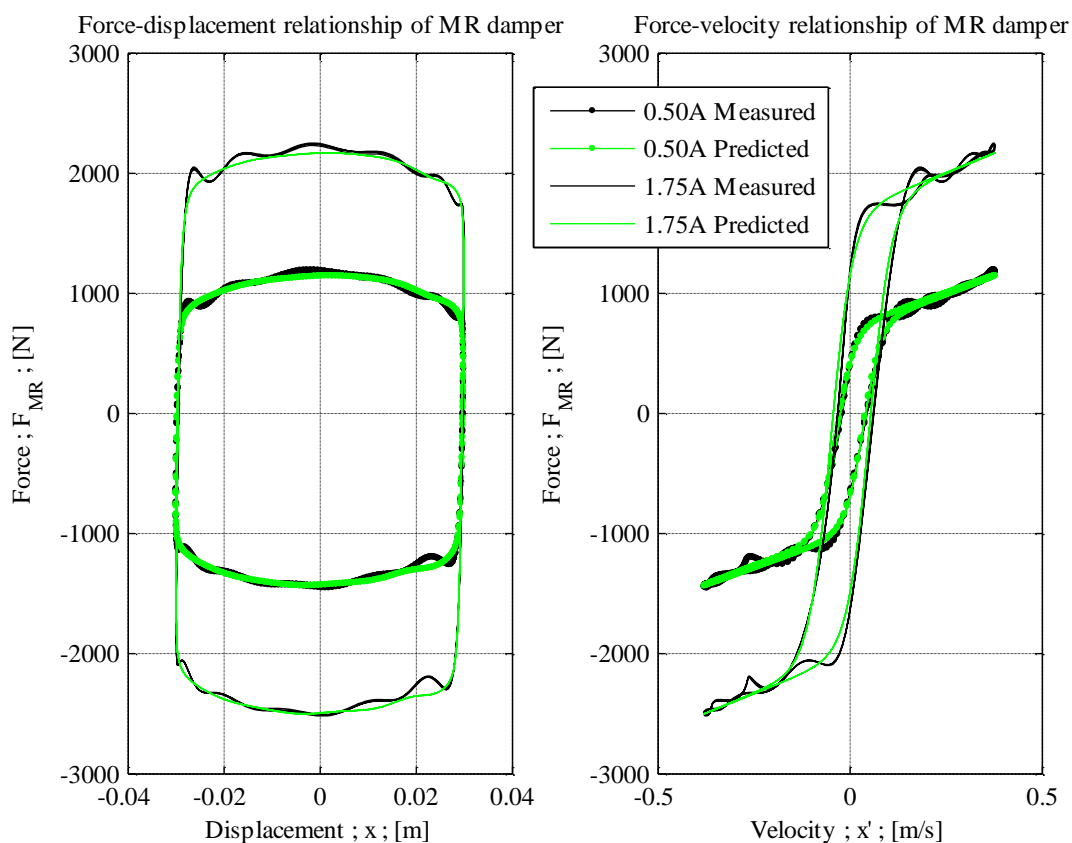


**Figure 3-15: Kwok model force-displacement (left) and force-velocity (right) relationship in response to 30mm amplitude at 2Hz sinusoidal excitation.**

compared to measured data in Figure 3-16, p3.19, and the top graph of Figure 3-17, p3.20. While the measured data exhibit a wide force range for a given velocity, the Kwok model is much more limited, the hysteresis behaviour is narrow and constrained to a loop.

To further evaluate the applicability of each Kwok model to changes in the displacement input signal, each of the models developed using Random signal #1 was implemented on a different random displacement input signal, referred to as Random signal #2. The RMS and NRMS errors of models developed from Random #1 (Table 3–10, p3.18) and implemented on a new random displacement input signal are given in Table 3–11, p3.19. The RMS and NRMS errors of the models implemented on Random signal #1 and #2 are comparable, and it is thus concluded that the Kwok models will deliver similar results when implemented on random displacement inputs with comparable frequency content. The MR damper force predicted by the model at 1.50A (from Table 3–10) is compared to the measured forces in response to the random input displacements in Figure 3-17, p3.20.

**Table 3–9: Computed Kwok model parameters for a sinusoidal input.**

<b>Kwok Model Parameters</b>								
30mm stroke at 2Hz sinusoidal input								
Parameters		$c$	$k$	$\alpha$	$\beta$	$\delta$	$F_0$	RMS Error [N] (NRMS Error)
Input Current	0.50A	1183.9	393.30	841.34	21.814	0.7497	-143.08	37.217 (2.56%)
	1.75A	1308.5	118.42	1839.7	17.820	0.9016	-163.19	91.956 (3.65%)

**Table 3–10: Computed Kwok model parameters for a random input signal.**

<b>Kwok Model Parameters</b>								
Random (#1) signal input								
Parameters		$c$	$k$	$\alpha$	$\beta$	$\delta$	$F_0$	RMS Error [N] (NRMS Error)
Input Current	0.00A	1238.6	52.410	-2.366	2.6295	5.4019	-135.96	23.671 (3.47%)
	0.25A	1191.2	77.829	393.29	15.344	0.1381	-135.11	101.01 (9.22%)
	0.50A	1497.4	112.87	801.31	14.677	0.1548	-147.01	229.92 (13.96%)
	0.75A	1872.5	294.79	1103.3	14.774	0.2010	-161.42	358.32 (17.14%)
	1.00A	2133.0	474.50	1284.3	14.363	0.2345	-189.57	472.42 (19.89%)
	1.25A	2329.6	663.97	1372.3	14.297	0.2524	-204.67	546.95 (21.40%)
	1.50A	2461.4	829.59	1433.0	14.218	0.2670	-216.81	605.33 (22.65%)
	1.75A	2875.7	36356	1374.8	15.282	0.1335	-241.55	626.20 (22.73%)
	2.00A	2793.1	2070.5	1472.0	13.975	0.2890	-246.40	701.92 (24.67%)

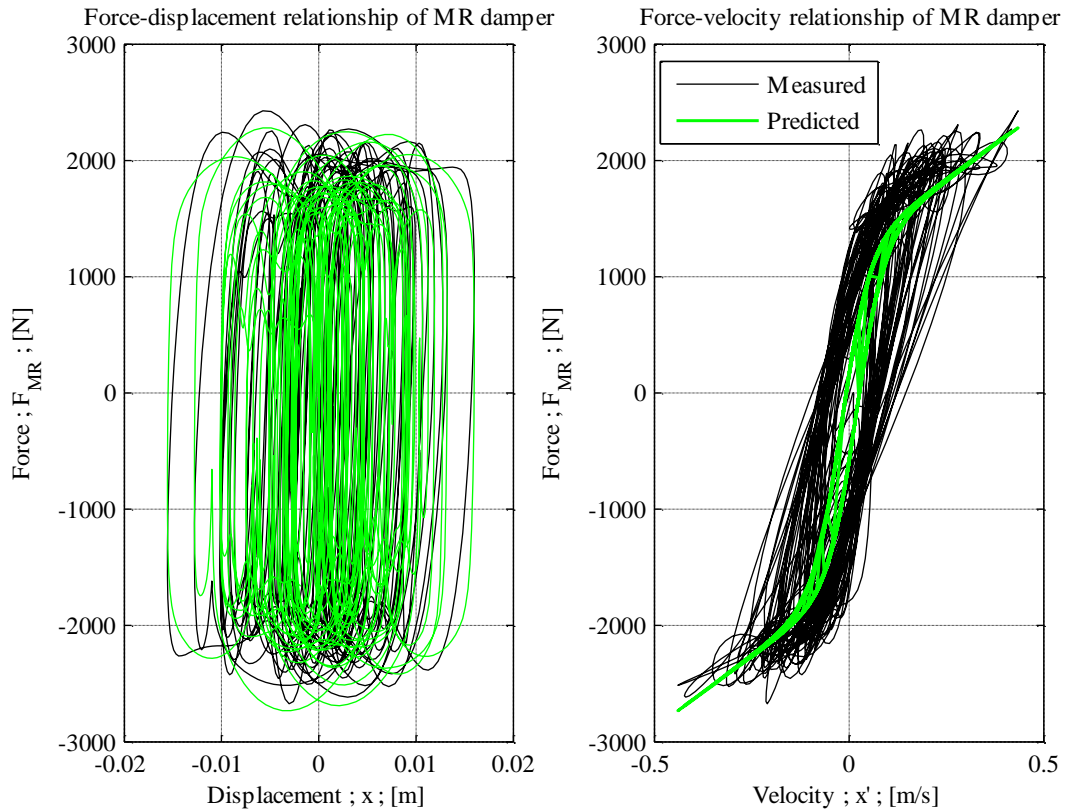


**Figure 3-16: Kwok model predicted force-displacement (left) and force-velocity (right) relationship in response to a random displacement input signal at 1.50A.**

**Table 3–11: Kwok model predicted force RMS and NRMS errors for random input signals.**

<b>Kwok Model Errors</b>				
Signals	Random #1		Random #2	
	RMS Error [N]	(NRMS Error)	RMS Error [N]	(NRMS Error)
Input Current	0.00A	23.671 (3.47%)	25.050 (2.97%)	
	0.25A	101.01 (9.22%)	106.47 (8.63%)	
	0.50A	229.92 (13.96%)	236.90 (13.44%)	
	0.75A	358.32 (17.14%)	363.50 (16.46%)	
	1.00A	472.42 (19.89%)	469.81 (18.79%)	
	1.25A	546.95 (21.40%)	540.45 (20.23%)	
	1.50A	605.33 (22.65%)	638.58 (22.08%)	
	1.75A	626.20 (22.73%)	672.65 (22.66%)	
	2.00A	701.92 (24.67%)	670.45 (22.82%)	

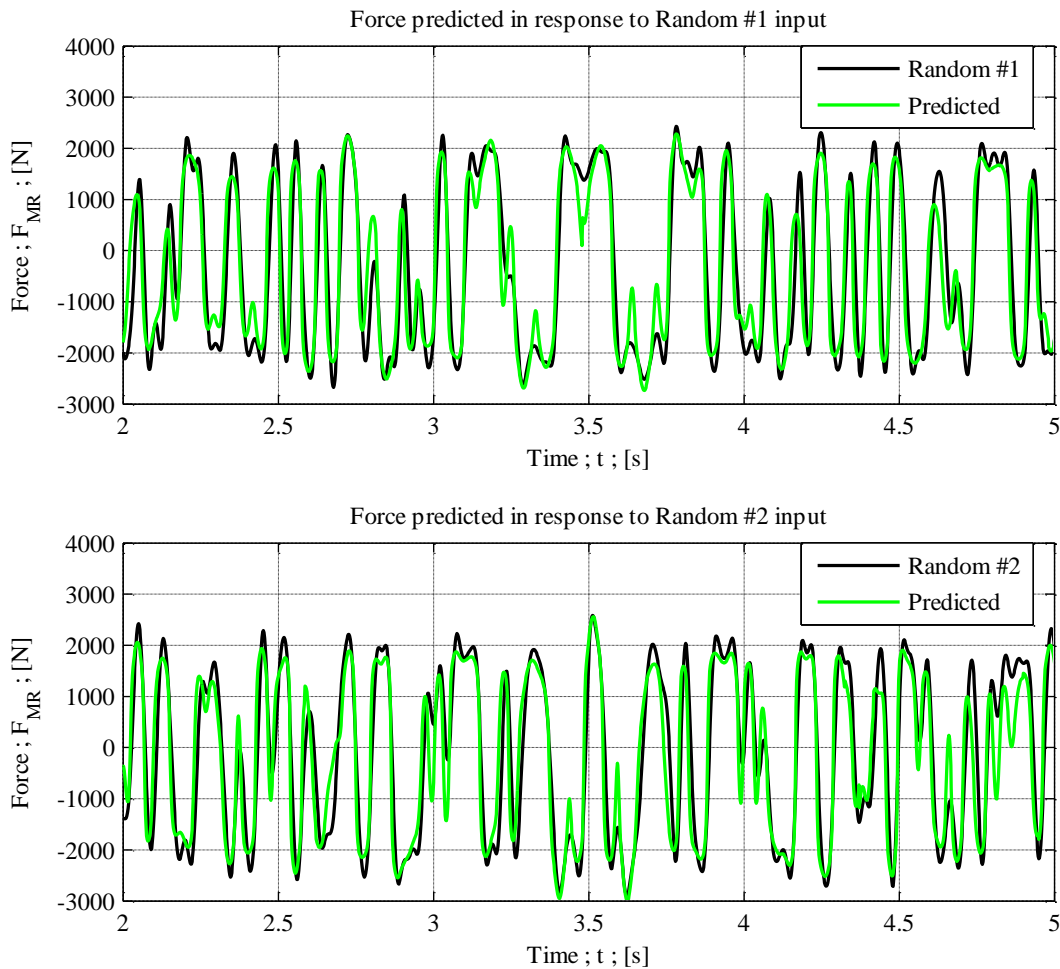


**Figure 3-17: Comparison of measured MR damper forces and forces predicted by Kwok model developed using Random #1 input at 1.50A.**

### 3.2.4 Polynomial Model

Since the polynomial model (previously discussed in Section 2.6.3.2.1, p2.27) is current dependent, one model has been developed for several current settings. The data set used to develop this model consists of a concatenation of measured data sets at six supplied current levels: 0.0A, 0.25A, 0.5A, 0.75A, 1.25A, and 1.75A. Two models are developed using a 30mm amplitude sinusoidal displacement input at 2Hz. In the first model the concatenated data set is used to determine the model parameters, and in the second model the hysteresis loops of the concatenated data set are divided into positive and negative displacement loops and a set of parameters is obtained for each loop. Usually the data set is divided according to positive and negative acceleration, but since the excitation is purely sinusoidal, displacement and acceleration are  $180^\circ$  out of phase and either can be used to separate the data. The displacement signal is used as it is the most readily available quantity and is relatively noise free.

The computed polynomial model parameters of the first model (implementing the data as it is), are given in Table 3–12, p3.21, and the corresponding predicted force-displacement and force-velocity relationship is compared to measured data in Figure 3-18, p3.21. The model order has been determined iteratively and  $n = 7$  has been chosen for this model, based on the trade-off between

**Table 3–12: Computed polynomial model parameters.**

<b>Polynomial Model Parameters</b>			
30mm amplitude at 2Hz sinusoidal input			
$i$	$b_i$	$c_i$	RMS Error [N] (NRMS Error)
0	-129.82	-66.87	316.50 (12.57%)
1	4299.9	9487.3	
2	-1023.5	2157.2	
3	$-76.311 \times 10^3$	$-148.1 \times 10^3$	
4	$15.682 \times 10^3$	$-21.256 \times 10^3$	
5	$750.52 \times 10^3$	$1.231 \times 10^6$	
6	$-62.226 \times 10^3$	$67.164 \times 10^3$	
7	$-2.4073 \times 10^6$	$-3.6607 \times 10^6$	

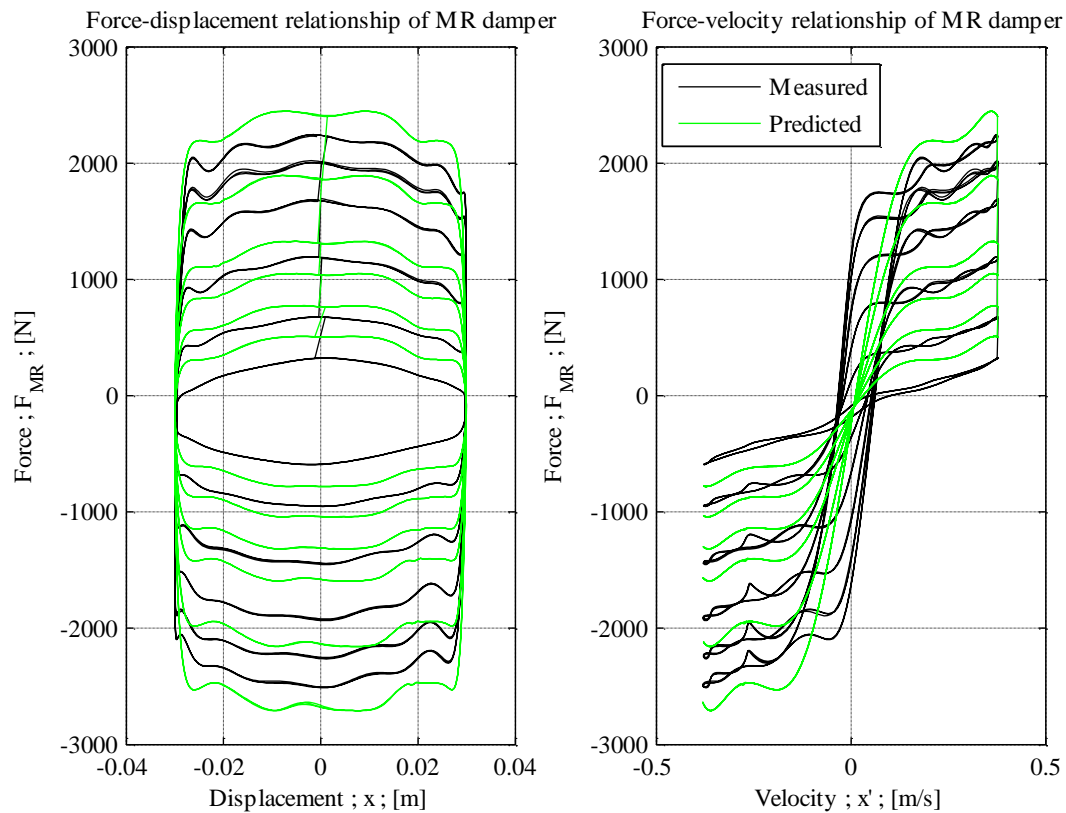


**Figure 3-18: Polynomial model force-displacement (left) and force-velocity (right) relationship in response to 30mm amplitude at 2Hz sinusoidal excitation.**

improvement in accuracy with a decrease in model stability as the model order increases. In Figure 3-18 it is demonstrated that the predicted force-velocity relationship does not exhibit hysteresis. Also, the post-yield force magnitudes predicted for each current setting is either over- or under- estimated by the polynomial model. However, a smooth roll-over from post-yield to pre-yield regions is presented.

The computed polynomial model parameters of the displacement divided data sets are given in Table 3–13, p3.22. A model order of  $n = 8$  has been chosen since there is no appreciable increase in accuracy obtained with higher order models. As can be deduced from the lower NRMS error in Table 3–13, this model more accurately represents the MR damper behaviour, mainly due to the presence of hysteresis, as shown in Figure 3-19, p3.23. As with the previous model, the post-yield force magnitudes predicted for each current setting is either over- or under- estimated. At high current levels, the post-yield region is poorly represented by this model. Although the polynomial model is less accurate than some of the other models presented in this section, its main benefit is its applicability to a wider range of input conditions, eliminating the need for re-characterization for changes in current settings. The polynomial model is also easily invertible and can therefore be used to prescribe the MR damper current setting.

A polynomial model has also been developed using a random displacement excitation signal, referred to as Random signal #1. As with the previous models, the measured data used to develop the model consists of a concatenation of measured data sets at the same six supplied current levels. Since the excitation is random, the data is divided into positive and negative acceleration groups. The computed polynomial model parameters of the acceleration divided data sets are provided in

**Table 3–13: Computed displacement determined polynomial model parameters.**

<b>Displacement Determined Polynomial Model Parameters</b>						
30mm amplitude at 2Hz sinusoidal input						
Positive Displacement			Negative Displacement			RMS Error [N] (NRMS Error)
$i$	$b_i$	$c_i$	$i$	$b_i$	$c_i$	
0	-42.346	567.21	0	-217.55	-734.60	195.49 (7.76%)
1	4221.3	$10.070 \times 10^3$	1	4384.5	8865.4	
2	-9030.8	$-46.475 \times 10^3$	2	7223.0	$54.213 \times 10^3$	
3	$-72.699 \times 10^3$	$-169.56 \times 10^3$	3	$-80.153 \times 10^3$	$-123.11 \times 10^3$	
4	$228.38 \times 10^3$	$1.1038 \times 10^6$	4	$-206.73 \times 10^3$	$-1.2177 \times 10^6$	
5	$708.46 \times 10^3$	$1.4826 \times 10^6$	5	$805.96 \times 10^3$	$958.28 \times 10^3$	
6	$-2.1140 \times 10^6$	$-10.028 \times 10^6$	6	$2.1014 \times 10^6$	$10.623 \times 10^6$	
7	$-2.2716 \times 10^6$	$-4.6045 \times 10^6$	7	$-2.6406 \times 10^6$	$-2.7780 \times 10^6$	
8	$6.5187 \times 10^6$	$30.920 \times 10^6$	8	$-6.9118 \times 10^6$	$-31.625 \times 10^6$	



Table 3–14, p3.23. The model order is determined iteratively with  $n = 7$  chosen as most appropriate. The force-displacement and force-velocity relationship predicted by the polynomial model is compared to measured data in Figure 3-20, p3.24, and the time trace of the measured force is

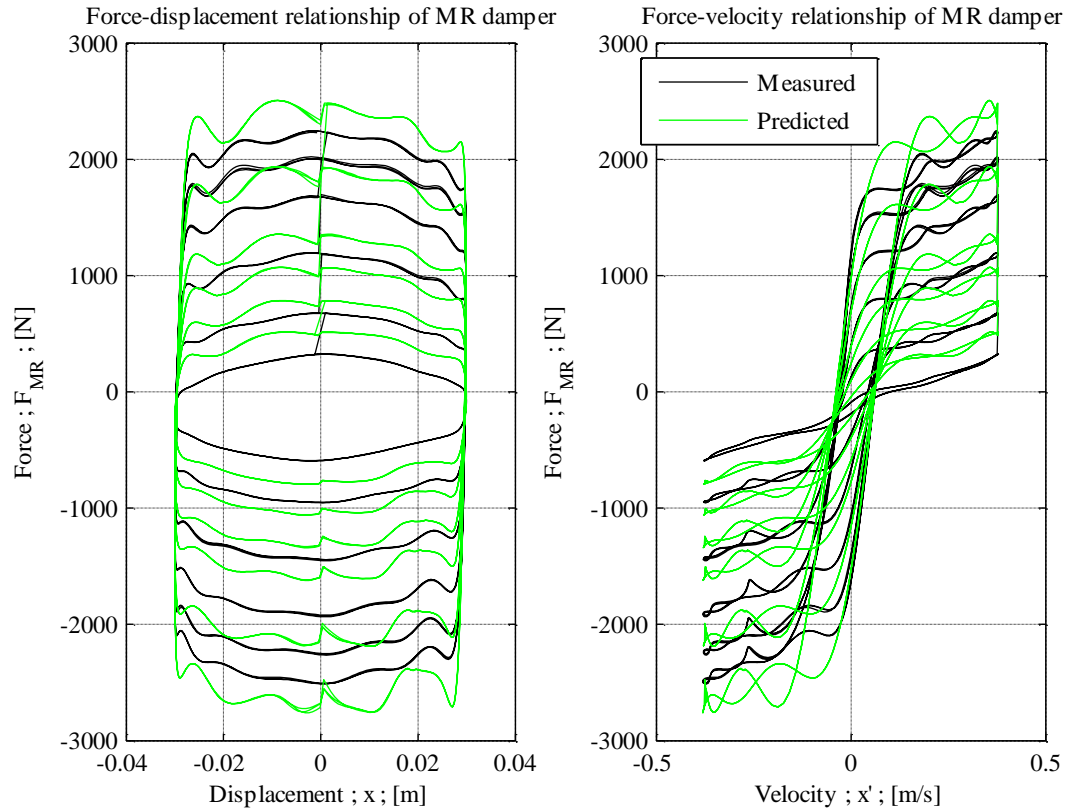
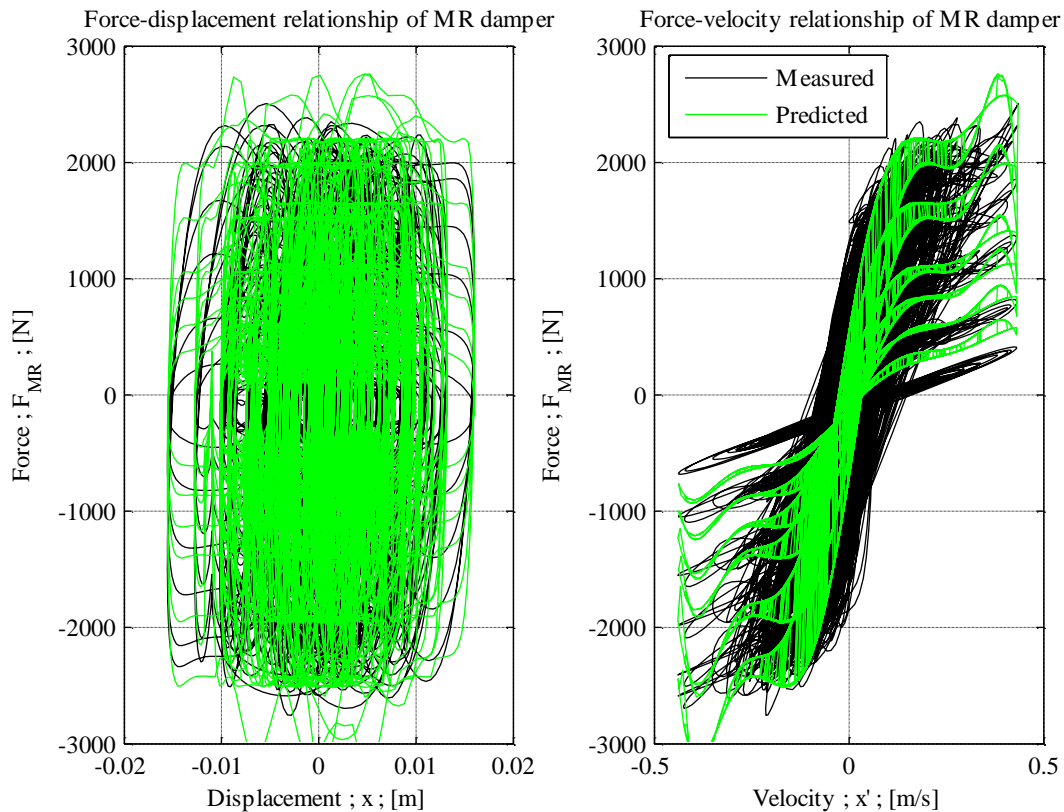


Figure 3-19: Displacement determined polynomial model force-displacement (left) and force-velocity (right) relationship in response to 30mm amplitude at 2Hz sinusoidal excitation.

Table 3–14: Computed acceleration determined polynomial model parameters.

Acceleration Determined Polynomial Model Parameters						
Random (#1) signal input						
Positive Acceleration			Negative Acceleration			RMS Error [N] (NRMS Error)
$i$	$b_i$	$c_i$	$i$	$b_i$	$c_i$	
0	-117.85	-326.63	0	-116.07	365.55	377.53 (13.71%)
1	4315.6	9308.9	1	3455.7	8962.3	
2	-222.42	$-14.651 \times 10^3$	2	-2344.5	$15.878 \times 10^3$	
3	$-69.371 \times 10^3$	$-161.68 \times 10^3$	3	$-42.468 \times 10^3$	$-147.56 \times 10^3$	
4	9960.6	$-278.95 \times 10^3$	4	$56.155 \times 10^3$	$305.33 \times 10^3$	
5	$637.92 \times 10^3$	$1.4131 \times 10^6$	5	$363.02 \times 10^3$	$1.2800 \times 10^6$	
6	$-82.360 \times 10^3$	$2.1054 \times 10^6$	6	$-520.22 \times 10^3$	$-2.5316 \times 10^6$	
7	$-1.8565 \times 10^6$	$-4.0640 \times 10^6$	7	$-1.0018 \times 10^6$	$-3.6935 \times 10^6$	
8	$160.92 \times 10^3$	$-5.4088 \times 10^6$	8	$1.5178 \times 10^6$	$7.1070 \times 10^6$	



**Figure 3-20: Acceleration determined polynomial model predicted force-displacement (left) and force-velocity (right) relationship in response to a random displacement input signal.**

compared to the predicted force in the top graph of Figure 3-21, p3.25. The behaviour of the damper is not accurately represented at high velocities, and the post-yield force magnitude predicted for each current setting is either over- or under- estimated. Also, hysteresis is not adequately represented since the predicted hysteresis curves are too narrow.

To evaluate the applicability of the polynomial model to changes in excitation conditions, the model from Table 3–14, p3.23 is implemented on a different random displacement signal, referred to as Random signal #2. Under certain conditions the model largely overestimates the force, resulting in a high RMS error of 940.48N, (NRMS error of 31.69%). This is shown in Figure 3-21, p3.25. To improve the stability of the model its order can be reduced. For  $n = 5$  the RMS error in response to Random #1 is increased to 387.61N, and the NRMS error is increased to 14.07% (refer to Table 3–14), while the RMS error in response to Random #2 is reduced to 542.97N, and the NRMS error is reduced to 18.29%. However, occasional over-estimation of the force still occurs under the same conditions. A model order as low as  $n = 3$  results in a RMS error of 418.94N (NRMS error of 15.21%) in response to Random #1, and 462.63N (NRMS error of 15.59%) in response to Random #2, without any over-estimation of force.

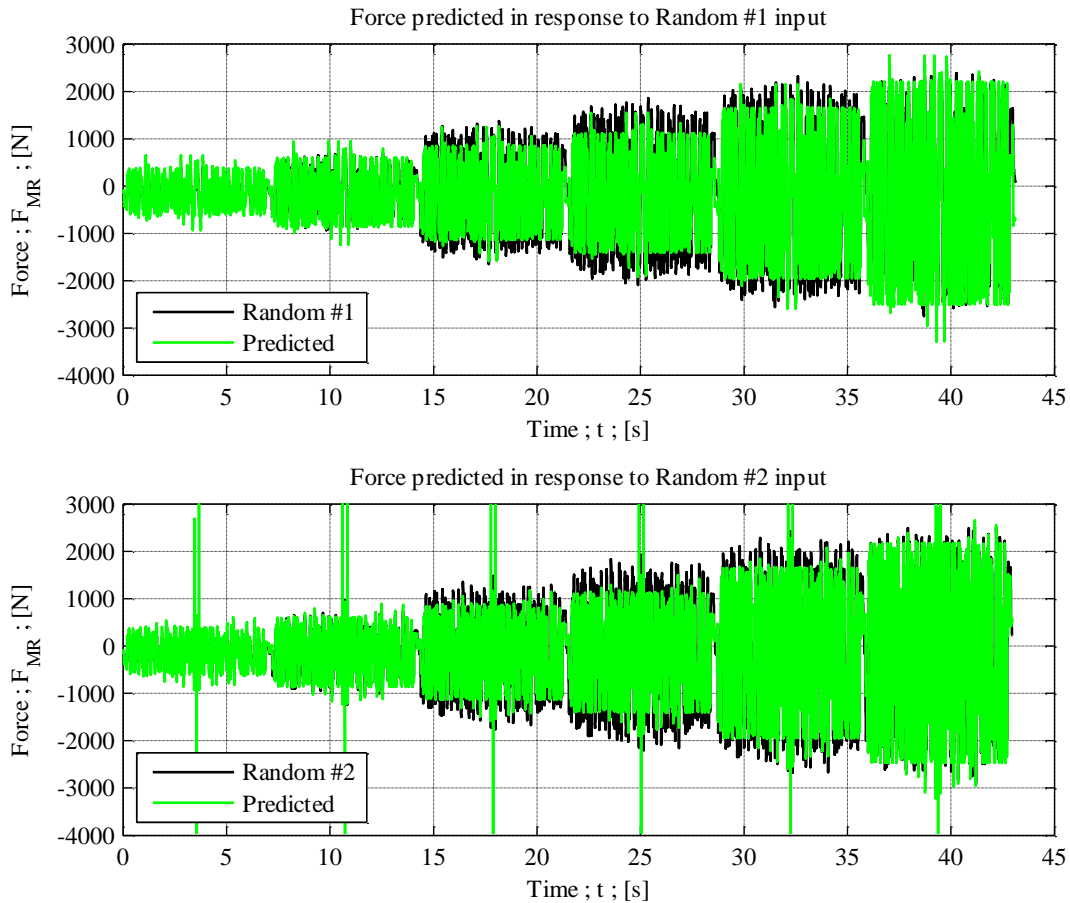


**Figure 3-21: Comparison of measured MR damper forces and forces predicted by polynomial model developed using Random #1 input at several current levels ( $n = 7$ ).**

### 3.2.5 Generalised Batch Least Square (BLS) Model

The composition of the regressor vector for the BLS model (previously discussed in Section 2.6.3.2.2, p2.28) has been chosen arbitrarily. Although the regressor vector developed by **Kaul (2011)** contains measured MR damper force data, measured damping force is not available from the test vehicle used for this study due to specific constraints. Therefore the regressor for the BLS model does not contain any terms related to the measured damping force. The measured current input has been included in the regressor to eliminate the need for re-characterization with a changing current input. To improve representation of saturation at higher current levels, a nonlinearity can be introduced by implementation of a nonlinear current term in the regressor. However, such a model will no longer be invertible. With model invertibility in mind, the power of all the current parameters is chosen to be unity. A constant term is included in the regressor vector in order to model the force-offset due to the accumulator in the MR damper. The regressor vector of the BLS model used in this study is:

$$\phi_t^T = [\dot{x}_t \quad \dot{x}_{t-1} \quad \dot{x}_{t-2} \quad |\dot{x}_t|x_t \quad I_t \quad \dot{x}_t^3 \quad I_t \dot{x}_t \quad I_t \dot{x}_t \quad I_{t-1} \dot{x}_{t-1} \quad \dots \quad I_{t-2} \dot{x}_{t-2} \quad I_t \dot{x}_t^2 \quad I_t \dot{x}_t^3 \quad I_{t-1} \dot{x}_{t-1}^3 \quad I_{t-2} \dot{x}_{t-2}^3 \quad 1] \quad [37]$$

The data set used to develop the BLS models consists of a concatenation of measured data sets at six supplied current levels: 0.0A, 0.25A, 0.5A, 0.75A, 1.25A, and 1.75A. The computed generalised BLS model parameters for a 30mm amplitude at 2Hz sinusoidal excitation are given in Table 3–15, p.3.26, and the model force-displacement and force-velocity relationships are compared to measured

Table 3–15: Computed BLS model parameters for a sinusoidal input.

BLS Model Parameters						
30mm amplitude at 2Hz sinusoidal input						
Parameter	Variable	Value	Parameter	Variable	Value	RMS Error [N] (NRMS Error)
$\hat{\theta}_1$	$\dot{x}_t$	$157.06 \times 10^3$	$\hat{\theta}_9$	$I_{t-1} \dot{x}_{t-1}$	$-116.39 \times 10^3$	287.03 (11.40%)
$\hat{\theta}_2$	$\dot{x}_{t-1}$	$-313.57 \times 10^3$	$\hat{\theta}_{10}$	$I_{t-2} \dot{x}_{t-2}$	$58.754 \times 10^3$	
$\hat{\theta}_3$	$\dot{x}_{t-2}$	$159.15 \times 10^3$	$\hat{\theta}_{11}$	$I_t \dot{x}_t^2$	288.5603	
$\hat{\theta}_4$	$ \dot{x}_t  x_t$	$-18.029 \times 10^3$	$\hat{\theta}_{12}$	$I_t \dot{x}_t^3$	$-393.86 \times 10^3$	
$\hat{\theta}_5$	$I_t$	-30.1617	$\hat{\theta}_{13}$	$I_{t-1} \dot{x}_{t-1}^3$	$825.99 \times 10^3$	
$\hat{\theta}_6$	$\dot{x}_t^3$	$-6.3392 \times 10^3$	$\hat{\theta}_{14}$	$I_{t-2} \dot{x}_{t-2}^3$	$-461.50 \times 10^3$	
$\hat{\theta}_7$	$I_t x_t$	$9.9857 \times 10^3$	$F_0$	1	-136.5418	
$\hat{\theta}_8$	$I_t \dot{x}_t$	$64.238 \times 10^3$				

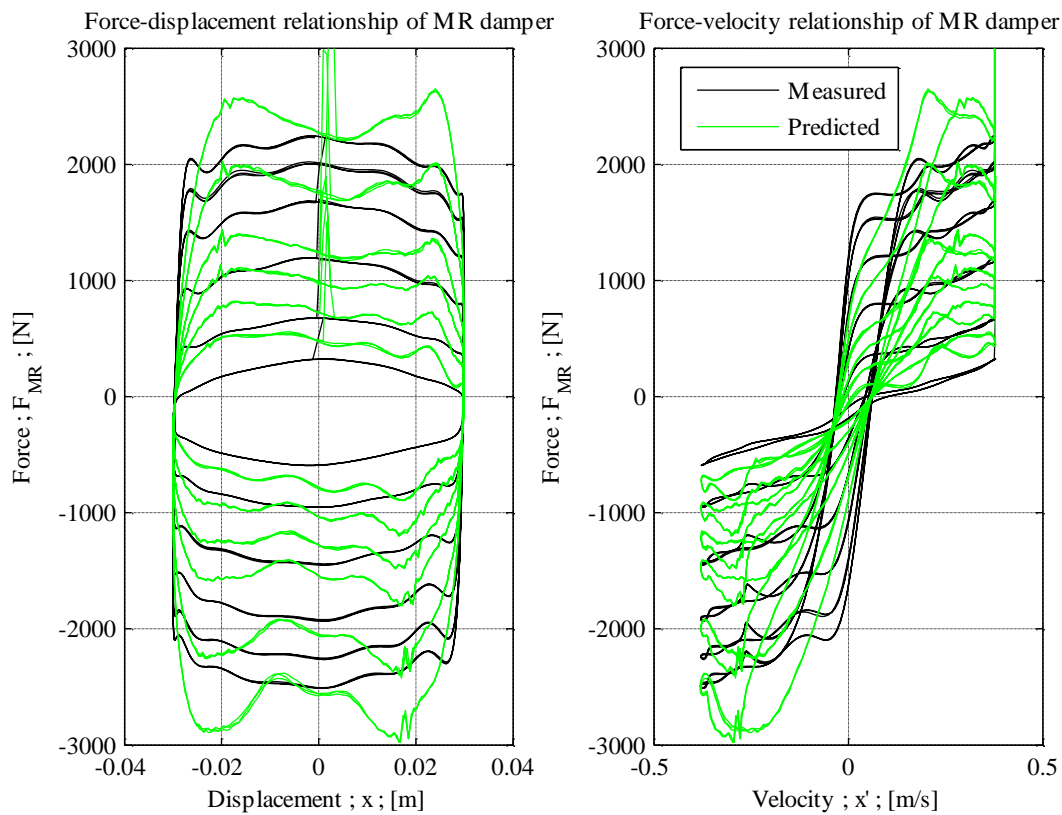


Figure 3-22: BLS model force-displacement (left) and force-velocity (right) relationship in response to 30mm amplitude at 2Hz sinusoidal excitation.

data in Figure 3-22, p3.26. From Figure 3-22 it is apparent that the model over-estimates the force exerted by the MR damper when changes in the current levels occur, which is the result of time history data ( $t - 1$ ,  $t - 2$ , etc.) implemented in the model. Although the hysteresis curves exhibited by the BLS model are wider than the polynomial models, the BLS model does not accurately represent the pre-yield and post-yield regions, and largely over-estimates the force at midrange velocity magnitudes. Although it has been demonstrated that a BLS model with a suitable regressor vector has the ability to accurately predict the MR damper force (**Kaul, 2011**), omission of measured damping force reduces model accuracy significantly. The BLS model may be improved by implementation of an alternate regressor vector (which may or may not include current as a variable) and by performing re-characterization for each current level, instead of characterization of concatenated data sets.

An additional BLS model has been developed by using a random displacement excitation signal (Random signal #1). As with the previous BLS model, the measured data used to develop the model consists of a concatenation of data sets at six input current levels. The computed BLS model parameters are provided in Table 3–16, p3.27. The force-displacement and force-velocity relationships of the model are compared to measured data in Figure 3-23, p3.28, and the time trace of the measured force is compared to the predicted force in the top graph of Figure 3-24, p3.29. Although hysteresis is adequately represented by the model, there is no clear distinction between the pre-yield and post-yield regions. The MR damper force is also over-estimated at midrange velocity magnitudes.

To evaluate the applicability of the BLS model to changes in excitation conditions, the model from Table 3–16, p3.27, is implemented on a different random displacement signal, referred to as Random signal #2. The RMS error between the measured MR damper force in response to Random signal #2

**Table 3–16: Computed BLS model parameters for a random input signal.**

BLS Model Parameters						
Random (#1) signal input						
Parameter	Variable	Value	Parameter	Variable	Value	RMS Error [N] (NRMS Error)
$\hat{\theta}_1$	$\dot{x}_t$	$14.880 \times 10^3$	$\hat{\theta}_9$	$I_{t-1} \dot{x}_{t-1}$	$-110.07 \times 10^3$	344.99 (12.13%)
$\hat{\theta}_2$	$\dot{x}_{t-1}$	$-20.725 \times 10^3$	$\hat{\theta}_{10}$	$I_{t-2} \dot{x}_{t-2}$	$63.683 \times 10^3$	
$\hat{\theta}_3$	$\dot{x}_{t-2}$	$8.9593 \times 10^3$	$\hat{\theta}_{11}$	$I_t \dot{x}_t^2$	453.7338	
$\hat{\theta}_4$	$ \dot{x}_t  x_t$	$-19.626 \times 10^3$	$\hat{\theta}_{12}$	$I_t \dot{x}_t^3$	$-321.79 \times 10^3$	
$\hat{\theta}_5$	$I_t$	-67.7292	$\hat{\theta}_{13}$	$I_{t-1} \dot{x}_{t-1}^3$	$638.55 \times 10^3$	
$\hat{\theta}_6$	$\dot{x}_t^3$	$-10.181 \times 10^3$	$\hat{\theta}_{14}$	$I_{t-2} \dot{x}_{t-2}^3$	$-366.14 \times 10^3$	
$\hat{\theta}_7$	$I_t x_t$	$8.7908 \times 10^3$	$F_0$	1	-127.6843	
$\hat{\theta}_8$	$I_t \dot{x}_t$	$55.081 \times 10^3$				

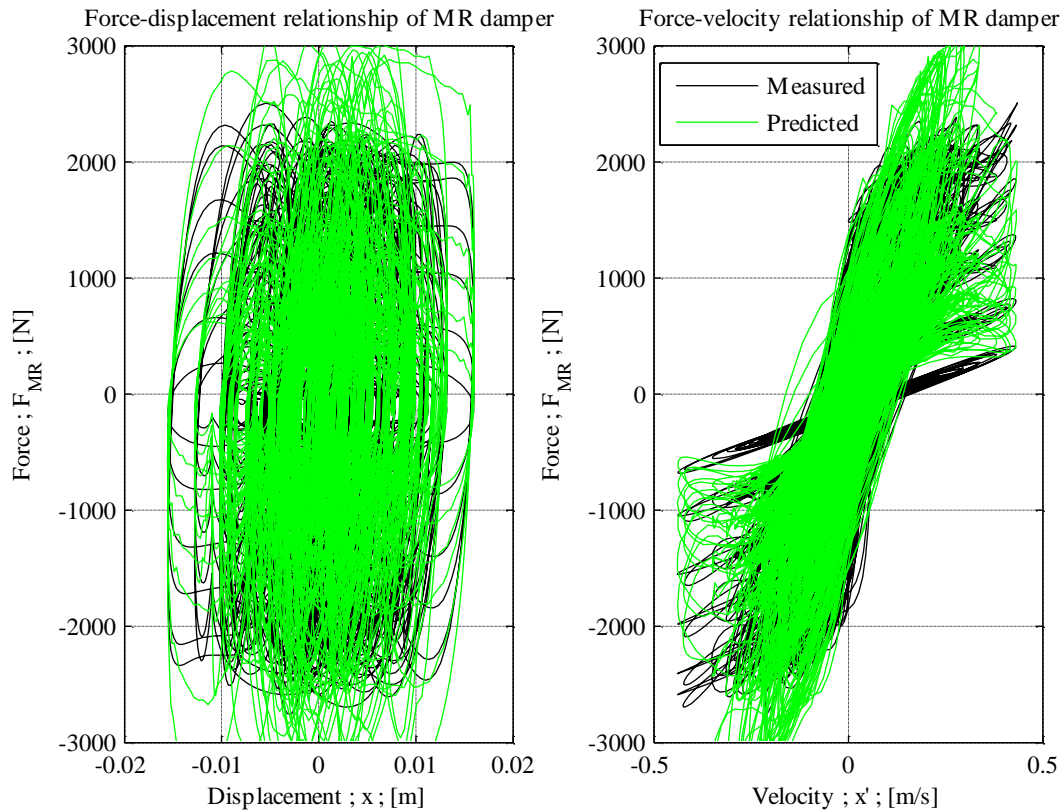


**Figure 3-23: BLS model predicted force-displacement (left) and force-velocity (right) relationship in response to a random displacement input signal.**

and the force predicted by the Random signal #1 model is 436.52N (NRMS error of 14.86%). The time trace of the measured force in response to the Random #2 input, and the corresponding force predicted by the model from Table 3–16, is shown in the bottom graph of Figure 3-24, p3.29. It can be clearly discerned that the BLS model is more stable than the polynomial model since there is no sudden increase in the predicted force, as compared to Figure 3-21, p3.25. To improve the stability of the polynomial model its order is reduced, while the BLS model remains stable without any changes in the regressor vector.

As with the polynomial model, one of the benefits associated with the developed BLS model is its invertibility, namely the ability to calculate the required current in order to deliver the prescribed damper force by using the BLS model and its computed parameters. From Equation 27, p2.29, and Equation 37, p3.25, the BLS model can also be written as:

$$\begin{aligned}
 F_t - (\hat{\theta}_1 \dot{x}_t + \hat{\theta}_2 \dot{x}_{t-1} + \hat{\theta}_3 \dot{x}_{t-2} + \hat{\theta}_4 |\dot{x}_t| x_t + \hat{\theta}_6 \dot{x}_t^3 + \hat{\theta}_9 I_{t-1} \dot{x}_{t-1} + \dots \\
 \hat{\theta}_{10} I_{t-2} \dot{x}_{t-2} + \hat{\theta}_{13} I_{t-1} \dot{x}_{t-1}^3 + \hat{\theta}_{14} I_{t-2} \dot{x}_{t-2}^3 + F_0) \quad [38] \\
 = I_t (\hat{\theta}_5 + \hat{\theta}_7 x_t + \hat{\theta}_8 \dot{x}_t + \hat{\theta}_{11} \dot{x}_t^2 + \hat{\theta}_{12} \dot{x}_t^3)
 \end{aligned}$$

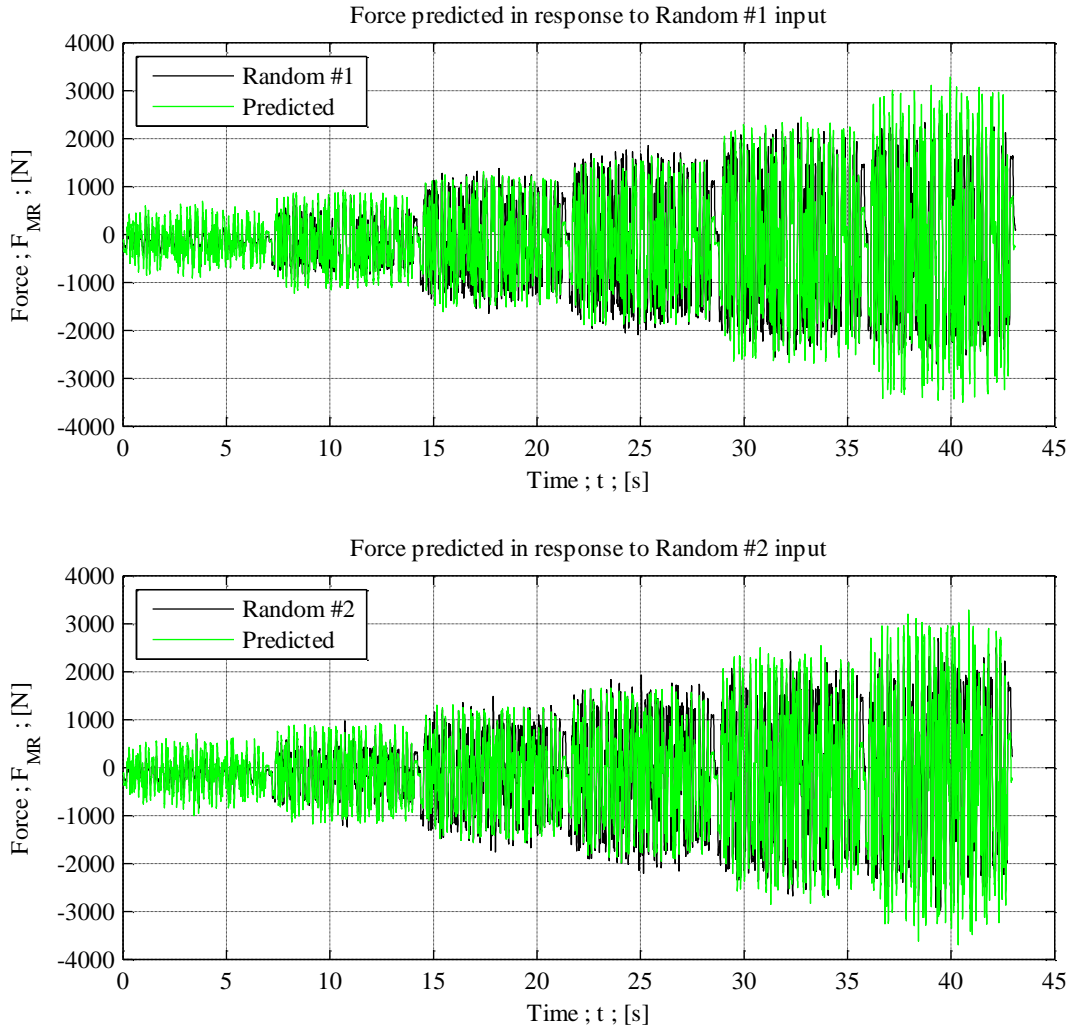


**Figure 3-24: Comparison of measured MR damper forces and forces predicted by BLS model developed using Random #1 input at several current levels.**

Let

$$\begin{aligned}
 \mathcal{A} = & (\hat{\theta}_1 \dot{x}_t + \hat{\theta}_2 \dot{x}_{t-1} + \hat{\theta}_3 \dot{x}_{t-2} + \hat{\theta}_4 |\dot{x}_t| x_t + \hat{\theta}_6 \dot{x}_t^3 + \hat{\theta}_9 I_{t-1} \dot{x}_{t-1} \\
 & + \hat{\theta}_{10} I_{t-2} \dot{x}_{t-2} + \hat{\theta}_{13} I_{t-1} \dot{x}_{t-1}^3 + \hat{\theta}_{14} I_{t-2} \dot{x}_{t-2}^3 + F_0)
 \end{aligned} \quad [39]$$

and

$$\mathcal{B} = (\hat{\theta}_5 + \hat{\theta}_7 x_t + \hat{\theta}_8 \dot{x}_t + \hat{\theta}_{11} \dot{x}_t^2 + \hat{\theta}_{12} \dot{x}_t^3) \quad [40]$$

The required current can be calculated from this model as follows:

$$I_t = \left( \frac{F_t - \mathcal{A}}{\mathcal{B}} \right) \quad [41]$$

In Equation 41,  $F_t$  is the prescribed semi-active damping force,  $F_{SA}$ .

### 3.2.6 Recursive Models

A significant shortcoming of the developed models is the need for re-characterization of model parameters with varying input conditions. This shortcoming can be overcome by using a recursive model. The need for re-characterization is avoided since the model parameters evolve as new data becomes available. This aspect makes recursive models suitable for online implementation and applicable to a wide range of input conditions. Although both the polynomial and BLS models are linear in the parameters and can therefore be implemented recursively, the BLS model (discussed in Section 3.2.5, p3.25) has been selected for recursive LMS implementation since it is superior to the polynomial model with regards to accuracy and stability.

The recursive algorithms investigated require the measured MR damper force,  $F_{t,meas}$ , as feedback to the algorithm. (Refer to Equations 28, 30, and 31, p2.31). However, the measured damper force is not available on the off-road application used in this study. Therefore the influence of the omission of the measured damping force on the accuracy of the LMS model is discussed in Section 3.2.6.2, p3.32, while the measured force feedback is included in the algorithm discussed in Section 3.2.6.1, p3.30.

#### 3.2.6.1 Least Mean Square (LMS) Model with Measured Force Feedback

The LMS algorithm (previously discussed in Section 2.6.3.3.1, p2.31) is implemented using the computed parameters of the generalised BLS models as the initial parameters,  $\hat{\theta}_0$ . The model parameters are continuously updated as per Equation 28, p2.31. The forgetting factor,  $\gamma_l$ , determines the extent to which new data influences the model parameters, and is chosen to yield relatively stable results without significantly compromising model tracking capability. A uniform forgetting factor of 0.2 has been chosen. The LMS algorithm is implemented on three excitation signals: 30mm amplitude at 2Hz sinusoidal displacement excitation, and two random displacement excitation signals. For LMS implementation on the sinusoidal excitation signal, the BLS model parameters from the same excitation signal are used as the initial parameters, (refer to Table 3–15, p3.26). For LMS implementation on both the random displacement excitation signals, the BLS model parameters from one of the random signals (Random #1) is used as the initial set of parameters, (refer to Table 3–16, p3.27). The LMS algorithm is also implemented on a concatenation of measured data sets at six input current levels: 0.0A, 0.25A, 0.5A, 0.75A, 1.25A, and 1.75A. The LMS algorithm results are compared to the corresponding BLS models in Table 3–17, p3.31.

The force-displacement and force-velocity relationship of the LMS model in response to the sinusoidal excitation is shown in Figure 3-25, p3.31. The model is unstable for low current levels, and the predicted response tracks the measured response well, except for a few outliers, as can be seen in Figure 3-25. The outliers coincide with the instances of changes in the supplied current. The



**Table 3–17: Comparison of BLS and LMS models.**

<b>BLS and LMS Models</b>						
Initial Parameters	Excitation Signal	BLS RMS Error [N]	BLS NRMS Error	LMS Forgetting Factor	LMS RMS Error [N]	LMS NRMS Error
Sinusoidal (30mm, 2Hz)	Sinusoidal (30mm, 2Hz)	287.03	11.40%	0.2	88.461	3.52%
Random 1	Random 1	344.99	12.13%	0.2	114.24	4.15%
Random 1	Random 2	436.52	14.86%	0.2	121.95	4.11%

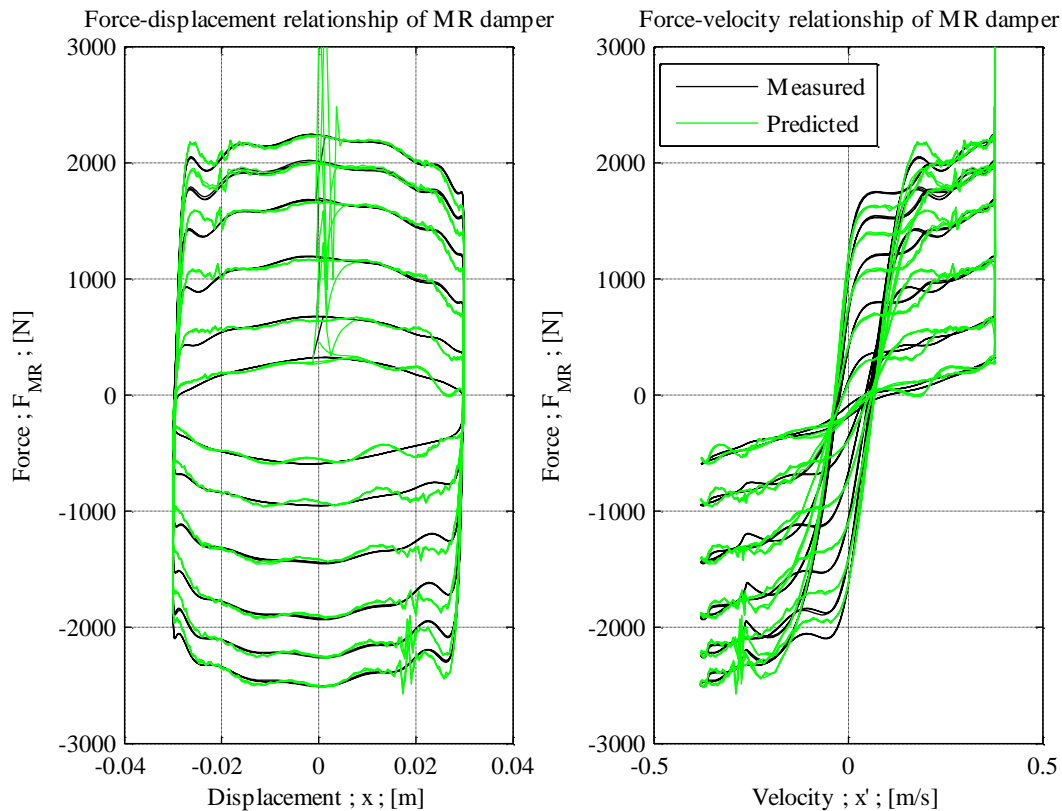


**Figure 3-25: LMS model with measured force feedback force-displacement (left) and force-velocity (right) relationship in response to 30mm amplitude at 2Hz sinusoidal excitation.**

LMS model yields a significant improvement over the BLS model, as indicated by the results in Table 3–17, p3.31, and as compared to Figure 3-22, p3.26. The transition from pre-yield to post-yield regions is more accurately represented by the LMS model, and the occurrence of over-estimation is also reduced.

The LMS algorithm has also been implemented on a random displacement excitation signal (Random #1). The force-displacement and force-velocity relationship of the LMS model is compared to measured data in Figure 3-26, p3.32, and the time trace of the measured force is compared to the

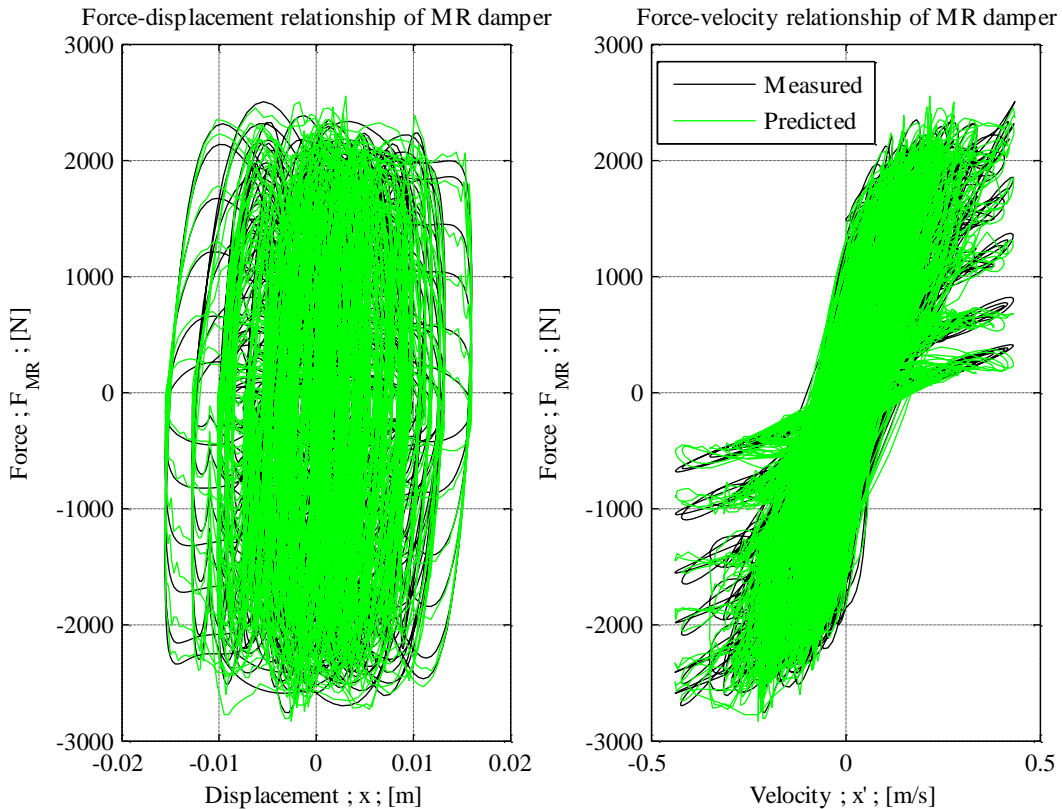


**Figure 3-26: LMS model with measured force feedback predicted force-displacement (left) and force-velocity (right) relationship in response to a random displacement input signal.**

predicted force in the top graph of Figure 3-27, p3.33. As can be seen, the predicted response closely tracks the measured response. The LMS model is a significant improvement over the BLS model from Table 3–16, p3.27, especially due to the elimination of over-estimation. The evolution of model parameters as more data becomes available is shown in Figure 3-28, p3.34.

To demonstrate the applicability of the LMS algorithm to changes in excitation conditions, the LMS algorithm is also implemented on another random displacement excitation, Random #2. The BLS model parameters obtained from Table 3–16, p3.27, are used as initial model parameters. The time trace of the predicted force is compared to the measured force in the bottom graph of Figure 3-27, p3.33. As indicated in Table 3–17, p3.31, similar accuracy is obtained even with a different excitation signal.

### 3.2.6.2 *Least Mean Square (LMS) Model with Calculated Force Feedback*

The LMS algorithm needs to be adjusted when the measured MR damper force is not available. In Equation 28, p2.31, the measured force is replaced by the predicted force from the previous time increment. The model parameters are thus updated as follows:

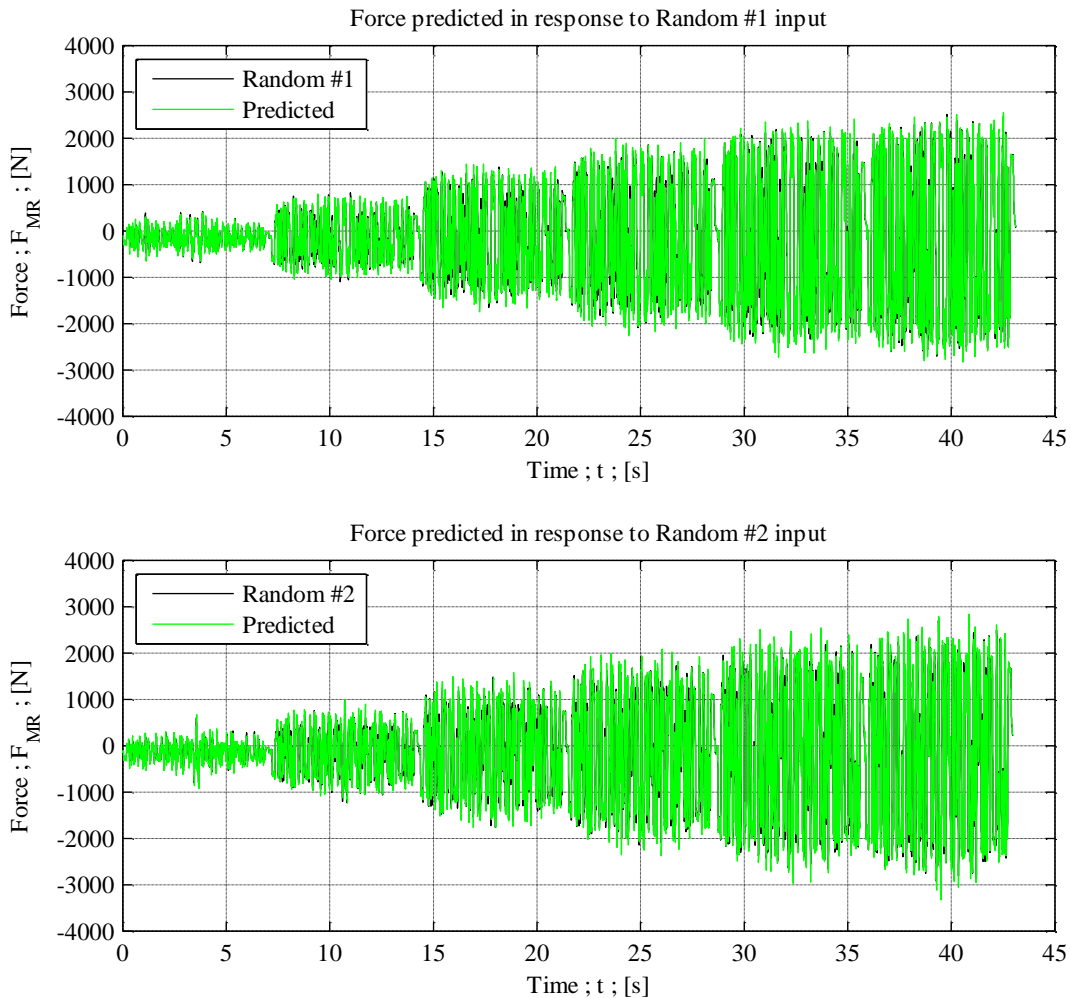


**Figure 3-27: Comparison of measured MR damper forces and forces predicted by LMS model with measured force feedback developed using Random #1 input at several current levels.**

$$\hat{\theta}_t = \hat{\theta}_{t-1} + \gamma_1 \phi_t [\hat{F}_{t-1} - \hat{F}_t] \quad [42]$$

The BLS model parameters developed from the same excitation conditions, shown in Table 3–15, p3.26, are used as initial parameters in the LMS algorithm. The LMS model without force feedback is implemented on a 30mm amplitude at 2Hz sinusoidal displacement excitation. The force-displacement and force-velocity relationship of the model is compared to measured data in Figure 3-29, p3.35. In order to obtain a stable model the forgetting factor is reduced to 0.02. The RMS error is 299.68N (NRMS error of 11.93%), which indicates a reduction in accuracy as compared to the BLS model from Table 3–15, p3.26.

Implementation of the LMS algorithm without measured MR damper force feedback exhibits poor model tracking and the model quickly becomes unstable. Reducing the model sensitivity by lowering the forgetting factor leads to reduced model tracking capability. In order to improve the stability of the model, the forgetting factor has to be made insignificantly small, effectively reducing the model to a

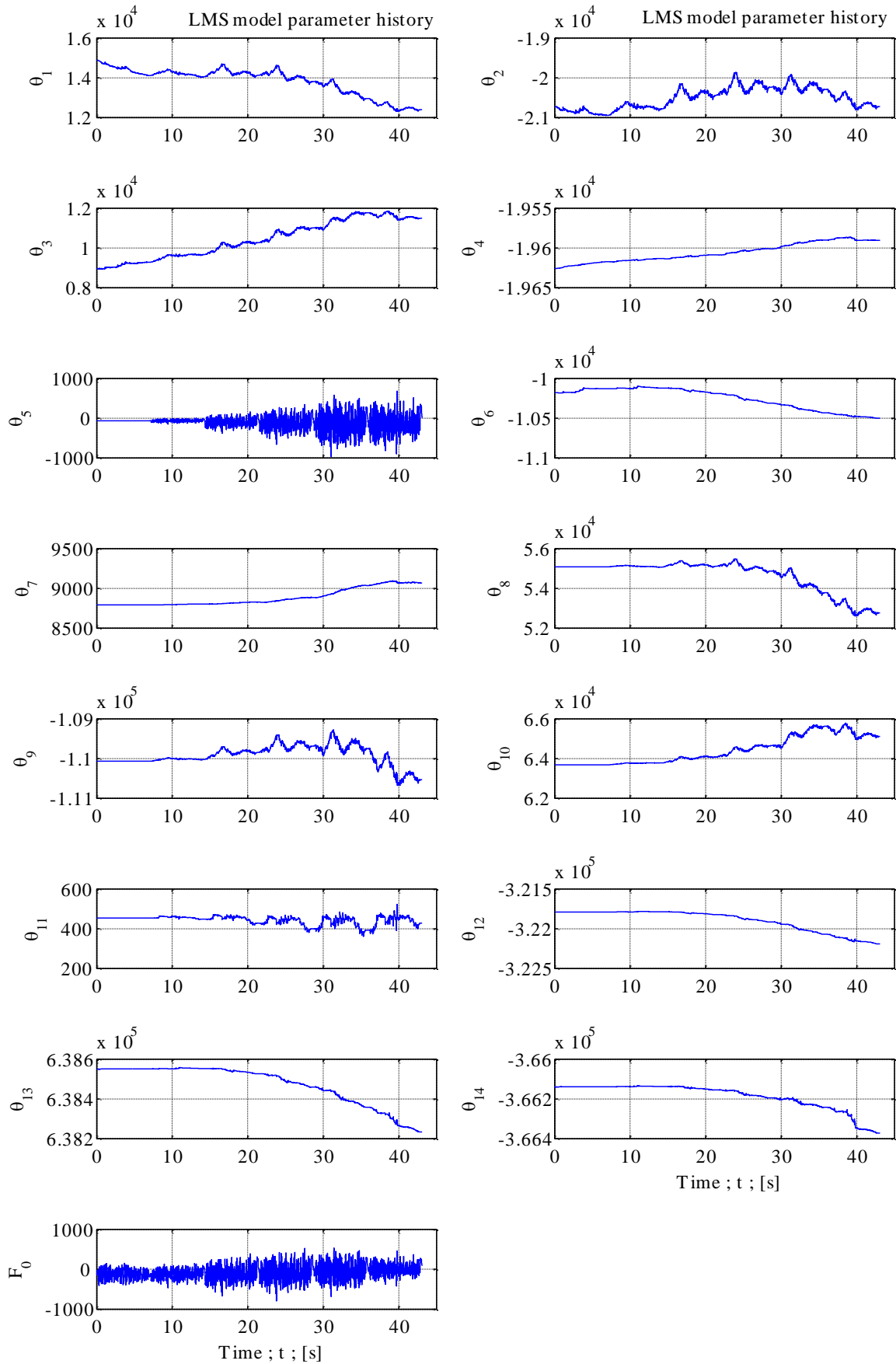
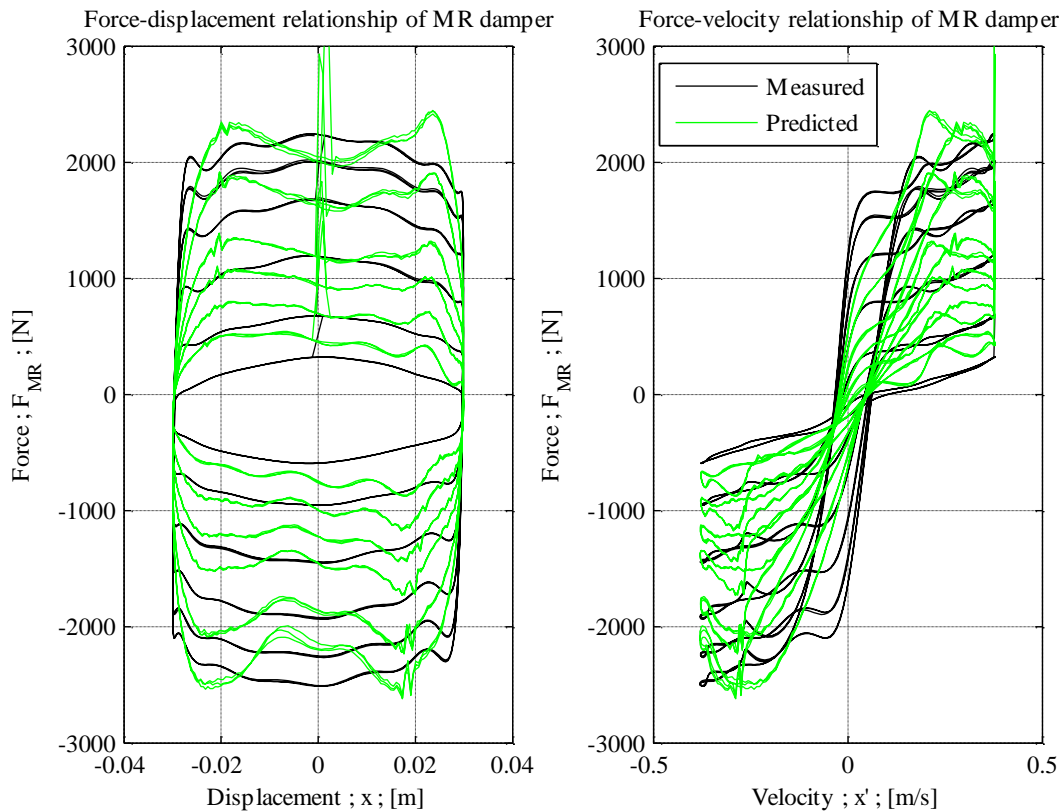


Figure 3-28: Parameter history of LMS algorithm with measured force feedback.



**Figure 3-29: LMS model with calculated force feedback force-displacement (left) and force-velocity (right) relationship in response to 30mm amplitude at 2Hz sinusoidal excitation.**

BLS model. The lack of measured force feedback to the LMS algorithm is found to significantly impair the working of this model. The use of the predicted force, instead of the measured force, introduces errors that cannot be overcome.

### 3.3 Conclusion

During the course of this work nine models have been developed to represent key characteristics of the MR damper used in this study: Bingham-, modified and delayed Bingham-, Bouc-Wen-, Kwok-, polynomial-, displacement or acceleration determined polynomial-, generalised BLS-, LMS with measured force feedback-, and LMS with calculated force feedback model. These models can be classified into three groups: current independent models, current dependent models, and recursive models.

The results of the current independent models are summarised in Table 3–18, p3.36. Due to the simplicity of the Bingham model some important MR damper characteristics, such as hysteresis and transition from the pre-yield to the post-yield region, are not captured by this model. Furthermore, the discontinuity of the model results in high computational requirements. Some of the shortcomings of

**Table 3–18: Summary of developed MR damper current independent models.**

Current Independent Models				
Model	Development Signal	Test Signal	Maximum RMS Error	Maximum NRMS Error
Bingham	Sinusoidal	Sinusoidal	503.55N	19.99%
Modified Bingham	Sinusoidal	Sinusoidal	100.10N	3.97%
	Random 1	Random 1	449.97N	15.82%
	Random 1	Random 2	464.40N	15.71%
Bouc-Wen	Sinusoidal	Sinusoidal	144.68N	5.74%
	Random 1	Random 1	304.11N	11.25%
	Random 1	Random 2	311.11N	10.67%
Kwok	Sinusoidal	Sinusoidal	91.956N	3.65%
	Random 1	Random 1	701.92N	24.67%
	Random 1	Random 2	672.65N	22.82%

the Bingham model are addressed by the modified Bingham model which introduces a delay in order to represent hysteretic behaviour. However, the optimal delay for improved accuracy needs to be determined iteratively and does not remain the same for all current levels and excitation conditions. Although the Bouc-Wen model delivers the most accurate results in response to non-uniform excitation, it is a complex model containing stiff differential equations and requires a very small time step in order to solve the governing differential equation. Of all the models developed in this study, the Bouc-Wen model is the most numerically inefficient. While the Kwok model is computationally efficient and straight forward, it is not as accurate under non-uniform excitation conditions. The major drawback of the current independent models listed in Table 3–18, p3.36, is the need for re-characterization of model parameters with changes in input current levels.

Current dependent models are favourable in terms of control implementation since the capability of the MR damper can be better utilised if a wide current range can be prescribed instead of a selection of discrete current levels. The results of the current dependent models are summarised in Table 3–19, p3.37. Although the polynomial model is straight forward and easy to implement, it is unable to represent hysteresis. The accuracy of the polynomial model can be improved by implementing two sets of parameters, one of each for either positive or negative acceleration. Implementation of this polynomial model may not be robust since the acceleration signal is inherently noisy, often resulting in the wrong parameter set being implemented. Also, in order to improve the stability of this model, its order is reduced at the expense of accuracy. The BLS model developed in this work is more stable and accurate in response to non-uniform excitation, and therefore superior to the polynomial model.

**Table 3–19: Summary of developed MR damper current dependent models.**

Current Dependent Models				
Model	Development Signal	Test Signal	Maximum RMS Error	Maximum NRMS Error
Polynomial	Sinusoidal	Sinusoidal	316.50N (n* = 7)	12.57%
Displacement or Acceleration Determined Polynomial	Sinusoidal	Sinusoidal	195.49N (n = 8)	7.76%
	Random 1	Random 1	387.61N (n = 5)	14.07%
	Random 1	Random 2	542.97N (n = 5)	18.29%
BLS	Sinusoidal	Sinusoidal	287.03N	11.40%
	Random 1	Random 1	344.99N	12.13%
	Random 1	Random 2	436.52N	14.86%

\* n denotes model order

**Table 3–20: Summary of developed MR damper recursive models.**

Recursive Models				
Model	Development Signal	Test Signal	Maximum RMS Error	Maximum NRMS Error
LMS with <i>Measured</i> Force Feedback	Sinusoidal	Sinusoidal	88.461N	3.52%
	Random 1	Random 1	114.24N	4.15%
	Random 1	Random 2	121.95N	4.11%
LMS with <i>Calculated</i> Force Feedback	Sinusoidal	Sinusoidal	299.68N	11.93%

The problem of required re-characterization with changes in input conditions is addressed by recursive models. These models are continuously updated as more data becomes available. The results of the recursive models are summarised in Table 3–20, p3.37. The non-recursive BLS model parameters are used as initial parameters for the LMS algorithm. The LMS model with measured force feedback shows a significant improvement over all the non-recursive models, especially with regard to non-uniform excitation conditions. Eliminating force feedback is important to overcome design and packaging constraints in off-road vehicles that use MR dampers, with the added benefit of being cost-effective. However, the lack of measured force feedback (and thus the use of calculated force feedback) inhibits the performance of the LMS algorithm, resulting in an unstable and therefore unusable model.

For this work an accurate and robust MR damper model is required to predict the MR damper force since some project constraints do not allow for the measuring of the damper force. Since this project involves implementation of semi-active control on an off-road application, the proposed model must be suitable for random excitation. In order to deliver the required damping forces prescribed by the system controller, the proposed model must also be invertible so as to determine the necessary current levels.

Both the polynomial and BLS models are invertible current dependent models suitable for semi-active control implementation. However, preliminary simulation results indicated that the polynomial model (refer to Table 3–14, p3.23) yields more stable results, and is therefore implemented in this study. The most accurate off-state (0A) model when subjected to random excitation is the Kwok model (refer to Table 3–11, p3.19) and is therefore used to calculate the force delivered by the MR dampers when the prescribed semi-active force is 0N and the current is consequently switched off.



---

## 4 BAJA VEHICLE MODELLING

---

A suitable vehicle model is required for suspension control simulation. The accuracy and reliability of simulation results depend on the validity of the model and its ability to represent the physical vehicle. To confirm that the model is reliable and truthfully represents the baseline vehicle it is validated for ride comfort and handling simulation. Ride comfort and handling baseline results are obtained by collecting several measurements as the test vehicle is driven over a rough Belgian paving track and performs a slalom test. These measured results are compared to simulation results to validate the vehicle model, and to compare the effect of suspension control to the uncontrolled (baseline) suspension. The development and validation of the test vehicle model is discussed in this chapter.

### 4.1 The Baja Vehicle

In this study suspension control has been implemented on a Baja vehicle. A Baja vehicle is a small single seat off-road racing vehicle similar in appearance to a dune buggy. The vehicle has been developed by a group of students of the University of Pretoria and competes in an intercollegiate design competition run by SAE International. The vehicle is designed and fabricated so as to be able to overcome several obstacles and perform several tasks, such as incline ascent, skid pull and rock crawl. The vehicle is tested for manoeuvrability, off-road mobility, endurance, and significant emphasis is placed on design evaluation. The Baja vehicle used for this study is shown in Figure 4-1, performing an incline ascent during the annual competition of 2009.



Figure 4-1: Baja vehicle on an incline during the 2009 competition.

The Baja vehicle body consists of a welded frame manufactured from 32mm diameter round tubing with a single seat driver compartment, a powertrain and a continuously variable transmission (CVT), along with steering as well as acceleration and brake components. The vehicle is rear wheel driven and the driveline consists of a 7.5kW engine, CVT, and hub-reduction gearbox. It should be noted that there is no differential to distribute the power between the driving wheels. The front and rear suspension is of the double wishbone type. The wheels are connected to the body via four hydro-pneumatic spring-damper units which are designed and developed by the Baja team at the University of Pretoria. Kenda Klaw XCF tyres are used at the front, and Kenda Dominator tyres are used at the rear (AT21x7-10). The straight-line top speed of the vehicle is approximately 40-45km/h reached after 100m from a standing start acceleration run.

## 4.2 Experimental Work

An accurate simulation model of the vehicle is required in order to simulate semi-active suspension control. While there are many simplified models discussed in the literature, these models often have significant shortcomings that have a considerable influence on accuracy, and don't apply directly to off-road vehicles, particularly the Baja vehicle that has been used for this project. Quarter car models only represent bounce motion and are therefore only applicable to situations where identical excitation is expected at all four wheels. "Full car" models often include pitch and roll motion, but the lateral and yaw degrees of freedom, which are essential in handling evaluation, are usually neglected in these models. Commonly used vertical tyre models disregard lateral forces which give an indication of directional response. Also, suspension kinematics may play a significant role in the dynamics of certain vehicles, such as the Baja, but is often ignored.

Several parameters are required in order to develop an accurate vehicle simulation model. These parameters include the mass of the vehicle components, the location of the centre of mass, moments of inertia, spring and damper properties, and tyre properties. The geometry of the model is obtained from solid models developed by the Baja team during the design stage of the vehicle. The location of the centre of mass and moments of inertia of the vehicle sprung mass are determined experimentally using the techniques discussed by **Uys et al. (2006b)**. In Section 4.2.1, p4.3, and Section 4.2.2, p4.5 the process that was used for determination of these parameters is described. The mass and inertia properties of the unsprung masses are obtained from the solid models. The characterization of the hydro-pneumatic spring-damper unit is discussed in Section 4.2.3, p4.9. The tyre model used in the vehicle simulation model is a Pacejka '89 tyre model (**Bakker et al. 1989**), developed using experimental data and is discussed in Section 4.2.4, p4.15.

Baseline testing has been performed in order to determine ride and handling quality of the original vehicle. The baseline tests are described in Section 4.4, p4.20, and their results are discussed in Section 5.2.1, p5.3 (ride comfort results) and Section 5.3.1, p5.13 (handling results). The data collected is also used to validate the Baja simulation model (developed using ADAMS software) and is discussed in Section 4.5, p4.24. Model development is discussed in Section 4.3, p4.16.

#### 4.2.1 Determination of Centre of Mass

The centre of mass and the moments of inertia of the vehicle sprung mass are determined using the complete vehicle body, including the driver and the testing equipment used for baseline testing. Usually the effect of the driver and testing equipment on the dynamics of a vehicle may be negligible, but the mass of the driver and equipment is approximately 30% of the total Baja vehicle mass, and needs to be taken into account. The experimental setup is shown in Figure 4-2, p4.3.

The centre of mass of the vehicle sprung mass is determined experimentally by measuring the force required to tilt the vehicle at a certain angle, as shown in Figure 4-3, p4.4. The vehicle is pivoted about an axis located at the front, point  $R$ , and lifted at the rear. The angle is increased in increments and the exerted force is measured at each increment. Taking moments about the pivot point,  $R$ , and equating to zero, results in Equation 43:

$$\sum T_R = LF \cos \theta - HF \sin \theta - mgb \cos \theta + mgh \sin \theta \quad [ 43 ]$$



Figure 4-2: Experimental determination of the centre of gravity.

The location of the centre of mass along the length of the vehicle, measure  $b$  in Figure 4-3, p4.4, and Equation 43, p4.3, is determined when the lifted angle is zero. The calculated centre of mass height,  $h$ , should converge as the angle increases. As shown in Figure 4-4, p4.4, the data did not converge, possibly due to movement of the driver as the tilted angle is increased. Accuracy is however acceptable at  $\pm 15\text{mm}$  on  $385\text{mm}$  (or  $\pm 4\%$ ). The results are summarised in Table 4-1, p4.5. The vehicle is assumed to be symmetrical in the lateral direction and the centre of mass is therefore located in the middle of the  $zy$ -plane (refer to Figure 4-3, and Figure 4-5, p4.5). The movement of the driver on the seat is not entirely constrained and thus has a substantial effect on the vehicle centre of

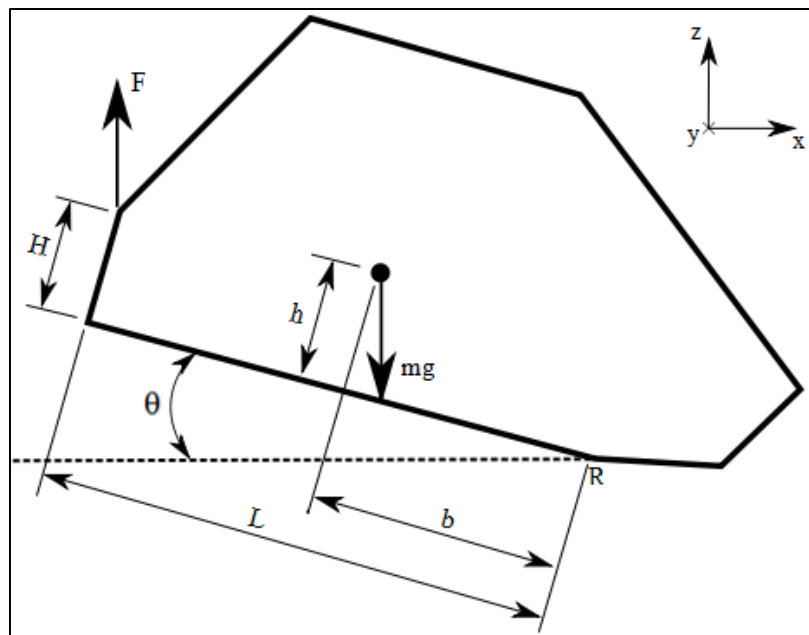


Figure 4-3: Obtaining the position of the centre of gravity.

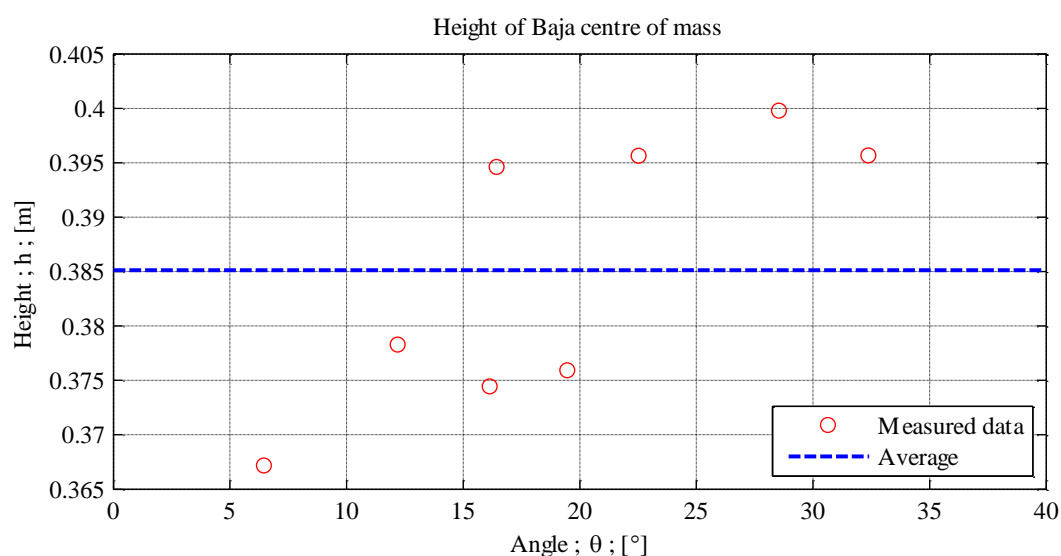


Figure 4-4: Height of Baja sprung mass centre of mass as a function of lifted angle.

mass position. Even though the sprung mass of the vehicle is treated as a rigid body in the simulation model used in this study, the rigid body assumption is not truly valid and further investigation is required in future work.

#### 4.2.2 Determination of Moments of Inertia

The moments of inertia of the vehicle sprung mass about its three axes (pitch, roll and yaw) are determined experimentally. The vehicle coordinate system is shown in Figure 4-5, p4.5. The sprung mass pivots about an axis and is allowed to oscillate using a spring, shown in Figure 4-6, p4.6. The experimental setup for the pitch moment of inertia is shown in Figure 4-7, p4.7. The procedure to calculate the moments of inertia from experimental measurements is as follows (with reference to Figure 4-6):

Newton's second law is applied to a rigid body pivoting in a plane:

$$\sum T_o = I_o \ddot{\theta} \quad [ 44 ]$$

**Table 4-1: Centre of mass properties of Baja sprung mass.**

Property	Symbol	Value
Mass of sprung mass	$M_s$	251.71kg
Centre of mass location along vehicle length	$b$	0.6096m
Average height of centre of mass	$h$	0.3851m

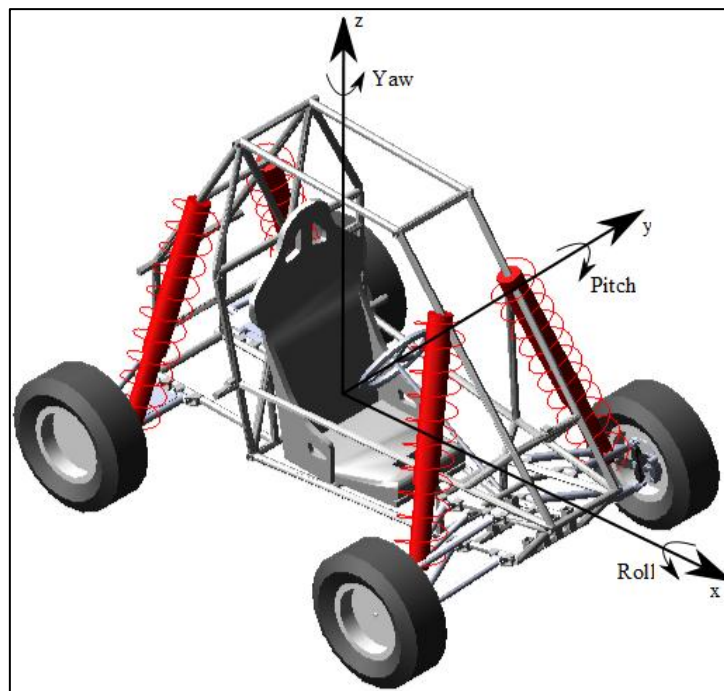


**Figure 4-5: Baja vehicle axis system.**

In Equation 44,  $\Sigma T_o$  is the sum of the moments of the external forces about the pivot axis at  $O$ ,  $\ddot{\theta}$  is the angular acceleration, and  $I_o$  is the moment of inertia about the axis of rotation. The spring of stiffness  $k$ , delivers a force due to its deflection  $x$  for an angular displacement  $\theta$ :  $kx = kL_{force} \sin \theta$ . The moment about  $O$  caused by the spring is  $kL_{force}^2 \sin \theta \cos \theta$ . For small rotational displacements  $\sin \theta \approx \theta$  and  $\cos \theta \approx 1$ , and thus:

$$\sum T_o = -kL_{force}^2 \theta \quad [45]$$

The homogeneous equation of motion of rotational vibration of a bar, usually written as  $\ddot{\theta} + \omega_n^2 \theta = 0$  is thus described by Equation 46 after setting Equation 44 equal to Equation 45:

$$\ddot{\theta} + \frac{kL_{force}^2}{I_o} \theta = 0 \quad [46]$$

The natural frequency of this system can be expressed as:

$$\omega_n = \sqrt{\frac{kL_{force}^2}{I_o}} \quad [47]$$

From Equation 47, the corresponding period of free vibration is given by:

$$\tau = 2\pi \sqrt{\frac{I_o}{kL_{force}^2}} \quad [48]$$

Thus, if the spring stiffness is known, the moment of inertia about the pivoting axis can be determined by measuring the period of oscillation using Equation 49:

$$I_o = \frac{\tau^2 kL_{force}^2}{(2\pi)^2} \quad [49]$$

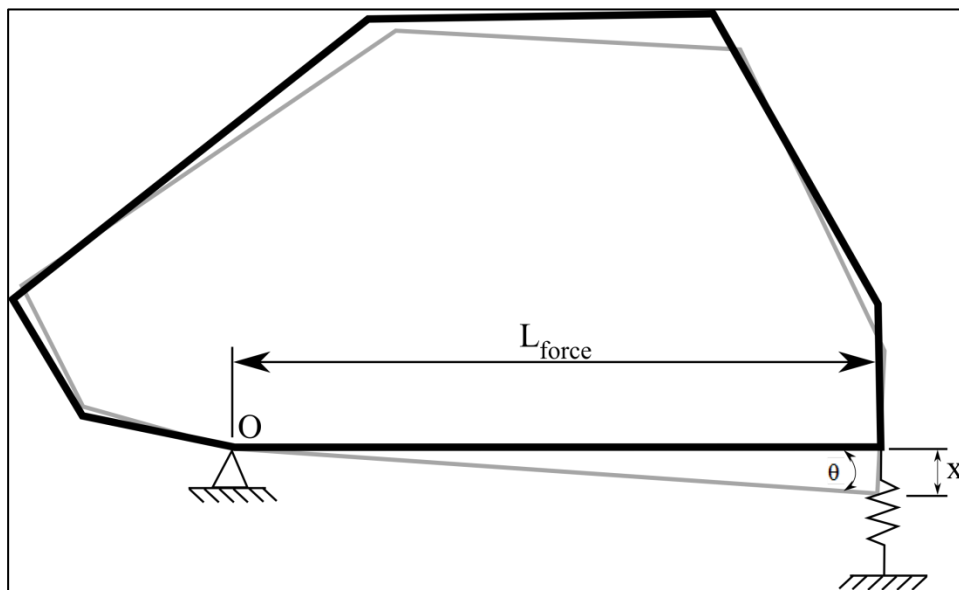


Figure 4-6: Schematic presentation of rigid body pivot motion (pitch).

The spring force and spring deflection are measured and used to determine the spring stiffness in Equation 49. It may be noted that the above equations apply to an undamped system only. Measured spring deflection data shown in Figure 4-8, p4.8, indicates that there is some damping present. Thus the measured period of oscillation corresponds to the damped period. Referring to the spring deflection as a function of time shown in Figure 4-8, the logarithmic decrement,  $\delta$ , is determined using the amplitude of the first oscillation,  $A_1$ , and the following amplitude,  $A_2$ :

$$\delta = \ln \frac{A_1}{A_2} \quad [ 50 ]$$

The damping ratio is determined as follows:

$$\zeta = \frac{\delta^2}{\sqrt{\delta^2 + (2\pi)^2}} \quad [ 51 ]$$

The undamped natural period,  $\tau$ , is then determined using the measured damped period,  $\tau_d$ :

$$\tau = \sqrt{1 - \zeta^2} \tau_d \quad [ 52 ]$$

Extra components were used in the experimental setup and contributed to the calculated inertia. The inertia of the added components,  $I_{components}$ , about the pivoting axis is subtracted. The moment of inertia about the axis through the centre of mass,  $I_{axis}$  (pitch, roll or yaw), is calculated using the parallel axis theorem:

$$I_{axis} = I_o - I_{components} - M_{Baja} d_{axis}^2 \quad [ 53 ]$$

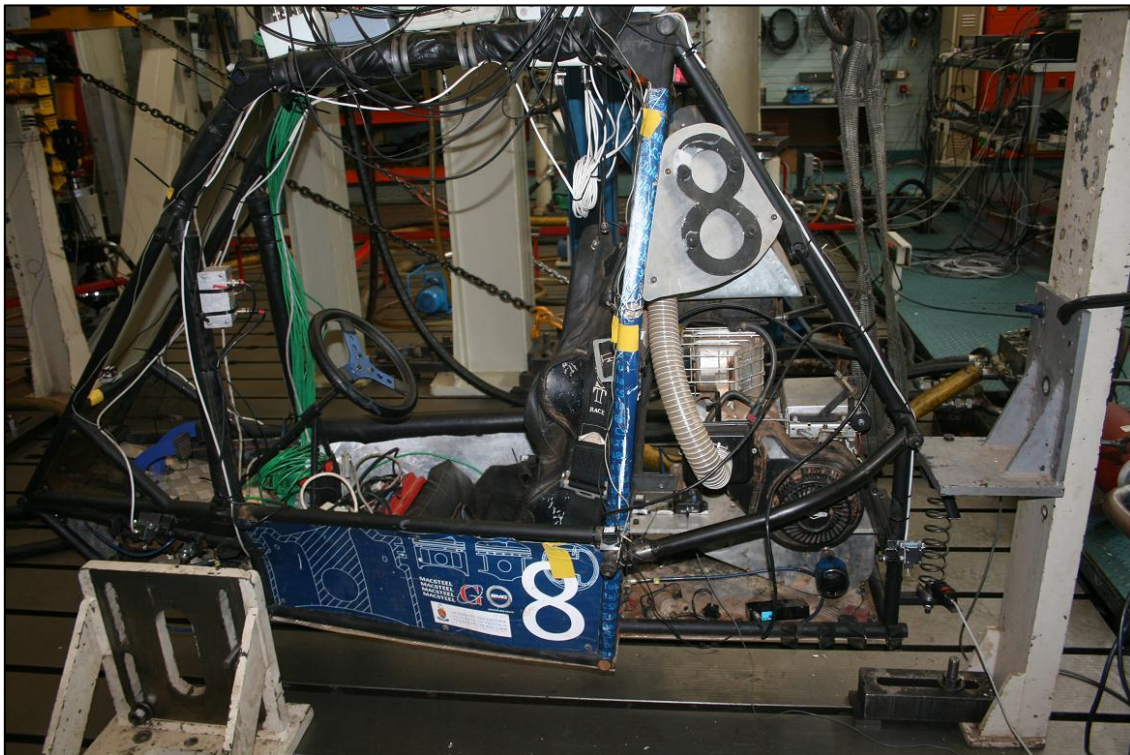


Figure 4-7: Experimental determination of pitch moment of inertia.

In Equation 53,  $M_{Baja}$  is the total mass of the sprung mass of the vehicle, including the driver and testing equipment, and  $d_{axis}$  is the distance between the pivoting axis and the corresponding parallel axis through the centre of mass.

The moment of inertia results of the vehicle are listed in Appendix A, Table A–1 to Table A–3, pA.1. The vehicle body was excited nine times about each of the three main axes. The degree of excitation was also varied between soft to strong. The average moments of inertia were used in the vehicle simulation model. An Inertial Measurement Unit (IMU) was used to measure the angular rate so as to verify that the correct degree of freedom was excited, as shown in Figure 4-9 to Figure 4-11, p4.8 to p4.9. The moment of inertia results from experimental work are given in Equation 54, 55 and Equation 56:

$$I_{roll} = 53.75 \text{kgm}^2 \quad [ 54 ]$$

$$I_{pitch} = 90.58 \text{kgm}^2 \quad [ 55 ]$$

$$I_{yaw} = 69.16 \text{kgm}^2 \quad [ 56 ]$$

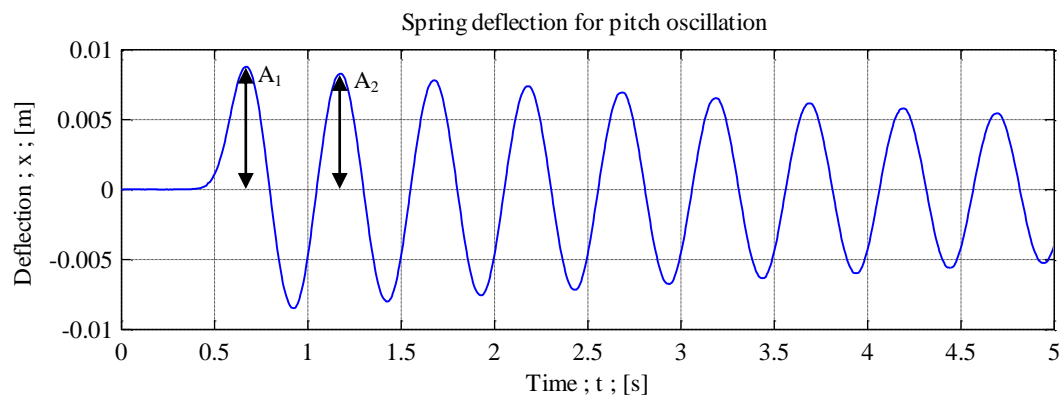


Figure 4-8: Spring deflection decay.

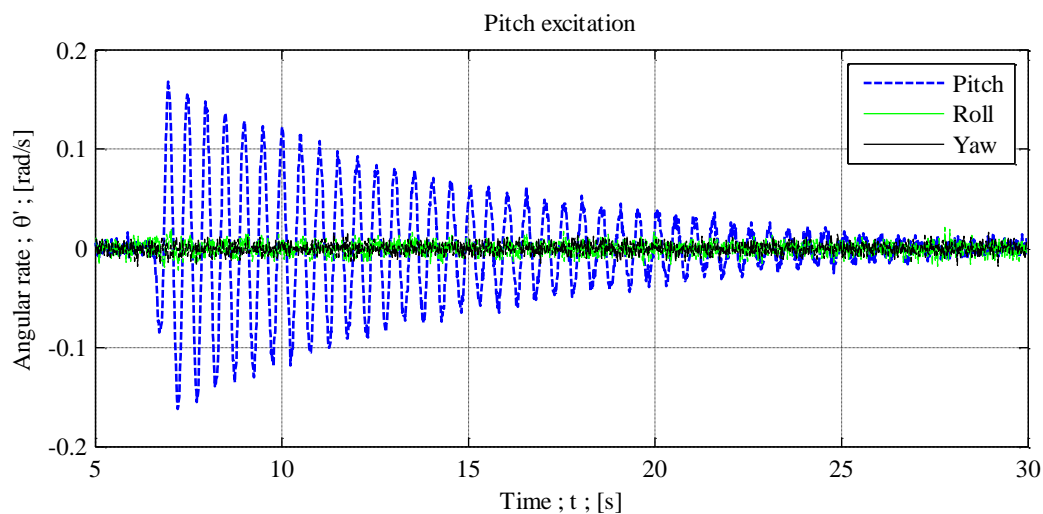


Figure 4-9: Measured angular rates during pitch excitation of vehicle sprung mass.



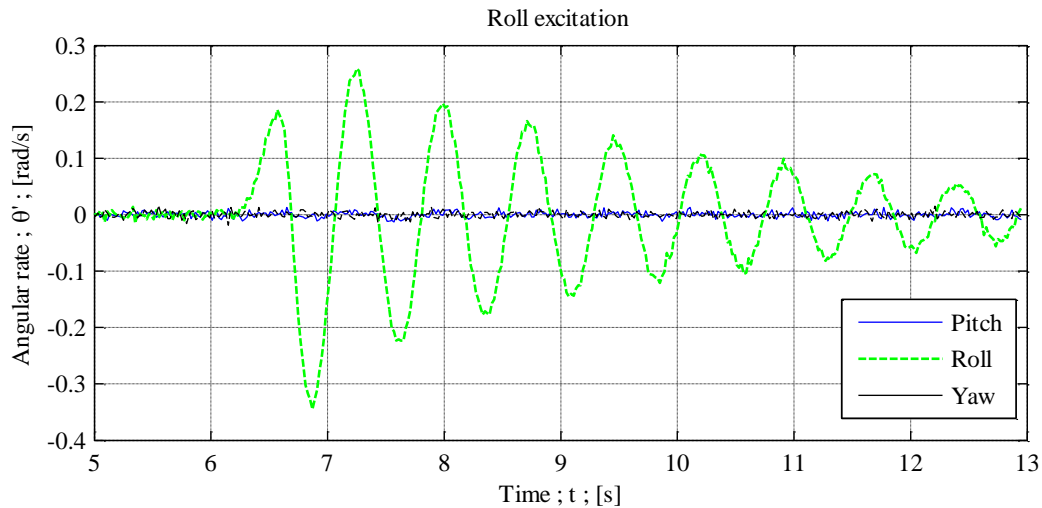


Figure 4-10: Measured angular rates during roll excitation of vehicle sprung mass.

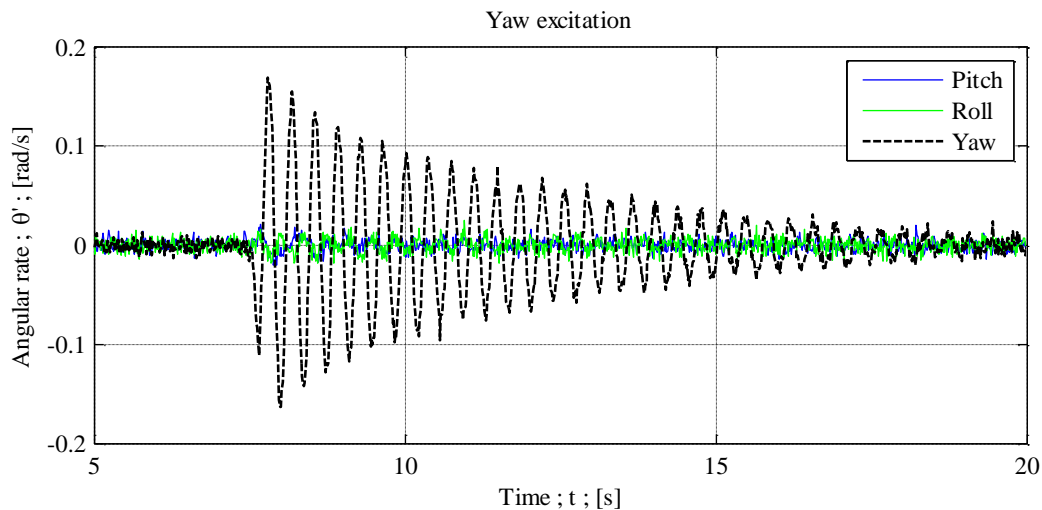


Figure 4-11: Measured angular rates during yaw excitation of vehicle sprung mass.

### 4.2.3 Hydro-Pneumatic Spring-Damper Unit Characterization

Characterization of the passive spring-damper units installed on the current vehicle is an accumulation of work done by previous research group members. The experimental setup assembly and data capturing performed by **Wehrmeyer (2011)** are briefly discussed in this section. A cross-section technical drawing including dimensions of the spring-damper unit is given in Figure 4-12, p4.10. Since the spring-damper behaviour is highly nonlinear, the characteristics have to be established and defined in the simulation model, rather than using a regular spring and damper with a constant stiffness and damping coefficient. Although the hydro-pneumatic spring-damper is a single unit, separate spring and damper characteristics are required by the simulation software.

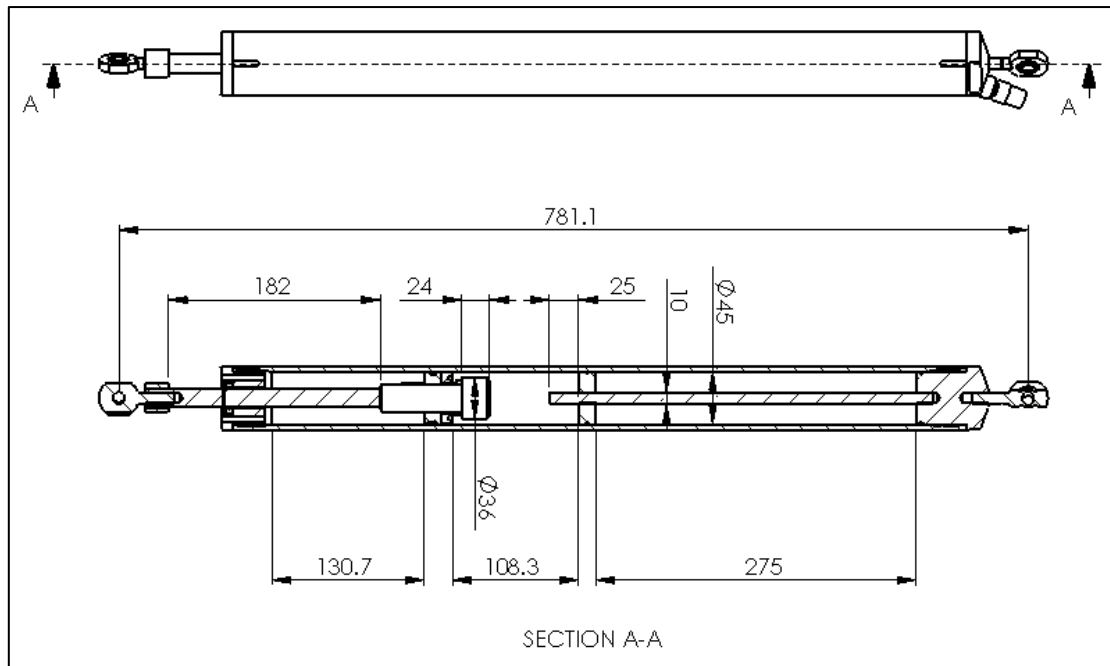


Figure 4-12: Hydro-pneumatic spring-damper unit section (Wehrmeyer 2011).

#### 4.2.3.1 Experimental Work

The hydro-pneumatic spring-damper unit characterization experimental setup is shown in Figure 4-13, p4.11. Optimal suspension settings require different suspension characteristics for the front and the rear of the vehicle, obtained by using different oil- and gas volumes, and holes in the piston. Therefore four characteristics are required: two different spring characteristics for the front and the rear, and two different damper characteristics for the front and the rear. In the experimental setup the spring-damper unit is connected in-line to a load cell and a hydraulic actuator via clevises. The setup is supported by a supporting frame mounted onto the hydraulic actuator body. The actuator imposes prescribed sinusoidal displacement inputs on the spring-damper unit, which is measured by the internal actuator linear variable differential transformer (LVDT) displacement transducer. The 10kN load cell measures the corresponding force exerted by the spring-damper unit. Sinusoidal displacement inputs of 0.08m amplitude at various frequencies are imposed on the damper and data is sampled at 1kHz.

#### 4.2.3.2 Pneumatic Spring Characteristic

The spring characteristics are determined by imposing a very slow sinusoidal displacement input, such that  $\dot{x} \approx 0$ , on the spring-damper units. By approximating a zero-velocity input, the presence of the damping characteristics should be minimized in the measured data. The stroke of the displacement input is 0.16m and the excitation frequency is 0.01Hz. The spring characteristic (force vs. displacement) for the front and rear springs are indicated in Figure 4-14 and Figure 4-15, p4.12. The

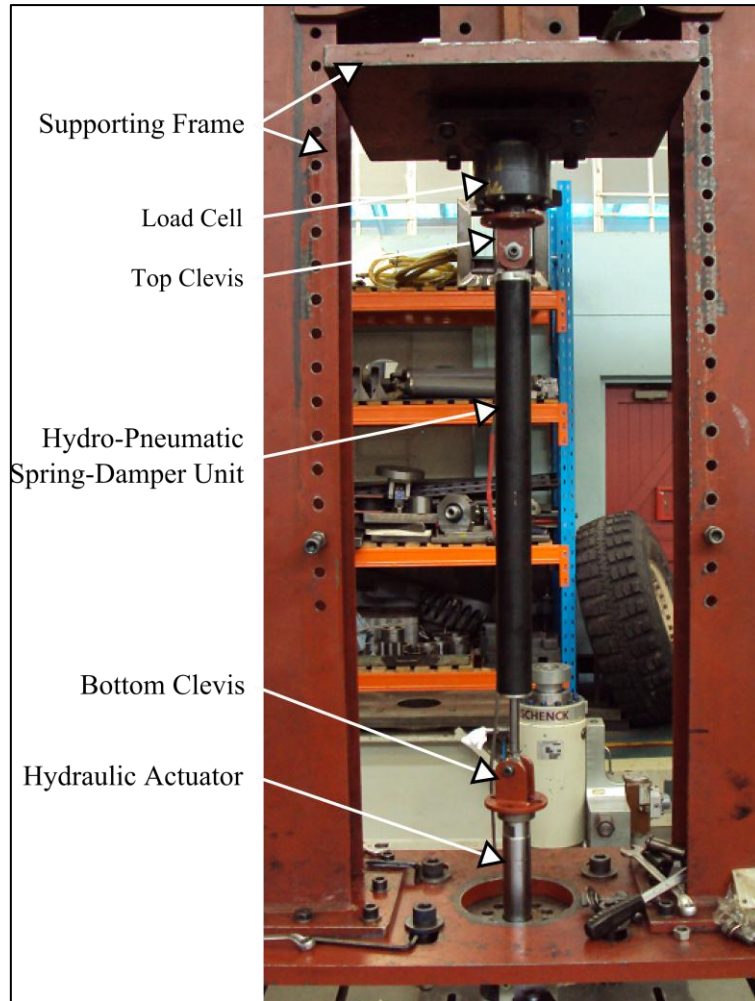


**Figure 4-13: Hydro-pneumatic spring-damper unit characterization experimental setup (Wehrmeyer 2011).**

characteristic exhibits a hysteresis loop (i.e. characteristics are different for compression and rebound). This can mostly be attributed to heat transfer effects and friction in the seals as a result of asymmetric seal geometry, but also to the fact that, although the speed is low, damping is not totally eliminated. Note that compressive forces are negative. The average force between the compression and rebound is used to determine the spring characteristics, while the hysteresis loop (friction) will be taken into account in the damper characteristics. The static pressure of the front and rear pneumatic springs is 6bar and 5bar respectively. This is the pre-charge pressure when the spring is fully extended against the built-in rebound stops. Due to the pre-load pressure an initial static force is required before the spring will start compressing, indicated in Equations 57 and 58, p4.11.

$$F_{s,f} = P \times A = (600 \times 10^3) \times \pi \times \left(\frac{0.0449}{2}\right)^2 = 950.0N \quad [ 57 ]$$

$$F_{s,r} = P \times A = (500 \times 10^3) \times \pi \times \left(\frac{0.0449}{2}\right)^2 = 791.7N \quad [ 58 ]$$

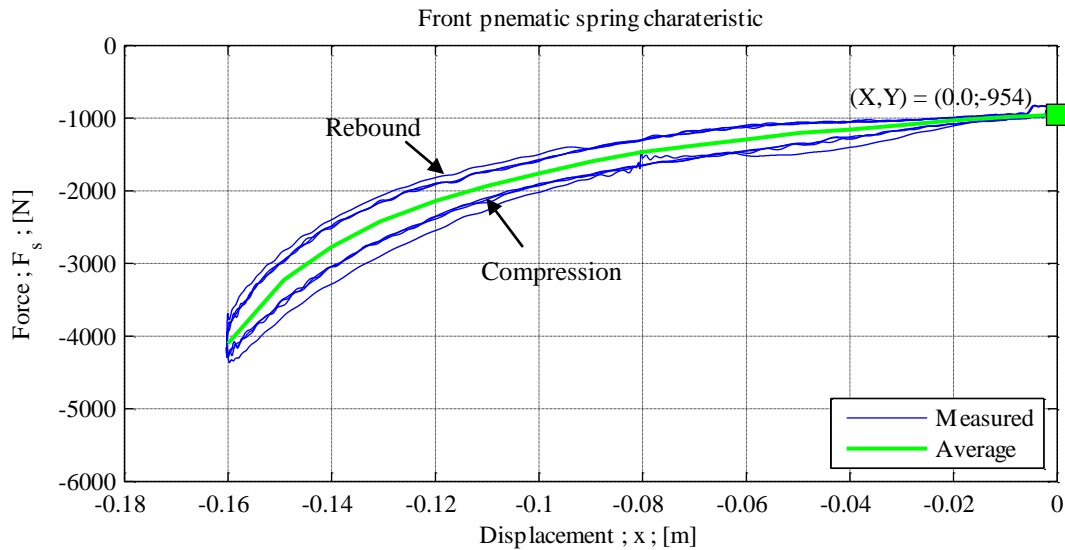


Figure 4-14: Average front spring characteristic.

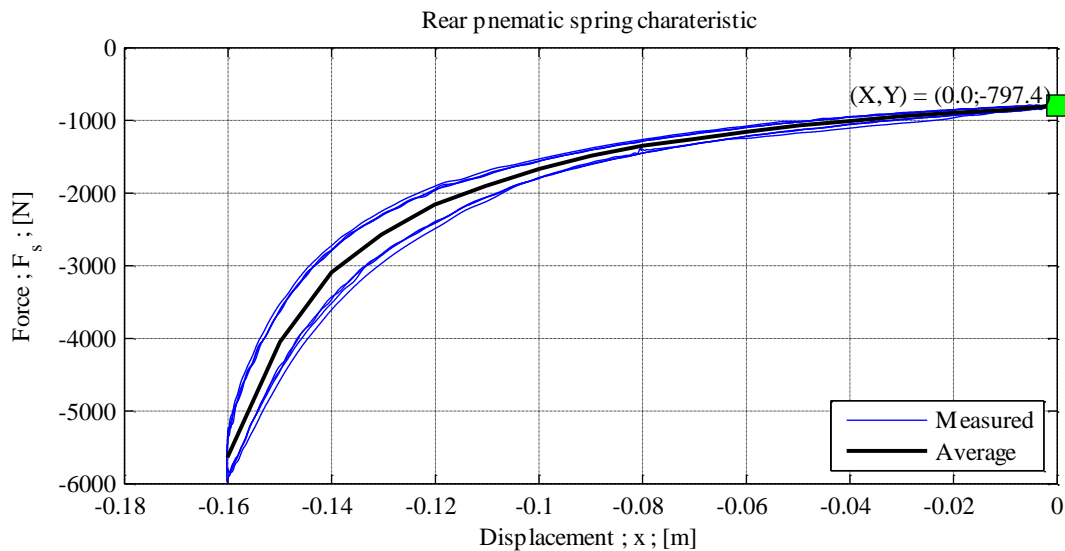


Figure 4-15: Average rear spring characteristic.

In Equations 57 and 58 the diameter of the piston is 0.0449m and the surface area is calculated using  $A = \pi r^2$ . The initial force values correspond well to the measured values at zero displacement in Figure 4-14 and Figure 4-15, p4.12.

If the spring piston reaches the rebound stop a sharp increase in extension force will be observed. Also, as the spring is compressed and approaches the stroke limit of 0.18m, a significant increase in force will be required to compress the spring further. The spring characteristic should include these phenomena to constrain the spring movement within realistic boundaries during simulations. The characteristics shown in Figure 4-16, p4.13 contain the rebound features indicated by a sharp increase in force for positive displacements, and the exponential increase in force when the spring compression exceeds 0.16m.

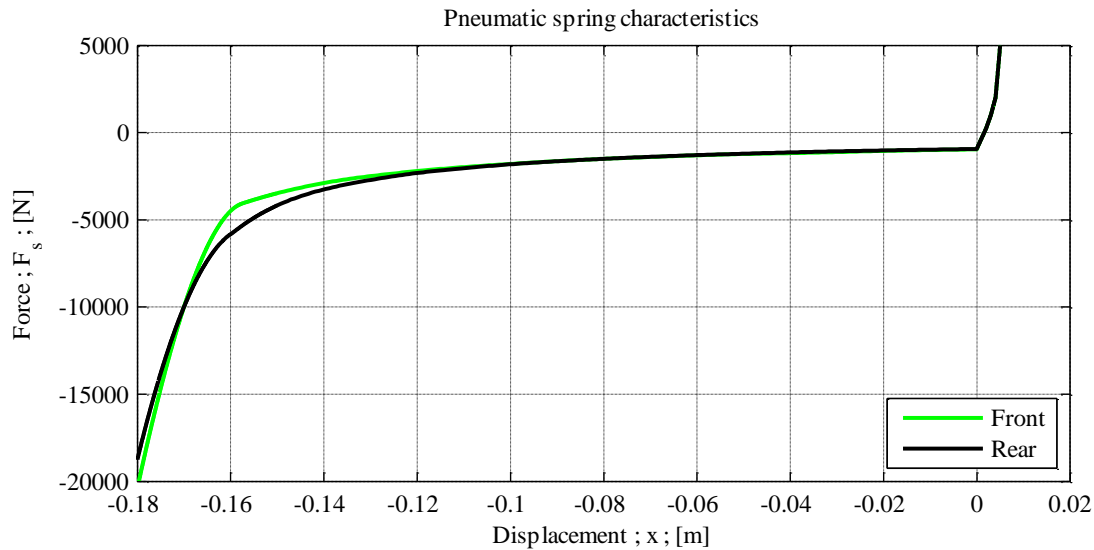
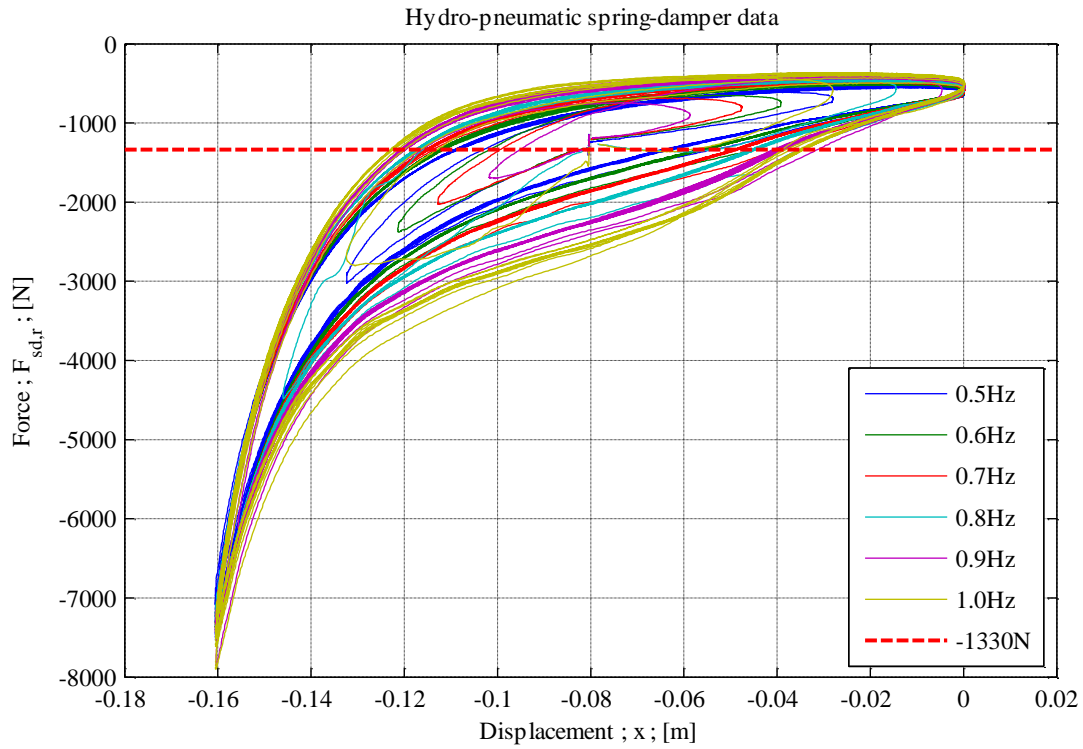


Figure 4-16: Front and rear pneumatic spring characteristics.

#### 4.2.3.3 Passive Hydraulic Damper Characteristic

The damper characteristic is determined by imposing sinusoidal displacement inputs of various frequencies and fixed amplitude of 0.08m on the hydro-pneumatic spring-damper units. By increasing the frequency the peak velocities are increased. To model the friction in the dampers low velocity inputs are also used. The dampers were excited with frequencies from 0.01Hz to 0.05Hz in increments of 0.01Hz, 0.5Hz to 1Hz in increments of 0.1Hz, and 2Hz. This excitation selection results in a maximum velocity input of 1.005m/s, which correspond to typical velocities a vehicle suspension experiences due to road irregularities (**Boada et al. 2011**). The measured force-displacement data at various frequencies is processed to generate force-velocity data. Measured forces of the rear spring-damper unit in response to displacement inputs at various frequencies are shown in Figure 4-17, p4.14. Velocity is obtained from measured displacement using the backward difference method. Negative velocity corresponds to compression and positive velocity corresponds to extension. The force-offset due to the pneumatic spring is removed by subtracting the static force when the spring-damper unit is compressed halfway (compressed by 0.08m), indicated by the red line (at -1330N) in Figure 4-17. The resulting force-velocity response is shown in Figure 4-18, p4.14. The damper characteristics are composed using the force magnitudes at the peak velocities for all measured data sets. Low excitation frequencies ( $\dot{x} \approx 0$ ) is used to capture the friction in the damper, and the data trend has been extrapolated to include higher velocities. The same process is used to determine the front damper characteristic. The damper characteristics, including the friction characteristic around the zero velocity point, are shown in Figure 4-19, p4.15.



**Figure 4-17: Force-displacement relationship of rear spring-damper unit.**

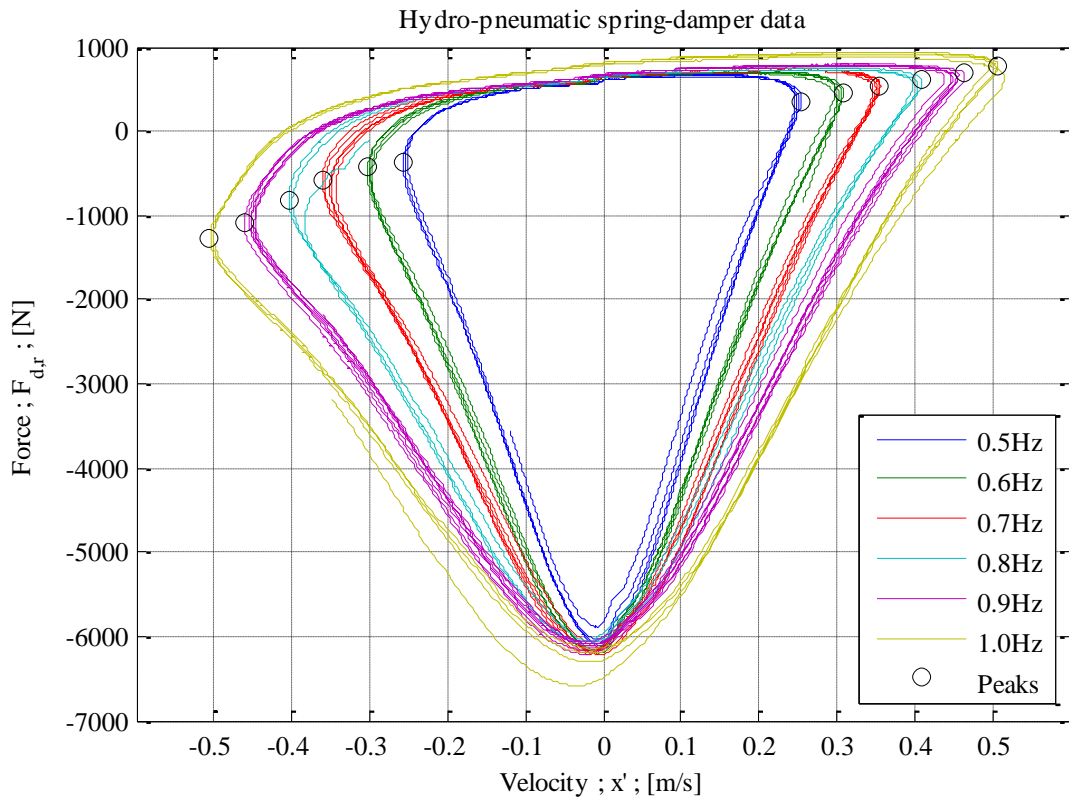


**Figure 4-18: Force-velocity relationship of rear spring-damper unit.**

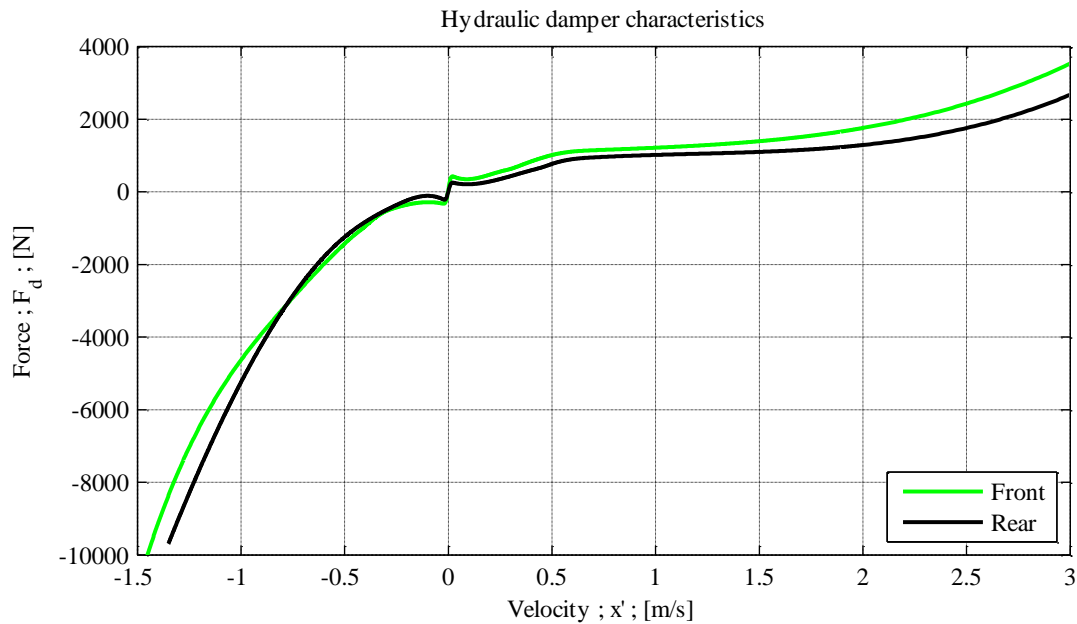


**Figure 4-19: Front and rear hydraulic damper characteristics.**

#### 4.2.4 The Tyre Model

To improve the controllability and predictability of vehicles in order to enhance vehicle safety, accurate vehicle simulation models are required. However, the accuracy of these vehicle models are often limited by the accuracy of the tyre models implemented. Except for aerodynamic forces applicable at high vehicle speeds, all the forces acting on the vehicle are transferred through the road-tyre contact area (**Gillespie 1992**). The tyre plays an important role in controlling the motion of the vehicle, therefore an accurate representation of the tyre is required in any model used for simulating vehicle dynamics. The Pacejka '89 tyre model is easy to work with, can be easily included in a vehicle model, and accurately represents the side force, brake force, and self-aligning torque in pure and combined slip conditions. Additional effects such as ply steer, conicity, rolling resistance and camber are also captured by this model (**Bakker et al. 1989**).

Therefore, the tyre model used in the simulation model is a Pacejka '89 model developed from experimental data, according to the methods described by **Van der Merwe (2007)**. The model is developed using a Maxxis Razr tyre, the old tyres used on the vehicle. Due to the lack of new tyre data of the Kenda tyres, the Maxxis Razr Pacejka '89 tyre model is implemented in the simulation model. The tyre characteristics were determined experimentally by towing a tyre tester behind a vehicle and measuring the side and brake forces for various slip angles and slip percentages. An updated version of the testing apparatus is shown in Figure 4-20, p4.16. In the previous test setup the slip angle is adjusted manually, and the lateral and longitudinal forces are measured using one longitudinal and two lateral load cells. The vertical load is increased by adding weights to the top surface of the tyre tester. The percentage slip is adjusted by braking the tyres through an adjustable



**Figure 4-20: Tyre characterization experimental setup.**

brake mechanism. Experimental data is processed and curve-fit methods are implemented to determine the Pacejka '89 model coefficients, listed in Appendix B, pB.1. The vertical stiffness and damping properties of the tyre has also been determined. This is done by dropping the tyre from a predetermined vertical height using a pendulum mechanism and measuring the rebound height for several oscillations. The logarithmic decrement in rebound height is used to determine the damping ratio (refer to Equation 50, p4.7 and Equation 51, p4.7). The side force, brake force, and self-aligning torque tyre characteristics are shown in Figure 4-21 to Figure 4-23, p4.17. The characteristics for a vertical load of 0.7358kN per tyre correspond to a vehicle mass of 300kg. The vertical load on the tyre varies in real time, and this variation is taken into account in the simulation model.

### 4.3 The Vehicle Simulation Model

The vehicle simulation model is three-dimensional with multiple degrees of freedom. The model is nonlinear and has been developed in ADAMS View software. The model consists of 20 moving bodies, 1 translational joint, 4 Hooke's joints, 8 spherical joints, and 12 revolute joints, resulting in a



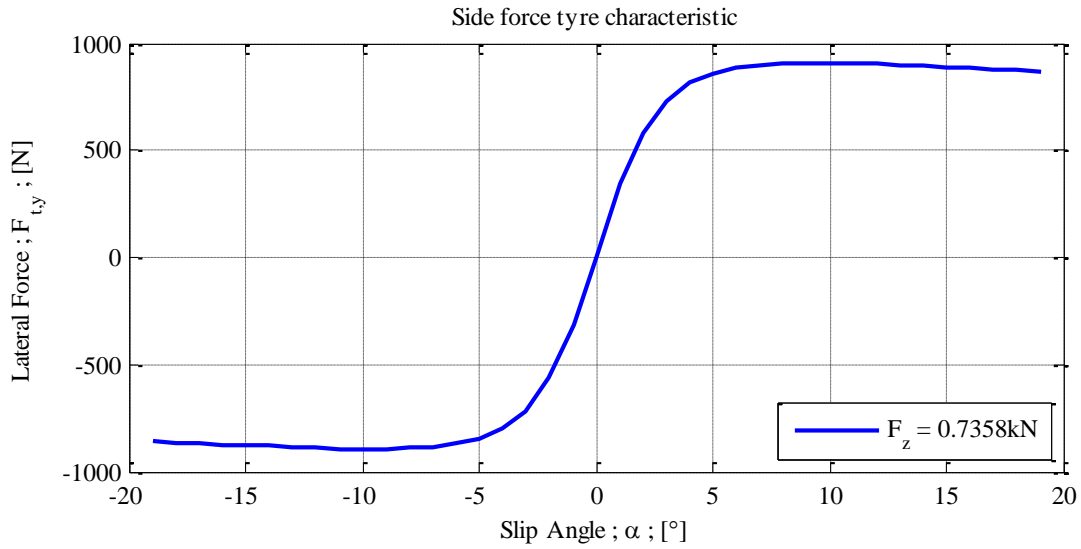


Figure 4-21: Pacejka '89 tyre model side force characteristic.

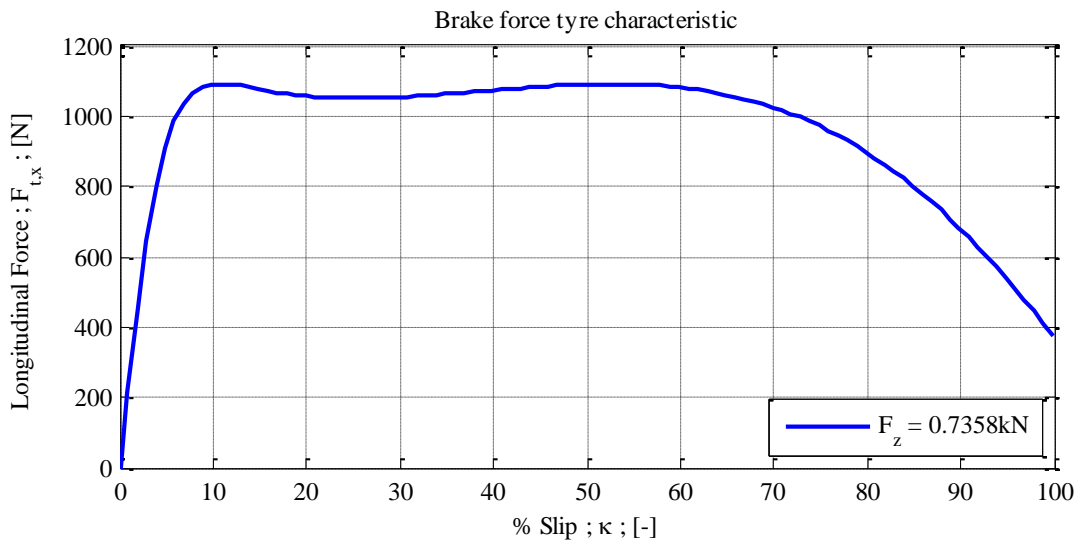


Figure 4-22: Pacejka '89 tyre model brake force characteristic.

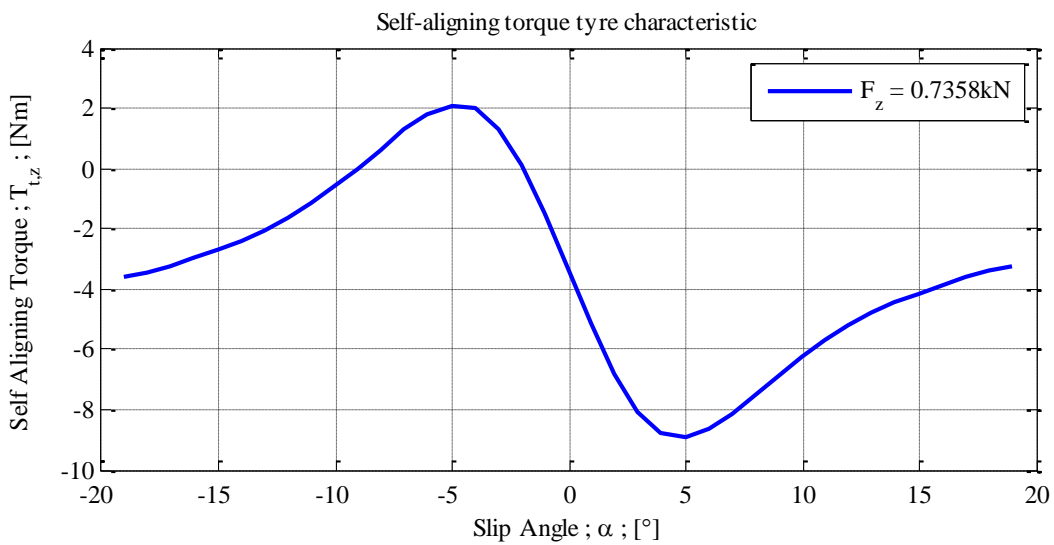
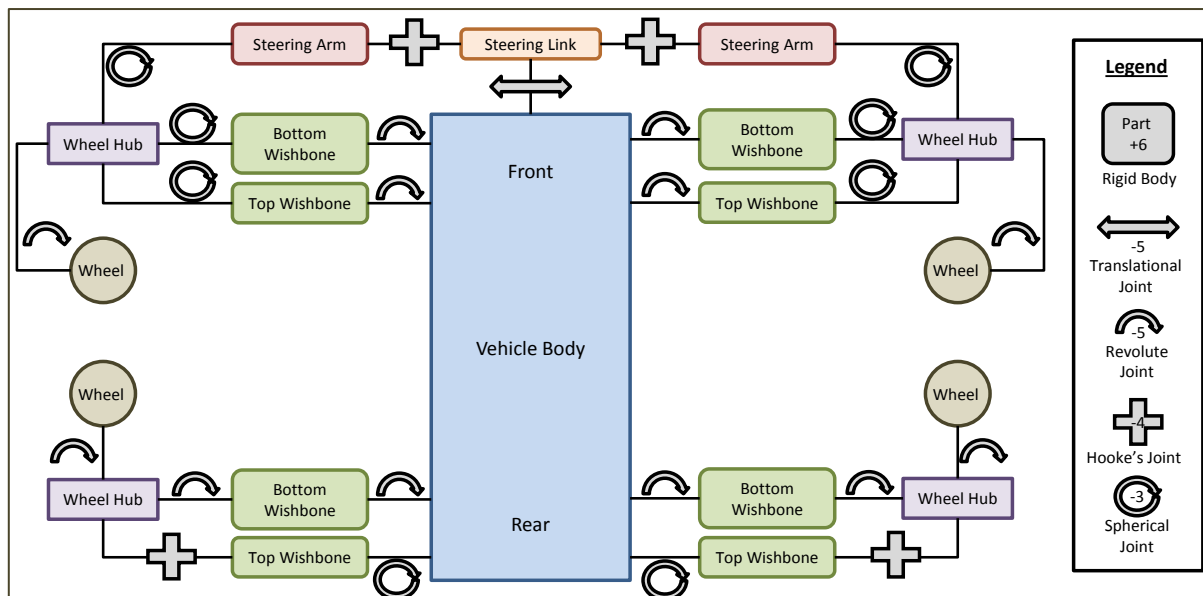


Figure 4-23: Pacejka '89 tyre model self-aligning torque characteristic.

model with 12 unconstrained degrees of freedom (DOF). The schematic layout of the model (indicating the joint constraints between the bodies) is shown in Figure 4-24, p4.18, and a graphic illustration of the model is shown in Figure 4-25, p4.19.

A detailed solid model of the vehicle has been used to define the geometry of the simulation model. The mass and inertia properties of the unsprung mass components were obtained from the computer aided design (CAD) model. The total mass of the sprung mass was obtained through physical measurements. The location of the centre of mass and the moment of inertia of the sprung mass about its three axes (roll, pitch and yaw) were determined experimentally as described in Section 4.2.1 and Section 4.2.2, p4.3 to p4.9. The unsprung mass components include the double wishbone parts, wheel hubs, brake disks and callipers, the steering rods, and hub-reduction gear boxes. The sprung mass consists of the vehicle body, including the driver and test equipment installed on the vehicle.

In most vehicle dynamics studies which entail larger vehicles the mass of the driver and additional testing equipment amounts to less than 10% of the total vehicle mass, and the effect of the driver and equipment are therefore simply added to the rigid body mass of the vehicle. Movement of the driver relative to the vehicle body results in negligible changes in the centre of mass position and moments of inertia. In this study the weight of the driver and testing equipment amounts to approximately 30% of the mass of the Baja vehicle body, which is a considerable amount. Movement of the driver relative to the vehicle body results in significant changes in centre of mass position and inertia properties and therefore has a significant influence on vehicle dynamics, especially over rough terrain and other severe excitation scenarios. It is very difficult to take these changes into account. This issue is



**Figure 4-24: Baja simulation model schematic.**

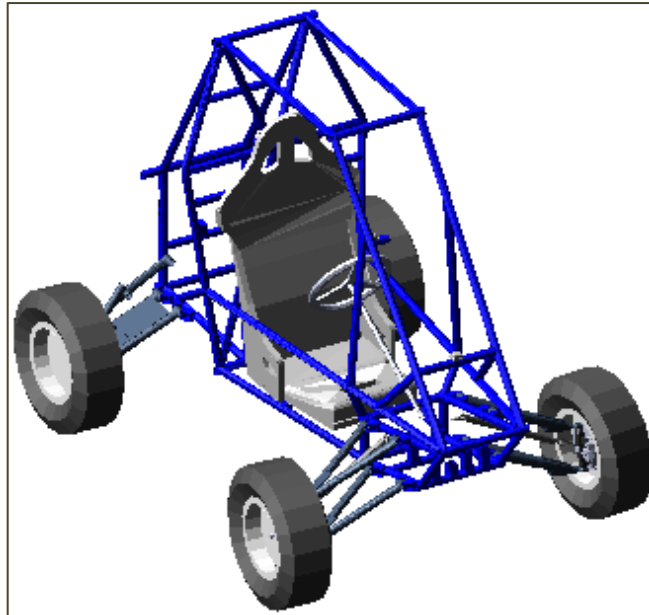


**Figure 4-25: Graphic illustration of Baja simulation model.**

currently addressed by only modelling the driver and testing equipment as part of the sprung mass. During testing the effects of the driver on the vehicle dynamics is minimized by proper fastening of the driver in the seat so that relative movement is limited.

The suspension of the vehicle consists of a double wishbone suspension system, with a hydro-pneumatic spring-damper unit positioned between the upper (front) or lower (back) wishbone and the vehicle body, as shown in Figure 4-1, p4.1, and Figure 4-26, p4.22. The hydro-pneumatic spring-damper units are modelled using forces acting between the Baja frame and wishbone components. The spring and damper characteristics of the spring-damper units are obtained separately as described in Section 4.2.3.2, p4.10, and Section 4.2.3.3, p4.13. Thus, for a given displacement and velocity input, the simulated springs and dampers will exert forces as defined by the spring and damper characteristic splines defined in the simulation model.

The tyre model implemented in the simulation model is the Maxxis Razr Pacejka '89 tyre model discussed in Section 4.2.4, p4.15. The road profile can be defined either as vertical displacement that is a function of longitudinal displacement for both tracks, or as a 3-dimensional surface that can be created using coordinates. The method of interpolation between prescribed coordinates has to be specified.

The simulation model requires three general motion inputs: the steering input and rotational inputs at the rear wheels. The motion inputs are used to drive the model to simulate manoeuvres performed by the vehicle. The steering is modelled as lateral displacement of the steering rack which imposes motion on the steering rods connected to the left and right front wheels. Steering inputs can either be

fixed (to drive straight ahead), or the lateral displacement of the steering rack is defined as a function of time. This is done either by implementation of measured data or by a driver model used to follow a prescribed path. The vehicle is driven forward by prescribing a rotational speed to the rear wheels as a function of time. To allow the simulation model to be comparable to the experimental tests, the measured steering and speed inputs are prescribed in the model as inputs.

## 4.4 Baseline Vehicle Testing

Baseline testing entails the execution of several repeatable tests while measuring parameters of interest for the purpose of generating data that can be used for model validation, and to determine the overall performance of the Baja. The performance of the baseline passive suspension is evaluated and later compared to the performance of the semi-active controlled suspension system in order to evaluate the performance of the control algorithm. Baseline testing was performed at Gerotek Test Facilities (**Gerotek, 2008**) on various concrete surfaces and the Belgian paving track.

To obtain an accurate simulation model it is required that the model be adequately validated for ride comfort as well as handling. Ride comfort can be assessed from the vertical and pitch degrees of freedom of the vehicle, while the lateral, roll, and yaw degrees of freedom can be used to comprehend handling performance. The bump test, discussed in Section 4.4.2, p4.22, is used to excite the vehicle in the vertical and pitch degrees of freedom, and the slalom test, discussed in Section 4.4.3, p4.23, is used to excite the vehicle in the lateral, yaw, and roll degrees of freedom. Several runs of each test were performed to confirm data trends and repeatability.

The instrumentation used for baseline testing is discussed in Section 4.4.1, p4.20, and the model validation procedure and test results are discussed in Section 4.5, p4.24.

### 4.4.1 Instrumentation

During baseline testing 24 channels of data were acquired using an eDAQ data acquisition system. An additional nine variables were measured using the IMU data measuring software. A list of measuring equipment, installation position, and corresponding measurements, is given in Table 4-2, p4.21. The instrumented Baja at Gerotek Testing Facilities is shown in Figure 4-26, p4.22. The location of the various testing equipment on the vehicle is indicated schematically in Figure 4-27, p4.22. All data was acquired at a sampling frequency of 100Hz.

Variables measured by the eDAQ system include (refer to Figure 4-27, p4.22):

1. Four MR damper relative displacements. These measurements can be converted to spring-damper displacements. (MR dampers not installed on the vehicle during baseline testing).
2. Steering rack displacement.
3. Nine vehicle body (sprung mass) accelerations, measured in three primary directions (longitudinal, lateral, and vertical) at three locations (front middle, rear left, and rear middle).
4. Four wheel (unsprung mass) accelerations, measured in the vertical direction only.
5. Three vehicle body angular velocities about the main axes of the vehicle (roll, pitch, and yaw rates).
6. Vehicle body vertical displacement relative to ground.
7. Secondary CVT rotational speed.
8. Vehicle absolute speed obtained from velocity box (VBox) unit.

Variables measured by the IMU system include:

- Three vehicle body angular displacements about the main axes of the vehicle (roll, pitch, and yaw angles).
- Three vehicle body angular velocities (roll, pitch, and yaw rates). These quantities are also measured by the eDAQ system via the gyroscope.
- Three vehicle body (sprung mass) accelerations, measured in the three primary directions.

The data acquisition system is powered by a 12V battery carried on board during testing and located under the seat. The eDAQ unit is located in the nose of the vehicle. Power is distributed to the testing equipment via specific power boxes either mounted on the roof or placed in the driver compartment next to the seat. Cables are secured to the vehicle frame.

**Table 4–2: Equipment installed on Baja vehicle for baseline testing.**

Equipment	Quantity	Position	Measurement
String displacement sensors	5	At all 4 MR damper locations	MR damper displacement
		1 at the steering rack	Steering rack displacement
Accelerometers	7	Vehicle body, 3 locations	X, Y, Z Sprung mass acceleration
		At all 4 wheels	Z Unsprung mass acceleration
Gyroscope	1	Vehicle body, roof	Pitch, roll and yaw rate
Laser displacement sensor	1	Vehicle body	Body height relative to ground
Optical sensor	1	Secondary CVT	Speed input to gearboxes
VBox	1	Vehicle body, middle	Vehicle velocity
IMU	1	Vehicle body, rear	Angular displacements, angular velocities, sprung mass accelerations



**Figure 4-26: Instrumented Baja vehicle for baseline testing.**

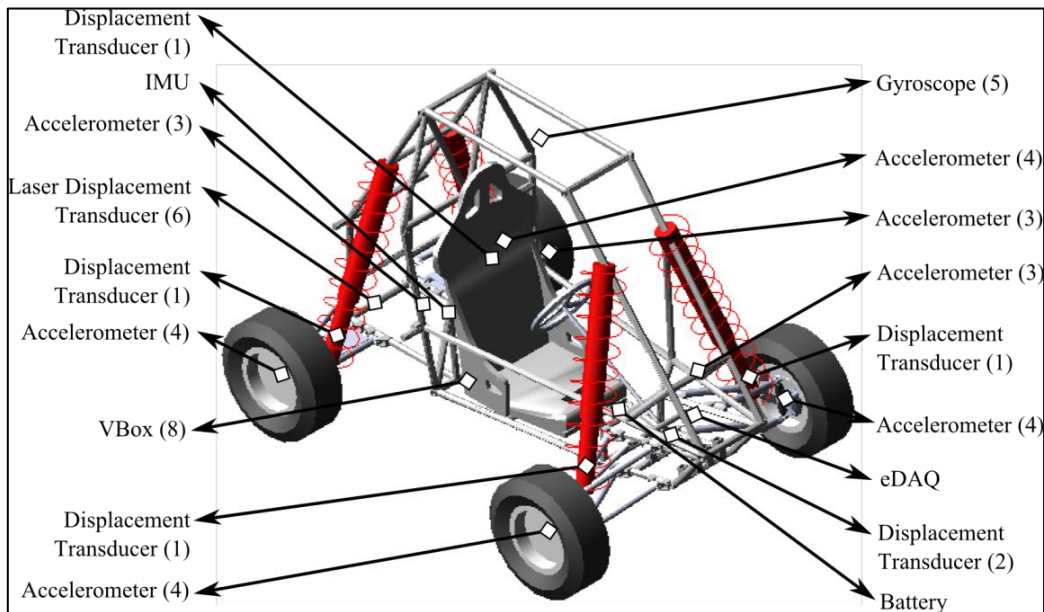


**Figure 4-27: Schematic representation of instrumentation installed on Baja vehicle.**

#### 4.4.2 Bump Test Experimental Setup

In the bump test the vehicle is driven over a set of bumps with pre-defined geometry in order to excite the vehicle in the pitch and vertical degrees of freedom. The vehicle accelerates from a stationary position at a defined distance from the bumps, and comes to a halt after it passed over the bumps. The test is performed at various bump entry speeds. The bump geometry and detailed profiles are shown in Figure 4-28, p4.23. The bumps are placed at the track width apart (1.35m) and are parallel to each other, as shown in the schematic in Figure 4-29, p4.23.

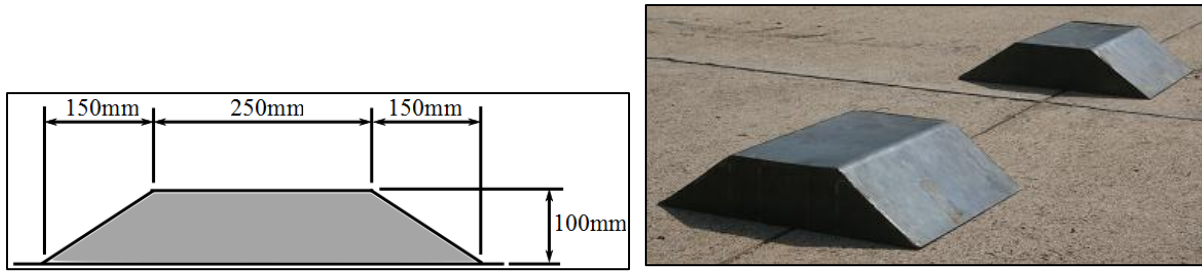


**Figure 4-28: Bumps implemented in bump test.**

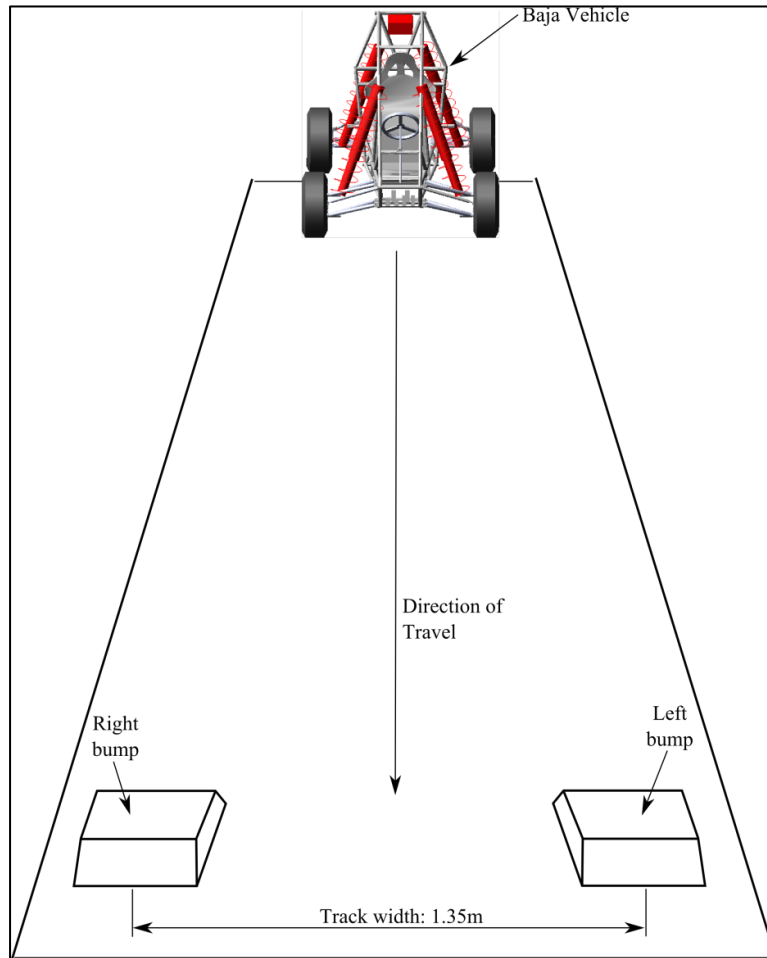


**Figure 4-29: Schematic of bump test setup.**

### 4.4.3 Slalom Test Experimental Setup

In the slalom test the vehicle is driven around cones placed in a straight line in order to excite the vehicle in the lateral, yaw and roll degrees of freedom. The vehicle accelerates from a stationary position at a defined distance from the first cone, and comes to a halt after it passed through all the cones. The distance between the five cones is arbitrarily chosen to be 7.5m. The test is performed at various speeds, and the vehicle speed does not remain constant during the test. A schematic of the slalom test setup is shown in Figure 4-30, p4.24.

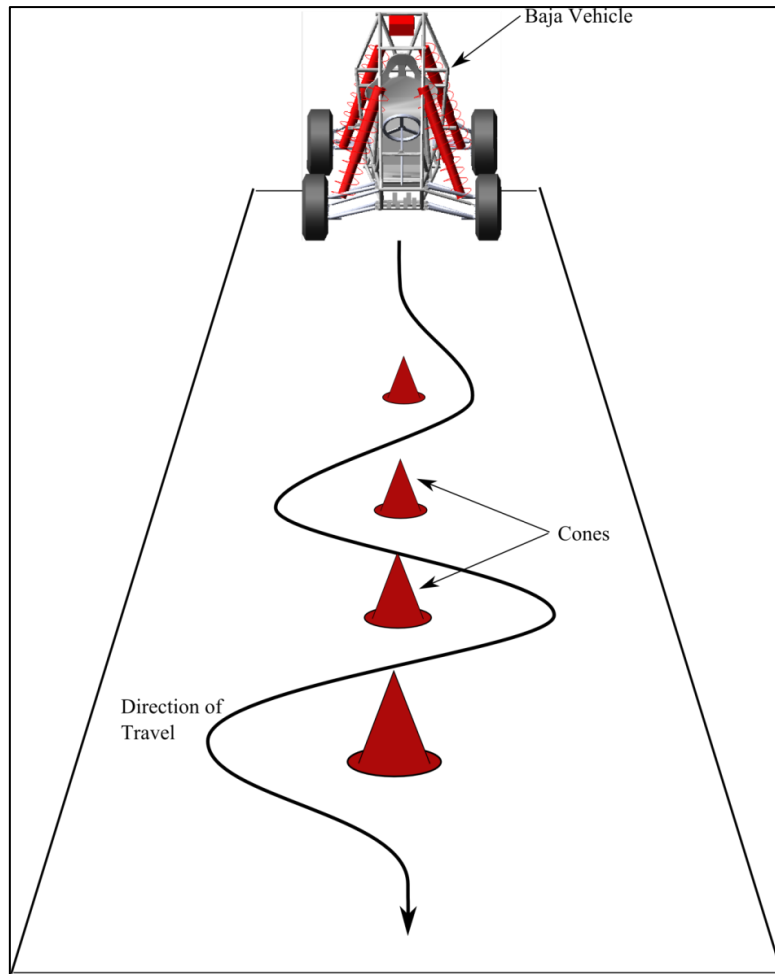


Figure 4-30: Schematic of slalom test setup.

## 4.5 Model Validation

To validate the Baja simulation model, measured data from the two baseline tests is compared to the simulation data. The baseline tests include the discrete bump test (discussed in Section 4.4.2, p4.22) and the slalom test (discussed in Section 4.4.3, p4.23). The measurement locations of the simulation model correspond to the physical locations on the vehicle that were used for data collection during testing, as indicated in Figure 4-27, p4.22. Since MR dampers are going to be installed on the vehicle as part of future work, the damper displacements were measured at the MR damper mounting locations during baseline testing and simulations. As a result, the measured data shows a maximum stroke of approximately 70mm, instead of 180mm (refer to Figure 4-16, p4.13) which is the approximate stroke of the hydro-pneumatic spring-damper units. All measured data has been filtered using a low pass filter with a cut-off frequency of 20Hz to eliminate the effects of the engine and transmission system vibration on the measured data, which is also not taken into account in the simulation model.



### 4.5.1 Bump Test Results

During the bump test, the vehicle is driven in a straight line, thus the steering input of the simulation model remains fixed in the neutral position. The road profile is altered to include the bump profile shown in Figure 4-28, p4.23. The measured secondary CVT rotational speed is converted to a rotational speed of the rear wheels using the fixed reduction ratio, and used as a prescribed motion in the simulation model in order to drive the vehicle. Since data capturing did not commence from a stationary position, the simulation speed input has been altered to allow for the decay of transient effects and to accelerate the vehicle to the measured speed magnitude. The speed input is shown in Figure 4-31, p4.25. The simulation results are compared to the measured data available, thus  $t = 32s$  in Figure 4-31 correspond to  $t = 0s$  in Figure 4-32, p4.26 to Figure 4-35, p4.28. The simulation solver step size is set to 0.002s.

The vehicle body angular rate correlation is shown in Figure 4-32, p4.26. While the simulation results show very little excitation in the roll and yaw degrees of freedom, the measured data exhibits significant excitation. This is due to an alignment error while driving over the bump (since both front wheels don't hit the bump at the same time). The measured yaw rate absolute magnitude increases after 3.5s, indicating that the vehicle was steered to the right after completion of the test. Since the steering is fixed in the simulation, the simulated yaw rate remains zero. The pitch rate simulation results correspond well to the measured data, especially for the first valley where the peak value is within 16% of the measured value. The simulation results are within 13% of the highest peak, and 46% of the last valley.

The suspension deflection results are shown in Figure 4-33, p4.27. It may be noted that compression of the dampers is indicated by negative displacements. The simulation results of the first compression of the front dampers correspond well to the measured data. According to the measured

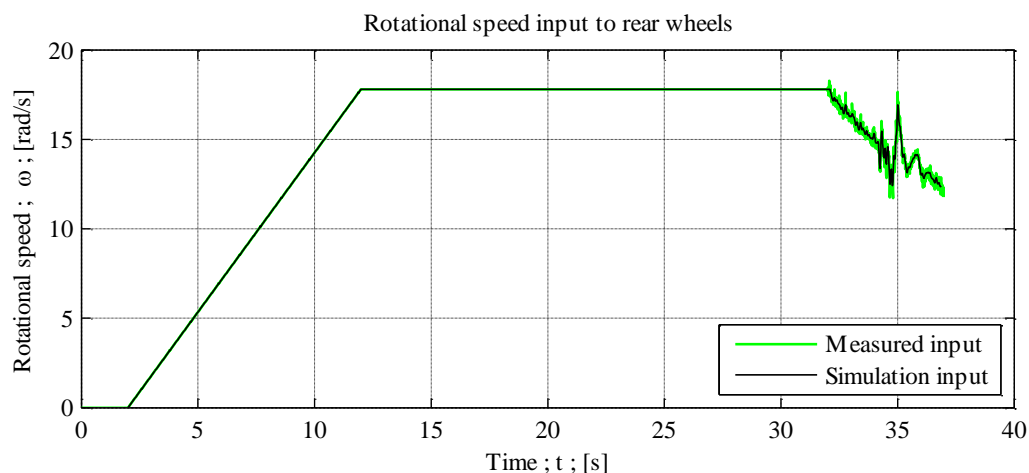
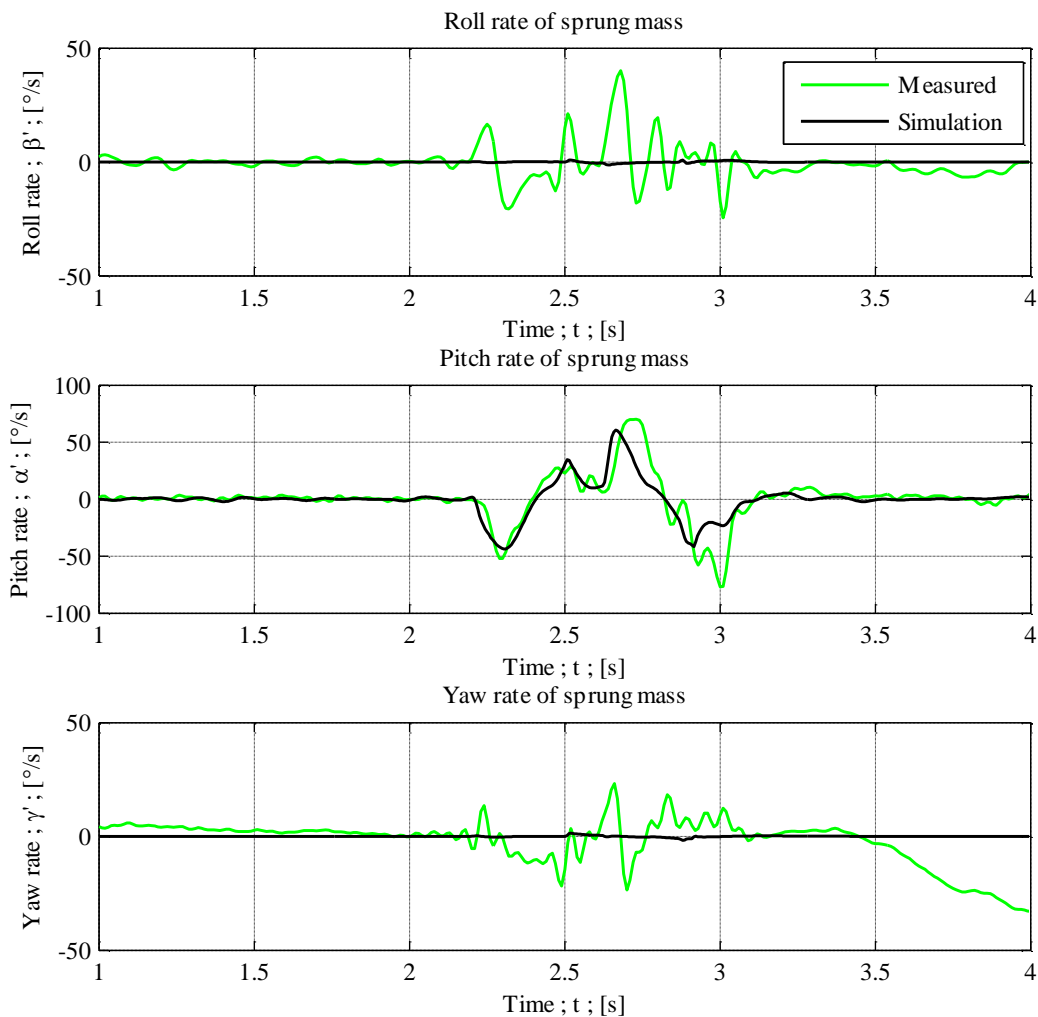


Figure 4-31: Bump test measured and simulation speed input.



**Figure 4-32: Bump test vehicle body angular rates results.**

data, the left rear damper compressed further than the right rear damper, indicating that the pneumatic springs may not have been at the same pressure setting at the time of data collection. As a result the simulation peaks correspond better to the rear right measured damper displacement data since the rear right damper was used to determine the spring-damper characteristics. Also, the suspension of a vehicle is a statically indeterminate system and small changes in variables such as tyre pressures or suspension displacements result in significant changes of the suspension forces. Friction present in the hydro-pneumatic spring-damper units also influence the static position of the suspension and may thus cause asymmetric compression. These factors could have contributed to increased yaw and roll motion seen in Figure 4-32, p4.26. The turn to the right after completion of the test is also visible in the damper displacement measured data, as indicated by the compression of the left dampers and extension of the right dampers after 3.5s. The suspension deflection simulation results are within 0.3-19.7% for the first valley, and 12-14% for the first peak. Rear left damper displacement results are not investigated due to the implementation of an incorrect spring-damper characteristic.

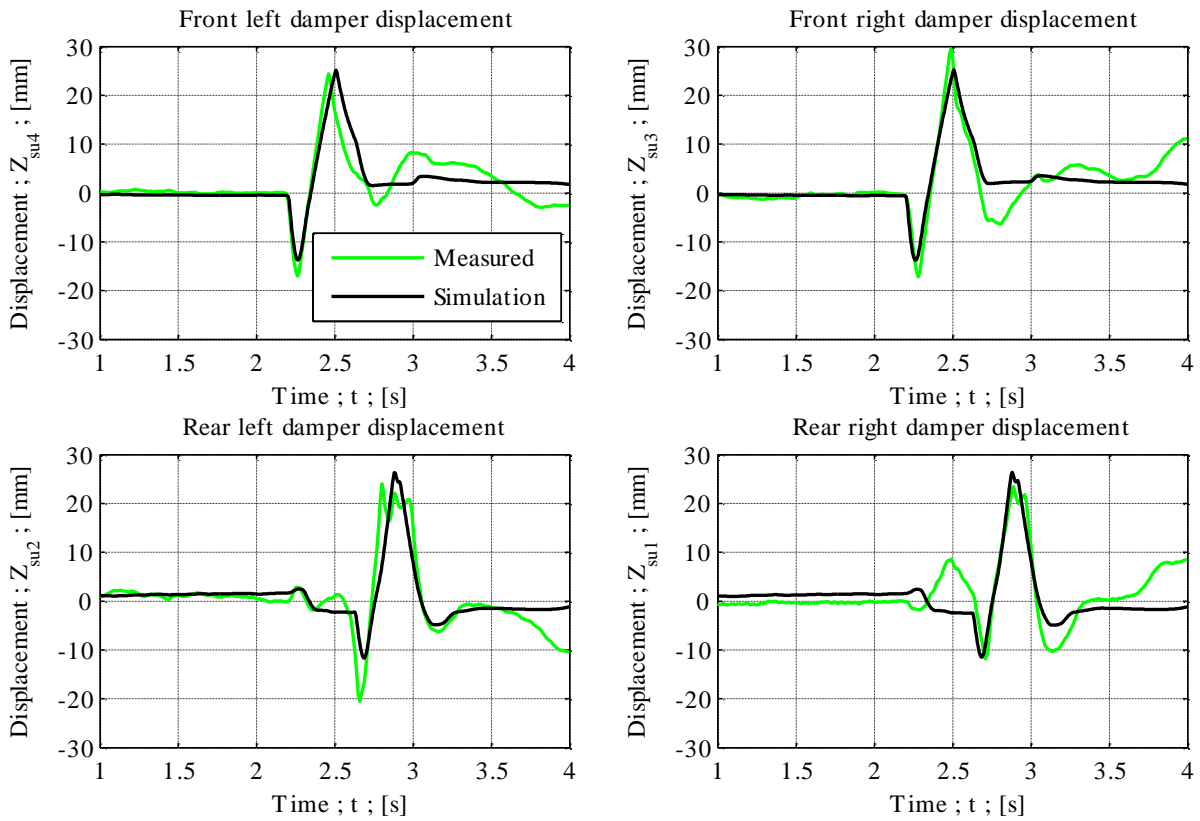


Figure 4-33: Bump test suspension deflection results.

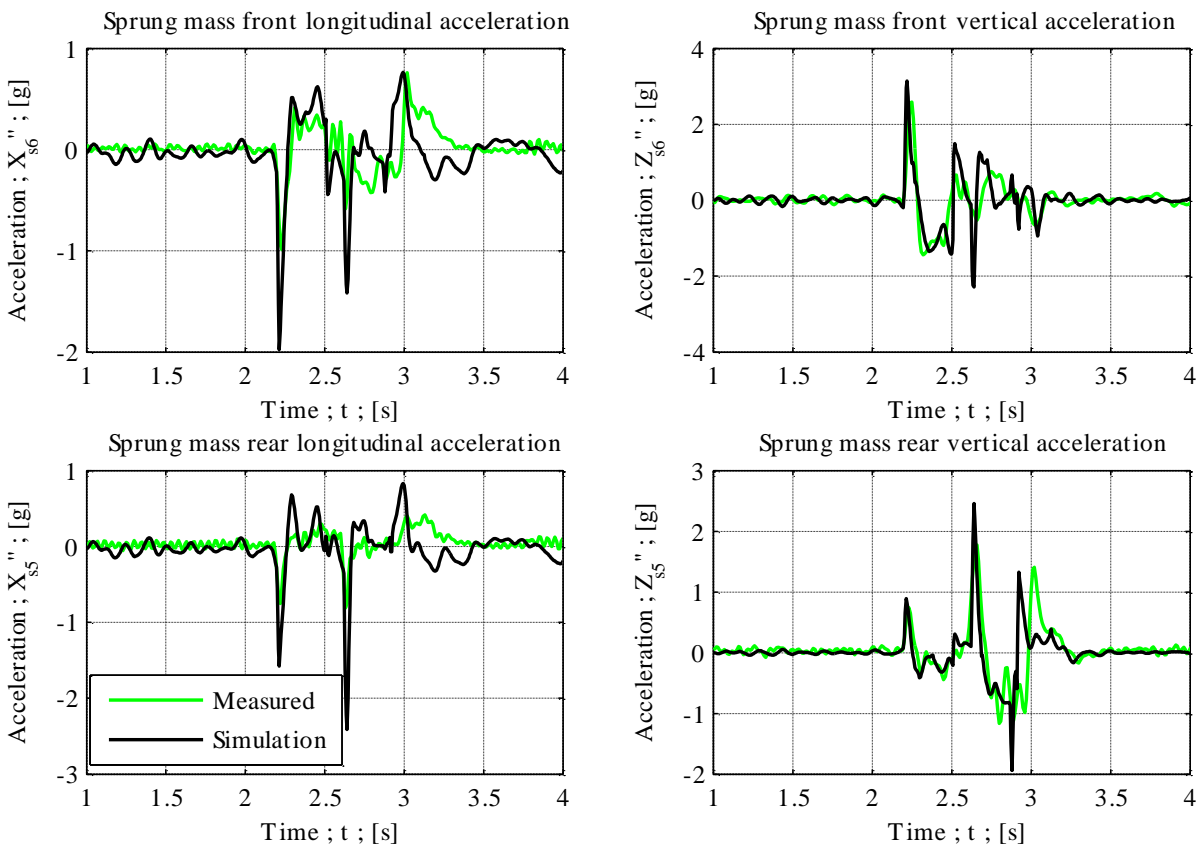
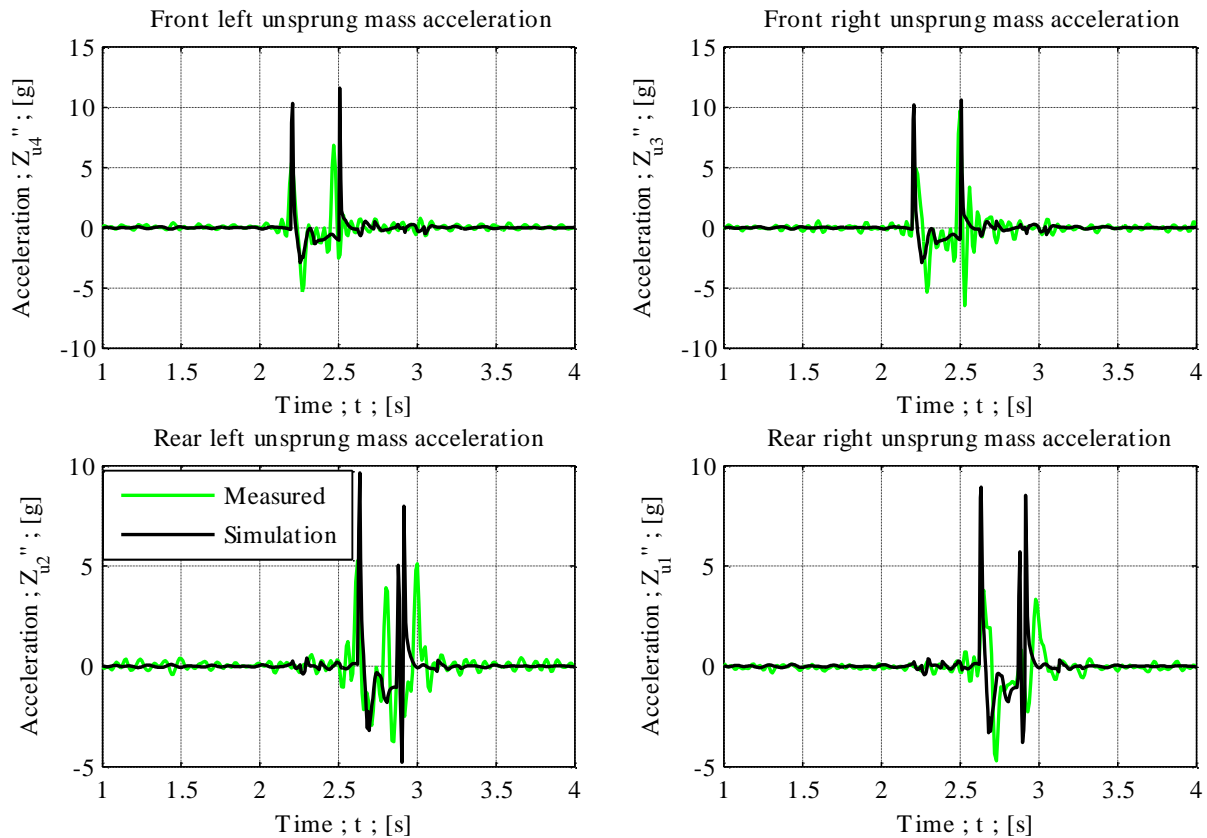


Figure 4-34: Bump test vehicle body acceleration results.



**Figure 4-35: Bump test unsprung mass vertical acceleration results.**

The correlation of the sprung mass longitudinal and vertical acceleration is shown in Figure 4-34, p4.27. The longitudinal acceleration results show that the simulation model experiences more braking when the bump is hit, as indicated by the larger negative peak values at 2.2s which exceed the measured data by approximately 96-114%. The sprung mass vertical acceleration simulation results correspond well to the measured data. All the peaks and valleys of the four measurements (consisting of two locations measured in two directions) exceed the measured data by between 4-128% and 6-337% respectively.

The unsprung mass vertical acceleration simulation results and measured data are shown in Figure 4-35, p4.28. The peak values of the simulation results are in general higher than the measured data. A possible explanation for the large discrepancies is the relatively low sampling frequency used during data collection.

Satisfactory pitch rate, suspension deflection, and sprung mass vertical acceleration correlation results are obtained for the bump test. It is thus concluded that the simulation model is satisfactory for the vertical and pitch degrees of freedom, and can therefore be used for simulating ride comfort.

## 4.5.2 Slalom Test Results

During the slalom test, the vehicle is driven around cones placed in a line. A flat road surface is used in the simulation model to represent this test. Various entry speeds were measured, and the speed did not remain constant throughout the test runs. The simulation solver step size is set to 0.002s. Two slalom test simulations are performed.

The first slalom test simulation (indicated by Simulation 1 in Figure 4-38, p4.30 to Figure 4-41, p4.33) incorporated the measured steering input and speed in the model, shown in Figure 4-36 and Figure 4-37, p4.29, respectively. The measured speed varied between 26rad/s and 33rad/s during entry to the first cone and exit from the last cone. Due to double integration during the solving process, a significant amount of lateral drift is present in the results of the simulation model, resulting in inaccurate suspension deflection predictions (refer to Figure 4-39, p4.31, Simulation 1 and Measured).

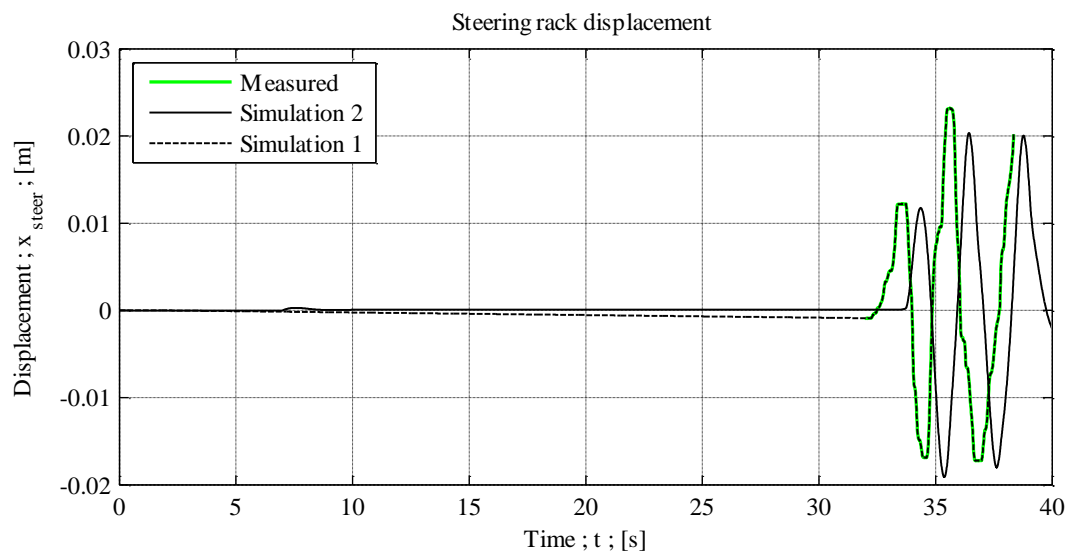


Figure 4-36: Slalom test measured and simulation steer input.

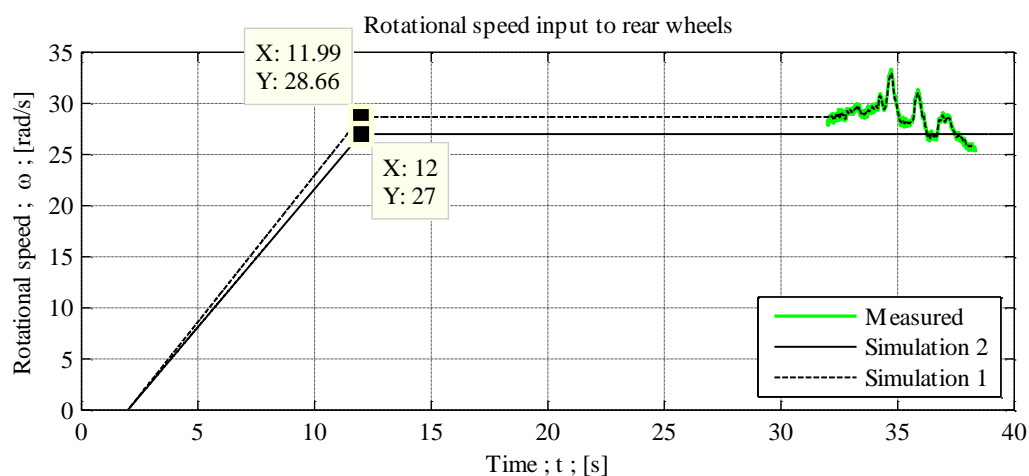


Figure 4-37: Slalom test measured and simulation speed input.

A satisfactory correlation of suspension deflection is particularly important because the simulation model is required to assess suspension control. The inaccurate results from the first simulation necessitated the implementation of a second simulation.

In the second simulation test (indicated by Simulation 2 in Figure 4-38, p4.30 to Figure 4-41, p4.33) a mathematical model of the steering controller is implemented to follow a prescribed path around the cones. The steering controller is very complex and directly incorporates the effect of tyre saturation and load transfer. A description of the model can be found in **Botha and Els, (2011)**. A constant rear wheel rotational speed input of 27rad/s is used for this simulation. The speed input was the highest possible speed selected such that the simulation model performed the slalom test successfully without roll over or slide-out occurring. The speed and steer inputs of Simulation 2 are shown in Figure 4-36, p4.29, and Figure 4-37, p4.29.

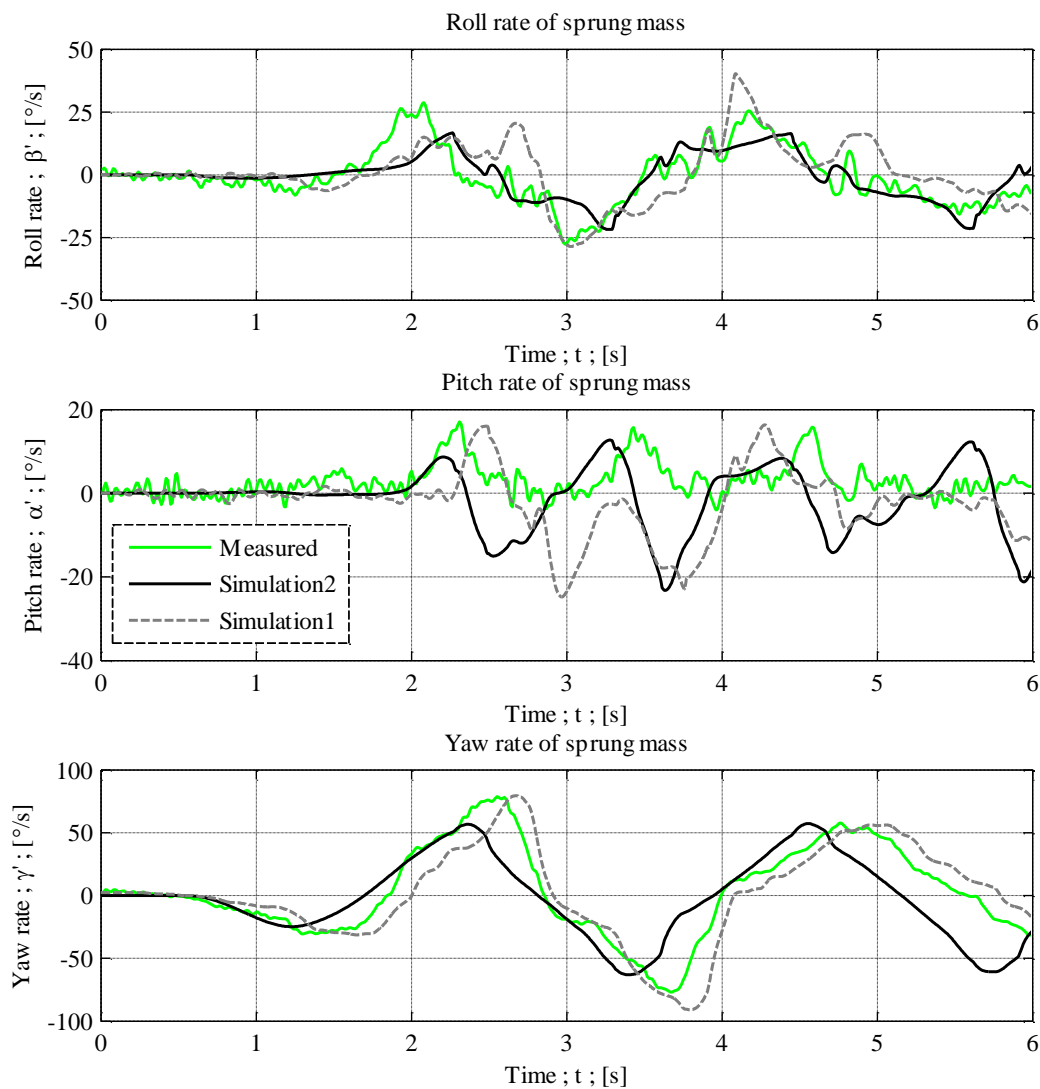


Figure 4-38: Slalom test vehicle body angular rates results.

The vehicle body angular rate correlation is shown in Figure 4-38, p4.30. The yaw rate simulation results correspond well to the measured data. The speed input for Simulation 2 is held constant, resulting in approximately equal magnitude peaks at different times (as compared to the measured data and Simulation 1 results). The peak values of Simulation 1 and Simulation 2 are within 1.4-18% and 0.7-28% of the measured values, respectively. The roll rate compares well with the measured data.

The suspension deflection results from the slalom test are shown in Figure 4-39, p4.31. According to the measured data the rear wheels lifted from the ground during the performance of the slalom test, indicated by extension of the rear dampers that remain constant when the piston reaches the rebound stops. It may be noted that the extension of the dampers is indicated by positive displacements. Simulation model 2 accurately captures the suspension stroke limitations whereas Simulation model 1 mistakenly predicts large compression magnitudes. Simulation 1 overshoots suspension compression by 82-179% and extension by up to 129%. Furthermore, suspension deflection results of Simulation 2 are much more comparable to the measured data than Simulation 1. However, the peaks in Simulation 2 occur at different times, this is due to a different speed input used for this simulation.

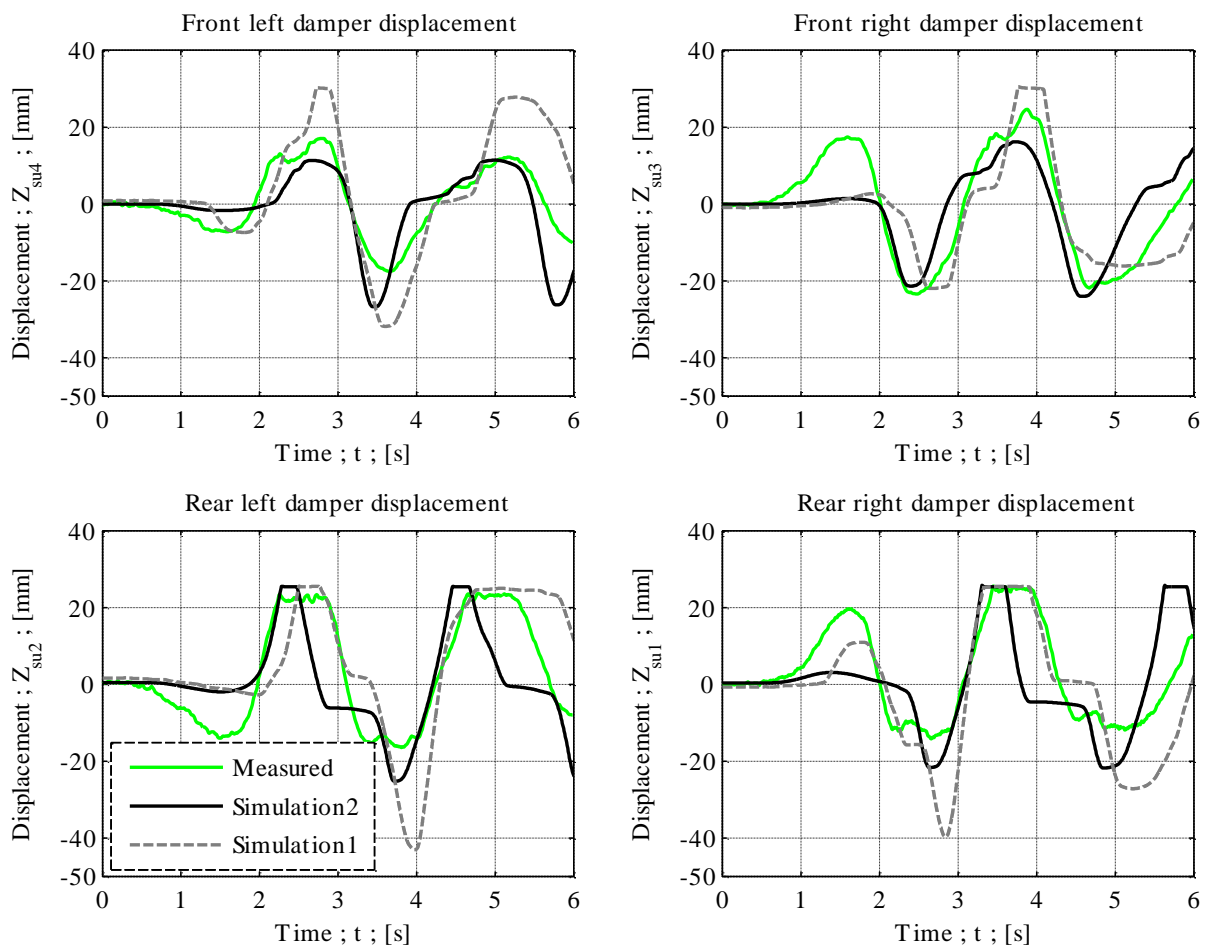


Figure 4-39: Slalom test suspension deflection results.

The correlation of the sprung mass longitudinal and lateral acceleration is shown in Figure 4-40, p4.32. The longitudinal acceleration behaviour is more accurately captured by Simulation 2 with acceleration peaks exceeding the measured values by up to 100%. The lateral acceleration simulation results correspond well to the measured data. Similar to the yaw rate results, the lateral acceleration is also accurately captured by Simulation 2, although the peaks occur at different times due to the different speed input.

The comparison for unsprung mass vertical acceleration is shown in Figure 4-41, p4.33. The road roughness is not taken into account in the simulation models, resulting in very low vertical acceleration magnitudes, especially visible up to 2s. When the front and rear rebound stops are reached in Simulation 1, sharp peaks in unsprung mass accelerations occur. Since the front rebound stops are never reached in Simulation 2, the model more accurately captures the front unsprung mass vertical acceleration behaviour. When the rear rebound stops are reached in both simulation models, a sharp peak occurs, followed by a negative acceleration magnitude for the duration of loss of contact with the road surface. The acceleration peaks could be attributed to the sharp rebound characteristic of the pneumatic spring. Since the measured signal is much noisier due to the road roughness, loss of ground contact is not visible as a constant negative acceleration value. Instead, the mean value of the signal drops below zero at the time intervals when the rebound stops are reached.

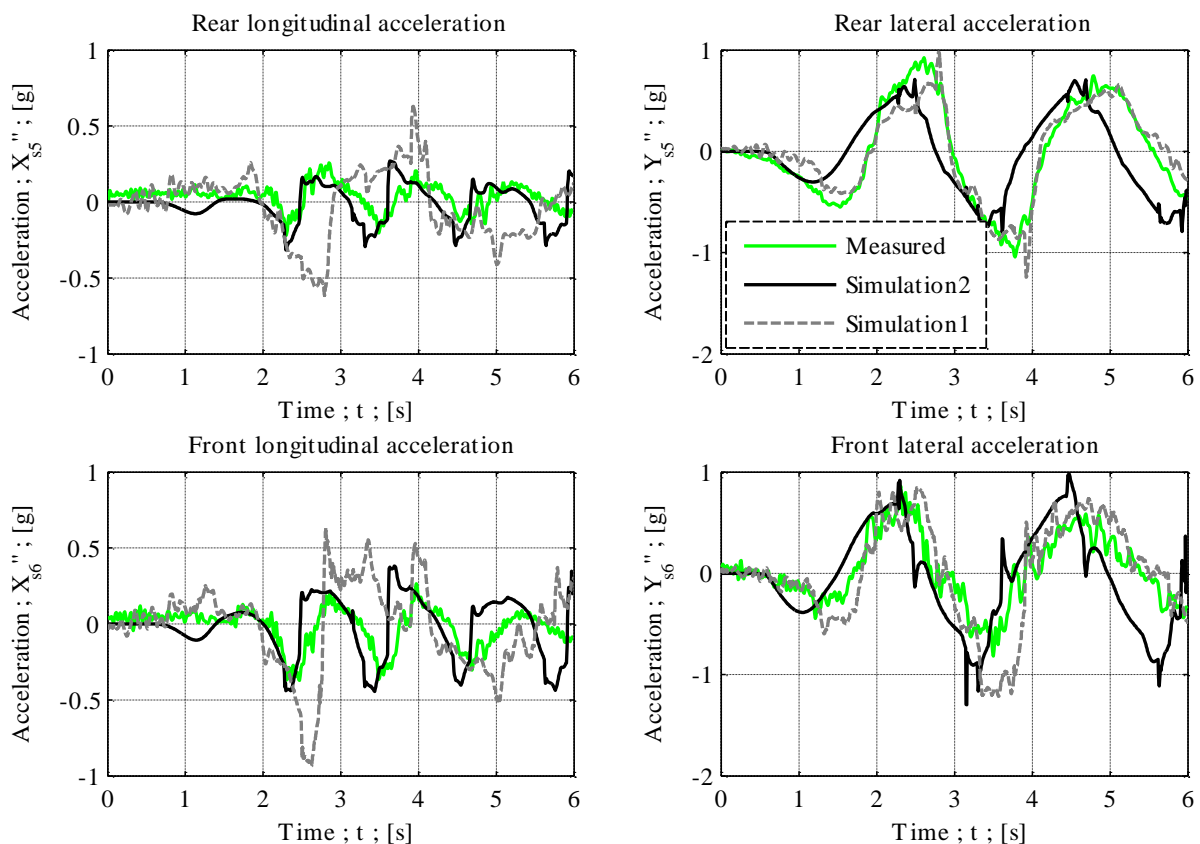
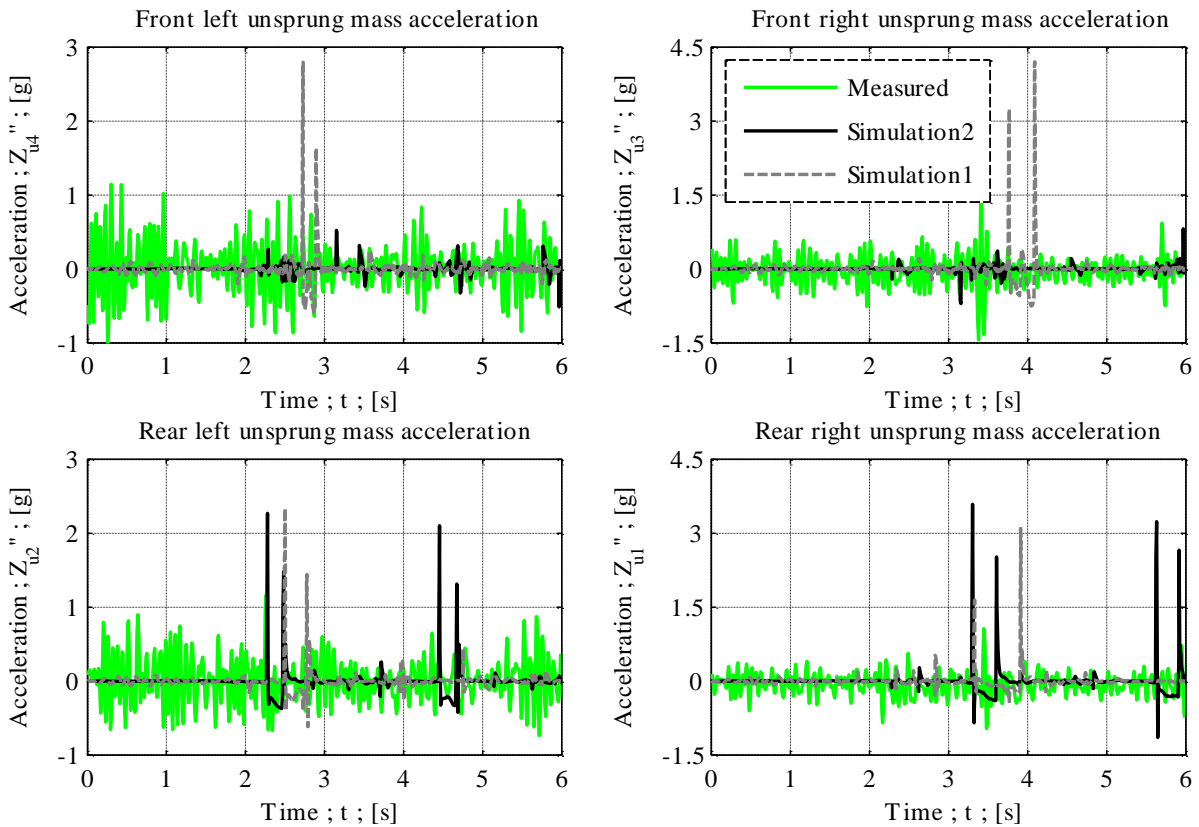


Figure 4-40: Slalom test vehicle body acceleration results.





**Figure 4-41: Slalom test unsprung mass vertical acceleration results.**

Poor correlation between the measured data and simulation results of the slalom test may be attributed to various effects, the main contributor being unrealistic lateral displacement due to errors introduced during double integration of the solving process. This sideways drift of the simulation model result in inaccurate suspension deflection during the simulation test, including loss of contact of the front wheels, which is not present in the measured data. Loss of contact of the steering wheels result in delayed steer, hence a delay in the results of Simulation 1 and measured data. In order to address the inaccuracies in the model as a result of lateral drift a steering controller is implemented in Simulation 2 to force the vehicle to follow the correct path. The delay between the results of Simulation 2 and measured data is a result of a different steering input obtained from the steering controller, as shown in Figure 4-36, p4.29, and a different speed input, as shown in Figure 4-37, p4.29. Another contributor to poor correlation between the measured data and the simulation results may be the Pacejka tyre model implemented in the simulation model. The tyre model does not take lateral damping into account although the double wishbone suspension geometry allows lateral displacement of the wheels as they move up and down. The implementation of a more complex tyre model becomes significant during handling studies where the simulation model is excited in the lateral and yaw degrees of freedom.

The slalom test correlation process can thus be summarised as follows: Unforeseen problems with the solver for vehicle handling simulation tests resulted in inaccurate predictions from Simulation 1. In an attempt to rectify the problem, steps were taken that deviated from the prescribed execution of the test. A constant speed input was used, and instead of using the measured steering input, a steering controller was implemented to follow a prescribed path. The slalom path was created by generating a sinusoidal curve through the cone locations. It is expected that the handling simulation correlation can be significantly improved by measurement of the followed path, and by performing the slalom test at a constant speed. Other tests such as a sinusoidal steer test, single lane change test, or double lane change test can also be implemented for further investigation of vehicle handling studies. It is therefore concluded that the model is satisfactory for preliminary handling studies only, and that there is significant scope for improving the testing process and the simulation model.

## 4.6 Conclusion

A full model of the Baja vehicle is required for suspension control studies. A nonlinear, three-dimensional, multiple degree of freedom model has been developed using ADAMS View software and has been discussed in detail in this chapter. This model incorporates experimentally determined moments of inertia, centre of mass location, spring and damper characteristics, and a Pacejka tyre model.

A discrete bump test and a slalom test have been performed to obtain measured sprung mass acceleration, unsprung mass acceleration, sprung mass angular rates, and suspension deflection data for the baseline vehicle. The results from the tests are discussed in detail in this chapter. The measured data has been used to validate the simulation model, and to evaluate the performance of the baseline vehicle.

Test data from the discrete bump test has been used to successfully validate the vehicle simulation model for ride comfort simulation. Two simulation models have been implemented for handling validation: the first model incorporates the measured steering and speed inputs, and the second model consists of a steering controller forcing the vehicle to follow a prescribed path at a constant speed. It is concluded that the handling simulation model is sufficient for preliminary studies, but might need modifications for detailed simulations of vehicle handling. The baseline data and the simulation model will be used to assess the performance of semi-active control and will be discussed in Chapter 5.

---

## 5 SIMULATION RESULTS: CONTROL IMPLEMENTATION ON VEHICLE MODEL

---

After completion of the Baja simulation model validation, a suitable model for suspension control simulation has been obtained. The model is altered by introducing controllable damping forces provided by the MR dampers. It is assumed that the mass of added suspension components is negligible compared to the vehicle body mass, and therefore the experimentally determined centre of mass location and moments of inertia need not be changed in the simulation model.

### 5.1 Simulated Suspension Control

The MR dampers used in this study are suitable for seat suspensions, and are thus only capable of delivering damping forces that are smaller than generally experienced in vehicle suspensions. Due to capability limitations of the available MR dampers, passive damping is not completely eliminated from the suspension of the test vehicle used for this study. Instead, a relatively small amount of passive damping, provided by the passive hydro-pneumatic spring-damper suspension system, is always present. This is the case with most suspension systems where passive damping due to friction or hysteresis in rubber bushes is always present. Also, a minimum level of passive damping is always present in variable dampers as damping can never be entirely removed from these devices. For suspension control performed in this study, a variable damping component prescribed by the control strategy is added to the passive component.

The passive damping is varied in the simulations by multiplying the hydraulic damper characteristic (discussed in Section 4.2.3.3, p4.13, and shown in Figure 4-19, p4.15) by a factor between 0 and 1. A passive damping factor,  $c_{fac}$ , of 0 corresponds to a zero passive damping suspension, and a passive damping factor of 1 corresponds to a fully passive suspension. The effect of the passive damping factor on the damper characteristics is demonstrated in Figure 5-1, p5.2.

The control strategy implemented in this study is commonly referred to as hybrid control, which is a combination of skyhook- and groundhook control, discussed in Section 2.4.1, p2.13. Since hybrid control is a strategy developed for quarter car suspensions, the vertical sprung mass and unsprung mass velocity, and relative vertical velocity, are implemented to prescribe the optimal vertical damping force for favourable ride comfort or handling. This variable damping component which is added to the passive component is altered by changing the control gain,  $G$ , in Equation 8, p2.16. The

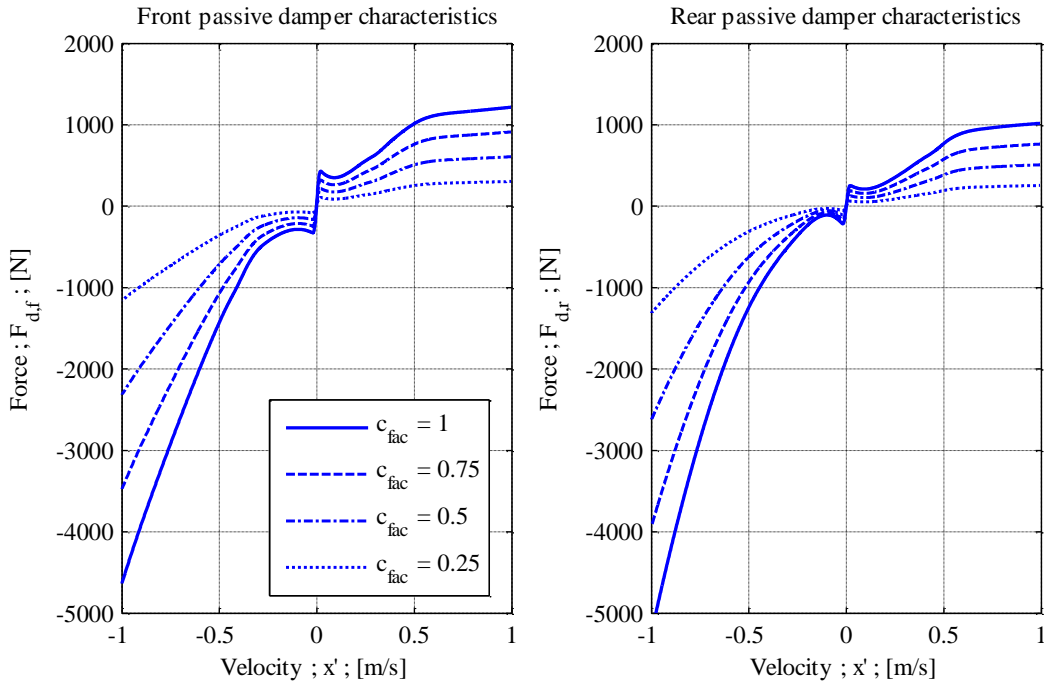


**Figure 5-1: Front and rear passive damper characteristics for various passive damping factors.**

damping force delivered by the passive spring-damper unit (see Figure 5-1, p5.2), is converted to its vertical component. The vertical MR damper force is then calculated as:

$$F_{MR,z} = F_{SA,z} - F_{d,z} \quad [ 59 ]$$

In Equation 59,  $F_{SA,z}$  is the semi-active hybrid control prescribed vertical damping force from Equation 8, p2.16,  $F_{d,z}$  is the vertical passive damping force provided by the hydro-pneumatic spring-damper unit, and  $F_{MR,z}$  is the corresponding vertical MR damper force. In the event that the vertical passive component is larger than the prescribed force, the MR damper force is set to a minimum, ideally  $F_{MR,z} = 0$ . The MR dampers and passive spring-damper units are inclined, as shown in Figure 4-1, p4.1, and Figure 4-26, p4.22. Therefore, for full vehicle model application, the optimal vertical damping force is converted to a MR damper force at an angle,  $F_{MR}$ .

A co-simulation is carried out in ADAMS and Simulink, as illustrated through a flowchart in Figure 5-2, p5.3. Simulink is a commercial software package developed by MathWorks and is used for modelling, simulating and analysing dynamic systems. While ADAMS is used to solve the dynamics of the vehicle model developed in Chapter 4, Simulink deals with the suspension control component of the simulation process. The model is excited in ADAMS by a road profile in the form of displacement inputs, rear wheel rotation inputs, and steering inputs. ADAMS supplies various measured outputs such as velocities and forces that are then used in the Simulink model. The model in Simulink calculates damping forces according to the control strategy and supplies the MR damper forces based on the prescribed passive damping level and MR damper model that is then passed back

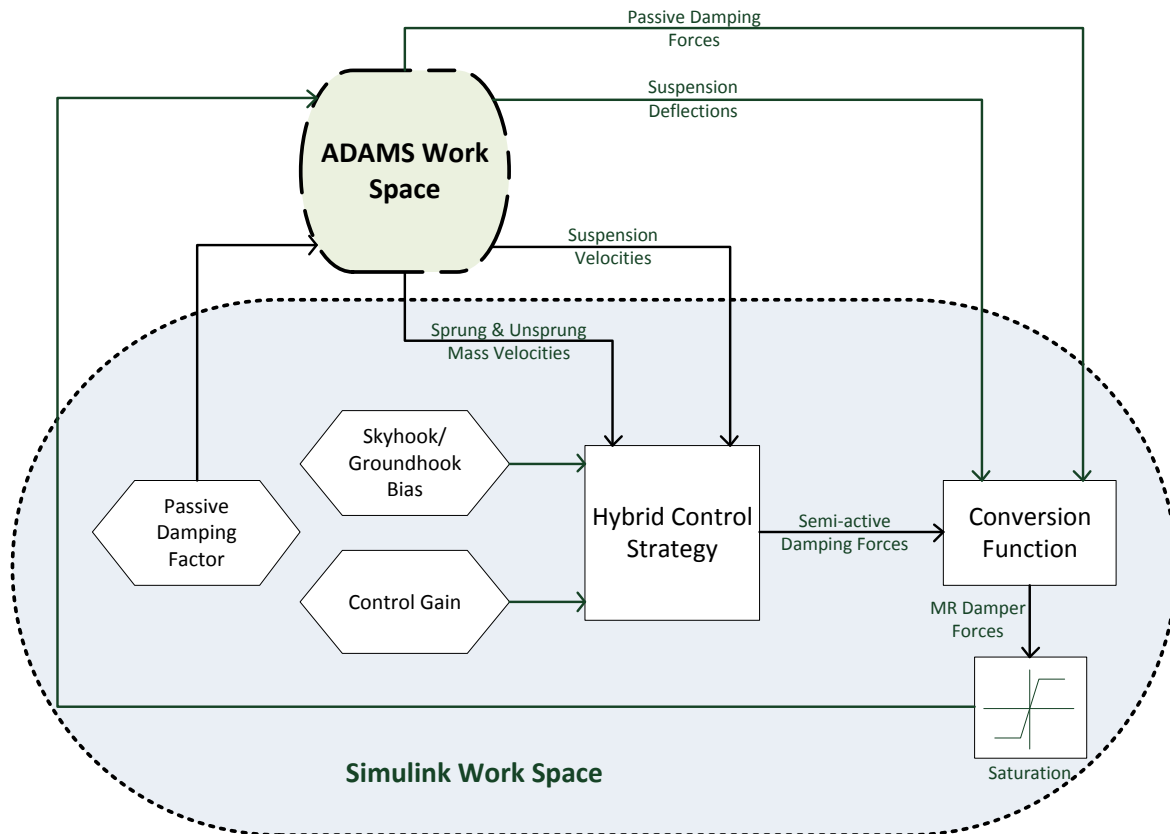


Figure 5-2: ADAMS/Simulink co-simulation environment.

to the ADAMS model. The ADAMS model then solves the system equations of motion through numerical integration to provide measured outputs to model in Simulink.

The ride comfort of the vehicle with suspension control is evaluated through Belgian paving tests, as discussed in Section 5.2, p5.3. The handling performance is evaluated through single lane change tests, as discussed in Section 5.3, p5.13. The effects of variations in passive damping and control gain on the ride comfort and handling capabilities of the test vehicle are also explored.

## 5.2 Ride Comfort Results

In this section the measured ride comfort of the baseline vehicle when driving over a rough Belgian paving track is presented and compared to suspension control simulation results.

### 5.2.1 Ride Comfort Baseline Results

The ride comfort of the baseline vehicle, (as well as the controlled suspension vehicle), is determined and evaluated as per BS 6841 (**British Standards Institution, 1987**). The weighted RMS vertical acceleration at the centre of mass (calculated from measured data) of the baseline

test vehicle body when driven over the Belgian paving track is  $2.1\text{m/s}^2$ , which is considered to be very high. The vertical acceleration of the sprung mass is shown in Figure 5-3, p5.4.

The RMS vertical acceleration of the four wheels when driven over the Belgian paving track is  $18.7\text{m/s}^2$  and  $25.4\text{m/s}^2$  at the front, and  $27.9\text{m/s}^2$  and  $27.6\text{m/s}^2$  at the rear. The measured vertical acceleration of the wheels is shown in Figure 5-4, p5.5. As mentioned in Section 4.5.1, p4.25, and confirmed by the rear suspension deflection in Figure 4-33, p4.27, the rear hydro-pneumatic spring-damper units were not at the same pressure during baseline testing. This can also be discerned from the difference in measured acceleration magnitudes at the rear wheels.

## 5.2.2 Ride Comfort Simulation Results

In the ride comfort simulation the vehicle model is driven over the Belgian paving surface, modelled as two tracks defined as vertical displacements as a function of longitudinal distance. The tracks have been measured experimentally using a Can-Can profilometer (**Becker and Els, 2013**). The simulation model is driven over the surface by prescribing a rotational speed input to the rear wheels. The speed input consists of a ramp section to gradually increase the speed of the vehicle up to the first measured value, and a filtered measured speed section. Once the vehicle is up to speed and the speed input switches to the filtered measured speed section, the test vehicle enters the Belgian

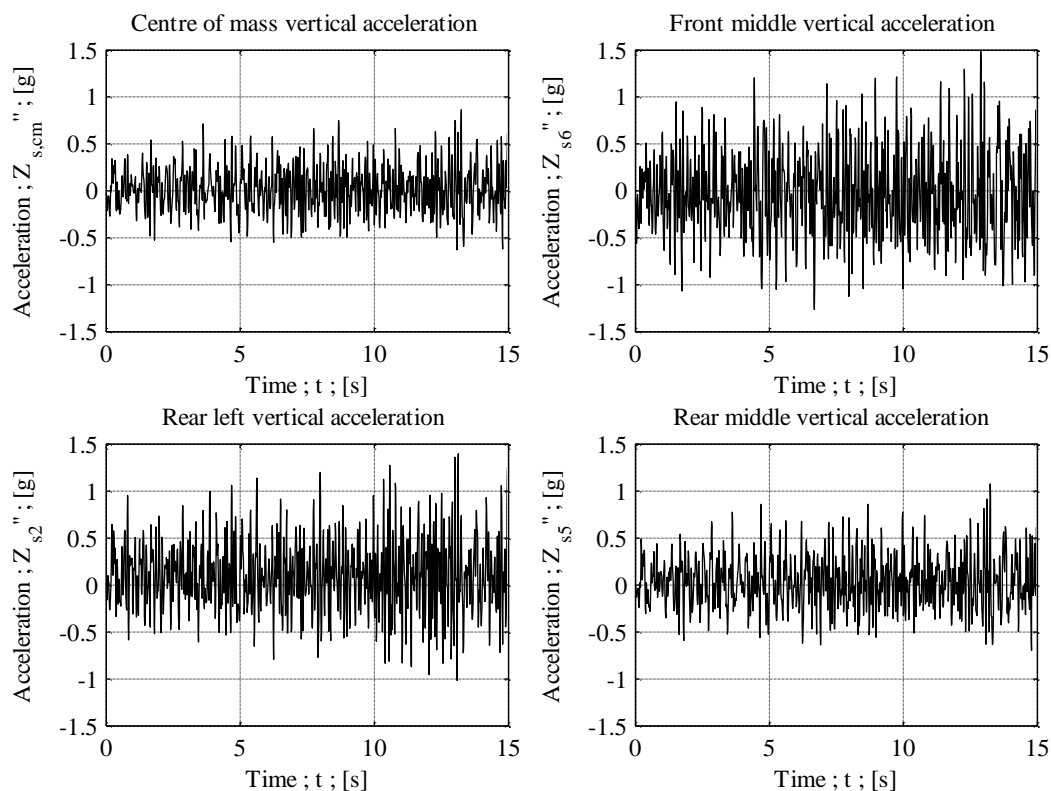


**Figure 5-3: Belgian paving measured results: Vertical acceleration of the sprung mass.**

paving track, at  $t = 0s$ . The speed input while driving over the rough surface is shown in Figure 5-5, p5.5. This corresponds to a longitudinal speed of between 23km/h and 26km/h. The steer input to the simulation model remains fixed at zero displacement of the steering rack. Skyhook- and groundhook control results are discussed in Section 5.2.2.1, p5.6, and Section 5.2.2.2, p5.8, respectively.

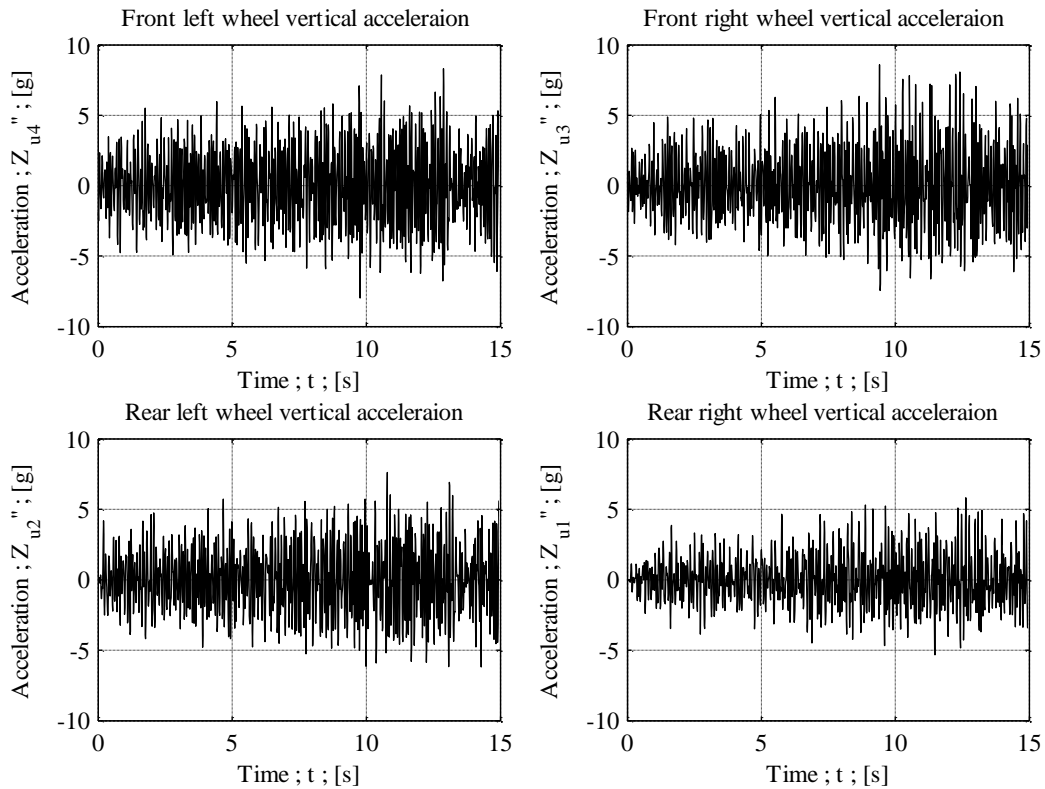


**Figure 5-4: Belgian paving measured results: Vertical acceleration of the four wheels.**

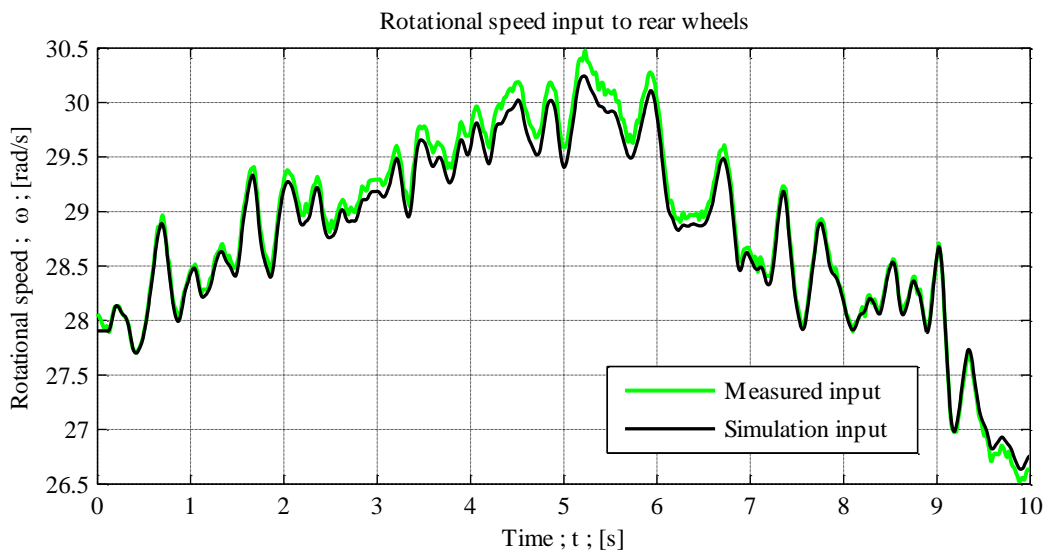


**Figure 5-5: Speed input for ride comfort (Belgian paving) tests.**

### 5.2.2.1 Skyhook Control Results

The weighted RMS vertical acceleration of the sprung mass (measured at the centre of mass) as a function of passive damping factor and skyhook gain is shown in Figure 5-6, p5.6. The simulated baseline vehicle (uncontrolled, thus  $G = 0$  and  $c_{fac} = 1$ ) weighted RMS vertical acceleration at the centre of mass is  $2.047\text{m/s}^2$ , which corresponds well to the measured results of  $2.1\text{m/s}^2$ . As the passive damping of the uncontrolled suspension ( $G = 0$ ) is reduced, the ride comfort improves, up to an optimal point occurring at approximately 7.5% of the baseline passive damping setting. The lowest weighted RMS vertical acceleration that can be achieved by a passive suspension when driving over the Belgian paving track at a speed between  $23\text{km/h}$  and  $26\text{km/h}$  is  $0.9533\text{m/s}^2$ . Better isolation of the vehicle body from road excitation is achieved with less damping, but better road-tyre contact is achieved with high damping (as discussed in Section 2.1.3, p2.5). Thus, if the passive damping is lowered beyond the optimal point, ride comfort deteriorates due to excessive wheel hop movement transferred to the sprung mass. The best ride comfort that can be accomplished by a controlled suspension system is achieved by a skyhook control gain of  $1200\text{Ns/m}$  with passive damping completely removed from the system. The weighted RMS acceleration at this point is  $0.8827\text{m/s}^2$ , which is considered to be fairly uncomfortable to uncomfortable (according to BS 6841). As the

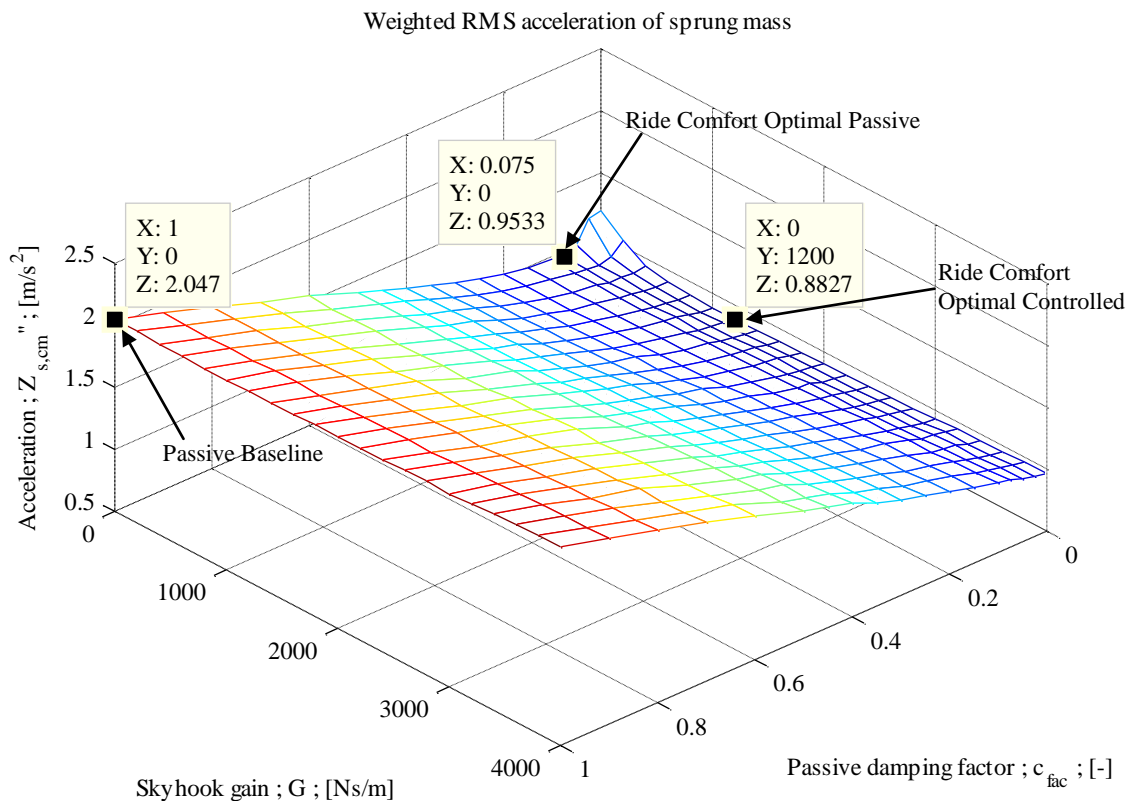


**Figure 5-6: Belgian paving simulation results: Weighted RMS acceleration of sprung mass for various skyhook gain and passive damping contributions.**



control gain increases above 1400Ns/m for all passive damping levels, the weighted RMS vertical acceleration magnitudes slowly increase. The weighted RMS vertical acceleration achieved by a pure skyhook controlled suspension remains below  $1\text{m/s}^2$ , while much higher accelerations are obtained by the pure passive suspension at all damping levels, except in the vicinity of the optimal at 7.5%.

The weighted RMS vertical acceleration of the rear right wheel as a function of passive damping factor and skyhook gain is shown in Figure 5-7, p5.7. For brevity, the results for the other wheels are omitted as they are similar to that of the rear right wheel. As the passive damping of the uncontrolled suspension is increased, the suspension becomes harder, and the vertical acceleration of the wheels decreases by limiting unnecessary suspension deflection. Since skyhook control is a ride comfort oriented strategy, the effect of the skyhook gain on the acceleration of the wheels is negligible. The RMS vertical acceleration of the rear right wheel for ride comfort optimal passive damping ( $c_{fac} = 0.075$ ) is  $38.73\text{m/s}^2$ , and for optimal controlled damping ( $G = 1200\text{Ns/m}$ ) is  $39.06\text{m/s}^2$ . The RMS vertical acceleration of the rear right wheel of the baseline vehicle predicted by the simulation ( $31.25\text{m/s}^2$ ) is higher than the measured results, as expected due to incorrect spring pressure settings during baseline testing. However, the RMS vertical acceleration of the baseline vehicle predicted by

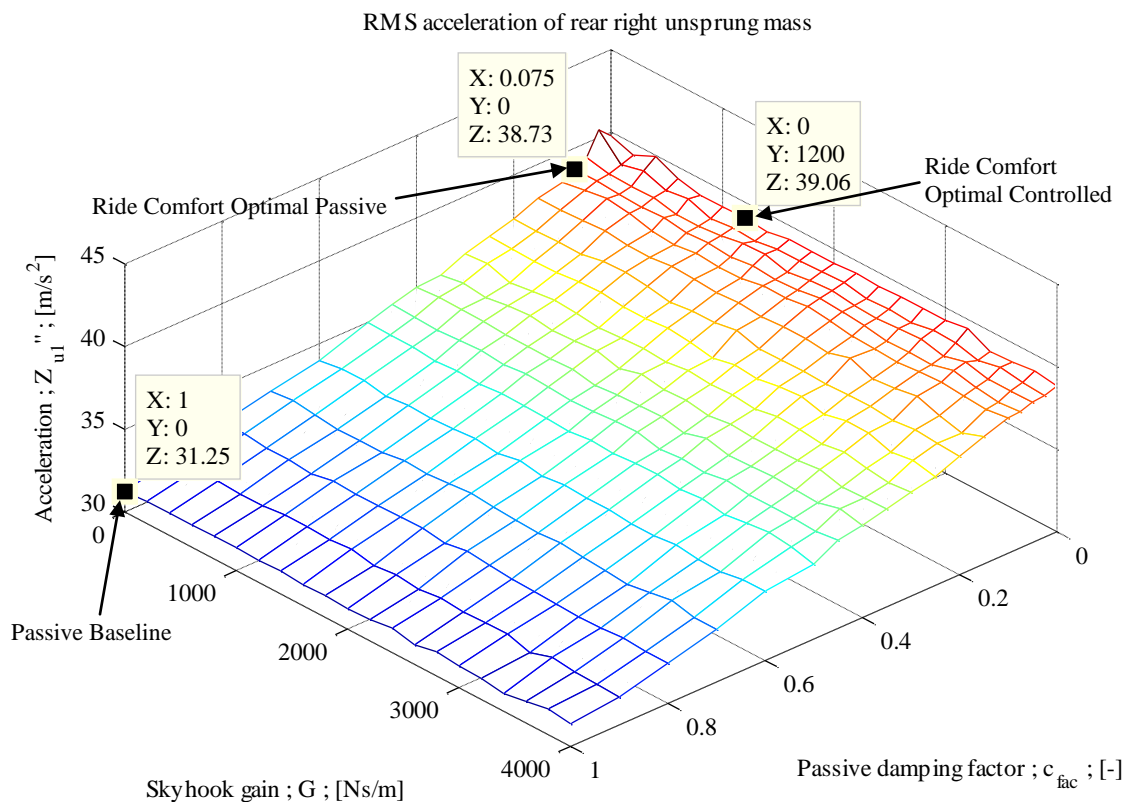


**Figure 5-7: Belgian paving simulation results: RMS acceleration of rear right wheel for various skyhook gain and passive damping contributions.**

the simulation for the front wheels corresponds well to the measured results, with a difference of only about  $1.5\text{m/s}^2$ . The RMS vertical acceleration of the rear left wheel is overestimated by approximately  $5\text{m/s}^2$ .

### 5.2.2.2 Groundhook Control Results

The weighted RMS vertical acceleration of the sprung mass (measured at the centre of mass) as a function of passive damping factor and groundhook gain is shown in Figure 5-8, p5.8. As with the skyhook results in Section 5.2.2.1, p5.6, the weighted RMS vertical acceleration of the vehicle body decreases as the passive damping of an uncontrolled suspension is decreased. Whereas the implementation of pure skyhook control ( $c_{fac} = 0$ ) yielded an improved ride comfort over the optimal passive suspension, groundhook control does not yield these results. The optimal ride comfort obtained by the fully controlled suspension is  $1.094\text{m/s}^2$  for a groundhook control gain of  $400\text{Ns/m}$ . Also, while pure skyhook control resulted in improved ride comfort levels compared to the uncontrolled suspension, pure groundhook control deteriorated the ride comfort levels with increased control gains. This is expected as groundhook control is a handling oriented control strategy and does not enhance ride.

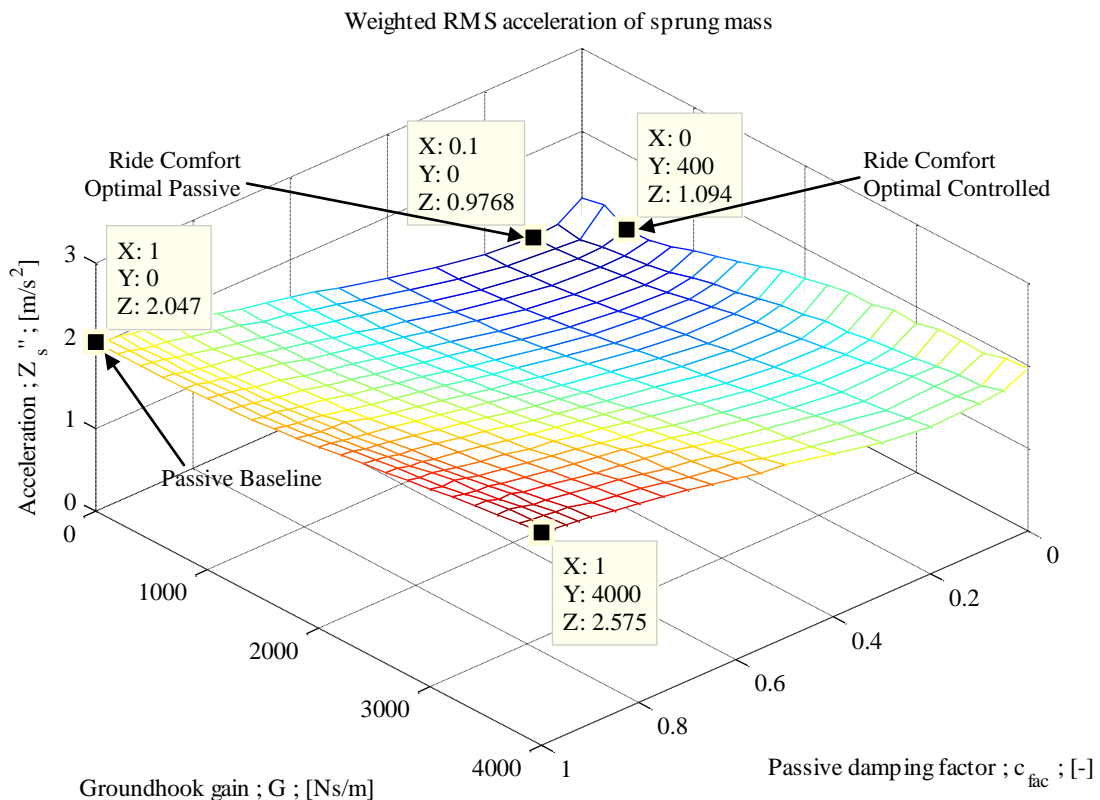


Figure 5-8: Belgian paving simulation results: Weighted RMS acceleration of sprung mass for various groundhook gain and passive damping contributions.

The weighted RMS vertical acceleration of the rear right wheel as a function of passive damping factor and groundhook gain is shown in Figure 5-9, p5.9. For brevity, the results for the other wheels are omitted as they are similar to the rear right wheel. As the damping of the uncontrolled suspension ( $G = 0$ ) is increased, the vertical acceleration of the wheels is decreased. For all passive damping levels, introduction of more damping by addition of groundhook control results in less vertical motion of the wheels (and thus possible improved road-holding). The lowest vertical acceleration of the rear right wheel,  $29\text{m/s}^2$ , is obtained for a combined full passive and controlled suspension with a groundhook gain of  $4000\text{Ns/m}$ . It may be noted that for this suspension configuration the weighted RMS vertical acceleration of the vehicle body is at its highest ( $2.575\text{m/s}^2$ , refer to Figure 5-8, p5.8). Lower RMS vertical accelerations may be obtained by increasing the control gain above  $4000\text{Ns/m}$ .

### 5.2.3 The Optimal Ride Comfort Suspension

From Figure 5-6, p5.6, the suspension setting for optimal ride comfort is a pure skyhook controlled suspension with a gain of  $1200\text{Ns/m}$ . However, this is under the assumption that the forces prescribed by the hybrid control strategy are deliverable by the MR dampers, and the dampers are limited to their maximum capacity. For a given excitation condition (even at minimum or maximum current levels)

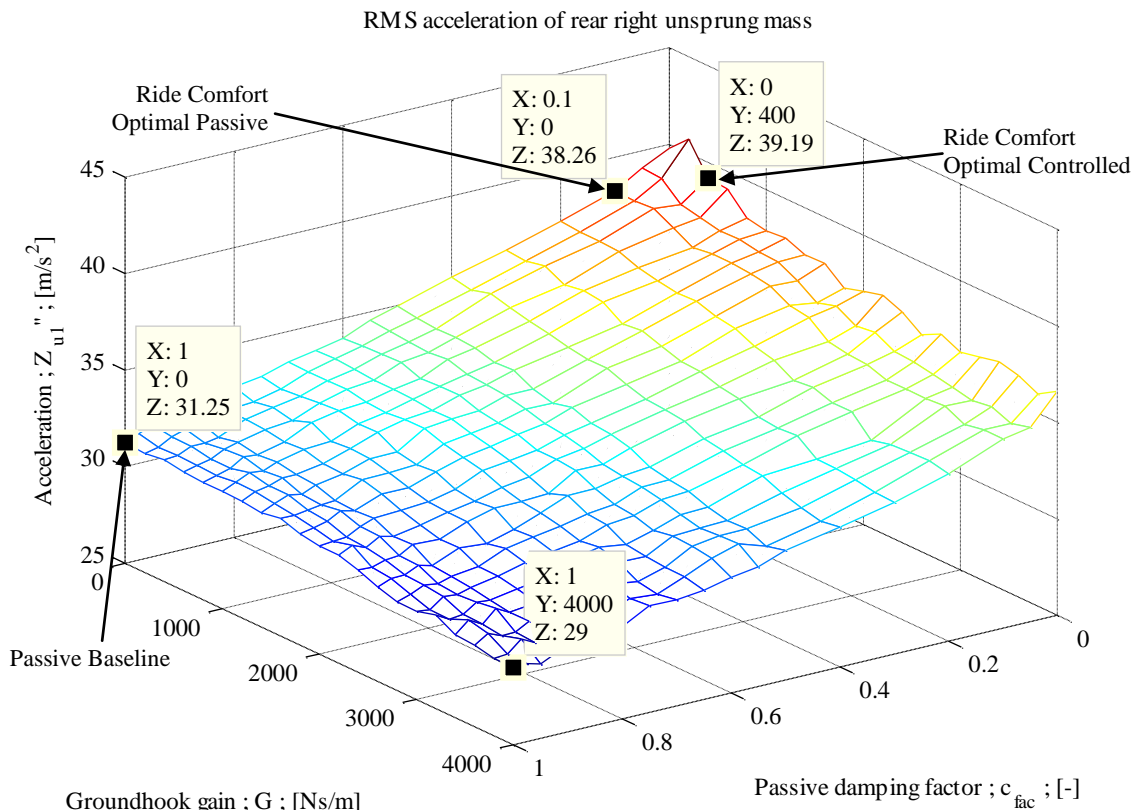


Figure 5-9: Belgian paving simulation results: RMS acceleration of rear right wheel for various groundhook gain and passive damping contributions.

the required MR damper forces may not be deliverable. For instance, from Figure 3-6, p3.7, it may be discerned that at high velocity magnitudes (above 0.5m/s) the minimum obtainable damping force is approximately 450N. A suitable MR damper model is used to calculate the actual damping force that can be delivered under the specific input conditions. For this study, the developed polynomial model (refer to Section 3.2.4, p3.20) is used to convert the hybrid control prescribed semi-active damping forces to the corresponding input current to the MR dampers.

The performance of the skyhook control principle is demonstrated in Figure 5-10, p5.10. As discussed in Section 2.4.1.1, p2.13, the vertical force prescribed by the skyhook control algorithm,  $F_{SA,z}$ , becomes zero when the sprung mass velocity and the relative vertical velocity of the sprung and unsprung mass are in opposite directions (refer to Equation 1 and 3, p2.14). Otherwise, the force is a scaled value ( $G = 1200\text{Ns/m}$ ) of the sprung mass velocity. In Figure 5-10 the prescribed control force has been scaled by a factor of 1/500 to obtain values that are comparable to the velocity magnitudes. Since the passive damping is removed from the suspension, the prescribed damping forces must be delivered by the MR dampers alone (refer to Equation 59, p5.2).

In order to track the desired force the polynomial MR damper model from Table 3–14, p3.23 is implemented to determine the required damper input current levels using Equation 21, p2.28. As discussed in Section 2.6.3.2.1, p2.27, the prescribed input current levels should be constrained to zero and the maximum value. The prescribed input current to the MR dampers during control implementation is shown in Figure 5-11, p5.11. In the event that the prescribed damping forces are beyond the capabilities of the MR dampers ( $I < 0A$  or  $I > 2A$ ) the input current is constrained and the

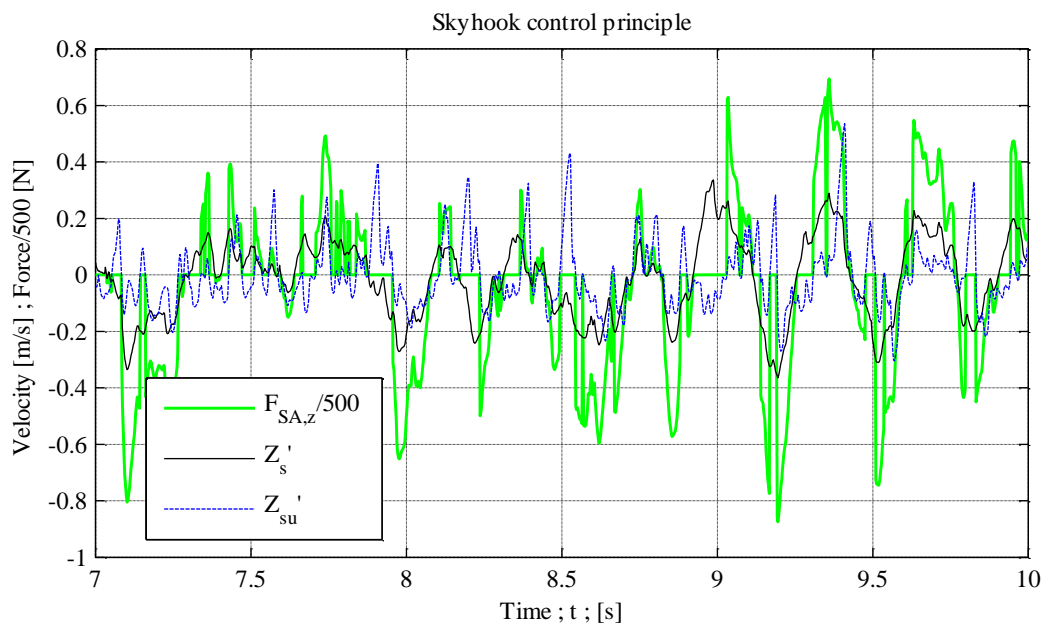
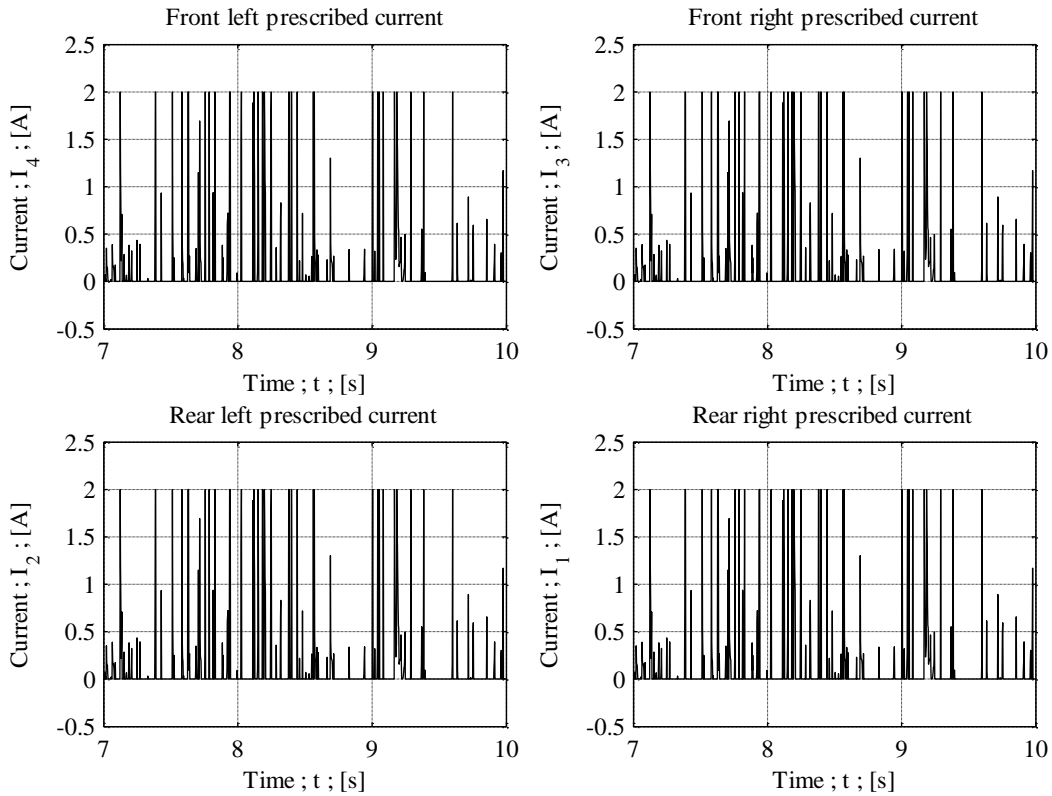
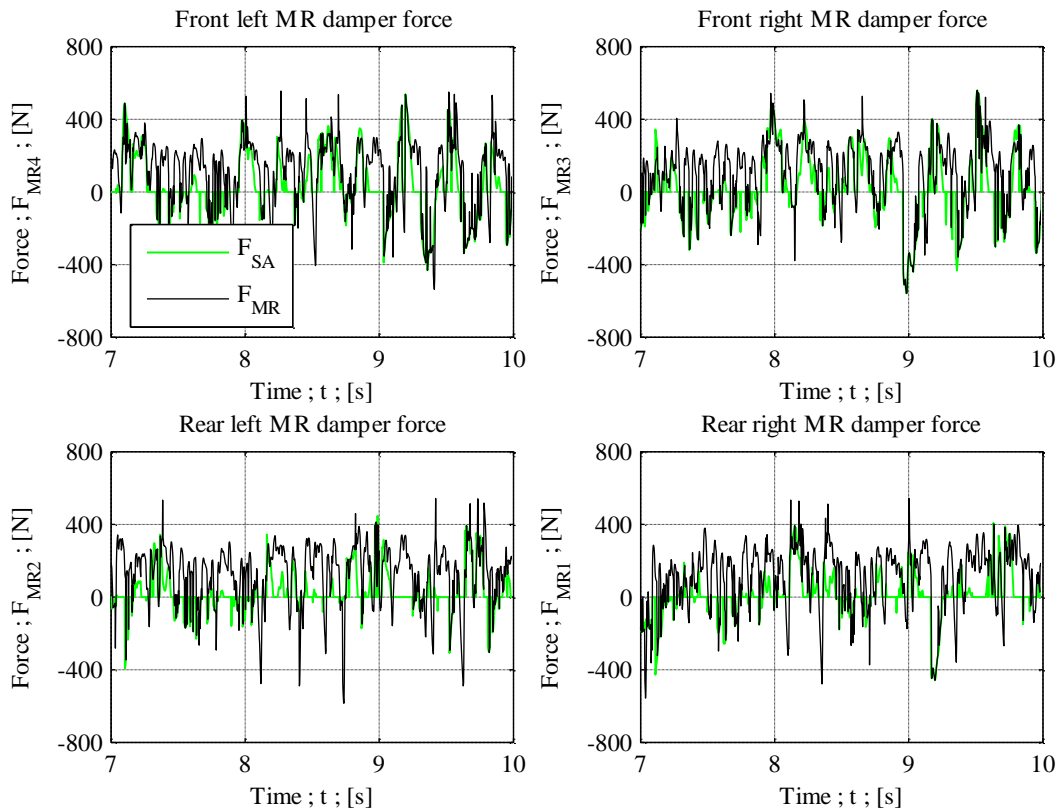


Figure 5-10: Optimal ride comfort: Time traces for skyhook control implementation (rear right corner).



**Figure 5-11: Prescribed input current to MR dampers.**



**Figure 5-12: Comparison of the prescribed semi-active forces and the forces delivered by the MR dampers.**

actual forces that can be delivered by the dampers are recalculated using the polynomial model. If the prescribed semi-active force is zero, the current supplied to the damper is switched off and the Kwok model from Table 3–10, p3.18 (0A), is used to determine the force delivered by the MR damper. The prescribed semi-active forces are compared to the actual MR damper forces in Figure 5-12, p5.11.

The force-velocity relationships of the prescribed semi-active damping forces are compared to the actual damping forces that can be delivered by the MR dampers in Figure 5-13, p5.12. The diagonal black lines correspond to the implementation of the Kwok model when the current is switched off. Shortcomings of the developed polynomial model are also highlighted as there are some regions where damping forces are prescribed but not deliverable according to the model. It may be discerned that inaccuracies in the utilised MR damper model lead to damping forces that may not be ideal.

The weighted RMS vertical acceleration of the vehicle sprung mass is  $1.02\text{m/s}^2$ . The increase in vertical acceleration is attributed to passive damping forces delivered by the MR dampers when the prescribed damping forces are zero and the input current is switched off. Simulation results show that implementation of a skyhook controlled suspension with a polynomial model to prescribe the damper current may yield a significant improvement in ride comfort over the baseline passive suspension.

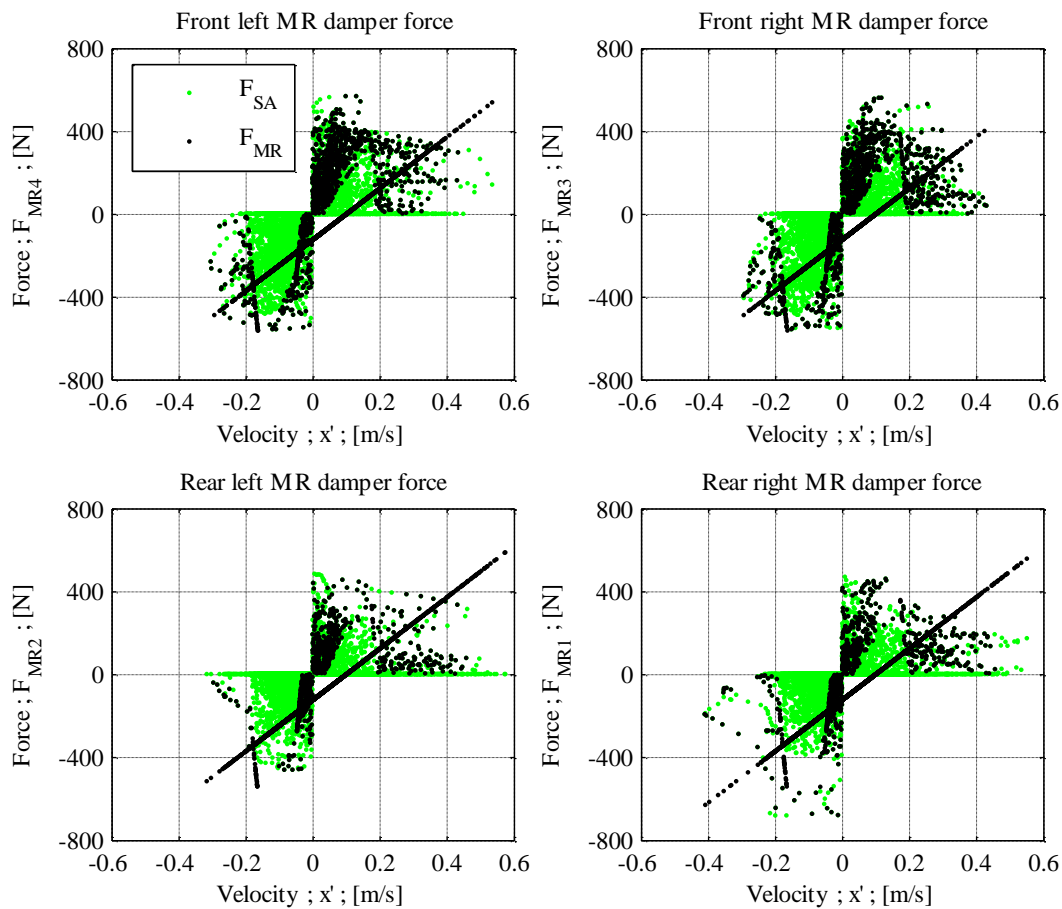


**Figure 5-13: Force-velocity relationship of polynomial model compared to prescribed semi-active forces.**

### 5.2.4 Ride Comfort Results Summary

To evaluate ride comfort the test vehicle is driven over a rough Belgian paving track. This is also evaluated through simulation. The weighted RMS vertical acceleration of the baseline vehicle sprung mass is  $2.1\text{m/s}^2$ , while simulation results show that the RMS acceleration resulting from an optimal passive suspension (at 7.5% damping of the baseline suspension) could be as low as  $0.95\text{m/s}^2$ . Optimal ride comfort ( $0.88\text{m/s}^2$ ) is obtained by implementation of skyhook control using a control gain of  $1200\text{Ns/m}$  and assuming that the prescribed semi-active forces (including  $0\text{N}$ ) are exactly deliverable by the MR dampers when subjected to the specific input conditions. Implementation of the polynomial- and Kwok MR damper models to more accurately determine the true damping forces results in a deterioration in ride comfort ( $1\text{m/s}^2$ ) as compared to the ideal optimal point ( $0.88\text{m/s}^2$ ). A significant improvement in ride comfort is however obtained as compared to the baseline test vehicle.

## 5.3 Handling Results

In this section some measured data of the baseline vehicle while performing a slalom test is presented. Handling simulation results of a single lane change test are also presented and analysed in this section.

### 5.3.1 Handling Baseline Results

The handling performance of the baseline test vehicle is determined by the achievable lateral acceleration, longitudinal acceleration and yaw rate during the execution of a slalom test. The duration of road-tyre contact is also considered.

While road-holding is often used in the literature to evaluate the handling of a vehicle, where maximum duration of road-tyre contact is desired, loss of road tyre contact is not necessarily disadvantageous in all situations. Road-tyre contact loss at the inner rear wheels in a turn may be desirable in order to increase the yaw response of the vehicle and to generate oversteer. Since there is no differential present in the driveline of the test vehicle to control the distribution of power between the left and right wheels, road-tyre contact loss is desired in order to aid the vehicle in the performance of handling manoeuvres. While this isn't applicable to conventional vehicles, it is required for the test vehicle used in this study.

The measured suspension deflection during the performance of a slalom test is shown in Figure 5-14, p5.14. Compression is denoted by negative displacement values. When the rear dampers extend, a maximum extension of approximately  $0.024\text{m}$  is reached for long durations of time,

indicating loss of road-tyre contact at the rear wheels. The percentage of road-tyre contact loss during the slalom test is estimated at 23% for the rear left wheel, and 10% for the rear right wheel.

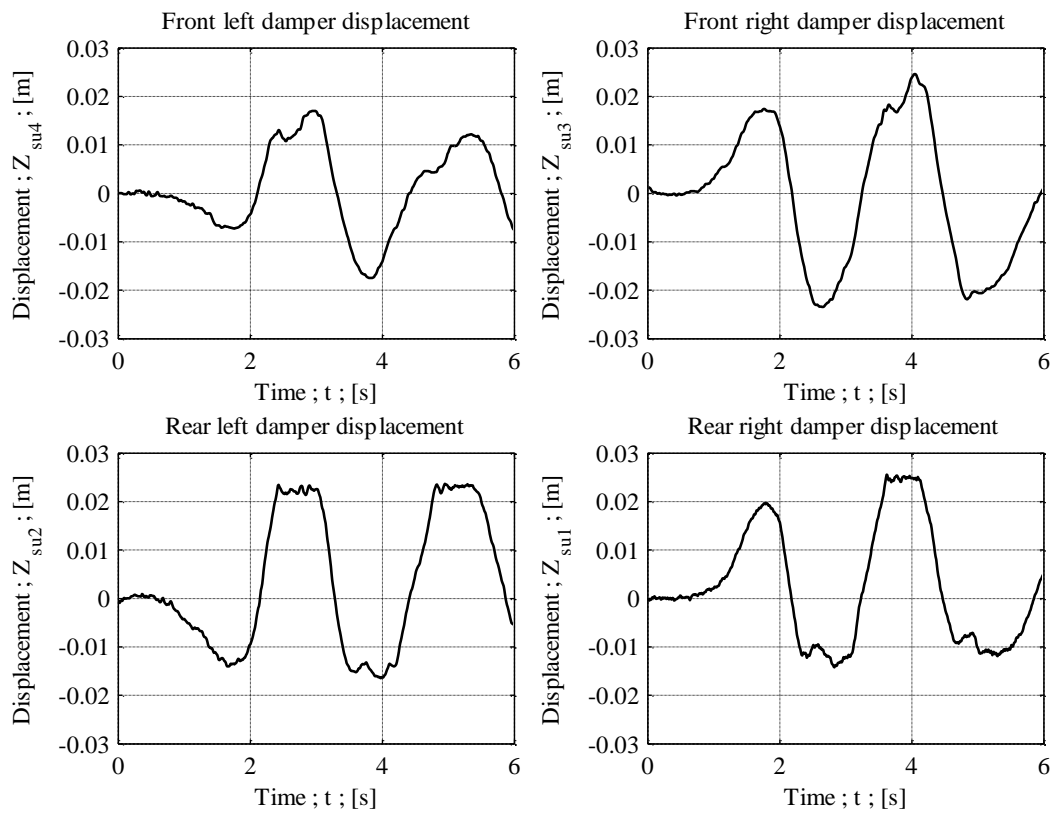


Figure 5-14: Slalom test measured results: Suspension deflection.

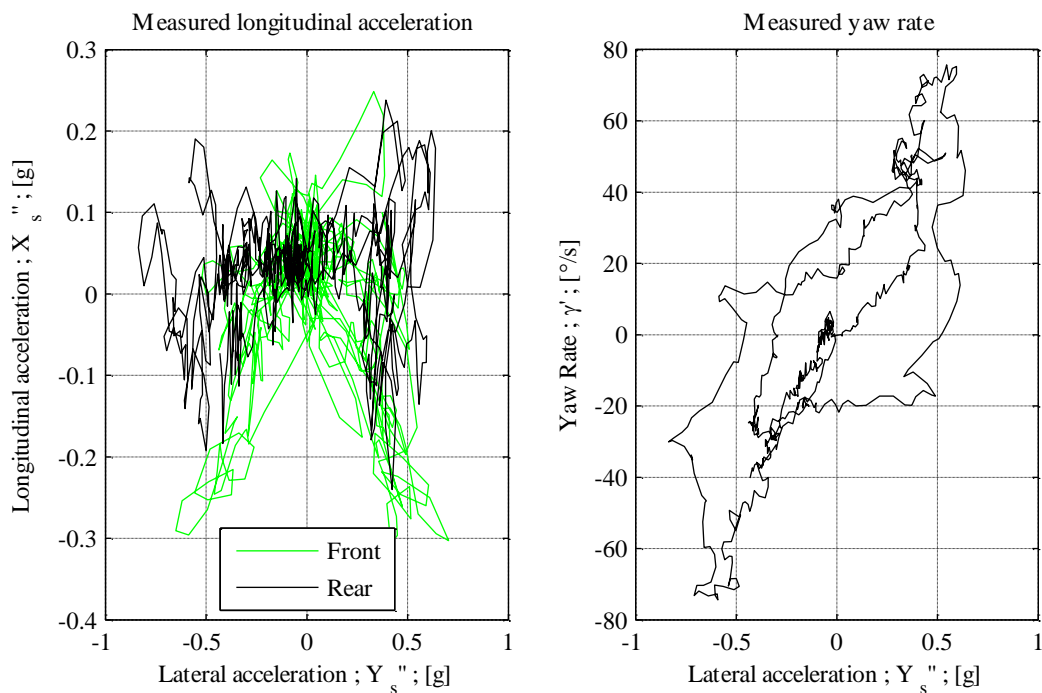


Figure 5-15: Slalom test measured results: Lateral- and longitudinal acceleration, and yaw rate.



As shown in Figure 5-15, p5.14, the maximum lateral acceleration obtained during the slalom test is approximately 0.85g, while the maximum longitudinal acceleration is 0.3g. The yaw rate obtained (approximately 75°/s) is high compared to results of other vehicles in handling studies by Uys et al. 2006a.

### 5.3.2 Handling Simulation Results

The single lane change test is used in this study to evaluate the handling capabilities of the combined passive and controlled suspension. A lane offset of 4m is chosen based on ISO 3888-1 (International Organisation for Standardisation, 1999) and a vehicle width of 1.51m. According to simulation results, the baseline vehicle (100% passive suspension) will travel a lateral distance of 4m in response to a steering input of 20mm amplitude with a period of 1.80s (as shown in Figure 5-16, p5.15). The test is performed on a flat surface and the rotational speed input to the rear wheels is the same as for the ride comfort simulation test discussed in Section 5.2.2, p5.4, and shown in Figure 5-5, p5.5.

Preliminary simulation results show that during control implementation the skyhook- and groundhook control principles would occasionally prescribe semi-active forces in the opposite direction than deliverable by the MR dampers. Even though the control condition is satisfied (Equation 3 and 6, p2.15 and p2.16), the relative velocity over the damper,  $x'_{MR}$ , is in the opposite direction as compared to the relative vertical velocity between the unsprung and sprung masses,  $Z'_{su}$ , as shown in the top graph of Figure 5-17, p5.16. This occurs when severe vehicle body pitch or roll is present, typically during handling manoeuvres such as the single lane change. In the bottom graph of Figure 5-17 it is shown that occasionally the prescribed semi-active force is in the opposite

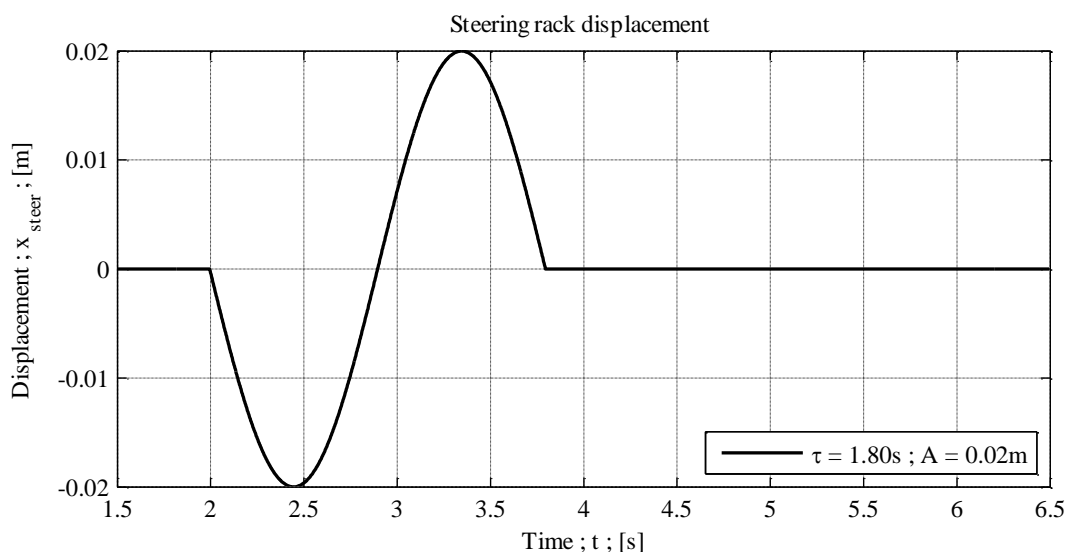
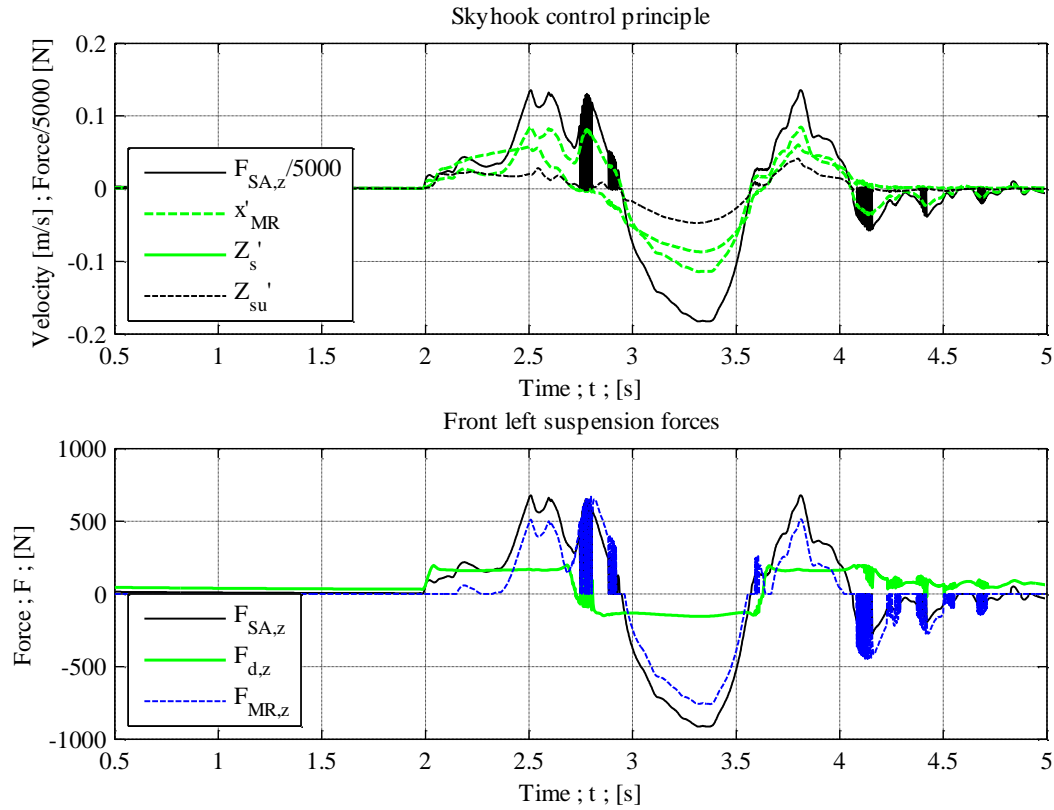


Figure 5-16: Steer input for handling (single lane change) tests.



**Figure 5-17: Inaccurate prescribed forces due to relative damper velocity error.**

direction than the passive damper force, thus requiring an active force. Thus for handling simulations in this study, to ensure that deliverable MR damper forces (and not active forces) are prescribed, the skyhook- and groundhook control conditions are adapted to include the relative velocity over the MR damper rather than vertical relative velocity:

$$\begin{aligned}
 \dot{Z}_s \dot{x}_{MR} > 0: \quad \sigma_{sky} &= \dot{Z}_s \\
 \dot{Z}_s \dot{x}_{MR} \leq 0: \quad \sigma_{sky} &= 0 \\
 \dot{Z}_u \dot{x}_{MR} < 0: \quad \sigma_{gnd} &= -\dot{Z}_u \\
 \dot{Z}_u \dot{x}_{MR} \geq 0: \quad \sigma_{gnd} &= 0
 \end{aligned}
 \tag{60}$$

In the handling simulations, the controlled suspension is combined with 20% and 50% passive damping levels, and only two control gain levels are implemented, 4000Ns/m and 8000Ns/m. These suspension settings were chosen so as to get an insight into a range of situations, varying from a low damping scenario (20% passive), up to a high damping scenario (50% passive with a control gain of 8000Ns/m). The lowest damping setting is selected as low as possible for successful completion of the single lane change test (i.e. without suspension bump-stop contact occurring that could lead to roll over), and the highest damping setting is chosen so as to limit the required damping forces to the capabilities of the MR dampers used in this study. Skyhook- and groundhook control results are discussed in Section 5.3.2.1, p5.17, and Section 5.3.2.2, p5.21, respectively.

### 5.3.2.1 Skyhook Control Results

The pitch, roll and yaw response of the vehicle sprung mass during the performance of the single lane change test for various passive damping levels and skyhook gains is shown in Figure 5-18, p5.17, and Figure 5-19, p5.18. The lower the passive damping levels present in the uncontrolled suspension system, the more the body rolls when turning, indicated by larger roll displacements and higher roll rates. This is especially visible during the second roll (vehicle tilts to the left, negative roll angles) when the uncontrolled suspension passive damping is limited to 20%. The high roll angle magnitude and roll rate suggests loss of road-tyre contact at the right, and is confirmed in Figure 5-20, p5.19 by zero vertical tyre forces during the time interval of 3.3s to 4.5s. Loss of road-tyre contact assists in generating oversteer in vehicles without a differential, resulting in improved directional response

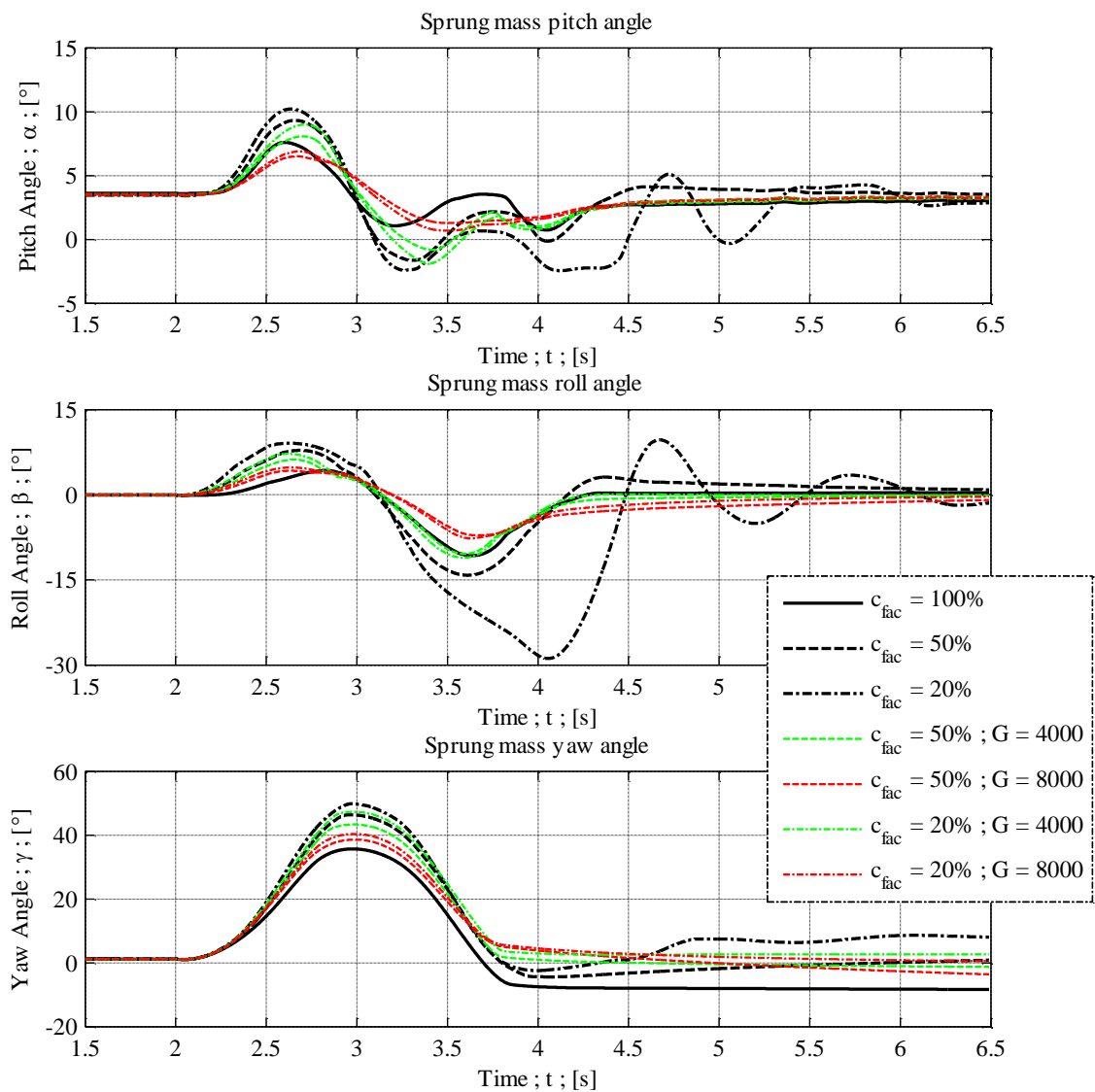


Figure 5-18: Sprung mass pitch, roll and yaw angles during single lane change test for various passive damping factors and skyhook gains.

indicated by larger yaw angles ( $50^\circ$  for a 20% passive setting and  $35^\circ$  for the original suspension) and higher yaw rates ( $88^\circ/s$  for a 20% passive setting compared to  $62^\circ/s$  for the original suspension). It is shown that the addition of a skyhook controlled suspension with sufficient damping forces (obtained through larger control gains,  $G$ ) may significantly reduce the pitch and roll response of the vehicle body through maintained road-tyre contact, as is desired for conventional vehicles.

The vertical tyre force results in Figure 5-20, p5.19 indicate that for improved road-tyre contact the passive damping must be high. The original passive suspension (solid black line) loses contact with the road surface at the front right, rear left and rear right wheels during the performance of the single lane change test. Increasing the control gain and the passive damping reduces the duration of loss of contact. A combined passive and controlled suspension, at 50% passive damping with a control gain

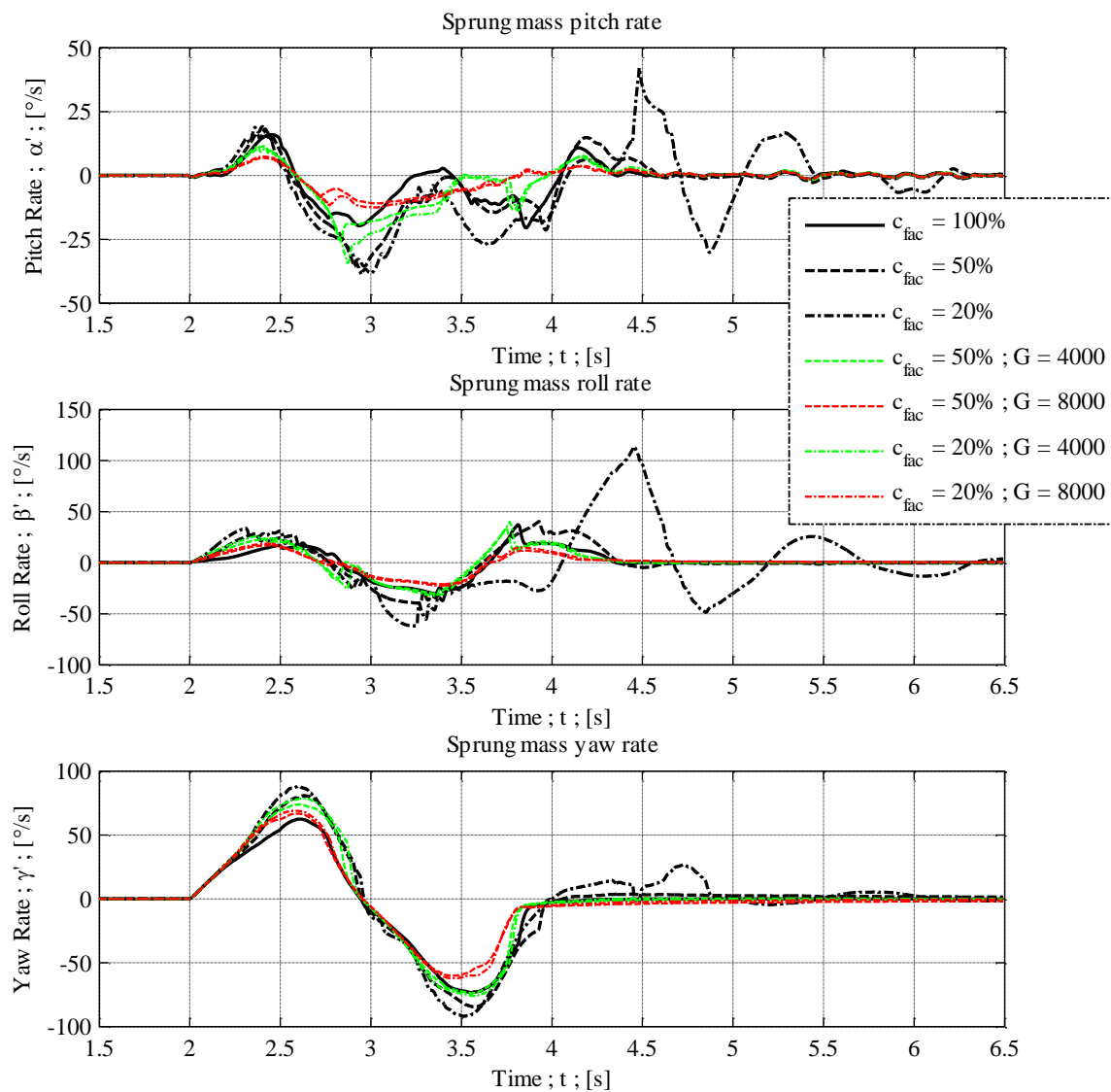
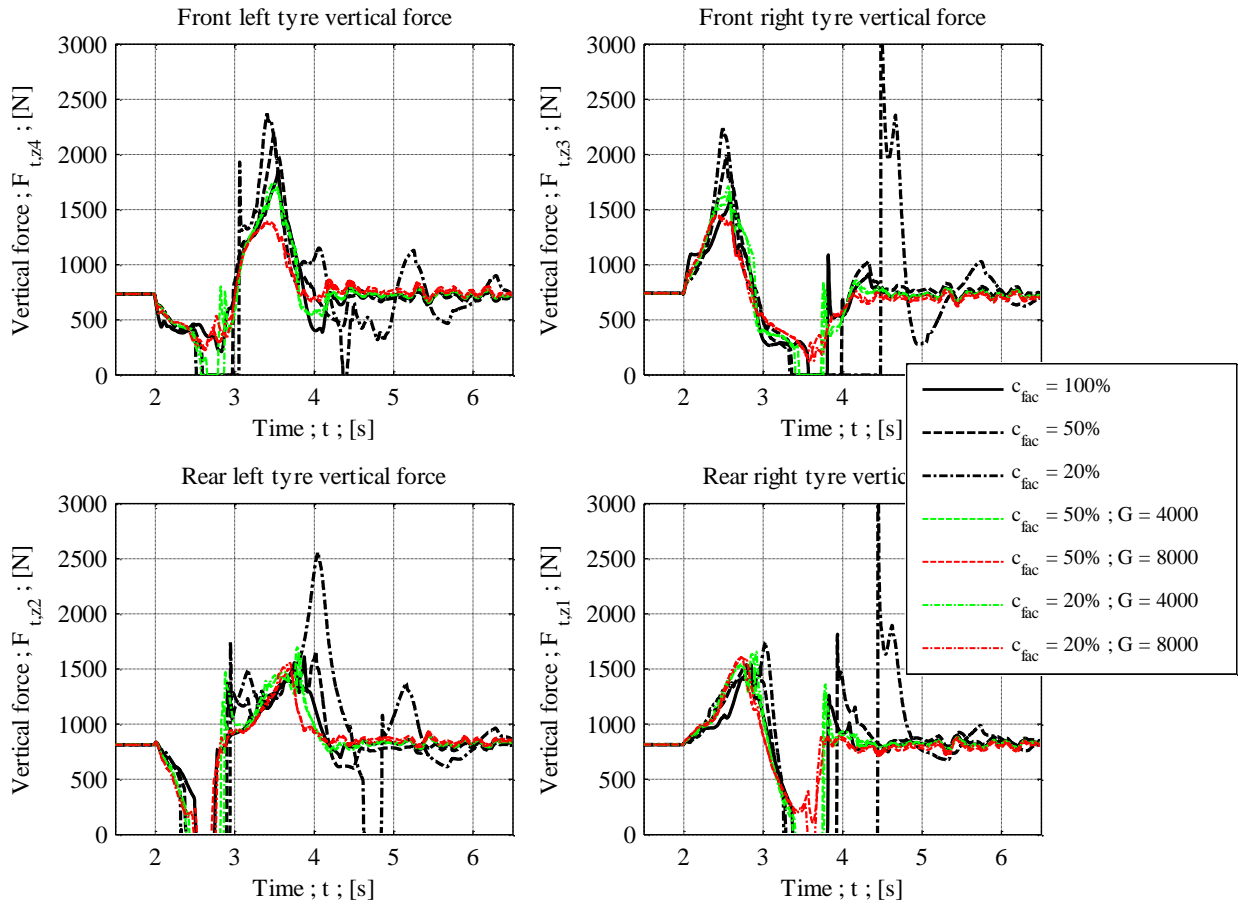
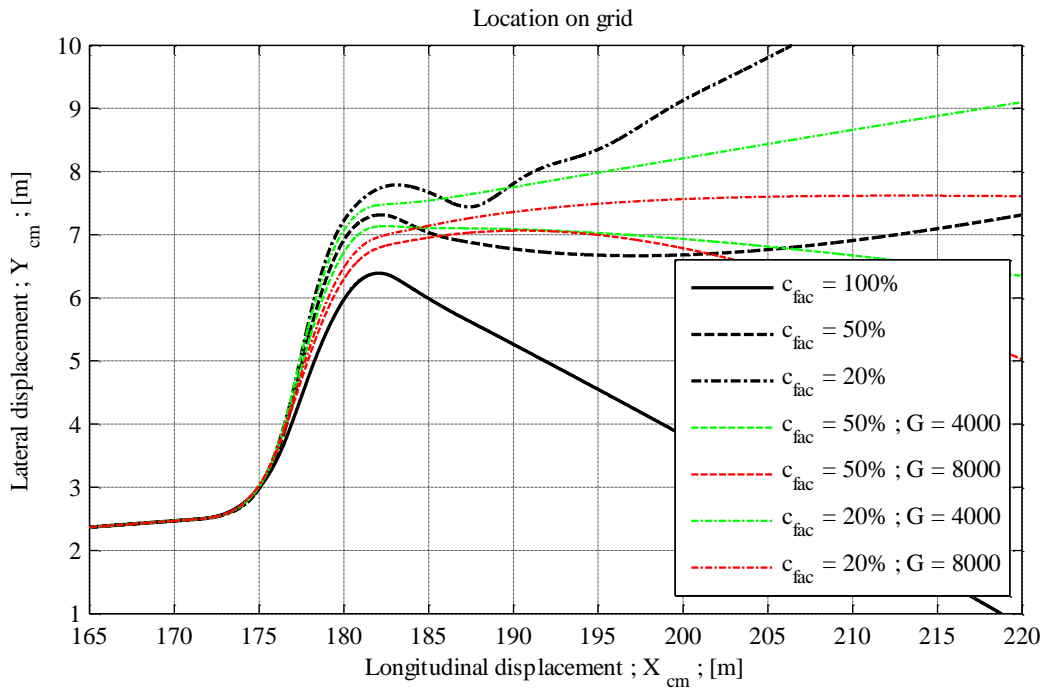


Figure 5-19: Sprung mass pitch, roll and yaw rates during single lane change test for various passive damping factors and skyhook gains.



**Figure 5-20: Vertical tyre forces during single lane change test for various passive damping factors and skyhook gains.**



**Figure 5-21: Path followed during single lane change test for various passive damping factors and skyhook gains.**

of 8000Ns/m, results in the best road-tyre contact during the performance of the test, with loss of contact only occurring briefly at the rear left wheel.

The path followed during the single lane change test for each suspension setting is shown in Figure 5-21, p5.19. The responses after the peak displacement vary for each test run due to lateral drift resulting from the double integration process. For reduced passive damping, the lateral distance travelled by the vehicle increases, indicating improved directional response as the vehicle has to turn more in order to achieve larger displacements. In turn, inclusion of a controlled component reduces the peak lateral displacement through increased road-tyre contact that is disadvantageous for vehicles without a differential, as the left and right driving wheels are required to rotate at different velocities in order to change the direction of travel.

As shown in Figure 5-22, p5.20, the maximum absolute longitudinal- and lateral acceleration (measured at the centre of mass) obtained by the baseline suspension is 0.60g and 0.91g respectively. Higher lateral acceleration is obtained for lower passive damping levels, with values larger than 1g occurring for a 20% passive suspension. Implementation of skyhook control reduces the lateral and longitudinal acceleration as a result of reduced body roll with increased road-tyre contact.

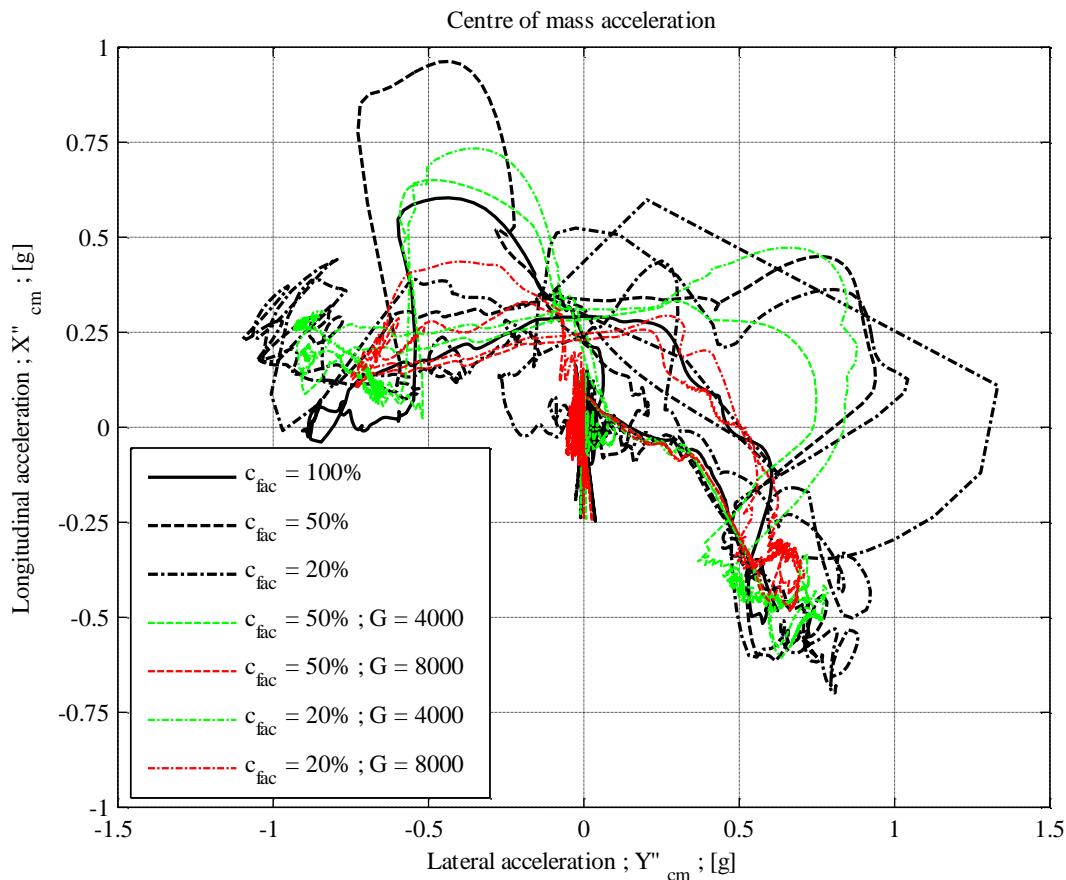


**Figure 5-22: Lateral- and longitudinal acceleration response during single lane change test for various passive damping factors and skyhook gains.**

### 5.3.2.2 Groundhook Control Results

The pitch, roll and yaw response of the vehicle sprung mass during the performance of the single lane change test for various passive damping levels and groundhook gains are shown in Figure 5-23, p5.21, and Figure 5-24, p5.22. As mentioned previously, lowering the passive damping levels in the uncontrolled suspension system results in more body roll while turning. While the implementation of skyhook control results in reduced vehicle body pitch, roll and yaw response, implementation of groundhook control does not yield favourable responses for all combinations of passive damping levels and control gains. Reduced body roll, favourable for handling of conventional off-road vehicles, is obtainable by implementation of skyhook control, while groundhook control is unable to reduce the body roll experienced by the baseline vehicle. Implementation of groundhook control is

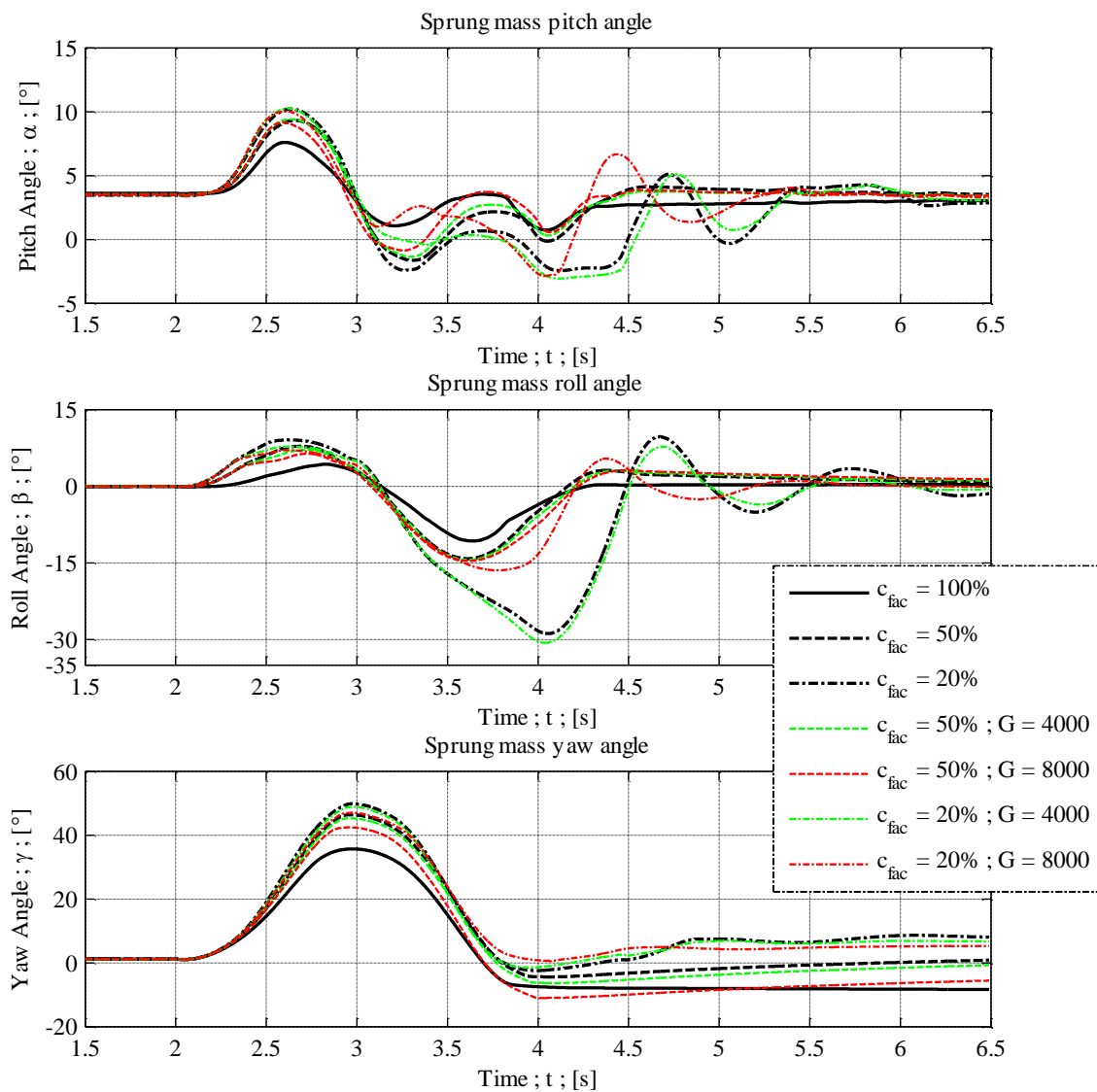


Figure 5-23: Sprung mass angles during single lane change test for various passive damping factors and groundhook gains.

also incapable of increasing the yaw response of the vehicle, even though the body rolls more than it does with the implementation of skyhook control. The highest yaw rate, and thus the best directional response, is obtained by implementation of an uncontrolled passive suspension limited to 20% damping.

The vertical tyre forces during the performance of the single lane change test are shown in Figure 5-25, p5.23. The original suspension system (solid black line) maintains the most road-tyre contact, while the implementation of a groundhook controlled suspension is incapable of increasing the duration of road-tyre contact provided by the corresponding uncontrolled passive level. The incapability of changing the duration of road-tyre contact with groundhook control leads to unchanged directional response as compared to the corresponding passive suspension (refer to Figure 5-23, p5.21

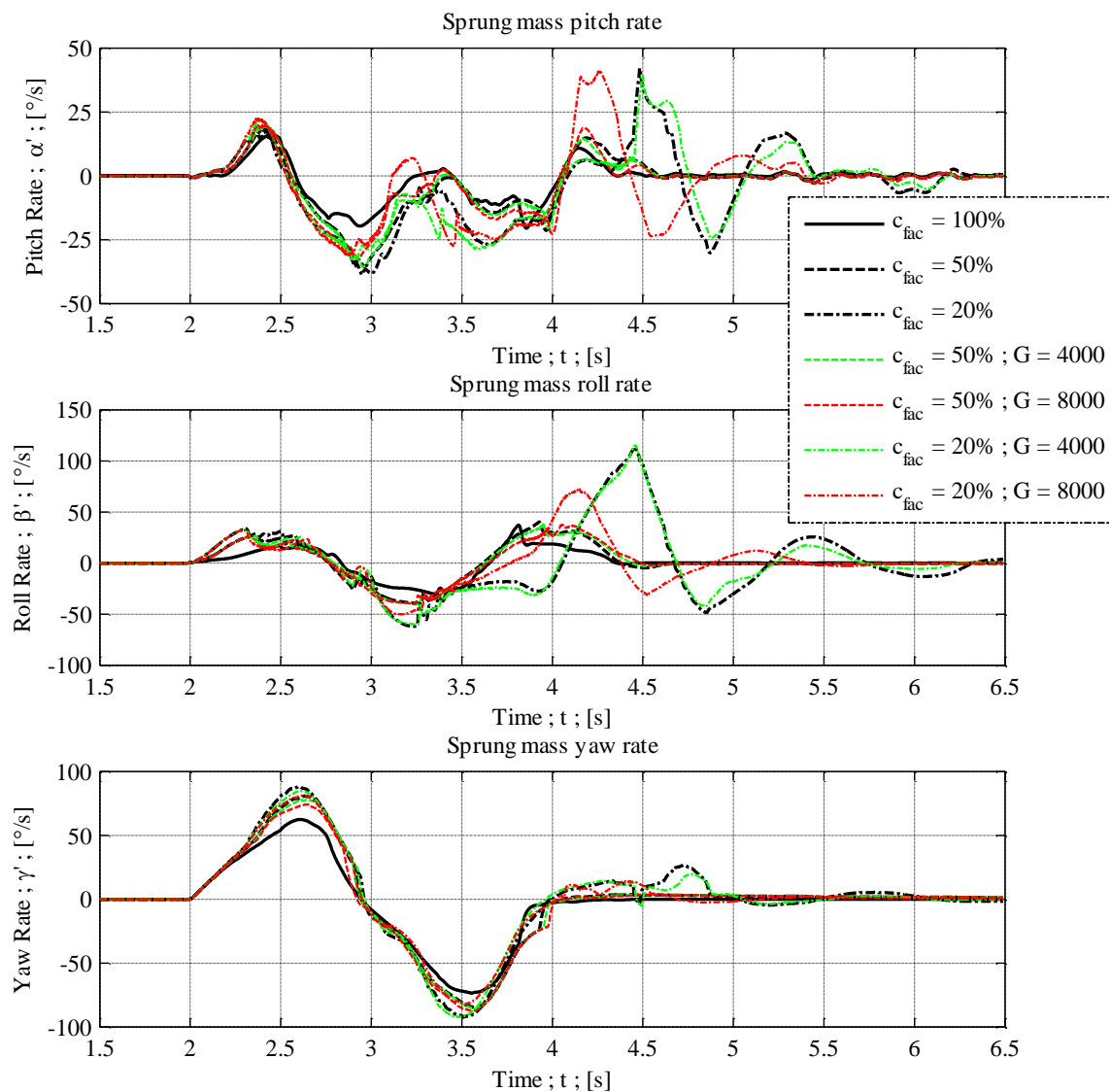
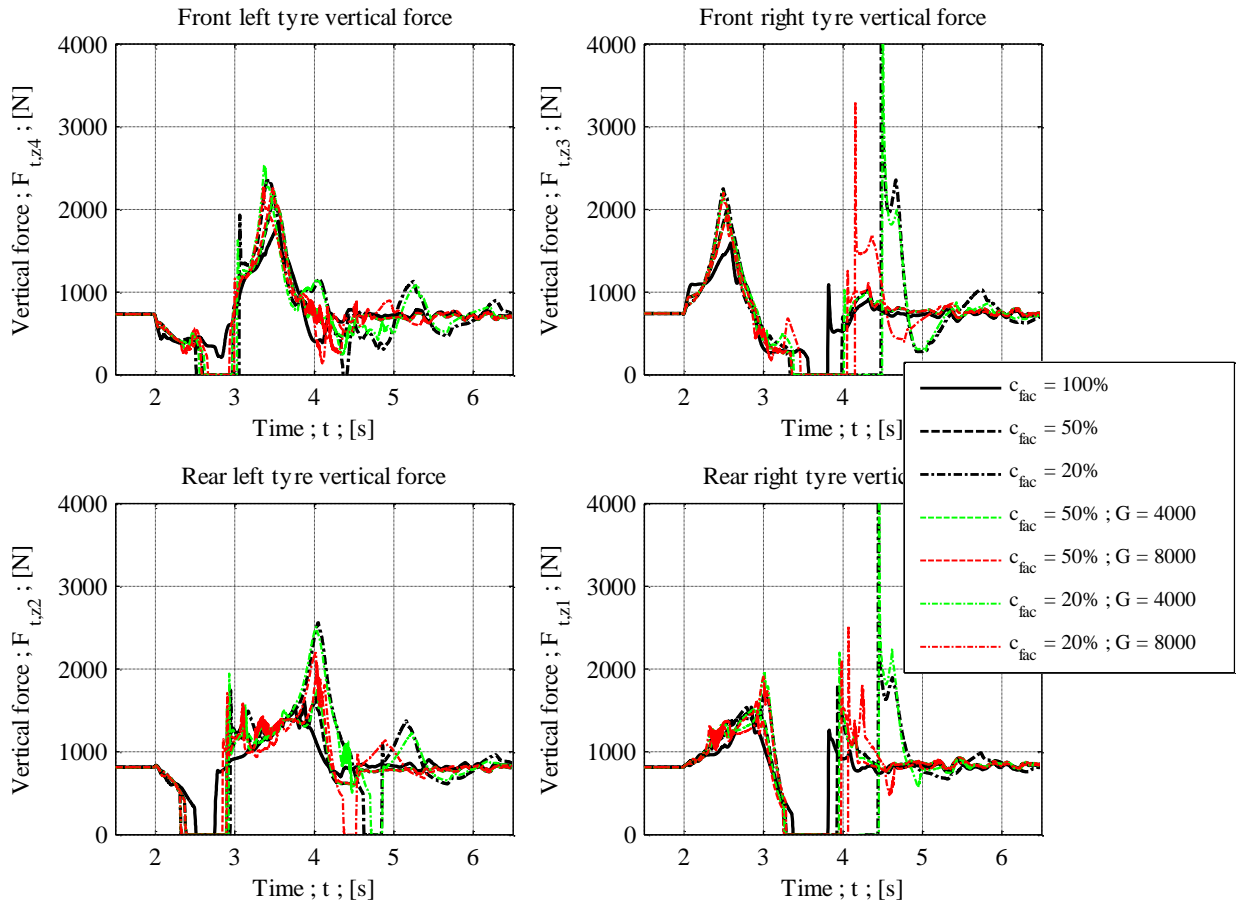
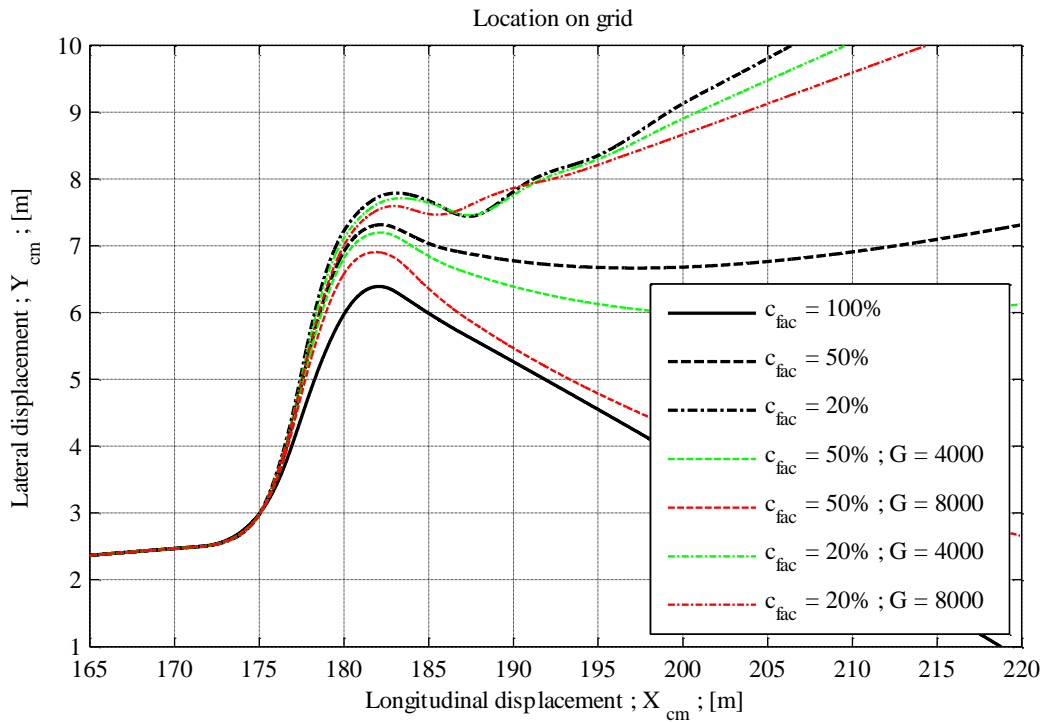


Figure 5-24: Sprung mass pitch, roll and yaw rates during single lane change test for various passive damping factors and groundhook gains.





**Figure 5-25: Vertical tyre forces during single lane change test for various passive damping factors and groundhook gains.**



**Figure 5-26: Path followed during single lane change test for various passive damping factors and groundhook gains.**

and Figure 5-24, p5.22). Sudden vertical force increases occur after tyre lift-off when the tyre again comes into contact with the road surface. This especially holds true for low passive damping levels and the tyres on the right when the vehicle stabilises after the second roll ( $t > 4s$ ).

The path followed during the single lane change test for each suspension setting is shown in Figure 5-26, p5.23. As mentioned before, the responses after the peak displacement vary for each test run due to lateral drift resulting from the double integration process. It can be concluded that the addition of a controlled suspension to the passive system results in similar lateral displacements as the directional response is unchanged.

As shown in Figure 5-27, p5.24, through the implementation of groundhook control, it is possible to increase the lateral and longitudinal acceleration response of the test vehicle during the performance of the single lane change test, as compared to the corresponding uncontrolled passive suspension. However, the acceleration response is reduced for higher control gains.

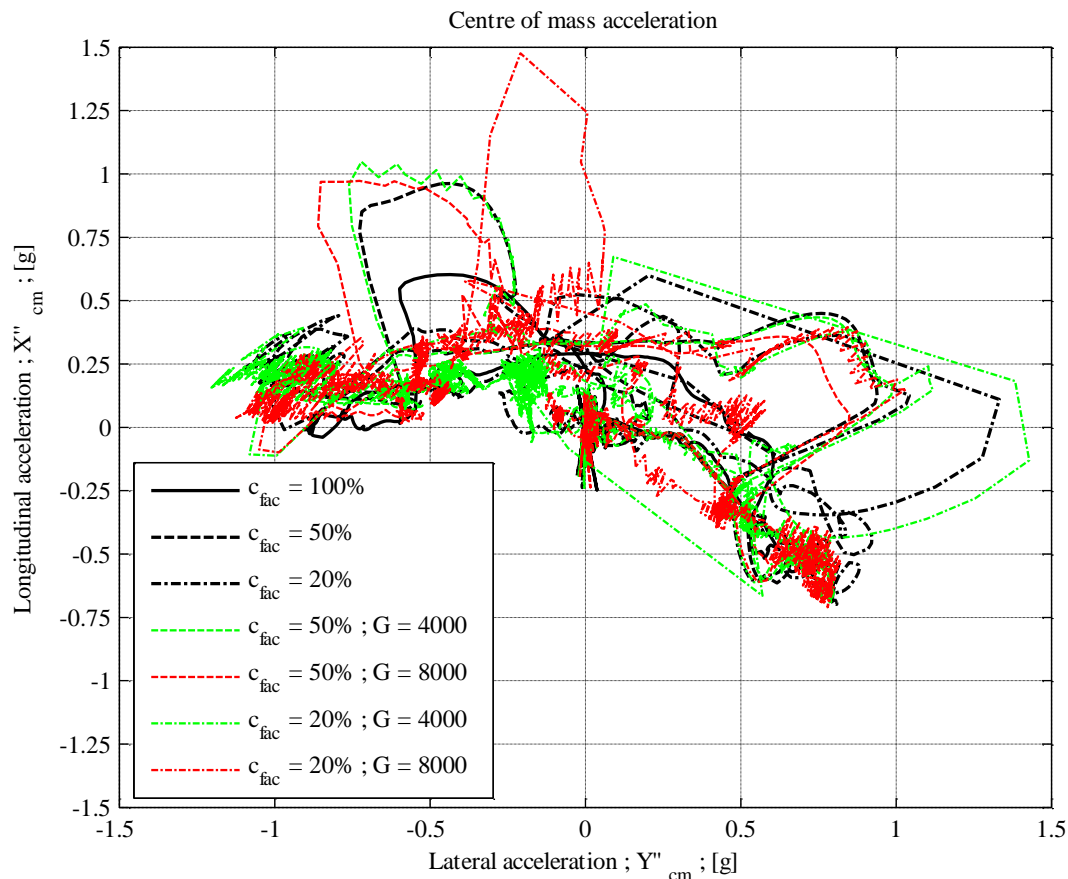


**Figure 5-27: Lateral- and longitudinal acceleration response during single lane change test for various passive damping factors and groundhook gains.**

### 5.3.3 The Optimal Handling Suspension

The results from Section 5.3.2, p5.15 reflect the implementation of ideal semi-active damping forces, assuming that the prescribed damping forces are exactly deliverable by the MR dampers regardless of the input conditions. In this section, results from the optimal handling suspension using the semi-active prescribed damping forces and the results from implementation of the MR damper models to determine the true damping forces are compared. The results from implementation of the semi-active forces are discussed in Section 5.3.3.1, p5.26, and the results from implementation of the true MR damper forces are discussed in Section 5.3.3.2, p5.29.

From the handling simulation results, it may be concluded that for a vehicle without a differential, such as the test vehicle used in this study, the best handling in a single lane change test is obtained by implementation of an uncontrolled suspension with low passive damping (20%). Lower damping results in an increase in body roll and loss of road-tyre contact at the rear wheels that is required to generate oversteer and thus enhance the directional response of the vehicle. Improved directional response is confirmed by a higher yaw rate obtained during the single lane change test, as shown in Figure 5-19, p5.18. However, the successful performance of other handling tests (such as jump manoeuvres that the test vehicle is subjected to) may require different suspension characteristics.

To enhance the handling of a conventional off-road vehicle the body roll should be reduced and the duration of road-tyre contact should be increased. Thus the best handling of a conventional off-road vehicle in a single lane change test is obtained by the implementation of skyhook control combined with a 50% passive setting (refer to Figure 5-18, p5.17 and Figure 5-20, p5.19). It should however be noted that in order to obtain the best handling solution, the degree of passive damping present in the suspension can be adjusted according to requirements of other handling tests, and the control gain can also be varied. A low level of passive damping can be used, given that the MR dampers are properly utilised by using an adequately high control gain. Yet, the passive damping should not be so low that controlled damping forces exceeding the capabilities of the MR dampers are required when performing severe handling manoeuvres.

For the purpose of this study, a 50% passive suspension in combination with a skyhook controlled suspension at a gain of 8000Ns/m is considered to be optimal, as significant improvement over the original passive suspension is obtained from an increased road-tyre contact and reduced body roll perspective, (refer to Figure 5-18, p5.17 and Figure 5-20, p5.19).

### 5.3.3.1 Implementation of Semi-active Force

In this section the optimal handling suspension (50% passive suspension with a skyhook control gain of 8000Ns/m), under the assumption that the prescribed semi-active forces are delivered exactly by the MR dampers (and therefore used as feedback to the vehicle model), is discussed.

The performance of the skyhook control principle during the single lane change test is shown in Figure 5-28, p5.26. As indicated in Equation 60, p5.16, the relative velocity of the MR damper and the vehicle body vertical acceleration are used to prescribe the semi-active damping force. In Figure 5-28 the prescribed control force has been scaled by a factor of 1/5000 to obtain values that are comparable to the velocity magnitudes.

Since there is passive damping present in the suspension, the prescribed damping forces must be delivered by the MR dampers and the passive hydro-pneumatic dampers together, as indicated in Equation 59, p5.2. The required total damping force,  $F_{SA,z}$ , passive damping force,  $F_{d,z}$ , and MR damper force,  $F_{MR,z}$ , are shown in Figure 5-29, p5.27. It may be noted that when the damping force delivered by the passive damper is bigger than the prescribed semi-active force, the MR damper is “switched off” and no force is delivered. This is possible under the mentioned assumption that the prescribed forces are deliverable by the MR dampers, regardless of other excitation conditions such as relative damper velocity.

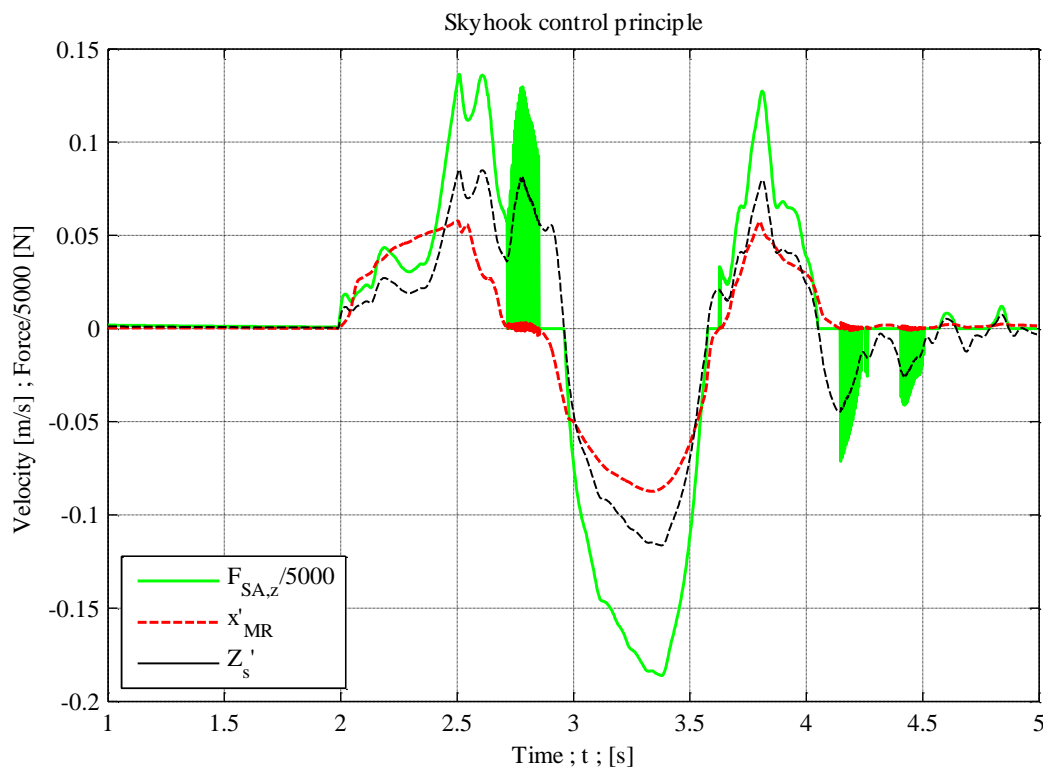
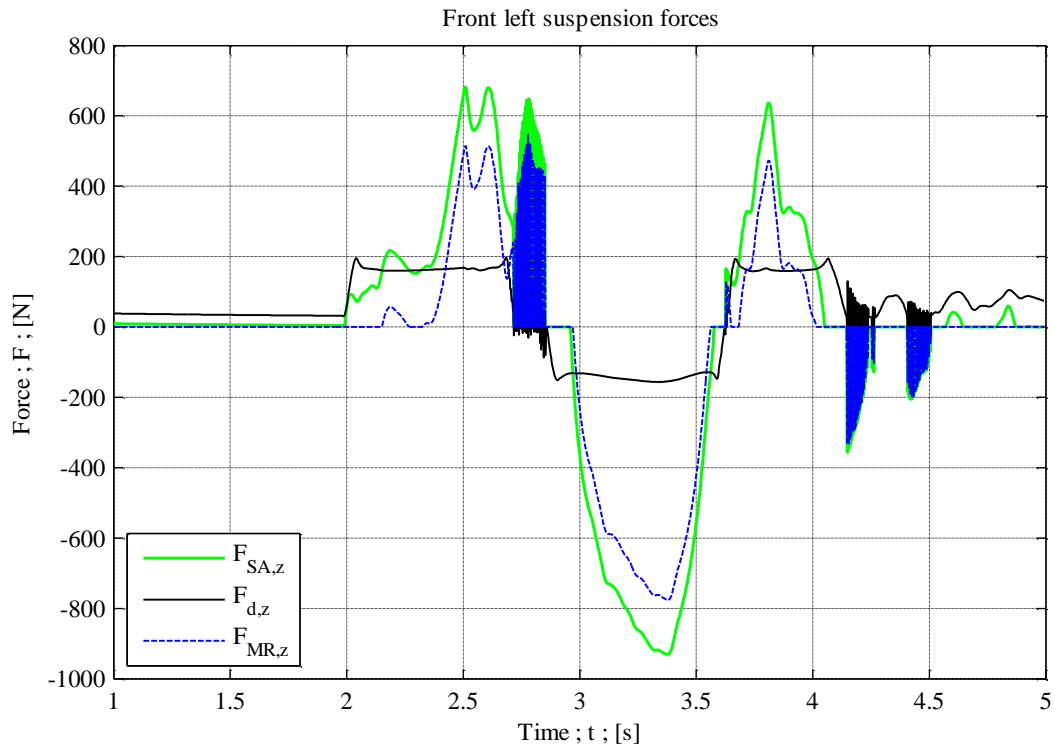
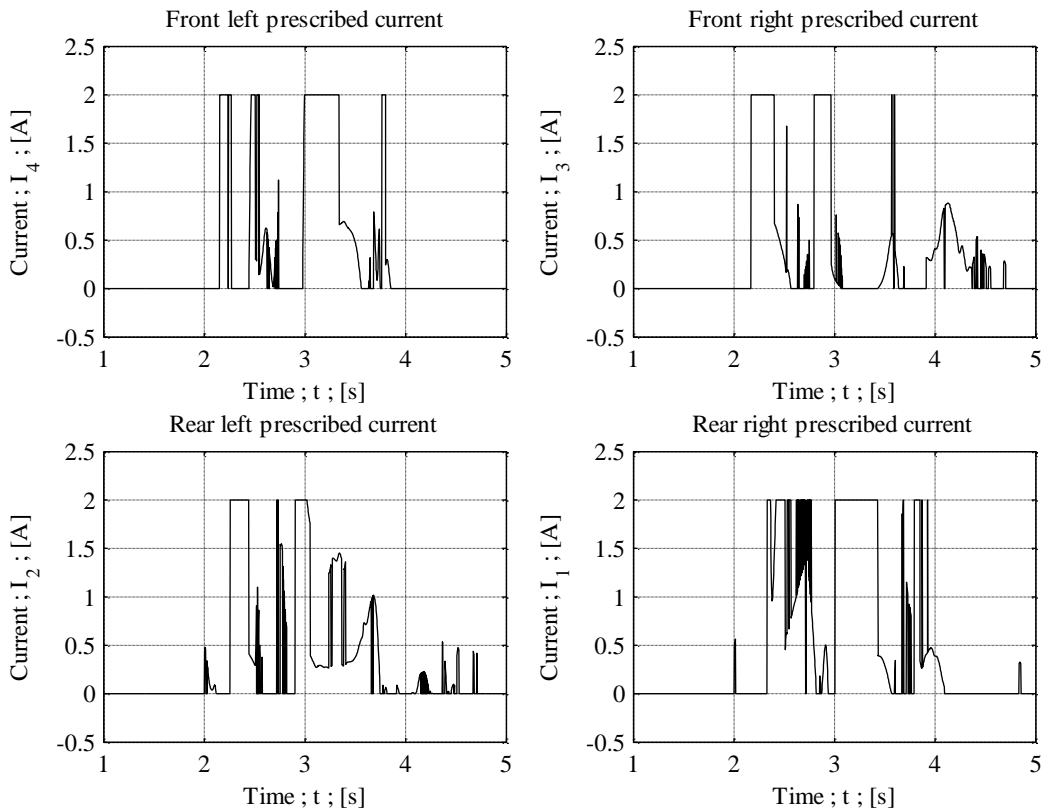


Figure 5-28: Optimal handling: Time traces for skyhook control implementation (front left corner).



**Figure 5-29: Optimal handling: Time traces for suspension forces (front left corner).**



**Figure 5-30: Prescribed input current to MR dampers.**

The polynomial model developed in this study is implemented to determine the damper input current. The current levels are constrained between 0A and the maximum allowable input current to the damper, 2A, as shown in Figure 5-30, p5.27. Here the MR damper force isn't recalculated when the current is constrained, instead, only the prescribed semi-active forces and the passive damping forces are used to calculate the force delivered by the MR damper. The discrepancies between the prescribed semi-active forces and those deliverable by the MR dampers according to the polynomial model are shown in Figure 5-31, p5.28.

According to simulation results, the percentage road-tyre contact loss of the original 100% passive suspension during the single lane change test is 6% at the front right wheel and rear left wheels, and 12% at the rear right wheel. The optimal handling suspension improves the road-tyre contact with only the rear left wheel losing contact for 6% of the duration of the test, and all the other wheels maintaining 100% road-tyre contact (refer to Figure 5-20, p5.19).

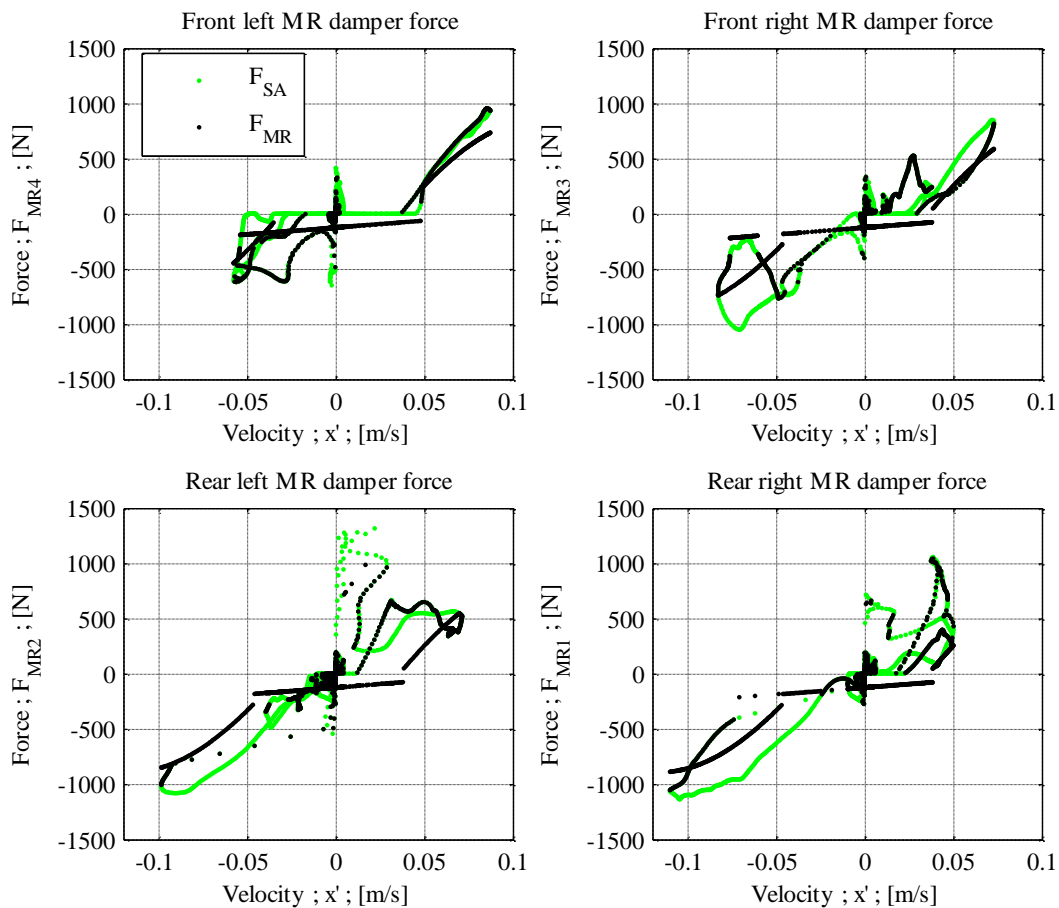


Figure 5-31: Force-velocity relationship of polynomial model compared to prescribed semi-active forces.

### 5.3.3.2 Implementation of the MR Damper Model

The handling simulation results from Section 5.3.2, p5.15 are only valid if the semi-active damping forces prescribed by the system controller are deliverable by the MR dampers. As mentioned in Section 5.2.3, p5.9, the MR damper polynomial model and the Kwok model (at 0A) are used to convert the prescribed semi-active forces to the damper input current, and to determine the actual deliverable MR damper forces under the specific input conditions. In this section the same optimal handling suspension is implemented ( $c_{fac} = 0.5$ ,  $G = 8000\text{Ns/m}$ ), but the actual deliverable MR damper forces are used as feedback to the vehicle model instead of the prescribed forces.

The shortcomings of the polynomial MR damper model and limitations of the MR dampers used in this study are demonstrated in Figure 5-32, p5.29. Saturation of MR damper forces occur at  $0.23 \times 10^4\text{N}$  and  $-0.26 \times 10^4\text{N}$ , which are the maximum deliverable MR damper forces according to experimental results (refer to Figure 3-4, p3.5). Although the semi-active forces prescribed in Figure 5-31, p5.28, fall within the capabilities of the dampers, shortcomings in the polynomial model and constraining of the prescribed input current levels between 0A and 2A, as shown in Figure 5-30, p5.27, lead to less than ideal damping forces being implemented, thus negatively affecting the

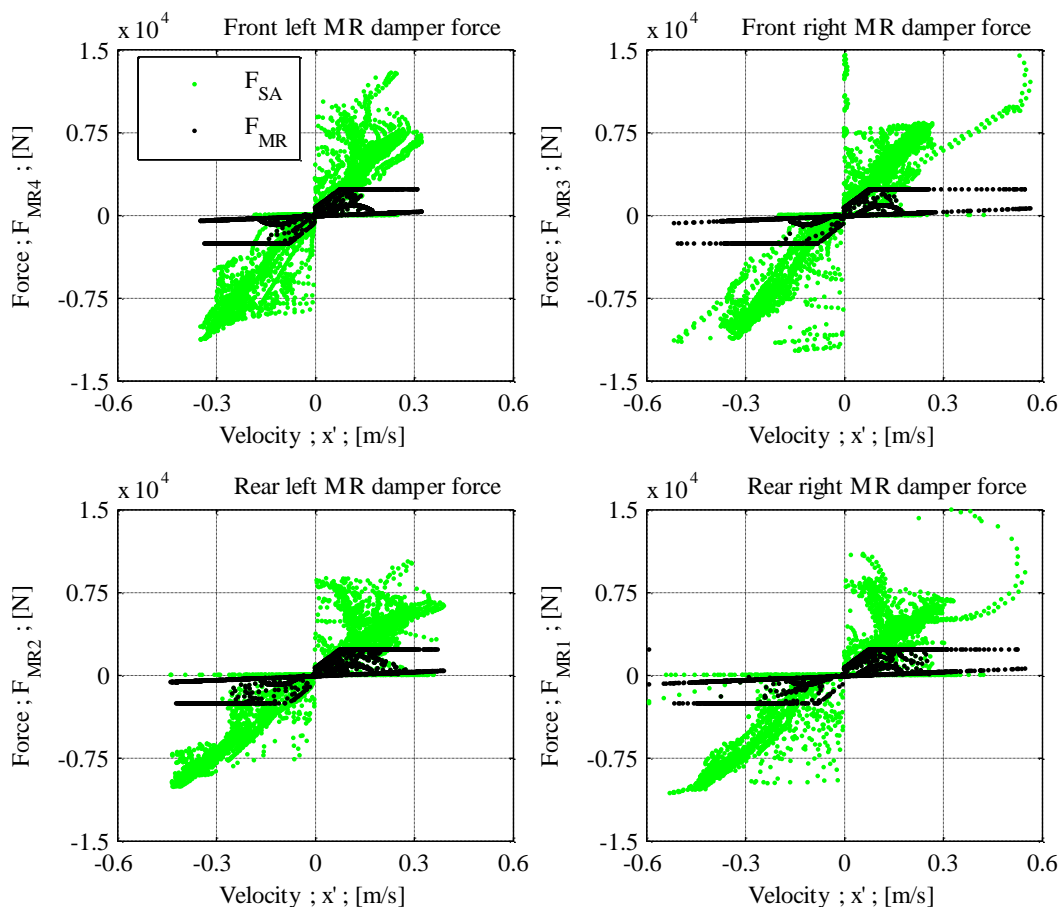


Figure 5-32: Force-velocity relationship of polynomial model compared to prescribed semi-active forces.

performance of suspension control. In order to compensate for dynamics resulting from faulty damping, even higher damping forces are prescribed by the skyhook control algorithm.

The vehicle body angular displacement results are shown in Figure 5-33, p5.30, and the vertical tyre forces are shown in Figure 5-34, p5.31. Compared to the simulation results in Figure 5-18, p5.17, the pitch and roll response of the suspension under consideration has increased significantly and is oscillatory in nature. From the second roll angle magnitude (almost  $-30^\circ$ ) it may be deduced that considerable loss of road-tyre contact of the right wheels occurs at around 4s. This is confirmed in Figure 5-34, p5.31. It may also be noted that wheel hop occurs.

Although simulation results have shown that road-tyre contact and vehicle body roll during the single lane change test can be improved by implementation of a 50% passive suspension in combination with a skyhook controlled suspension with a control gain of 8000Ns/m, shortcomings in the implemented MR damper model and saturation of the prescribed damper input current considerably impair the control of the suspension, resulting in an ineffective solution. While the implementation of the prescribed semi-active damping forces result in a significant improvement, once the MR damper input current is controlled, the results are no longer desirable.

### 5.3.4 Handling Results Summary

In order to investigate the handling capabilities of the baseline vehicle, slalom tests have been performed. Semi-active suspension control has been evaluated by simulating the test vehicle while performing a single lane change. Road-tyre contact loss occurred during both handling manoeuvres. Two sets of suspension characteristics for optimal handling behaviour during the single lane change test have been identified:

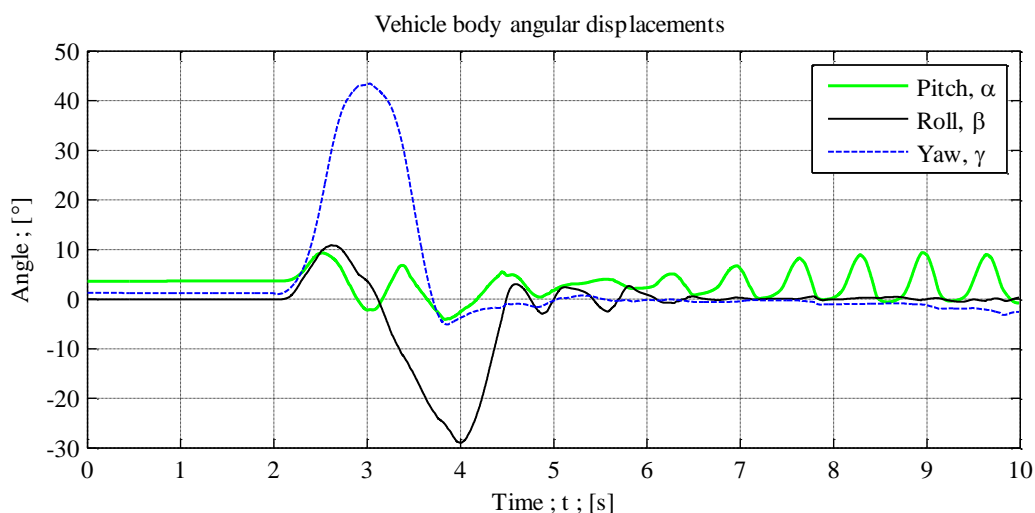
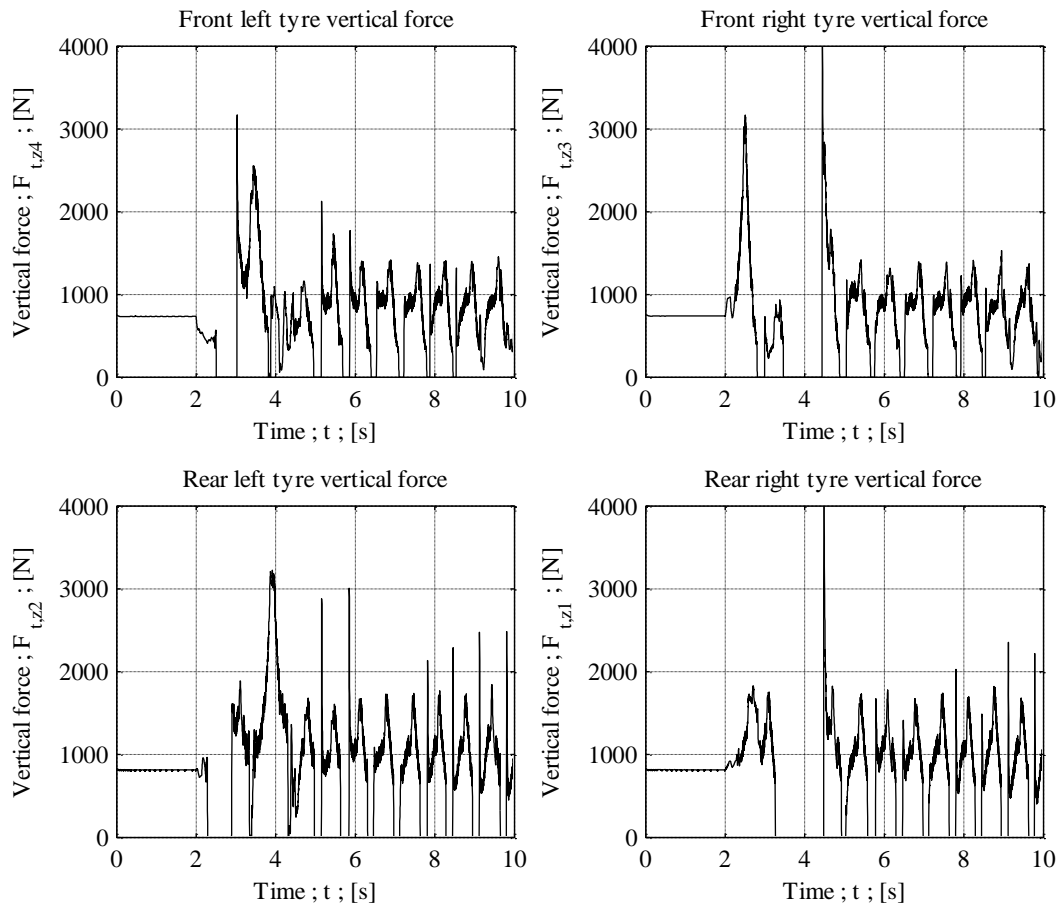


Figure 5-33: Sprung mass angles during single lane change test with implementation of MR damper model.





**Figure 5-34: Vertical tyre forces during single lane change test with implementation of MR damper model.**

- A 50% passive damping setting combined with skyhook controlled MR dampers with a control gain of 8000Ns/m to enhance the handling of *conventional off-road vehicles* by significantly reducing body roll and road-tyre contact loss. While the simulation results showed that three wheels of the baseline vehicle lose contact with the road, road-tyre contact loss occurs at only the rear left wheel when the optimal handling suspension is implemented. The body roll occurring during the second roll movement is also reduced as compared to the baseline vehicle.
- An uncontrolled 20% passive suspension to enhance the handling of the *test vehicle used in this study*, which has no differential, by allowing sufficient body roll to induce road-tyre contact loss at the rear of the vehicle that is required to generate oversteer and thus improve the directional response of the vehicle. Simulation results showed an increase in yaw rate, lateral acceleration and lateral displacement.

The prescribed semi-active damping forces (see Figure 5-31, p5.28) remained well within the physical limits of the MR dampers used in this study, indicating that the road-holding of the test vehicle could potentially be increased by implementation of higher control gains. However, due to shortcomings in the utilised MR damper models, prescribed input current saturation, and possibly

limitations in the MR damper capabilities, simulation results showed that the implementation of skyhook control with the polynomial and Kwok MR damper models may be ineffective in controlling the road-holding and the body roll of the vehicle.

## 5.4 Addressing the Combined Ride Comfort and Handling Problem

While the passive damping for optimal handling of the test vehicle in a single lane change is 20% of the original suspension, for optimal ride comfort while driving over a rough track passive damping should be as low as 7.5% (refer to Sections 5.2.2, p5.4, and 5.3.2, p5.15). Implementation of a passive suspension lower than 20% leads to suspension bump-stop contact occurring during the single lane change test and could result in roll over during more severe handling manoeuvres. Although 20% damping for the passive suspension has been identified as the optimal handling suspension, different suspension characteristics may be favourable for the successful completion of other handling manoeuvres.

Implementation of lower passive damping levels with variable control gains entail that both the ride comfort and handling issues can be addressed with one suspension design, given that sufficient damping forces can be obtained with increased control gains. *Optimal ride comfort when driving over a rough track* can be obtained by implementation of a hydro-pneumatic passive suspension combined with MR dampers in the “off” state (when no current is applied to the MR dampers), resulting in damping characteristics equivalent to 7.5% of the original suspension. Although a lower weighted RMS vertical acceleration can be obtained by implementation of skyhook control (as discussed in Section 5.2.2.1, p5.6), the improvement is minimal and there are some uncertainties regarding the actual improvement that can be obtained since there is always some minimum level of passive damping provided by MR dampers. *Optimal handling in a single lane change* can be obtained by providing a constant current to the MR dampers, resulting in damping characteristics equivalent to 20% of the original suspension. When larger damping forces are required for more severe handling manoeuvres, the current supplied to the MR dampers can be increased, effectively producing damping characteristics higher than 20% of the original suspension, but limited by the capabilities of the MR dampers used in this study. Also, for other manoeuvres it may be desired that the body roll be reduced and the duration of road-tyre contact be increased. Simulation results have shown that this can be achieved by passive suspensions with higher damping (such as the baseline suspension), and by the implementation of skyhook control (refer to Section 5.3.2.1, p5.17).

Furthermore, a “decision-making strategy” could be implemented to switch from ride comfort mode (MR dampers “off”) to handling mode (MR dampers “on” and skyhook controlled using an

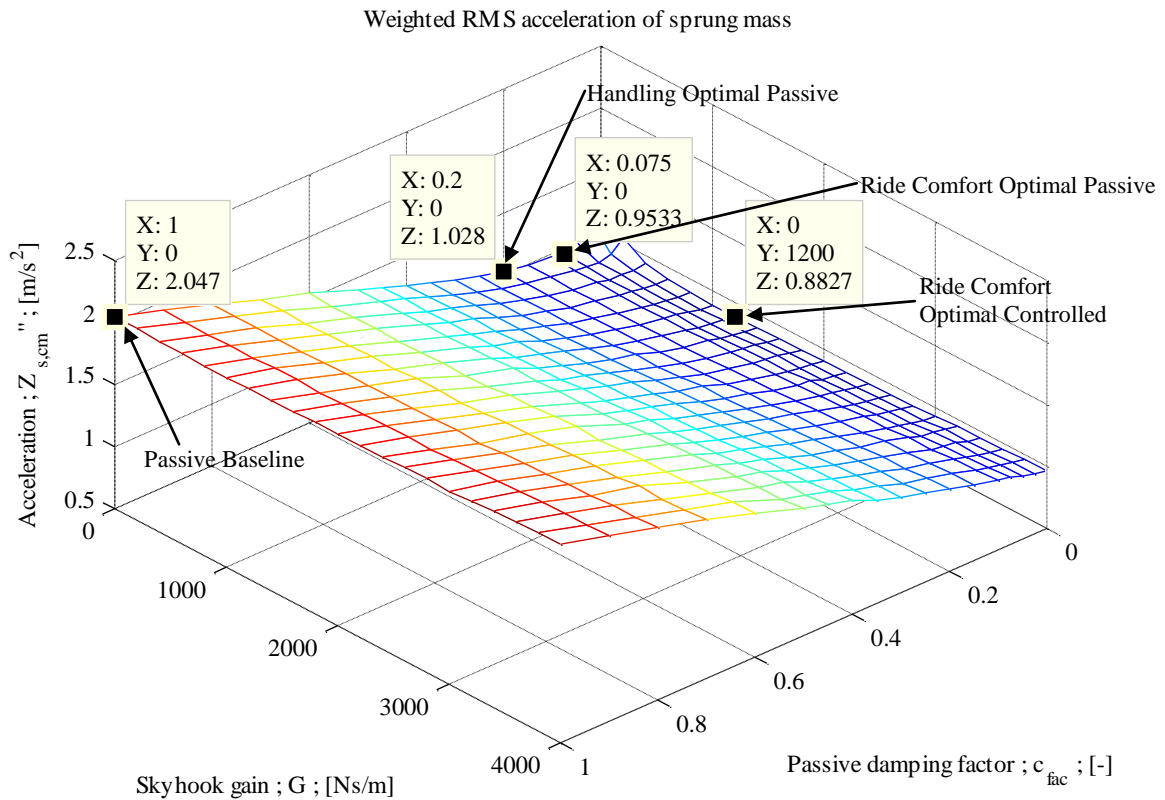


**Figure 5-35: Belgian paving simulation results: Weighted RMS acceleration of sprung mass for various skyhook gain and passive damping contributions.**

adequate control gain) when required, as proposed by **Els et al. (2007)**. Such a decision-making strategy is also described by **Els (2006)**.

In Figure 5-35, p5.33 it is shown that the weighted RMS vertical acceleration of the vehicle body when driven over the Belgian paving track is  $0.9533\text{m/s}^2$  for a 7.5% passive damping level, and  $1.028\text{m/s}^2$  for a 20% passive damping level. Although this passive damping level results in an increase in weighted RMS vertical acceleration compared to the ride comfort optimal controlled suspension ( $0.8827\text{m/s}^2$ ), it is still a significant improvement over the acceleration levels transmitted by the original uncontrolled suspension ( $2.047\text{m/s}^2$ ). Considerations such as added system complexity could possibly lead to the implementation of a 20% damping level for optimal ride comfort and handling, with a decision making strategy to increase the current supplied to the damper when severe handling manoeuvres are performed.

## 5.5 Conclusion

In this chapter, the vehicle model developed in Chapter 4 has been used for simulation runs in order to determine a suitable suspension that could be used to improve the ride comfort and handling

performance of the test vehicle. Ride comfort is investigated by using the input from a rough Belgian paving track, and handling is evaluated by subjecting the test vehicle to a single lane change manoeuvre. Skyhook- and groundhook control schemes are implemented jointly with a passive suspension at multiple damping levels.

Since skyhook control is aimed at reducing the vertical motion of the sprung mass, it is expected to improve the pitch and roll movement and vertical acceleration of the vehicle body, without taking the response at the wheels into consideration. On the contrary, groundhook control is expected to improve the response at the wheels without accounting for vehicle body movement. Skyhook control should therefore yield favourable ride comfort characteristics, while groundhook control should yield favourable handling characteristics. Simulation results in this chapter indicate that skyhook control could be capable of improving both the ride comfort and handling performance of conventional off-road vehicles, while groundhook control could only reduce the wheel hop motion when driving over a rough surface. The control strategies implemented in this chapter were originally developed for two degree of freedom vertical models, and it has been demonstrated that the control principle is less effective when applied to higher order models, especially when the roll and pitch degrees of freedom are included in the model.

It is concluded that for optimal ride comfort the passive damping should be at a minimum, either 7.5% passive or 0% passive combined with a controlled suspension. The ideal ride comfort suspension is a pure skyhook controlled suspension with a gain of 1200Ns/m. The RMS weighted vertical acceleration of the sprung mass is reduced from  $2.1\text{m/s}^2$  (of the baseline vehicle) to  $0.8827\text{m/s}^2$ . It has also been shown that the ride comfort optimal passive suspension (at 7.5% passive damping of the baseline vehicle) can reduce the RMS vertical acceleration of the vehicle body ( $0.9533\text{m/s}^2$ ) to levels comparable to the optimal controlled suspension ( $0.8827\text{m/s}^2$ ), without the added system complexity and cost associated with semi-active controlled suspensions. Furthermore, the choice of skyhook control gain is not obvious as there exists an optimal value above which the RMS vertical acceleration of the vehicle body gradually increases. It should therefore be carefully considered, when ride comfort alone is the design goal and other suspension performance requirements are not factored in, whether implementation of a semi-active controlled suspension really is worth the extra effort as compared to merely reducing the damping of the passive suspension to an acceptable level.

For optimal handling of conventional off-road vehicles it is concluded that the total damping in the system should be as high as possible, ideally 100% passive damping with the maximum possible control gain without exceeding the capability of the MR dampers. Among the suspension configurations investigated, the 50% passive damping with skyhook controlled MR dampers with a

control gain of 8000Ns/m was found to be the most effective in reducing body roll and loss of road-tyre contact. Where three wheels of the baseline vehicle lose road-tyre contact, with the implementation of skyhook control, it is reduced to one wheel. It is expected that a 7.5% passive suspension in combination with a skyhook controlled suspension can address both the ride comfort and handling problems by altering the control gain as the damping need changes.

While reducing body roll and maintaining road-tyre contact are important design objectives for improving handling of conventional off-road vehicles, suspension requirements are different for vehicles without a differential, such as the test vehicle used in this study. Since the driving wheels of these vehicles rotate at the same velocity, the ability to change direction is impaired. In order to improve handling, suitable body roll is required to induce loss of road-tyre contact at the inside driving wheel and simultaneously overload the outside driving wheel, so as to generate oversteer for improving the directional response. Thus for the optimal handling of the test vehicle used in this study, it is concluded that the uncontrolled damping should be the lowest possible, that is just enough to avoid bump-stop contact, so as to prevent roll over in more severe handling manoeuvres. Among the suspension configurations investigated, the 20% passive suspension has been found to be the most effective in improving the directional response of the test vehicle. Simulation results showed that the baseline vehicle is capable of achieving a yaw rate of 62°/s during the single lane change test, but the implementation of a 20% damping suspension resulted in a yaw rate of 88°/s.

Simulation results demonstrate that skyhook control is effective in improving both the ride comfort and the handling capabilities of conventional off-road vehicles. While a low level of damping is required for optimal ride comfort, higher damping levels are required for improved handling. Therefore, it is recommended that a passive suspension equivalent to 7.5% of the baseline suspension be implemented with skyhook controlled MR dampers with varying control gains. This requires a system controller that selects a suitable control gain according to desirable ride comfort or handling, and a damper controller to regulate the damper input current.

While groundhook control has been implemented in the existing literature to improve the road-holding of vehicles, in this study it is found to be ineffective in this regard. Implementation of groundhook control yielded no apparent benefit as compared to the corresponding uncontrolled suspensions at a higher passive damping level (50%). Skyhook control was able to increase the duration of road-tyre contact in the single lane change test, but there was no noticeable improvement achieved by groundhook control. This raises some questions regarding the ability of groundhook control to enhance the drivability of vehicles when performing handling manoeuvres involving the lateral, roll and yaw degrees of freedom, and whether limiting of the vertical movement of the wheels is in fact beneficial for handling manoeuvres.

The simulation results are summarised in Table 5–1, p5.36. These results reflect the implementation of the prescribed semi-active forces, and the effects of the MR damper model are thus omitted.

**Table 5–1: Ride comfort and handling simulation results summary.**

	<b>Control</b>	<b>Gain</b>	<b>Passive Level</b>	<b>Result</b>	<b>Baseline Result</b>
Ride Comfort	Skyhook	1200Ns/m	0%	0.88m/s <sup>2</sup> RMS vertical acceleration.	2.1m/s <sup>2</sup> RMS vertical acceleration.
	Optimal Passive		7.5%	0.95m/s <sup>2</sup> RMS vertical acceleration.	
Handling ( <i>Conventional off-road vehicles</i> )	Skyhook	8000Ns/m	50%	Up to 6% contact loss at 1 wheel. Body roll reduced.	Up to 12% contact loss at 3 wheels.
Handling ( <i>Test vehicle</i> )	Optimal Passive		20%	Yaw rate of 88°/s obtained.	Yaw rate of 62°/s obtained.
Combined Ride Comfort and Handling	Skyhook	Varied by decision making strategy.	7.5% (Proposed value.)	- (To be investigated.)	- (To be investigated.)

---

## 6 CONCLUSIONS AND FUTURE WORK

---

The design of passive suspension systems of vehicles generally involves a compromise between ride comfort and drivability due to the contrasting requirements of suspension characteristics. A soft spring and low damping is required for improved ride comfort, whereas a stiff spring with high damping is required for improved handling. A trade-off situation is created since the passive suspension characteristics remain fixed at the design state. This compromise can be resolved by using a fully active suspension system. However, such a system is energy intensive, expensive, and can be extremely complex. Semi-active suspensions have the potential to deliver results that are comparable to active suspensions, but require less energy, are more cost effective, and require minimal modifications to already developed vehicles. MR dampers are a class of controllable semi-active dampers that offer continuous and fast switching between damping levels constrained by upper and lower limits. MR dampers are gaining widespread recognition and are being increasingly used in vehicle suspension systems.

This study attempts to mitigate the compromise between ride comfort and handling by investigating the use of MR dampers. A controllable suspension for an off-road vehicle has been designed, consisting of MR dampers and passive hydro-pneumatic spring-damper units. Passive damping has not been eliminated due to limitations of the MR dampers used in this study. The conclusions from this study are discussed in Section 6.1, p6.1, shortcomings identified during the course of this work are discussed in Section 6.2, p6.4, and future work is discussed in Section 6.3, p6.5.

### 6.1 Conclusions

Numerous MR damper models have been developed and evaluated during the course of this study. Although the LMS recursive model has demonstrated great potential in addressing MR damper model shortcomings, this model requires measured force feedback in order to operate accurately. The use of calculated force feedback has been investigated in this study, but was not found to yield acceptable results. Therefore, it can be concluded that LMS models are difficult to implement in combined damper and vehicle simulations, and may not be feasible in experimental applications due to the added cost and complexity associated with real-time measurement of the damping forces. Also, for control purposes, a current dependent invertible damper model is required in order to prescribe the damper input current levels so as to achieve the desired damping forces. While the Bouc-Wen models

are found to be the most accurate, these models are numerically inefficient, and cannot be used to calculate the required damper current. Two current dependent invertible MR damper models suitable for control purposes have been developed in this study, but simulation results indicate that the polynomial model is superior.

For suspension control analysis, a three-dimensional multiple degrees of freedom vehicle model has been developed using ADAMS View software. This model incorporates experimentally determined characteristics, including moments of inertia, spring and damper characteristics, and a Pacejka tyre model. The model has been validated by comparing simulation results to measured data from discrete bump tests and slalom tests. While the model has been adequately validated for ride comfort simulation, there are some shortcomings regarding handling.

For ride comfort simulation the vehicle model is driven over a rough Belgian paving track, and for handling simulation the vehicle model executes a single lane change test. The influence of several passive damping levels as well as skyhook- and groundhook control gains on the ride comfort and handling ability of the test vehicle has been investigated. It is concluded from the simulation results that lower passive damping levels yield improved ride comfort, with only marginal improvement obtained by the implementation of skyhook control as compared to optimal passive damping. Lower passive damping levels also yield improved handling. This is because the test vehicle used in this study has no differential, and loss of road-tyre contact induced by body roll is required to generate oversteer and so improve the directional response of the vehicle. The implementation of skyhook control has a positive influence on the reduction of vehicle body roll and maintaining road-tyre contact, while groundhook control provides no benefit over uncontrolled damping. The ability of skyhook control to improve handling, and the inability of groundhook control to improve road-holding in this study, raise questions regarding the applicability of hybrid control to higher order vehicle models, and therefore the performance improvement that can actually be obtained regardless of the assertions made in the literature.

The ride comfort optimal passive suspension (7.5% of baseline damping) reduces the weighted RMS vertical acceleration of the test vehicle sprung mass when driven over a rough Belgian paving track from  $2.1\text{m/s}^2$  to  $0.95\text{m/s}^2$ , an improvement of 55%. Implementation of skyhook control further reduces the RMS vertical acceleration to  $0.88\text{m/s}^2$ , which is an improvement of 3% compared to the passive suspension. Such a small improvement in ride comfort may not be worth the extra complexity (sensors and filters) associated with continuous variable damping control. The handling optimal passive suspension (20% of baseline damping) increases the yaw rate obtained in a single lane change from  $62^\circ/\text{s}$  to  $88^\circ/\text{s}$ , an improvement of 42%, and reduces the weighted RMS vertical acceleration to  $1.03\text{m/s}^2$ , an improvement of 51% compared to the baseline suspension. Higher damping may be required for more severe handling manoeuvres, such as jump manoeuvres. The ride comfort and



handling trade-off may be resolved by implementing passive hydro-pneumatic spring-damper units combined with MR dampers in the “off” state (when no current is supplied to the dampers) to provide a characteristic equivalent to 20% of the baseline suspension for “optimal” ride comfort and handling. The damping may be increased or controlled by implementing a decision-making strategy or variable damping control such as skyhook control when more severe handling manoeuvres are performed.

Since there are some capability constraints associated with MR dampers, for instance that the prescribed ideal damping forces may not be deliverable by the dampers under specific excitation conditions, a MR damper polynomial model has been implemented to provide a more realistic indication of the possible performance of the test vehicle. It has been demonstrated that shortcomings in the MR damper model impairs suspension control, yielding poor results as compared to initial simulations. Under ideal conditions (when the prescribed damping forces are precisely provided by the MR dampers) the lowest RMS vertical acceleration (and thus best ride comfort) achievable by skyhook control is  $0.88\text{m/s}^2$ , once the MR damper model is implemented the RMS vertical acceleration is increased to  $1.02\text{m/s}^2$ . Also, when the MR damper model is implemented in the single lane change test, skyhook control is ineffective in reducing body roll and improving road-holding as compared to implementation of the prescribed semi-active damping forces. These findings demonstrate the need for force feedback in order to adequately control the MR dampers.

The important conclusions drawn by this study are summarised as follows:

- A passive suspension equivalent to 20% of the baseline damping is capable of improving the ride comfort and handling of the test vehicle used in this study.
- The improvement in ride comfort obtained by implementation of skyhook control is marginal compared to ride comfort levels obtained by the optimal passive suspension (at 7.5% of the baseline damping).
- In order to reduce the ride comfort and handling compromise when severe handling manoeuvres are expected, implementation of a decision-making strategy for switching between low and high damping is proposed.
- Skyhook control may be adequate to control body roll and improve road-holding during severe handling manoeuvres. This is in contrast to the implementation of groundhook control that is generally proposed in the literature. These findings eliminate the need for hybrid control and a strategy to choose the skyhook-/ groundhook control bias factor according to ride comfort and drivability requirements.
- Shortcomings in the MR damper models result in a decrease in improvement levels obtained by the simulation tests.

The main research question addressed by this study is thus answered as follows: *A passive suspension delivering 20% damping of the baseline suspension is capable of significantly improving the ride comfort and handling of a Baja vehicle, with minimal trade-off in ride comfort. However, the proposed suspension may be insufficient for severe handling manoeuvres. Therefore implementation of controllable MR dampers combined with passive spring-damper units and an on-off decision-making strategy is proposed to increase the damping when required. If improved road-holding and reduced body roll are required, rather than improved directional response, the implementation of skyhook control is recommended.*

## **6.2 Recommendations**

Recommendations and shortcomings identified during the course of this work are discussed in this section. This section also discusses possible areas of improvement that could be incorporated in a future study.

### **6.2.1 MR Damper Models**

The MR damper force response shows a strong dependence on the temperature of the MR fluid in the damper. Inclusion of temperature as a parameter in MR damper models may aid in improving of the model.

While there are many MR damper models discussed in the literature, no outright superior model has been identified. Accurate MR damper models are either numerically intensive, applicable to specific input conditions (such as the frequency content of the excitation signal and the current supplied to the damper), and/or unable to calculate the required input current. Invertible current dependent models that are applicable to a wide range of input conditions are not accurate, and implementation of these models leads to ineffective suspension control, as demonstrated in this study. A model for MR dampers that can overcome the discussed shortcomings needs to be developed.

### **6.2.2 Vehicle Modelling**

The vehicle model can be more adequately validated for ride comfort simulation by elimination of accidental roll and yaw excitation during performance of the bump test. Both front wheels should hit the bump at the same time. This can be achieved by ensuring that the bumps are parallel to each other, and by using a guide line perpendicular to the bumps. The vehicle model should also be improved for handling simulation. Lateral drift resulting from double integration during simulations is removed by

implementation of a steering controller. Therefore, a closed loop handling test is required and the path followed by the vehicle during data collection should be measured.

As a result of low excitation frequencies used in the experimental work to determine the damping characteristics of the hydro-pneumatic spring-damper units, limited information was available to generate adequate force-velocity relationships. A wider velocity range has been obtained through extrapolation, which introduces uncertainties and inaccuracies in the model. A more accurate model of the spring-damper units would enhance the accuracy of the simulations. The spring-damper units should also be characterised for various passive damping levels to obtain improved accuracy in passive damping forces deliverable by the suspension system.

### **6.2.3 Suspension Control Simulations**

The only handling simulations performed in this study were open loop single lane change tests. It is recommended that results from other handling tests also be analysed, especially since a single unambiguous objective handling criterion has not been agreed upon in the literature.

Shortcomings in the utilised MR damper model have led to ineffective suspension control. For ride comfort analysis MR damper model shortcomings can be addressed by hardware-in-the-loop (HiL) tests, where the damper is experimentally excited in real-time according to ADAMS/Simulink outputs, and the measured MR damper forces are imported to ADAMS. HiL tests may also be helpful in the development and testing of a damper controller. HiL is however not feasible for handling analysis due to the high number of the degrees of freedom that are involved, and due to certain tyre effects.

## **6.3 Future Work**

Recursive MR damper models will be developed as part of future work. This can be accomplished by using strain gauge inputs to provide feedback to the recursive algorithm in order to update model parameters. Other classes of models will also be developed, such as fuzzy logic and neural network based models.

The vehicle model will be improved in future work: an updated tyre model will be implemented, and the hydro-pneumatic spring-damper units will be re-characterised to eliminate errors. To improve the handling simulation model, the path the vehicle follows during the handling tests (such as single lane change, double lane change, and slalom tests) will also be measured. Alignment errors will be reduced in the performance of the bump test. In addition to the bump test and slalom test, a static test and a sinusoidal steer test will also be performed.

A damper controller that regulates the input current to the MR dampers will be developed and tested. This includes semi-active damper control schemes such as on-off control and continuous state control (**Lai and Liao 2002**).

Suspension control algorithms, such as optimal-, robust- and sliding mode control will also be investigated in future studies. Effective control algorithms identified through simulation studies will be implemented experimentally on the test vehicle to compare simulation results with experimental work.

---

---

## REFERENCES

---

---

### A

Ahmadian, M., Pare, C.A. (2000). *A quarter-car experimental analysis of alternative semi-active control methods*, Journal of Intelligent Material Systems and Structures, Vol.11, pp.604-612.

Alvarez, L., Jiménez, R. (2002). *Real-time identification of magneto-rheological dampers*, Proc. 15<sup>th</sup> Triennial IFAC World Congress, Barcelona, Spain, Paper 2252.

### B

Babuska, I., Oden, J.T. (2004). *Verification and validation in computational engineering and science: basic concepts*. Computational methods in applied mechanics and engineering, Vol.193, pp.4057-4066.

Baja SAE. (2013). *SAE Collegiate Design Series: Baja SAE*, [Online] Available at: <http://students.sae.org/competitions/bajasae/> [Accessed 4 April 2013].

Bakker, E., Pacejka, H.B., Lidner, L. (1989). *A new tire model with an application in vehicle dynamics studies*, In: Proc. Int. Congress and Exposition, SAE paper 890087, Detroit, Michigan.

Becker, C.M., Els, P.S. (2013). *Profiling of rough terrain*, Accepted for publication in International Journal of Vehicle Design, 2013.

Bernard, J.E., Clover, C.L. (1994). *Validation of Computer Simulations of Vehicle Dynamics*, SAE Transactions, 940231.

Blundell, M., Harty, D. (2004). *The Multibody Systems Approach to Vehicle Dynamics*. Butterworth-Heinemann; Elsevier, Oxford.

Boada, M.J.L., Calvo, J.A., Boada, B.L., Díaz, V. (2011). *Modeling of a magnetorheological damper by recursive lazy learning*, International Journal of Non-Linear Mechanics, Vol.46, pp.479-485.

Botha, T.R., Els, P.S. (2011). *High speed autonomous off-road vehicle steering*. 17<sup>th</sup> International Conference of the International Society for Terrain-Vehicle Systems, Blacksburg, Virginia, USA.

Bouc, R. (1971). *Mathematical model for hysteresis*, Acustica, Vol.24, pp.16-25.

British Standards Institution. (1987). *British Standards Guide to Measurement and Evaluation of Human Exposure to Whole Body Mechanical Vibration and Repeated Shock*, BS 6841, 1987.

## C

Cao, D., Song, X., Ahmadian, M. (2011). *Editors' perspectives: road vehicles suspension design, dynamics, and control*, Journal of Vehicle System Dynamics, Vol.49, Nos.1-2, pp.3-28.

Carrera Akutain, X., Vinolas, J., Sacall, J., Castro, M. (2007). *Comparing the performance and limitations of semi-active suspensions*, International Journal of Vehicle Systems Modelling and Testing, Vol.2, No.3, pp296-314.

Chen, Y., Wang, Z., Qiu, J., Huang, H. (2012). *Hybrid Fuzzy Skyhook Surface Control Using Multi-Objective Microgenetic Algorithm for Semi-Active Vehicle Suspension System Ride Comfort Stability Analysis*, Journal of Dynamic Systems, Measurement, and Control, Vol.134.

Choi, S.B., Lee, H.K., Chang, E.G. (2001). *Field test results of a semi-active ER suspension system associated with skyhook controller*, Mechatronics, Vol.11, pp345-353.

Choi, S.B., Lee, S.K., Park, Y.P. (2001). *A hysteresis model for the field-dependent damping force of a magnetorheological damper*, Journal of Sound and Vibration, Vol.245, No.2, pp375-383.

Crosby, M.J., Karnopp, D.C. (1973). *The Active Damper*, The Shock and Vibration Bulletin, Number 43, Naval Research Laboratory, Washington, D.C.

## D

De Wit, C.C., Olsson, H., Åström, K.J., Lischinsky, P. (1995). *A new model for control of systems with friction*, IEEE Transactions on Automatic Control, Vol.40, pp.419-425.

Dong, X., Yu, M., Liao, C., Chen, W. (2010). *Comparative research on semi-active control strategies for magneto-rheological suspension*, Nonlinear Dynamics, Vol.59, p433-453.

Du, H., Sze, K.Y., Lam, J. (2005). *Semi-active  $H_\infty$  control of vehicle suspension with magneto-rheological dampers*, Journal of Sound and Vibration, Vol.283, pp.981-996.

Dyke, S.J., Spencer, B.F. (1997). *A Comparison of Semi-Active Control Strategies for the MR Damper*, Proceedings of International Conference on Intelligent Information Systems, The Bahamas.

Dyke, S.J., Spencer, B.F., Sain, M.K., Carlson, J.D. (1998). *An experimental study of MR dampers for seismic protection*, Smart Materials and Structures: Special Issue on Large Civil Structures, Vol.7, pp.693-703.

## E

Els, P.S. (2005). *The applicability of ride comfort standards to off-road vehicles*. Journal of Terramechanics, Vol.42, pp.47-64.

Els, P.S. (2006). *The ride comfort vs. handling compromise for off-road vehicles*, PhD Dissertation, Department of Mechanical and Aeronautical Engineering, University of Pretoria. [Online] Available at: <http://upetd.up.ac.za/thesis/available/etd-07152008-102911/> [Accessed 10 April 2012].

Els, P.S., Theron, N.J., Uys, P.E., Thoresson, M.J. (2007). *The ride comfort vs. handling compromise for off-road vehicles*, Journal of Terramechanics, Vol.44, pp.303-317.

## F

Fischer, D., Isermann, R. (2004). *Mechatronic semi-active and active vehicle suspensions*, Control Engineering Practice, Vol.12, pp.1353-1367.

## G

Gamota, D.R., Filisko, F.E. (1991). *Dynamic mechanical studies of electrorheological materials: Moderate frequencies*, Journal of Rheology, Vol.35, pp.399-425.

Garrott, W.R., Howe, J.G., Forkenbrock, G. (2001). *Results from NHTSA's Experimental Examination of Selected Maneuvers that may Induce On-Road Untripped Light Vehicle Rollover*, NHTSA 2001-01-0131.

Gerotek. (2008). *Gerotek Test Facilities, South Africa*. [Online] Available at: [http://www.armscordi.com/SubSites/Gerotek1/Gerotek01\\_landing.asp](http://www.armscordi.com/SubSites/Gerotek1/Gerotek01_landing.asp) [Accessed 23 October 2012].

Gillespie, T.D. (1992). *Fundamentals of vehicle dynamics*. Warrendale, PA: Society of Automotive Engineers, Inc.

Guglielmino, E., Sireteanu, T., Stammers, C.W., Ghita, G., Giuclea, M. (2008). *Semi-active Suspension Control: Improved Vehicle Ride and Road Friendliness*. Springer, London.

## H

Ha, S.H., Nguyen, Q., Choi, S., Rhee, E., Kang, P. (2009). *Performance Evaluation of a 6WD Military Vehicle Featured by MR Suspension System Considering Lumped Parameter Model of MR Damper*. Second International Conference on Smart Materials & Nanotechnology in Engineering, Weihai, China.

Heydinger, G., Garrott, W., Chrstos, J., Guenther, D. (1990). *A Methodology for Validating Vehicle Dynamics Simulations*. SAE Technical Paper 900128.

Hirai, J., Naruse, M., Abiru, H. (1996). *Structural control with variable friction damper for seismic response*, 11<sup>th</sup> World Conference on Earthquake Engineering. Paper 1934.

Hohl, G.H. (1984). *Ride Comfort of Off-Road Vehicles*, In Proceedings of the 8<sup>th</sup> International Conference of the ISTVS, Vol. I of III, Cambridge, England, August 5-11, 1984.

Housner, G.W., Bergman, L.A., Caughey, T.K., Chassiakos, A.G., Claus, R.O., Masri, S.F., Skelton, R.E., Soong, T.T., Spencer, B.F., Yao, J.T.P.(1997). *Structural control: Past, present, and future*, ASCE Journal of Engineering Mechanics, Vol.123, No.9, pp.897-971.

## I

International Organisation for Standardisation. (1988). *International Standard ISO 7401: Road vehicles – Lateral transient response test methods*, ISO 7401:1988(E).

International Organisation for Standardisation. (1997). *Mechanical Vibration and Shock – Evaluation of Human Exposure to Whole-Body Vibration, Part 1: General Requirements*. ISO 2631-1, Second Edition, The International Organisation for Standardisation, 15 July 1997.

International Organisation for Standardisation. (1999). *International Standard ISO 3888-1: Passenger cars – Test track for a severe lane-change manoeuvre – Part 1: Double lane-change*. ISO 3888-1:1999(E).

Ivers, D.E., Miller, L.R. (1989). *Experimental comparison of passive, semi-active on/off, and semi-active continuous suspensions*, SAE Technical Paper 892484.

Ivers, D.E., Miller, L.R. (1991). *Semi-active suspension technology: An evolutionary view*, Advanced Automotive Technologies, DE-Vol.40, ASME.



## J

Jansen, L.M., Dyke, S.J. (2000). *Semi-active control strategies for MR dampers: A comparative study*, ASCE Journal of Engineering Mechanics, Vol.126, No.8, pp.795-803.

Jolly, M.R., Bender, J.W., Carlson, J.D. (1999). *Properties and Applications of Commercial Magnetorheological Fluids*, Journal of Intelligent Material Systems and Structures, Vol.10, No.5, pp.5-13.

## K

Kat, C., Els, P.S. (2011). *Importance of correct validation of simulation models*, ASME 2011 International Design Engineering Technical Conferences and Computers and Information in Engineering Conference, Washington, DC, USA.

Kaul, S. (2011). *Recursive modeling of a magnetorheological damper*, International Journal of Mechanical and Materials Engineering, Vol.6, No.1, pp.31-40.

Kwok, N.M., Ha, Q.P., Nguyen, T.H., Li, J., Samali, B. (2006). *A novel hysteretic model for magnetorheological fluid dampers and parameter identification using particle swarm optimization*, Sensors and Actuators A, Vol.132, pp.441-451.

## L

Lai, C.Y., Liao, W.H. (2002). *Vibration control of a suspension system via a magnetorheological fluid damper*, Journal of Vibration and Control, Vol.8, pp.527-547.

Ljung, L., Soderstrom, T. (1985). *Theory and Practice of Recursive Identification*, MIT Press, Cambridge, MA, USA.

LORD Corporation. (2013). *LORD Ask Us How, Products & Solutions*, Cary, North Carolina. [Online] Available at: [http://www.lord.com/products-and-solutions/magneto-rheological-\(mr\)/product.xml/1652](http://www.lord.com/products-and-solutions/magneto-rheological-(mr)/product.xml/1652) [Accessed 2 June 2010].

## N

Nell, S., Steyn, J.L. (2003). *Development and experimental evaluation of translational semi-active dampers on a high mobility off-road vehicle*, Journal of Terramechanics, Vol.40, pp.25-32.

## P

Pradko, F., Lee, R.A. (1966). *Vibration Comfort Criteria*, SAE Technical Paper 660139, Society of Automotive Engineers, Warrendale.

## S

Şahin, İ., Engin, T., Çeşmeci, Ş. (2010). *Comparison of some existing parametric models for magnetorheological fluid dampers*, Smart Materials and Structures, Vol.19.

Savaresi, S.M., Poussot-Vassal, C., Spelta, C., Sename, O., Dugard, L. (2010). *Semi-Active Suspension Control Design for Vehicles*. Butterworth-Heinemann; Elsevier, Oxford.

Sharp, R.S., Pan, D. (1991). *On active control for automobiles*, In: 12<sup>th</sup> IAVSD Symposium August 26-30, 1991. Supplement to Vehicle System Dynamics, Vol.20.

Simon, D.E. (2001). *An investigation of the effectiveness of skyhook suspensions for controlling roll dynamics of sport utility vehicles using magneto-rheological dampers*, PhD Thesis, Virginia Polytechnic Institute and State University, Blacksburg, VA, USA.

Song, X. (1999). *Design of adaptive vibration control systems with application to magneto-rheological dampers*, PhD Thesis, Virginia Polytechnic Institute and State University, Blacksburg, VA, USA.

Song, X., Ahmadian, M., Southward, S.C. (2005). *Modeling magnetorheological dampers with application of nonparametric approach*, Journal of Intelligent Material Systems and Structures, Vol.16, pp.421-432.

Spencer, B.F., Dyke, S.J., Sain, M.K., Carlson, J.D. (1997). *Phenomenological model for magnetorheological dampers*, ASCE Journal of Engineering Mechanics, Vol.123, No.3, pp.230-238.

Stanway, R., Sproston, J.L., Stevens, N.G. (1987). *Non-linear modelling of an electro-rheological vibration damper*, Journal of Electrostatics, Vol.20, pp.167-184.

## T

Tham, M.T. (1999). *Principles of Linear Least Squares*, School of Chemical Engineering and Advanced Materials, Newcastle University. [Online] Available at: <http://lorien.ncl.ac.uk/ming/leastqs/leastqs.htm> [Accessed 3 October 2012].

Thoresson, M., Uys, P.E., Els, P.S., Snyman, J.A. (2009). *Efficient optimization of a vehicle suspension system, using a gradient-based approximation method, Part 1: Mathematical modelling*, Mathematical and Computer Modelling, Vol.50, pp.1421-1436.

Terasawa, T., Sakai, C., Ohmori, H., Sano, A. (2004). *Adaptive identification of MR damper for vibration control*, CDC: Proc. 43<sup>rd</sup> IEEE Conference on Decision and Control, Vol.3, pp.2297-2303.

## U

Uys, P.E., Els, P.S., Thoresson, M.J. (2006a). *Criteria for Handling Measurement*, Journal of Terramechanics, Vol.43, pp.43-67.

Uys, P.E., Els, P.S., Thoresson, M.J., Voigt, K.G., Combrinck, W.C. (2006b). *Experimental determination of moments of inertia for an off-road vehicle in a regular engineering laboratory*, International Journal of Mechanical Engineering Education, Vol.34, No.4, pp.291-341.

## V

Van der Merwe, W. (2007). *Band Evaluasie (English: Tyre Evaluation)*, Unpublished Final Year Thesis, Department of Mechanical and Aeronautical Engineering, University of Pretoria.

## W

Wang, D.H., Liao, W.H. (2011). *Magnetorheological fluid dampers: a review of parametric modeling*, Smart Materials and Structures, Vol.20, pp.1-34.

Wehrmeyer, V.H. (2011). *Baja Suspension Optimization*, Unpublished Final Year Thesis, Department of Mechanical and Aeronautical Engineering, University of Pretoria.

Wen, Y.K. (1976). *Method for random vibration of hysteretic systems*, Journal of Engineering Mechanics Division, ASCE, Vol.102, pp.249-263.

## Y

Yildirim, Ş. (2004). *Vibration control of suspension systems using a proposed neural network*, Journal of Sound and Vibration, Vol.277, pp.1059-1069.

Yu, M., Choi, S.B., Dong, X.M., Liao, C.R. (2009). *Fuzzy Neural Network Control for Vehicle Stability Utilizing Magnetorheological Suspension System*, Journal of Intelligent Material Systems and Structures, Vol.20, pp.457-466.

Yu, M., Liao, C.R., Chen, W.M., Huang, S.L. (2006). *Study on MR semi-active suspension system and its road testing*, Journal of Intelligent Material Systems and Structures, Vol.17, pp.801-806.

# APPENDIX A: EXPERIMENTAL MOMENT OF INERTIA RESULTS

**Table A-1: Roll moment of inertia results.**

Dataset:	1	2	3	4	5	6	7	8	9	Average
$I_O$ [kgm <sup>2</sup> ]	129.35	129.24	129.27	125.34	127.64	130.77	129.72	129.69	129.61	128.96
$I_{roll}$ [kgm <sup>2</sup> ]	54.14	54.03	54.06	50.13	52.43	55.56	54.50	54.48	54.40	53.75
$\tau_d$ [s]	0.74	0.74	0.73	0.72	0.73	0.73	0.73	0.73	0.73	0.73
$\omega_d$ [rad/s]	8.50	8.55	8.67	8.74	8.65	8.58	8.60	8.58	8.61	8.61
$\tau_n$ [s]	0.74	0.74	0.73	0.72	0.73	0.73	0.73	0.73	0.73	0.73
$\omega_n$ [rad/s]	8.50	8.55	8.67	8.74	8.65	8.58	8.60	8.58	8.61	8.61
$\zeta$ [-]	0.00920	0.00730	0.00620	0.01000	0.00610	0.00480	0.00430	0.00450	0.00410	0.00628
$k$ [N/m]	14759	14907	15324	15119	15062	15186	15132	15060	15154	15078.11

**Table A-2: Pitch moment of inertia results.**

Dataset:	1	2	3	4	5	6	7	8	9	Average
$I_O$ [kgm <sup>2</sup> ]	223.73	222.73	222.55	223.23	223.23	223.50	223.96	224.52	223.75	223.47
$I_{pitch}$ [kgm <sup>2</sup> ]	90.85	89.85	89.67	90.35	90.35	90.62	91.08	91.63	90.87	90.58
$\tau_d$ [s]	0.51	0.50	0.50	0.51	0.51	0.51	0.51	0.51	0.51	0.51
$\omega_d$ [rad/s]	12.40	12.48	12.46	12.40	12.40	12.42	12.37	12.34	12.34	12.40
$\tau_n$ [s]	0.51	0.50	0.50	0.51	0.51	0.51	0.51	0.51	0.51	0.51
$\omega_n$ [rad/s]	12.40	12.48	12.46	12.40	12.40	12.42	12.37	12.34	12.34	12.40
$\zeta$ [-]	0.00069	0.00064	0.00050	0.00064	0.00056	0.00038	0.00063	0.00064	0.00061	0.00059
$k$ [N/m]	15000	15131	15069	14966	14966	15041	14945	14905	14854	14986.33

**Table A-3: Yaw moment of inertia results.**

Dataset:	1	2	3	4	5	6	7	8	9	Average
$I_O$ [kgm <sup>2</sup> ]	70.81	72.14	71.71	71.39	72.01	72.51	73.26	73.18	73.08	72.23
$I_{yaw}$ [kgm <sup>2</sup> ]	67.74	69.06	68.64	68.31	68.93	69.44	70.19	70.10	70.01	69.16
$\tau_d$ [s]	0.37	0.37	0.37	0.37	0.37	0.38	0.38	0.38	0.38	0.37
$\omega_d$ [rad/s]	17.10	16.94	17.14	16.91	16.94	16.72	16.57	16.57	16.57	16.83
$\tau_n$ [s]	0.37	0.37	0.37	0.37	0.37	0.38	0.38	0.38	0.38	0.37
$\omega_n$ [rad/s]	17.10	16.94	17.14	16.91	16.94	16.72	16.57	16.57	16.57	16.83
$\zeta$ [-]	0.00170	0.00210	0.00091	0.00260	0.00210	0.00400	0.00530	0.00500	0.00460	0.00315
$k$ [N/m]	14927	14934	15185	14712	14907	14615	14508	14491	14472	14750.11



---



---

## *APPENDIX B: BAJA PACEJKA '89 TYRE MODEL PROPERTIES*

---



---

<pre>[MDI_HEADER] FILE_TYPE = 'tir' FILE_VERSION = 3.0 FILE_FORMAT = 'ASCII' (COMMENTS) {comment_string} 'Tire - XXXXXX' 'Pressure - XXXXXX' 'Test Date - XXXXXX' 'Test tire' 'New File Format v2.1' [UNITS] LENGTH = 'mm' FORCE = 'newton' ANGLE = 'radians' MASS = 'kg' TIME = 'sec' [MODEL] ! use mode 1 2 3 4 ! ----- ----- ! smoothing X X ! combined X X ! PROPERTY_FILE_FORMAT = 'PAC89' USE_MODE = 4.0 [DIMENSION] UNLOADED_RADIUS = 267 WIDTH = 150 ASPECT_RATIO = 0.75 [PARAMETER] VERTICAL_STIFFNESS = 80 VERTICAL_DAMPING = 3.1 LATERAL_STIFFNESS = 150 ROLLING_RESISTANCE = 0.02 [LATERAL_COEFFICIENTS] a0 = 1.65000 a1 = -34.0 a2 = 1250.00 a3 = 3036.00 a4 = 12.80</pre>	<pre>a5 = 0.00501 a6 = -0.02103 a7 = 0.77394 a8 = 0.0022890 a9 = 0.013442 a10 = 0.003709 a11 = 19.1656 a12 = 1.21356 a13 = 6.26206 [LONGITUDINAL_COEFFICIENTS] b0 = 2.37272 b1 = -9.46000 b2 = 1490.00 b3 = 130 b4 = 276 b5 = 0.08860 b6 = 0.00402 b7 = -0.06150 b8 = 1.2 b9 = 0.02990 b10 = -0.17600 [ALIGNING_COEFFICIENTS] c0 = 2.34000 c1 = 1.4950 c2 = 6.416654 c3 = -3.57403 c4 = -0.087737 c5 = 0.098410 c6 = 0.0027699 c7 = -0.0001151 c8 = 0.1000 c9 = -1.33329 c10 = 0.025501 c11 = -0.02357 c12 = 0.03027 c13 = -0.0647 c14 = 0.0211329 c15 = 0.89469 c16 = -0.099443 c17 = -3.336941</pre>
---	--